

**Die solvothermale Synthese von
Thioantimonaten(III),
Kupfer(I)- und Silber(I)haltigen Thioantimonaten(III)**

Kumulative Dissertation
zur Erlangung des Doktorgrades
der Naturwissenschaften

vorgelegt von Oberstudienrat i. R. Volker Spetzler

beim Fachbereich Chemie
der Christian-Albrechts-Universität zu Kiel

Kiel, Mai 2006

Referent: Prof. Dr. W. Bensch

Koreferent: Prof. Dr. N. Stock

Tag der mündlichen Prüfung: 13. 7. 06

Zum Druck genehmigt: Kiel, 19. 6. 06

gez. Prof. Dr. J. Grottemeyer
Dekan

Meiner Frau gewidmet

Die Hoffnung
ist der
Regenbogen
über den
herabstürzenden
Bach des
Lebens.

Friedrich Nietzsche
(1844-1900)

Die solvothermale Synthese von

Thioantimonaten(III),

Kupfer(I)- und Silber(I)haltigen Thioantimonaten(III)

Die Arbeit bestand darin, unter solvothermalen Bedingungen offene Netzwerkstrukturen aus Übergangsmetallhaltigen-Thioantimonaten und Aminen als Strukturdirektoren zu synthetisieren und zu charakterisieren. Zunächst wurden reine Thioantimonate(III) der allgemeinen Formel RSb_xS_y (R = Amin) wie $(C_6N_3H_{17})Sb_6S_{10}$ und $(C_6N_2H_{18})Sb_4S_7$ hergestellt. Sie sind in die Reihen der Thioantimonate(III) mit dem Sb:S-Verhältnissen 1:1.667 und 1:1.75 einzureihen. Im Unterschied zu diesen Verbindungen sind in der Literatur nur wenige auf Kupfer und Silber basierende Thioantimonate(III) beschrieben. Unter nahezu gleichen Versuchsbedingungen gelang es, Kupfer(I)-Thioantimonate(III) der allgemeinen Formeln RCu_2SbS_3 und $RCu_3Sb_2S_5$ (R = Amin) zu synthetisieren. Die fünf hergestellten Verbindungen $(C_4N_2H_{14})_{0.5}Cu_2SbS_3$ [$C_4N_2H_{12}$ = 1,4-Diaminobutan], $(C_6N_2H_{18})_{0.5}Cu_2SbS_3$ [$C_6N_2H_{16}$ = 1,6-Diaminohexan], $(C_4N_3H_{15})_{0.5}Cu_2SbS_3$ [$C_4N_3H_{13}$ = Diethylentriamin] und $(C_8N_4H_{22})_{0.5}Cu_2SbS_3$ [$C_8N_4H_{20}$ = 1,4-bis(2-aminoethyl)-Piperazin] kristallisieren in der monoklinen Raumgruppe $P2_1/n$ und weisen alle die gleiche Topologie des Cu_2SbS_3 -Netzwerkes auf und können als anorganisch-organische Hybridverbindungen aufgefasst werden. Die Sb-S-, Cu-S-, Cu-Sb- und Cu-Cu-Abstände, sowie die entsprechenden Winkel unterscheiden sich nur geringfügig. Dagegen weisen die Verbindungen $(C_4N_3H_{14})Cu_3Sb_2S_5$ [$C_4N_3H_{13}$ = Diethylentriamin] und $(C_6N_4H_{20})_{0.5}Cu_3Sb_2S_5$ [$C_6N_4H_{18}$ = Triethylentetramin] trotz des identischen Cu:Sb:S-Verhältnisses völlig verschiedenartige Strukturen auf. Alle Verbindungen zeigen eine sandwichartige Anordnung der Anionenschicht und des protonierten Amins auf. Dabei variieren die Schichtabstände zwischen 4.4 und 8.8 Å. Schichtverbindungen sind ebenfalls die beiden Silber(I)-Thioantimonate(III) $(C_4N_2H_{14})Ag_3Sb_3S_7$ ($C_4N_2H_{12}$ = 1,4-Diaminobutan) und $(C_2N_2H_9)_2Ag_5Sb_3S_8$ ($C_2N_2H_8$ = Ethylendiamin). Sie kristallisieren in der orthorhombischen Raumgruppe Pnma bzw. der monoklinen Raumgruppe $P2_1/n$.

Um Kenntnis über weitere Materialeigenschaften zu erhalten, wurden zusätzlich Messungen zur magnetischen Suszeptibilität χ , der diffusen Reflexion und der Impedanzspektroskopie durchgeführt.

The Solvothermal Synthesis of

Thioantimonates(III),

Copper(I)- and Silver(I)-Thioantimonates(III)

The thioantimonates(III) were synthesized under solvothermal conditions with the amines as structure directing molecules. The two compounds $(C_6N_3H_{17})Sb_6S_{10}$ and $(C_6N_2H_{18})Sb_4S_7$ belong to the groups of thioantimonates(III) with a Sb:S ratio of 1:1.667 respectively 1:1.75. Only few copper- and silver-based thioantimonates were described in the literature. The compounds $(C_4N_2H_{14})_{0.5}Cu_2SbS_3$ [$C_4N_2H_{12}$ = 1,4-diaminobutane], $(C_6N_2H_{18})_{0.5}Cu_2SbS_3$ [$C_6N_2H_{16}$ = 1,6-diaminohexane], $(C_4N_3H_{15})_{0.5}Cu_2SbS_3$ [$C_4N_3H_{13}$ = diethylenetriamine], $(C_8N_4H_{22})_{0.5}Cu_2SbS_3$ [$C_8N_4H_{20}$ = 1,4-di-(2-aminoethyl)-piperazine] $(C_4N_3H_{14})Cu_3Sb_2S_5$ [$C_4N_3H_{13}$ = diethylenetriamine] and $(C_6N_4H_{20})_{0.5}Cu_3Sb_2S_5$ [$C_6N_4H_{18}$ = triethylenetetramine] are new members of the copper(I)-thioantimonate(III) families with the general formulas RCu_2SbS_3 respectively $RCu_3Sb_2S_5$ with R being an amine of different size and shape. The compounds with the general formula RCu_2SbS_3 crystallize in the monoclinic space group $P2_1/n$ and a comparison of the geometrical parameters of the compounds reveals small differences. The anions in the other two compounds have the same chemical composition but very different structures. The layers of these inorganic/organic hybrid compounds are separated by the organic amine cations and a sandwich-like arrangement of anions and cations is observed. The interlayer separation reaches from 4.4 Å to 8.4 Å. This sandwich-like arrangement was observed in the silver(I)-thioantimonates(III) $(C_4N_2H_{14})Ag_3Sb_3S_7$ ($C_4N_2H_{12}$ = 1,4-diaminobutane) and $(C_2N_2H_9)_2Ag_5Sb_3S_8$ ($C_2N_2H_8$ = ethylenediamine) too. The two compounds crystallize in the orthorhombic space group $Pnma$ respectively in the monoclinic space group $P2_1/n$.

The crystal structures, thermoanalytical measurements, optical properties, magnetic susceptibilities χ and impedance spectroscopy were presented.

Inhaltsverzeichnis

1. Einleitung	1
1.1 Motivation und Ziel	1
1.2 Sb(III) und das lone-pair (LP)	4
2. Experimentelles	6
2.1 Syntheseapparaturen	6
2.2 Verwendete Chemikalien und Geräte	7
2.3 Die Impedanzspektroskopie	8
3. Synthese und Struktur von Thioantimonaten	13
3.1 Synthese und Struktur von $(C_6N_3H_{17})Sb_6S_{10}$ und $(C_7N_2H_{13})_3Sb_9S_{15}$	13
3.2 Synthese und Struktur von $(C_6N_2H_{18})Sb_4S_7$	22
3.3 Synthese und Struktur von Kupfer(I)-Thioantimonaten(III) mit der allgemeinen Formel RCu_2SbS_3 ($R = \text{Amin}$)	37
3.4 Synthese und Struktur von Kupfer(I)-Thioantimonaten(III) mit den allgemeinen Formeln RCu_2SbS_3 und $RCu_3Sb_2S_5$ ($R = \text{Amin}$)	50
3.5 Synthese und Struktur von $(C_4N_2H_{14})Ag_3Sb_3S_7$ und $(C_2N_2H_9)_2Ag_5Sb_3S_8$	64
4. Zusammenfassung und Ausblick	87
4.1 Thioantimonate (III) mit der allgemeinen Formel RSb_xS_y ($R = \text{Amin}$)	87
4.2 Kupfer(I)-Thioantimonate(III) mit der allgemeinen Formel RCu_2SbS_3 ($R = \text{Amin}$)	90
4.3 Kupfer(I)-Thioantimonate(III) mit der allgemeinen Formel $RCu_3Sb_2S_5$ ($R = \text{Amin}$)	96
4.4 Die Silber(I)-Thioantimonate(III) $(C_4N_2H_{14})_2Ag_3Sb_3S_7$ und $(C_2N_2H_9)_2Ag_5Sb_3S_8$	98
4.5 Synthese von Kupfer(I)- Silber(I)- Thioantimonat(III): ein Anfang?	100
5. Publikationsliste und Tagungsbeiträge	103
5.1 Publikationsliste	103
5.2 Tagungsbeitrag	104
6. Strukturdaten	105
6.1 Single Crystal Structure Determination of $(1,6-DAHH_2)Sb_4S_7$	105
6.2 Single Crystal Structure Determination of $(1-\text{pip}H_2)Sb_6S_{10}$	109
6.3 Single Crystal Structure Determination of $(1,4-DABH_2)_{0,5}Cu_2SbS_3$	114
6.4 Single Crystal Structure Determination of $(1,6-DAHH_2)_{0,5}Cu_2SbS_3$	118

6.5 Single Crystal Structure Determination of (dienH ₂) _{0.5} Cu ₂ SbS ₃	122
6.6 Single Crystal Structure Determination of (1,4-pipH ₂) _{0.5} Cu ₂ SbS ₃	127
6.7 Single Crystal Structure Determination of (dienH)Cu ₃ Sb ₂ S ₅	131
6.8 Single Crystal Structure Determination of (TETNH ₂) _{0.5} Cu ₃ Sb ₂ S ₅	135
6.9 Single Crystal Structure Determination of (1,4-DAB)Ag ₃ Sb ₃ S ₇	139
6.10 Single Crystal Structure Determination of (en) ₂ Ag ₅ Sb ₃ S ₈	143
6.11 Single Crystal Structure Determination of (enH ₂) ₂ Cu ₃ Ag ₅ Sb ₄ S ₁₂	149

7. Literatur **155**

1. Einleitung

1.1 Motivation und Ziel

In der modernen Technologie nimmt die **Festkörperchemie** einen bedeutenden Platz ein [1]. Dabei wird der Synthese von Festkörpern mit offenen Gerüststrukturen eine besondere Aufmerksamkeit gewidmet [2]. Diese Festkörper finden Verwendung als Katalysatoren und Ionenaustauscher und dienen zur Sorption gasförmiger und flüssiger Stoffe [3, 4]. Zunehmend gewinnen sie an Bedeutung in der nichtlinearen Optik (NLO) [5] und auch als Halbleiter [6, 7, 8]. Die im Rahmen dieser Arbeit durchgeföhrten Synthesen konzentrierten sich darauf, durch Einsatz von Übergangsmetallen (ÜM) neue nanoporöse Thioantimonat-Produkte mit offenen Gerüststrukturen zu erhalten, welche Kanäle, Käfige oder andere Hohlräume aufweisen. Eine Möglichkeit, derartige “zeotype” Materialien zu synthetisieren, bietet die Substitution der brückenbildenden Sauerstoffatome in Zeolithen durch Homologe wie Schwefel, Selen oder Tellur.

Die “Chimie-douce“-Anwendungen der **Solvothermalsynthese** haben den Zugang zu einem neuen Bereich der Festkörperchemie geschaffen [9]. Diese “milden” Bedingungen begünstigen bei Einsatz stark polarer Lösungsmittel wie Wasser, Methanol oder Aminen und Temperaturen zwischen 100-200°C einerseits das Kristallwachstum, andererseits werden molekulare Bausteine, die zur Bildung polymerer Strukturen führen können, nicht zerstört.

Meine Motivation für diese Arbeit bestand darin, unter solvothermalen Bedingungen **offene Netzwerkstrukturen** aus ÜM-Thioantimonaten und Aminen als **Strukturdirektoren** zu synthetisieren und zu charakterisieren [10-18]. In der Literatur sind nur wenige auf Kupfer basierende Thioantimonate beschrieben. Die Verbindung CuSbS₂ bildet eine Schichtstruktur mit den primären Baueinheiten (PBE) SbS₃ und CuS₄, wobei Sb^{III} an drei Schwefelatome gebunden ist und eine trigonal-pyramidal Geometrie aufweist und Cu^I von vier Schwefelatomen tetraedrisch koordiniert ist [19]. Tetrahedrit, Cu₁₂Sb₄S₁₃, gehört zur Gruppe der Sulfosalze der allgemeinen Zusammensetzung X₁₂Z₄S₁₃ und in der Struktur liegen ein nahezu regulärer CuS₄-Tetraeder und ein CuS₃-Dreieck vor. In dieser Verbindung ist die Oxidationszahl des

Kupfers nicht eindeutig. Unter Berücksichtigung der Ladungsneutralität müssten zwei Cu^{II}, 10 Cu^I und 4 Sb^{III} vorhanden sein. Die Sb-S-Abstände betragen ca. 2.446 Å und die Cu-S-Abstände variieren zwischen 2.272 und 2.342 Å [20]. Auch in der Verbindung Cu₃SbS₃ weisen die Cu-S-Abstände von 2.239 und 2.359 Å auf Cu^I hin. Bemerkenswert sind die kurzen Cu-Cu-Abstände von 2.627 Å, die nur unwesentlich länger als in elementarem Kupfer von 2.556 Å sind [21], so dass eine d¹⁰-d¹⁰ Wechselwirkung anzunehmen ist [22]. Beispiele für fünfwertiges Antimon stellen die beiden Verbindungen Cu₃SbS₄ und Cu₃SbSe₄ dar, die zum Famatinit Strukturtyp gehören [23]. Auch die auf Kupfer basierenden Selenoantimonate CuSbSe₂ [24], Cu₃SbSe₃ [25] und Cu₃SbSe₄ [23] sind bei relativ hohen Temperaturen synthetisiert worden, wobei CuSbSe₂ eine Schichtstruktur und die beiden anderen Verbindungen ein 3-D Netzwerk aufweisen. Na₂CuSbS₃ bildet eine zweidimensionale anionische Schicht aus den trigonal planaren Cu^IS₃- und den trigonal pyramidalen SbS₃-Einheiten, wobei der Ladungsausgleich durch 2 Na⁺ erfolgt [26]. Unter **solvothermalen Bedingungen** gelang es, Selenoantimonate(III) und Kupferthioantimonate(III) in Form von Schichtverbindungen mit sandwichartig eingelagerten Aminen zu synthetisieren. So ist Ethylendiamin in der Verbindung Cu₂SbSe₃·en nahezu senkrecht zwischen den Schichten orientiert, während in Cu₂SbSe₃·0.5en das Amin fast parallel zu den anionischen Schichten angeordnet ist [27]. Für Cu₂SbS₃·0.5en wurden die zwei Wertigkeiten Cu^I/Cu^{II} mit nicht protoniertem Amin postuliert [28], während Cu^I und ein vollständig protoniertes Amin in der Verbindung [C₄H₁₂N₂]_{0.5}[CuSb₆S₁₀] vorliegen [29].

Diese aufgeführten Beispiele machen die strukturelle Vielfalt der Kupferthioantimonate deutlich. Um Kenntnis über weitere Materialeigenschaften zu erhalten, kommt der Impedanzspektroskopie eine grosse Bedeutung zu. Es ist eine überaus wichtige elektrochemische Messmethode, mit welcher der Wechselstromwiderstand als Funktion der Frequenz gemessen wird. Mit dieser Technik ist es möglich, Informationen über Widerstände, Kapazitäten, Leitfähigkeiten und Aktivierungsenergien zu erhalten [30-36].

Die erfolgreichen Synthesen der Kupfer(I)-Thioantimonate(III) der allgemeinen Formel RCu₂SbS₃ und RCu₃Sb₂S₅ (R = Amin) führten zu der Überlegung, Silber(I)-Thioantimonate(III) unter ähnlichen Versuchsbedingungen zu synthetisieren.

In der Literatur ist über nur wenige Silberthioantimonate berichtet worden. Dazu gehören die Verbindungen AgSbS_2 (Miargyrit) [37], Ag_3SbS_3 (Pyrargyrit) [38] und Ag_5SbS_4 (Stephanit) [39]. Im Miargyrit und Pyrargyrit werden eine primäre Baueinheit AgS_3 mit drei kurzen Ag-S-Abständen (2.44, 2.50, 2.58 Å) und eine AgS_3 -Gruppe mit zwei kurzen und einem langen Ag-S-Abstand (2.36, 2.46, 2.89 Å) beobachtet. Der Ag-Ag-Abstand im Miargyrit beträgt 4.00 Å, während im Stephanit mit 2.88, 2.95 und 2.99 Å drei kurze Ag-Ag-Abstände beobachtet werden und hierbei von einer Metall-Metall-Bindung ausgegangen werden kann, da der Ag-Ag-Abstand im Metall 2.88 Å beträgt [39, 22]. Unter solvothermalen Bedingungen wurden die acht quaternären Thioantimonate $\text{RbAg}_2\text{SbS}_4$, $\text{Rb}_2\text{AgSbS}_4$, KAg_2SbS_4 , K_2AgSbS_4 [40], $\text{Cs}_3\text{Ag}_2\text{Sb}_3\text{S}_8$, α - und β - $\text{Cs}_2\text{AgSbS}_4$, und $\text{Cs}_2\text{AgAsS}_4$ [41] sowie $[\text{C}_2\text{H}_9\text{N}_2]_2[\text{Ag}_2\text{SbS}_3]$, $[\text{C}_2\text{H}_9\text{N}_2]_2[\text{Ag}_5\text{Sb}_3\text{S}_8]$ [42] und $[\text{C}_6\text{H}_{20}\text{N}_4][\text{Ag}_5\text{Sb}_3\text{S}_8]$ [43] hergestellt. Alle vier quaternären Verbindungen im M-Ag-Sb-S-System (M = Rb, K) bestehen aus anionischen Netzwerken, die durch Kondensation nahezu idealer SbS_4^- und verzerrter AgS_4 -Tetraeder gebildet werden. Für die Verbindungen KAg_2SbS_4 , K_2AgSbS_4 und $\text{RbAg}_2\text{SbS}_4$ wird ein dreidimensionales anionisches Netzwerk, für $\text{Rb}_2\text{AgSbS}_4$ eine Schichtstruktur gefunden. Messungen der diffusen Reflexion ergeben für diese Verbindungen relativ grosse optische Bandlücken von 2.2 bis 3.9 eV. Die Oxidationszahlen M(I) (M = Rb, K), Ag(I), Sb(V) und S²⁻ sind eindeutig zuordnen [40]. Die vier Verbindungen im Cs-Ag-M-S-System (M = As, Sb) bestehen aus eindimensionalen Ketten [41]. Sandwichartig aufgebaute Schichten werden bei den drei Verbindungen $[\text{C}_2\text{H}_9\text{N}_2]_2[\text{Ag}_2\text{SbS}_3]$, $[\text{C}_2\text{H}_9\text{N}_2]_2[\text{Ag}_5\text{Sb}_3\text{S}_8]$ [42] und $[\text{C}_6\text{H}_{20}\text{N}_4][\text{Ag}_5\text{Sb}_3\text{S}_8]$ [43] gefunden. In diesen Verbindungen ist das Amin nahezu senkrecht zwischen den Schichten unter Bildung eines Schichtabstands von ca. 6 Å lokalisiert.

Im Unterschied zu den Kupfer(I)- und Silber(I)-Thioantimonaten(III) werden bei den reinen Thioantimonat(III)-Verbindungen verschiedene Sb:S-Verhältnisse beobachtet, wie z. B.: 1:1.625 ($[\text{Sb}_8\text{S}_{13}]^{2-}$ [44-48]), 1:1.667 ($[\text{Sb}_3\text{S}_5]^-$ [49-53], $[\text{Sb}_6\text{S}_{10}]^{2-}$ [54, 55, 56], $[\text{Sb}_9\text{S}_{15}]^{3-}$ [56], $[\text{Sb}_{12}\text{S}_{20}]^{4-}$ [57]), 1:1.75 ($[\text{Sb}_4\text{S}_7]^{2-}$ [58-71], $[\text{Sb}_{12}\text{S}_{21}]^{6-}$ [69]), 1:1.8 ($[\text{Sb}_5\text{S}_9]^{3-}$ [72], $[\text{Sb}_{10}\text{S}_{18}]^{6-}$ [73]) und 1:2 ($[\text{SbS}_2]^-$ [74, 75], $[\text{Sb}_2\text{S}_4]^{2-}$ [76], $[\text{Sb}_3\text{S}_6]^{3-}$ [77], $[\text{Sb}_4\text{S}_8]^{2-}$ [78], $[\text{Sb}_4\text{S}_8]^{4-}$ [79]).

Die Thioantimonate zeichnen sich durch eine grosse Vielfalt in bezug auf ihre Zusammensetzung und Dimensionalität der Anionenteilstrukturen wie Ketten, Schichten und Netzwerke aus [44-85]. Eine wichtige Voraussetzung dafür ist das stereochemisch aktive, einsame Elektronenpaar am Antimonatom [86].

1.2 Sb(III) und das lone-pair (LP)

Das lone-pair (LP) prägt die Koordinationsumgebung von Sb(III). Diese nicht-bindenden Elektronen im $5s^2$ -Niveau beanspruchen ungefähr den Platz eines O^{2-} -Liganden.

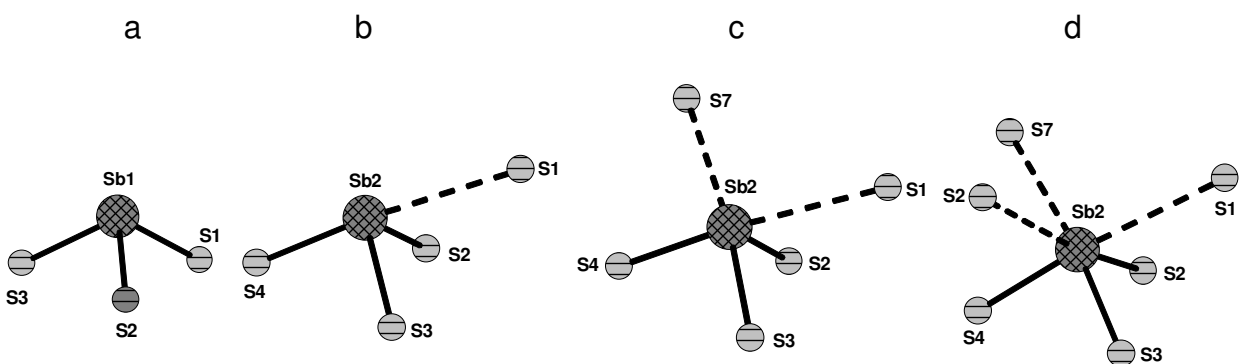


Abb. 1.2.1 Die Koordinationspolyeder um das Sb(III)-Ion am Beispiel der Verbindung $(DIEN)Cu_3Sb_2S_5$ (DIEN = Diethylentriamin)

Die einfachste Baueinheit ist trigonal-pyramidales SbS_3 , welches die **primäre Baueinheit** der Thioantimonate(III) darstellt (Abb. 1.2.1a). Isoliert kommt $[SbS_3]^{3-}$ wegen der Tendenz zur Bildung polymerer Thioantimonate selten vor, allerdings wird $[SbS_3]^{3-}$ in den Verbindungen A_3SbS_3 ($A = Na, K, Tl$), $Ca_2Sb_2S_5$ [81] und $Ba_8Sb_6S_{17}$ [87] gefunden. Unter Berücksichtigung des LP kann die Geometrie als SbS_3 -Tetraeder beschrieben werden. Die Erweiterung der Koordinationszahl über 3 hinaus führt zu ψ - SbS_4 -trigonalen Bipyramiden (Abb. 1.2.1b), ψ - SbS_5 -Oktaedern (Abb. 1.2.1c) und den SbS_6 -Oktaedern (Abb. 1.2.1d). Dabei ist anzumerken, dass sich die längeren Sb-S-Abstände immer in trans-Stellung zu den kürzeren Sb-S-Abständen befinden (Abb. 1.2.1). In der SbS_3 -Baugruppe variieren die Sb-S-Bindungsabstände zwischen ca. 2.4 und 2.6 Å. Die Sb-S-Bindungen in den anderen Baugruppen sind meistens deutlich länger und eine Analyse der Sb-S-Bindungen (s. Abb. 1.2.2) zeigt,

dass bis zur Summe der van-der-Waals-Radien von Sb und S (3.8 \AA [88]) solche so genannten sekundären Wechselwirkungen auftreten [89]. Das erschwert die eindeutige Zuordnung der Dimensionalität der Thioantimonatnetzwerke. Damit eine Konsistenz bei der Strukturbeschreibung erreicht wird, wurden Sb-S-Abstände bis etwa 3 \AA als bindend eingestuft. Es ist klar, dass dieser Wert etwas willkürlich gewählt ist und letztlich nur quantenchemische Rechnungen Auskunft geben würden, bis zu welchem Sb-S-Abstand bindende Wechselwirkungen vorliegen. Solche Rechnungen müssten für jede Struktur durchgeführt werden. Die Analyse der S-Sb-S-Winkel ergibt (Abb. 1.2.2), dass zwischen 85 und 110° ein Maximum auftritt. Im Vergleich zu den O-Si-O/O-Al-O-Winkeln in Zeolithen/Silikaten ist der S-Sb-S-Winkel weniger flexibel, was auf die hohe Kovalenz der Sb-S-Bindungen zurückzuführen ist.

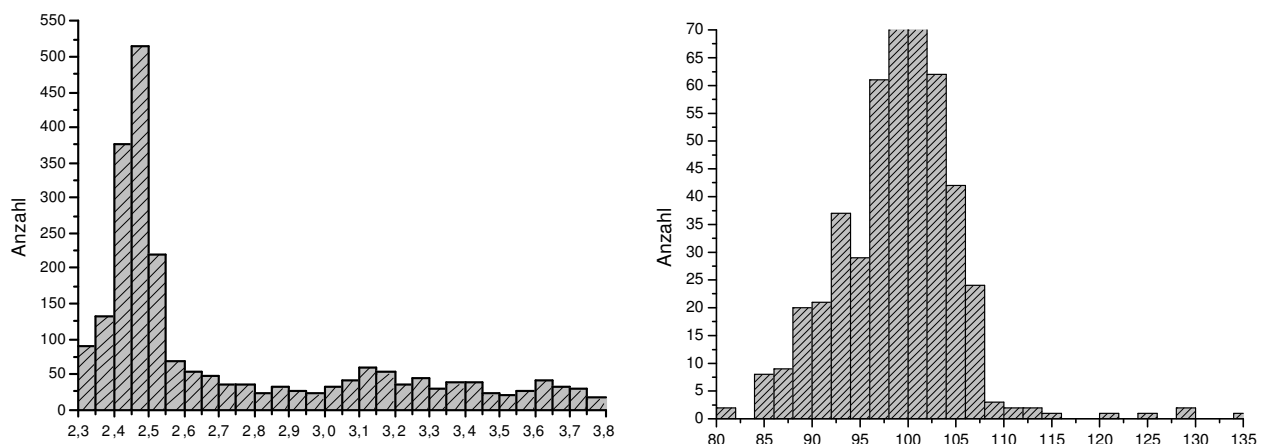


Abb. 1.2.2 Sb-S-Abstände (\AA) (links) und Sb-S-Sb-Winkel ($^\circ$) (rechts)

2. Experimentelles

2.1 Syntheseapparaturen

Zur solvothermalen Synthese wurden Edelstahlautoklaven verwendet. In diesen wurden Teflonbecher als schwimmender Einsatz eingesetzt (Abb. 2.1.1). Die Teflonbecher, die mit einem dicht schließenden Deckel versehen werden, haben einen Reaktionsraum von ca. 30 ml. Wegen seiner Korrosionsbeständigkeit ist Teflon das ideale Gefäßmaterial. Die Ausgangssubstanzen wurden mit einer Analysenwaage abgewogen, in den Tefloneinsatz überführt und mit dem Lösungsmittel versetzt. Der Füllgrad des Bechers betrug ca. 15%. Anschließend wurde der Becher in den Autoklaven gestellt und fest verschraubt. In einem Trockenschrank wurde das Reaktionsgemisch bei Temperaturen zwischen 100-170 °C erhitzt.



Abb. 2.1.1 Edelstahlautoklav mit Tefloneinsatz

Der Einsatz von Teflon ist jedoch nicht unproblematisch, da es porös ist. Dies kann zu einer ungewollten Aufnahme der Reaktionslösungen führen, und bei weiteren Synthesen werden diese dann freigesetzt und kontaminieren die Produkte. Daher dürfen Teflongefäße immer nur mit einem bestimmten Lösungsmittel (Amin) gefüllt werden. Ein Einsatz von geschlossenen Glasampullen in der Solvothermal-synthese bei 100-200 °C und damit verbundenen Druck unter 30 bar ist überlegenswert, da eine visuelle Beurteilung des Reaktionsverlaufs möglich und eine unbeabsichtigte Kontamination ausgeschlossen ist.

2.2 Verwendete Chemikalien und Geräte

Tab. 2.2.1: Verwendete Chemikalien

Chemikalien	Hersteller	Reinheit	Solvantien	Hersteller	Konzentration
Sb	Merck	99.5%	Ethylendiamin	Fluka	99%
Sb ₂ S ₃ (Stibnit)	Fluka	97%	1,3-Diamino-propan	Fluka	99%
S	Merck		1,4-Diaminobutan	Fluka	99%
Cu	Fluka	99.7%	1,6-Diaminohexan	Fluka	99%
CuCl ₂ ·2H ₂ O	Merck	99%	1-(2-aminoethyl)-Piperazin	Fluka	97%
AgNO ₃	Fluka	99.8%	Diethylenetriamin	Fluka	97%
Ag	Fluka	99.9%	Triethylentetramin	Fluka	70% / 97%

Tab. 2.2.2: Verwendete Geräte

Methode	Gerät	Bemerkungen
Einkristallstruktur-analyse	STOE AED 4	Mo K _α (0.71073 Å), Graphitmonochromator
	NONIUS CAD 4	Mo K _α (0.71073 Å), Graphitmonochromator
	STOE IPDS	Mo K _α (0.71073 Å), Graphitmonochromator
	Phillips PW 1100	Mo K _α (0.71073 Å), Graphitmonochromator
Pulver-diffraktometrie	Stadi-P (STOE)	Transmissionsgeometrie; Cu K _α (1.54051 Å)
DTA/TG	Netzsch STA-409 CD	Pt-Pt/Rh Thermoelement, Messung im Argonstrom, 100 mL/min, Heizrate 4 K/min, Messbereich bis 450 °C
FT-Raman	Bruker IFS 66	Raman Spektrometer mit 514.5 nm bei T = 20 K, Messbereich von 100-500 cm ⁻¹ , Auflösung: 2 cm ⁻¹
FIR	Bruker IFS 66	in Polyethylen-Matrix, 80-500 cm ⁻¹ , 1cm ⁻¹
MIR	ATI Mattson Genesis	Messbereich: 400-4000 cm ⁻¹ , in KBr-Pressling, Auflösung: 1cm ⁻¹
Elementaranalyse	Eurovector EuroEA Elemental Analyzer	CHNS-Analyse; He-Trägergas; Detektion über eine Wärmeleitzelle

Diffuse Reflektion	Cary5Varian TechtronPty. Darmstadt	Messbereich: 250-2000 nm, als Standard mit 100% Reflektion wurde BaSO ₄ benutzt.
Magnetmessung	MPMS SQUID, PPMS(Quantum Design)	H = 1 T H = 5 T
Impedanzspektroskopie	Kieler Zelle	Goldelektroden
ESEM	Philips ESEM XL30	Rasterelektronenmikroskop mit EDX- Aufsatz der Firma EDAX

2.3 Die Impedanzspektroskopie

Eine wichtige elektrochemische Messmethode ist die Impedanzspektroskopie, die den Wechselstromwiderstand als Funktion der Frequenz misst. Mit solchen Messungen werden Kenntnisse über elektrische Leitfähigkeiten, Kapazitäten, Widerstände, Beweglichkeiten von Ladungsträgern, elektrische Transportmechanismen, Diffusionskonstanten und Aktivierungsenergien erhalten [30-36]. Für die im Rahmen dieser Arbeit gemessenen Impedanzspektren gelten die in der Abbildung 2.3.1 und 2.3.2 dargestellten Nyquistplots und Ersatzschaltbilder.

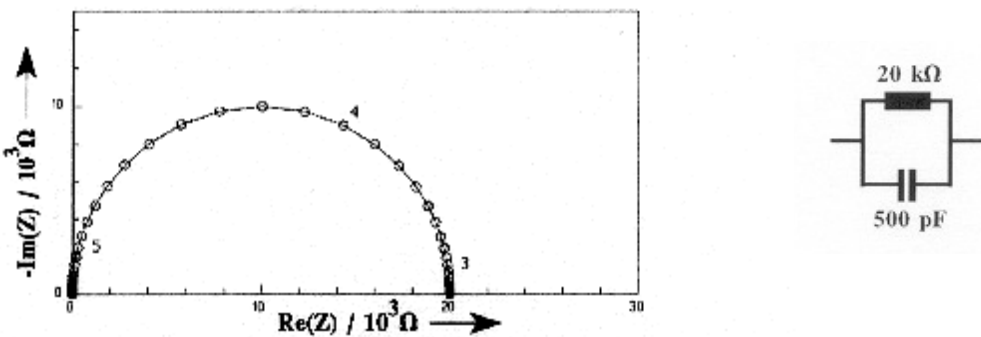


Abb. 2.3.1 Impedanzdiagramm mit dem zugehörigen Ersatzschaltbild für eine RC-Parallelschaltung [30]

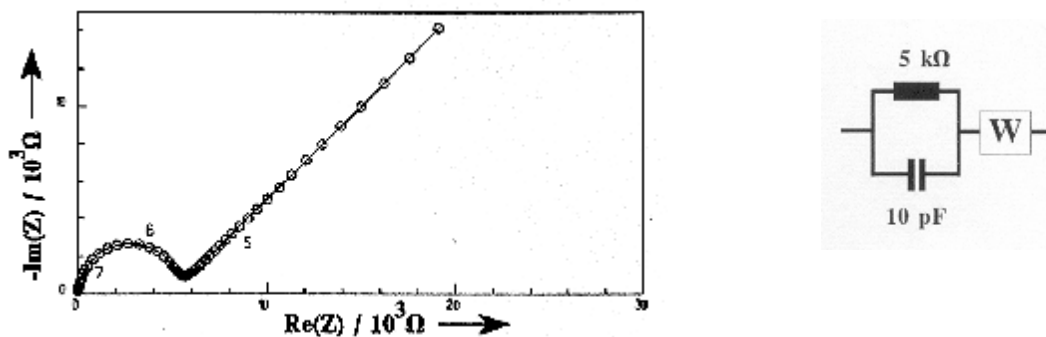


Abb. 2.3.2 Impedanzdiagramm mit dem zugehörigen Ersatzschaltbild für eine RC-Parallelschaltung und einer zusätzlichen Warburg-Impedanz W [30]

Die Kombination aus Ohm'schem Widerstand R und Kondensator C wird als komplexer Widerstand oder Impedanz Z des Systems bezeichnet. Der komplexe Widerstand setzt sich aus dem imaginären Z'' - und realen Z' -Teil zusammen. Der Impedanzverlauf wird im so genannten Nyquistplot dargestellt, in welcher der Imaginärteil des komplexen Widerstandes $-Z''$ über den Realteil Z' aufgetragen wird. Die RC-Parallelschaltung und der dazugehörige Nyquistplot stehen für ionenblockierende Elektroden (Abb. 2.3.1). Bei nicht ionenblockierenden Elektroden finden Reaktionen an der Phasengrenze zwischen dem Festkörperelektrolyten und den Elektroden statt. Dabei tritt im Ersatzschaltkreis ein Konstantphasenelement auf, wobei der Spezialfall dieses Elements mit $\alpha = 45^\circ$ als Warburg-Impedanz bezeichnet wird (Abb. 2.3.2). Diese Impedanz tritt dann auf, wenn in der zu messenden Probe Ladungstransportprozesse diffusionsbestimmend sind, wobei die Konzentration der Teilchen an der Elektrodenoberfläche um 45° mit dem Teilchenfluss über der Grenzschicht phasenverschoben ist [30-36]. In der Literatur wird auch von blockierender bzw. nicht blockierender Grenzschicht gesprochen [32]. Die Impedanzmessung wurde mit Hilfe einer in Kiel entwickelten Zelle durchgeführt (Abb. 2.3.3).

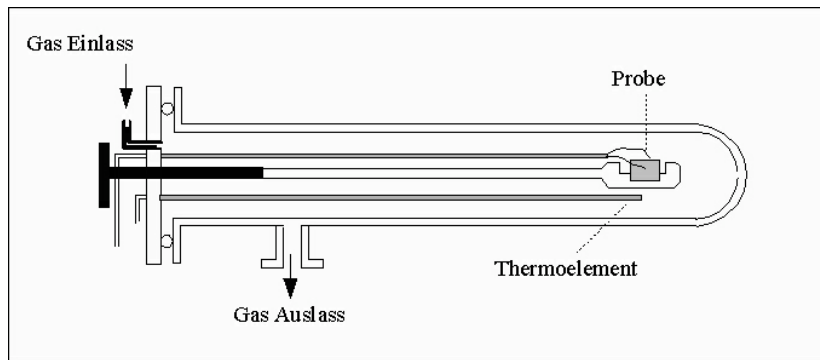


Abb. 2.3.3 Kieler Zelle [31]

Die Verbindungen $(en)_{0.5}Cu_2SbS_3$ und $(C_2N_2H_9)_2Ag_5Sb_3S_8$ wurden in Form von Presslingen in die Kieler Zelle eingebracht, wobei zur elektrischen Kontaktierung Goldfolie verwendet wurde. Diese Messzelle wird an eine Impedanzbrücke („HP 4192 Impedance–Analizer“) angeschlossen. Die Messung erfolgte im Frequenzbereich $\nu = 5 \text{ Hz} – 13 \text{ MHz}$ mit einer Spannung von 50 mV und wurde in einem mit Argon gefüllten Duranglaszyylinder durchgeführt. Zusätzlich stand ein Ofen und ein Cr/CrNi–Thermoelement für die Impedanzmessung bei unterschiedlichen Temperaturen zur Verfügung.

Die Verwendung von ionenblockierenden Elektroden bietet eine weitere Möglichkeit, elektrochemische Prozesse mit Hilfe des Nyquistplots und des entsprechenden Ersatzschaltbildes darzustellen (Abb. 2.3.4).

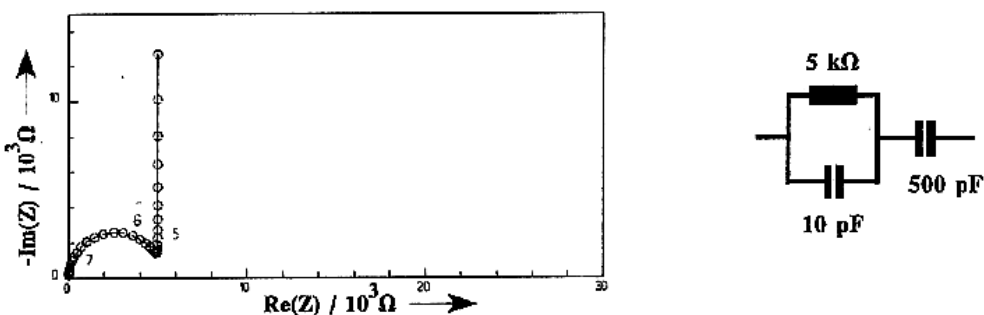


Abb. 2.3.4 Ersatzschaltbild für einen Festkörperelektrolyten zwischen zwei ionenblockierenden Elektroden (rechts) und der dazugehörige Nyquistplot (links) [30]

Bei Verwendung dieser Elektroden findet keine Entladung oder Reaktion an der Phasengrenze Elektrolyt/Elektrode statt. Dieses Ersatzschaltbild wird auch als Debye-Circuit bezeichnet. Hierbei verhält sich die Grenzschicht zwischen den Elektroden und dem Elektrolyten wie ein Doppelschicht-Kondensator C_{dl} , der parallel zum Elektrolytwiderstand liegt. Mit diesem ist noch zusätzlich ein Kondensator C_b in Reihe geschaltet, der von der Geometrie der Elektroden und der dielektrischen Zahl des Elektrolyten abhängt: $C_b = \epsilon \epsilon_0 A d^{-1}$ (ϵ = Dielektrizitätszahl, ϵ_0 = Dielektrizitätszahl im Vakuum, A = Fläche, d = Abstand der Platten). Die Dielektrizitätszahl erhöht demnach die Kapazität eines Kondensators, wobei allerdings entscheidend ist, dass keine Ionenwanderung stattfindet. Dieses ist nur dann möglich, wenn die Messung bei hoher Frequenz erfolgt, wodurch die Polarität des elektrischen Feldes schnell wechselt und sich daher die Ionen gar nicht oder nur sehr langsam bewegen [31].

Ein weiteres Beispiel für ionenblockierende Elektroden zeigt die Abbildung 2.3.5 mit zwei RC-Parallelschaltungen in Reihe und dem Nyquistplot mit einem grossen und einem kleinen Halbkreis. Dieser berücksichtigt die Beschaffenheit des Elektrolyten in Bezug auf seinen Korngrenzenwiderstand und seine Korngrenzenkapazität.

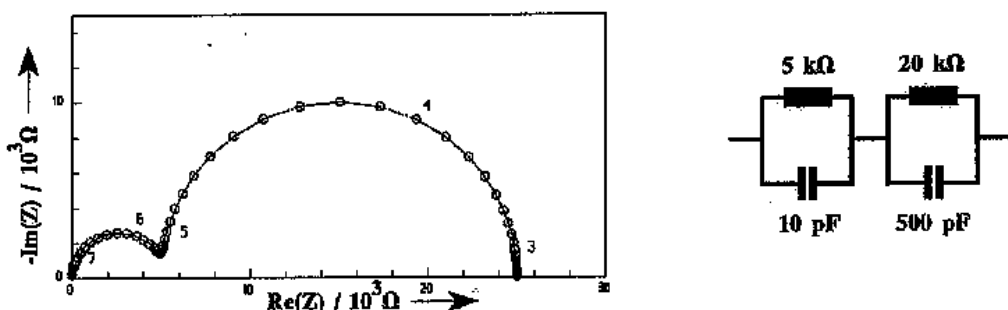


Abb. 2.3.5 Ersatzschaltbild für einen Festkörperelektrolyten zwischen zwei ionen-blockierenden Elektroden (rechts) und der dazu gehörige Nyquistplot (links) bei Korngrenzenwiderständen [30]

Die Vielfalt der Messungen zeigt das so genannte “Fünfkreis-Modell” (Abb. 2.3.6).

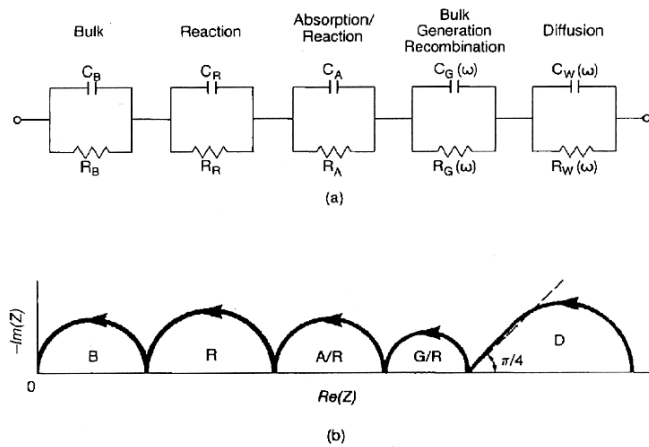


Abb. 2.3.6 Fünfkreis-Modell eines Festkörperelektrolyten: (a) Ersatzschaltung, (b) entsprechendes Impedanzdiagramm [30]

Dabei treten folgende elektrochemische Prozesse auf [30]:

- I. Ladungstrennung im Probenmaterial/Bulk, Leitfähigkeit der Probe (B)
- II. Ladungstransportreaktionen an den Korngrenzen (R)
- III. Absorptionsreaktion/Elektrodeneffekt (A/R)
- IV. Generation und Rekombination (G/R)
- V. Diffusion, Warburg-Impedanz (D)

3. Synthese und Struktur von Thioantimonaten

3.1 Synthese und Struktur von $(C_6N_3H_{17})Sb_6S_{10}$ und $(C_7N_2H_{13})_3Sb_9S_{15}$

Thioantimonate(III) mit gleichen stöchiometrischen Sb:S-Verhältnissen haben meistens unterschiedliche Kristallstrukturen. In die Reihe der Thioantimonate(III) mit dem Sb:S-Verhältnis von 1:1.667 ($[Sb_3S_5]^-$ [49-53], $[Sb_6S_{10}]^{2-}$ [54, 55] und $[Sb_{12}S_{20}]^{4-}$ [57]) gehören auch die beiden unter solvothermalen Bedingungen synthetisierten Verbindungen $(C_6N_3H_{17})Sb_6S_{10}$ (**I**) und $(C_7N_2H_{13})_3Sb_9S_{15}$ (**II**) [56], die in der monoklinen nicht-zentrosymmetrischen Raumgruppe $P2_1$ (**I**) und in der monoklinen zentrosymmetrischen Raumgruppe $P2_1/c$ (**II**) in Form roter Nadeln kristallisieren. Die Verbindungen $(C_6N_3H_{17})Sb_6S_{10}$ (**I**) und $(C_7N_2H_{13})_3Sb_9S_{15}$ (**II**) (dargestellt von R. Kiebach) wurden mit den Edukten Sb und S im Molverhältnis 1:3 in 5 mL AEP (1-(2-aminoethyl)-Piperazin) bzw. 2 mL DBN (1,5-diazabicyclo [4.3.0.]non-5-en) und 2 mL Wasser bei 170 °C (**I**) bzw. 160 °C (**II**) nach 7 Tagen erhalten. Die **optischen Bandlücken** von ca. 2 eV weisen darauf hin, dass es sich um Halbleiter handelt. Die **primären Baueinheiten** sind trigonale SbS_3 -Pyramiden und SbS_4 -Einheiten. Diese sind in Verbindung **I** zu sechsgliedrigen Sb_3S_3 -Ringen und Sb_3S_4 -Halbwürfeln verknüpft, die über gemeinsame S-Atome zu eindimensionalen $(Sb_6S_{10})^{2-}$ -**Kettenanionen** verbunden sind. Unter Berücksichtigung der längeren Sb-S-Bindungen über 3 Å wird ein **dreidimensionales Netzwerk** mit Käfigen ausgebildet, in denen die protonierten Amine eingeschlossen sind. In Verbindung **II** sind die SbS_4 -Einheiten zu einer zentralen Kette verknüpft, während die beiden anderen Ketten aus trigonalen SbS_3 -Pyramiden bestehen. Die einzelnen Ketten sind über gemeinsame Ecken zu einem eindimensionalen $(Sb_9S_{15})^{3-}$ -**Kettenanion** verknüpft. Dabei werden Sb_4S_4 -Ringe gebildet, die aneinander kondensiert sind. Unter Berücksichtigung der längeren Sb-S-Bindungen werden **Schichten** in der (100)-Ebene ausgebildet.

In den **Ramanspektren** werden Resonanzen zwischen 256 und 362 cm⁻¹ beobachtet, wobei die Banden zwischen 339 und 362 cm⁻¹ charakteristisch für SbS_3 -Einheiten sind. Banden um 280 und 318 cm⁻¹ (**I**) bzw. 289 und 315 cm⁻¹ (**II**) weisen auf SbS_x -Einheiten mit $x > 3$ hin [90, 91].

Die **thermische Zersetzung** von **I** beginnt bei ca. 238 °C und bei 245 °C für **II**, wobei der Massenabbau in einem (**I**) bzw. in zwei Schritten (**II**) erfolgt. Als Abbauprodukte konnten elementares Sb und Sb₂S₃ im Pulverdiffraktogramm identifiziert werden.

Two Novel Thioantimonates(III) with the Same Stoichiometric Sb:S Ratio but Different Crystal Structures: Solvothermal Synthesis, Crystal Structures, Thermal Stability and Spectroscopy of $(C_6N_3H_{17})Sb_6S_{10}$ and $(C_7N_2H_{13})_3Sb_9S_{15}$

Volker Spetzler, Ragnar Kiebach, Christian Näther, and Wolfgang Bensch*

Kiel, Institut für Anorganische Chemie der Christian-Albrechts Universität

Received Mai 28th, 2004.

Dedicated to Professor Martin Jansen on the Occasion of his 60th Birthday

Abstract. The two novel thioantimonates(III) $(C_6N_3H_{17}^{2+})Sb_6S_{10}$ (**I**) and $(C_7N_2H_{13}^{+})_3Sb_9S_{15}$ (**II**) were synthesized under solvothermal conditions reacting Sb and S with the amines 1-(2-aminoethyl)-piperazine ($C_6N_3H_{15}$) and 1,5-diazabicyclo[4.3.0]non-5-en (DBN, $C_7N_2H_{12}$), respectively. The compounds crystallize as red needles in the monoclinic non-centrosymmetric space group $P2_1$ (**I**) and in the monoclinic space group $P2_1/c$ (**II**) with lattice parameters $a = 6.120(4)$ Å, $b = 17.759(1)$ Å, $c = 11.478(7)$ Å, $\beta = 90.70(7)^\circ$ for **I** and $a = 10.2643(6)$ Å, $b = 23.648(2)$ Å, $c = 20.4655(11)$ Å, $\beta = 104.430(7)^\circ$ for **II**.

In both compounds the primary building units (PBUs) are trigonal Sb_3S_3 pyramids and Sb_4S_4 moieties. The interconnection of these PBUs leads to the formation of six-membered rings Sb_3S_3 and Sb_3S_4 semi-cubes in **I** which are joined via common S atoms to form the one-dimensional $[\![Sb_6S_{10}]^2]$ -anion being directed along [001]. Neighbored chains are arranged in a way that pockets are formed which host the organic cations. The ammonium groups of the organic molecules are oriented towards the anion ensuring optimal S···H bonding interactions. Taking into account the longer

Sb–S bonds above 3 Å a three-dimensional network is formed with large cages containing the organic cations. In compound **II** the Sb_3S_3 pyramids and the Sb_4S_4 units each form individual chains by vertex linking. The central chain is exclusively formed by Sb_4S_4 units whereas the other two chains are composed of Sb_3S_3 pyramids. The interconnection of the chains via common corners yields the one-dimensional $[\![Sb_9S_{15}]^3]$ -multiple chain anion. Due to the connection mode Sb_4S_4 rings are formed which are condensed along [001]. The chains are stacked along [100] with an inter-chain separation of about 7 Å. In the [010] direction the anions are lined-up with the shortest distance between neighbored anions of about 3.4 Å. With the long Sb–S distances layers within the (100) plane are formed. At elevated temperatures both compounds decompose via an internal redox reaction into Sb_2S_3 (Stibnite) and Sb. The optical band gaps of about 2 eV indicate that both compounds are semiconductors.

Keywords: Thioantimonates; Solvothermal synthesis; Crystal structure; Spectroscopy; Thermal investigation; Hybrid compounds

Zwei neue Thioantimonate(III) mit identischem stöchiometrischem Sb:S-Verhältnis aber unterschiedlichen Kristallstrukturen: Solvothermale Synthese, Kristallstrukturen, thermische Stabilität und optische Spektren von $(C_6N_3H_{17})Sb_6S_{10}$ und $(C_7N_2H_{13})_3Sb_9S_{15}$

Inhaltsübersicht. Die zwei neuen Thioantimonate(III) $(C_6N_3H_{17}^{2+})Sb_6S_{10}$ (**I**) und $(C_7N_2H_{13}^{+})_3Sb_9S_{15}$ (**II**) wurden unter solvothermalen Bedingungen bei der Reaktion von Antimon und Schwefel mit den Aminen 1-(2-aminoethyl)-Piperazin ($C_6N_3H_{15}$) (**I**) und 1,5-diazabicyclo[4.3.0]non-5-en (DBN, $C_7N_2H_{12}$) (**II**) erhalten. Die Verbindungen kristallisieren in Form roter Nadeln in der monoklinen nicht-zentrosymmetrischen Raumgruppe $P2_1$ (**I**) und in der monoklinen Raumgruppe $P2_1/c$ (**II**) mit den Gitterparametern $a = 6.120(4)$ Å, $b = 17.759(1)$ Å, $c = 11.478(7)$ Å, $\beta = 90.70(7)^\circ$ für **I** und $a = 10.2643(6)$ Å, $b = 23.648(2)$ Å, $c = 20.4655(11)$ Å, $\beta = 104.430(7)^\circ$ für **II**.

In beiden Verbindungen bilden trigonale Sb_3S_3 -Pyramiden und Sb_4S_4 -Einheiten die primären Baugruppen. In Verbindung **I** werden diese zu sechsgliedrigen Sb_3S_3 -Ringen und Sb_3S_4 -Halbwürfeln verknüpft, welche über gemeinsame S-Atome zu dem eindimensionalen $[\![Sb_6S_{10}]^2]$ -Kettenanion verbunden sind. Die Ketten verlaufen parallel zu [001] und benachbarte Ketten sind so angeordnet, dass Taschen gebildet werden, in welchen sich die organischen Kationen befinden. Die Ammoniumgruppen des Kations sind in Bezug auf das Anion so angeordnet, dass S···H-Bindungen gebildet werden

können. Werden bei der Strukturbeschreibung Sb–S-Kontakte länger als 3 Å berücksichtigt, dann kann ein dreidimensionales Netzwerk mit großen Käfigen identifiziert werden, in denen sich die organischen Kationen befinden. In Verbindung **II** bilden die Sb_3S_3 -Pyramiden und die Sb_4S_4 -Gruppen individuelle Ketten durch Eckverknüpfung. Die zentrale Kette wird ausschließlich von Sb_4S_4 -Einheiten gebildet, während zwei weitere Ketten nur Sb_3S_3 -Pyramiden enthalten. Die individuellen Ketten sind über gemeinsame Ecken zu dem eindimensionalen $[\![Sb_9S_{15}]^3]$ -Anion verknüpft. Durch den Verknüpfungsmodus werden Sb_4S_4 -Ringe gebildet, welche längs [001] aneinander kondensiert sind. Die Ketten sind entlang [100] gestapelt und der kürzeste Interkettenabstand beträgt etwa 7 Å. In der [010]-Richtung liegen die Ketten mit einem Abstand von etwa 3.4 Å nebeneinander. Unter Berücksichtigung der längeren Sb–S-Abstände werden Schichten in der (100)-Ebene ausgebildet. Bei erhöhten Temperaturen zersetzen sich die Verbindungen über eine interne Redoxreaktion zu Sb und Sb_2S_3 . Die optischen Bandlücken von ca. 2 eV weisen darauf hin, dass es sich bei den Verbindungen um Halbleiter handelt.

Two Novel Thioantimonates(III), $(C_6N_3H_{17})Sb_6S_{10}$ and $(C_7N_2H_{13})_3Sb_9S_{15}$

1 Introduction

A detailed analysis of the structures of thioantimonate(III) compounds reveals some remarkable and unique features. Starting with the most dense antimony sulfide Sb_2S_3 all negatively charged Sb–S compounds must have a Sb : S ratio which is larger than 1 : 1.5. In addition, for an identical Sb:S ratio different chemical compositions are observed, and examples are thioantimonates(III) with Sb : S ratios of 1 : 1.75 ($[Sb_4S_7]^{2-}$) [1–9], $[Sb_{12}S_{21}]^{6-}$ [10], 1:2 ($[Sb_2S_2]^-$) [11, 12], $[Sb_2S_4]^{2-}$ [13], $[Sb_3S_6]^{3-}$ [14], $[Sb_4S_8]^{4-}$ [15], $[Sb_4S_8]^{4-}$ [16]), 1 : 1.67 ($[Sb_3S_5]^-$) [17–21], $[Sb_6S_{10}]^{2-}$ [22, 23], $[Sb_{12}S_{20}]^{4-}$ [24]), or 1 : 1.8 ($[Sb_5S_9]^{3-}$) [25], $[Sb_{10}S_{18}]^{6-}$ [26]). Furthermore, for a given composition different connectivities of the primary Sb_3S_3 and Sb_2S_4 building units and different dimensionalities of the thioantimonate(III) anions are observed. The dimensionality of a given thioantimonate(III) anion is mainly determined by the size of the counter cation. Hence, the cation supplied during the syntheses has a structure directing effect. This can be demonstrated on the series of compounds containing the $[Sb_4S_7]^{2-}$ anion [1–9]. Only $K_2Sb_4S_7$ shows a three-dimensional interconnected $[Sb_4S_7]^{2-}$ anion [1] and with increasing size of the cation the dimensionality is reduced to two-dimensional layers [3, 5, 6, 7, 8] and finally to one-dimensional chains [2, 4, 9]. Another example are compounds with a Sb:S ratio of 1:1.67. Five different thioantimonates(III) were reported with the $[Sb_3S_5]^-$ anion [17–21], two with the $[Sb_6S_{10}]^{2-}$ anion [22, 23] and one with the $[Sb_{12}S_{20}]^{4-}$ anion [24]. In the compound $[C_6H_{15}N_2][Sb_3S_5]$ the anions form layers with Sb_2S_2 , Sb_4S_4 and Sb_5S_5 rings as the secondary building units [21]. A very different type of an one-dimensional chain is observed in $[N(C_3H_7)_4][Sb_3S_5]$ [19] and in $[Ph_4P_2][Sb_6S_{10}]$ [22]. In both compounds the Sb_3S_3 pyramids joined to form Sb_5S_5 rings which are condensed yielding the chain anions. In $RbSb_3S_5 \cdot H_2O$ small Sb_2S_2 and large $Sb_{12}S_{12}$ heterorings are joined to form a two atoms thick layered anion [18]. Finally, a complex three-dimensional network is formed in $TlSb_3S_5$ [20]. The topology of the anion in $[M(C_6H_{13}N_3)_2]Sb_6S_{10} \cdot 0.5 H_2O$ ($M = Fe, Ni$) [23] is complex and may be shortly described as chains built up by the interconnection of $-Sb_4S_4-Sb_3S_3-Sb_4S_4-$ units. These chains are then further joined into the final layered anion via common corners and edges. The largest ring contains 32 atoms ($Sb_{16}S_{16}$) [23]. The one-dimensional $[Sb_{12}S_{20}]^{4-}$ chain anion in $((MA)_{1.03}K_{2.97})[Sb_{12}S_{20}] \cdot 1.34 H_2O$ is two atoms thick. A central Sb_4S_4 ring is bound to 6 Sb_3S_3 units forming the next hierarchical building block. These blocks are joined via S atoms and larger Sb_8S_8 heterorings are formed [24]. The description of the struc-

tures presented above base on a cut-off for the Sb–S distances of about 3 Å. But the assignment of the dimensionality is arbitrary in thioantimonates(III) because Sb–S distances scatter in the large range between 2.2 and 3.9 Å. Therefore, the description of the structures of thioantimonates(III) and the final assignment of the dimensionality is not straight forward.

During our continuing efforts to synthesize new thioantimonates(III) we prepared the two new compounds $(C_6N_3H_{17}^{2+})Sb_6S_{10}$ and $(C_7N_2H_{13}^+)_3Sb_9S_{15}$. In the present contribution we report on the syntheses, crystal structures, thermal stability and optical properties of these new thioantimonates(III).

2 Experimental details

Syntheses

The compounds $(C_6N_3H_{17}^{2+})Sb_6S_{10}$ (I) and $(C_7N_2H_{13}^+)_3Sb_9S_{15}$ (II) were prepared under solvothermal conditions in a Teflon-lined steel autoclave. A mixture of Sb (1 mmol), S (3 mmol) and 5 ml 1-(2-aminoethyl)-piperazine respectively 2 ml DBN (1,5-diazabicyclo [4.3.0]non-5-en) diluted with 2 ml water were heated at 170 °C (I) or 160 °C (II) for 7 days followed by cooling to room temperature. The products were collected by filtration and washed with deionised water and acetone. The yields of the products were about 95% based on Sb. The compounds consist of red needle-like crystals (see Fig. 1). Elemental analysis I: found: C 6.0, H 1.4, N 3.5%; calc.: C 5.5, H 1.2, N 3.4%; II: found: C 13.3, H 2.1, N 4.7; calc.: C 12.9, H 2.1, N 4.6%. We also prepared compound I under the same experimental conditions with a mixture of Cu (2 mmol), Sb (2 mmol), S (5 mmol) and 5 ml 1-(2-aminoethyl)-piperazine yielding only 30% based on Sb. In the X-ray powder pattern of this product $CuSb_2S_2$ could be identified as the second product.

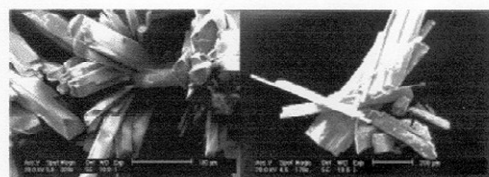


Fig. 1 SEM micrographs of the needle-like crystals of $(C_6N_3H_{17}^{2+})Sb_6S_{10}$ (I) (left) and $(C_7N_2H_{13}^+)_3Sb_9S_{15}$ (II) (right).

X-Ray scattering studies

The X-ray intensity data of single crystals of I and II were collected at 293 K using a STOE AED 4 diffractometer with graphite monochromated MoK_α radiation ($\lambda = 0.71073$ Å). The raw intensities were treated in the usual way applying a Lorentz, polarization as well as an absorption correction. The structures were solved using SHELXS-97 [27]. Crystal structure refinements were done against F^2 with SHELXL 97 [28]. All non-hydrogen atoms in compound II except those which are disordered were refined with anisotropic displacement parameters. The hydrogen atoms in compound I were positioned with idealized geometry and refined with fixed isotropic

* Prof. Dr. W. Bensch
Institut für Anorganische Chemie der Universität Kiel
Olshausenstr. 40
D-24098 Kiel
Fax: +49 (0)431/880-1520
e-mail: wbensch@ac.uni-kiel.de

V. Spetzler, R. Kiebach, C. Näther, W. Bensch

Table 1 Details of the data collections and selected refinement results for $(C_6N_3H_{17}^{2+})Sb_6S_{10}$ (**I**) and $(C_7N_2H_{13}^+)_3Sb_9S_{15}$ (**II**).

	I	II
<i>a</i> / Å	6.120(4)	10.2634(6)
<i>b</i> / Å	17.759(1)	23.648(2)
<i>c</i> / Å	11.478(7)	20.4655(11)
β / °	90.70(7)	102.430(7)
<i>V</i> / Å ³	1247.4(1)	4858.2(5)
<i>Z</i>	2	4
μ / mm ⁻¹	7.25	5.48
MW / g·mol ⁻¹	1128.33	1872.08
Space group	P2 ₁	P2 ₁ /c
ρ_{calc} / g·cm ⁻³	3.148	2.560
2θ range / °	4–56	4–53
Data collected	12066	42188
R_{int}	0.0370	0.0310
unique data	5770	10341
Data $F_0 > 4\sigma(F_0)$	5465	7063
parameters	228	461
R_1 for $F_0 > 4\sigma(F_0)$	0.0322	0.0341
wR2 all reflections	0.0810	0.0880
wR2 for $F_0 > 4\sigma(F_0)$	0.0789	0.0784
$\delta F/(e\text{\AA}^3)$	1.25/-1.31	0.85/-1.28

displacement parameters using a riding model. The absolute structure of compound **I** was determined and is in agreement with the selected setting (Flack-x parameter: 0.03(3)). In addition, refinement of the inverse structure leads to significant poorer reliability factors. Because compound **I** was additionally merohedrally twinned a twin refinement was performed using the twin option in SHELXL-97 leading to significant better reliability factors (BASF parameter: 0.02626). In compound **II** several atoms of the organic cations are disordered and were refined using a split model and isotropic displacement parameters. Details of the data collections and refinement results are summarized in Table 1. Bond lengths and angles for the two compounds are listed in Table 2 and 5. Crystallographic data (excluding structure factors) for the structures reported in this paper have been deposited with the Cambridge Crystallographic Data Centre as supplementary publication no. CCDC 240308 for **I** and CCDC 240309 for **II**. Copies of the data can be obtained, free of charge, on application to CCDC, 12 Union Road, Cambridge CB2 1EZ, UK. (fax: +44-(0)1223-336033 or email: deposit@ccdc.cam.ac.uk).

Spectroscopy

The Raman spectra were measured from 100 to 500 cm⁻¹ with a Bruker IFS 66 Fourier transform Raman spectrometer (wavelength: 514.5 nm, T = 20 K).

Thermoanalytical investigations

Thermogravimetry analyses were performed using a Netzsch STA 429 DTA-TG device. The samples were heated in Al₂O₃ crucibles at a rate of 4 K·min⁻¹ to 400 °C under a flow of argon of 100 ml min⁻¹.

3 Results and Discussion

The new compound $(C_6N_3H_{17}^{2+})Sb_6S_{10}$ (**I**) crystallizes as red needles (Fig. 1 left) in the monoclinic non-centrosymmetric space group P2₁ with two formula units. In the fol-

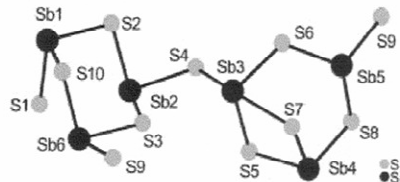


Fig. 2 Interconnection of the primary building units in $(C_6N_3H_{17}^{2+})Sb_6S_{10}$ (**I**) together with labelling.

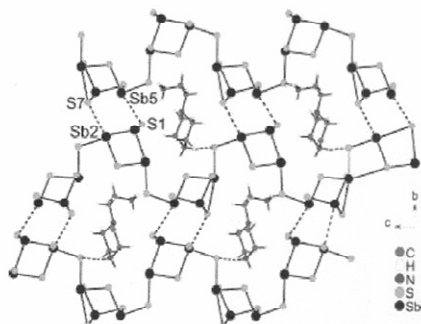


Fig. 3 Interconnection of the $\frac{1}{2}[Sb_6S_{10}]^{2-}$ chains which are directed along [001] via the long Sb–S bonds (dotted lines) forming a three-dimensional network with large cages accommodating the organic cations in $(C_6N_3H_{17}^{2+})Sb_6S_{10}$ (**I**) (The S···H bonds are indicated as dotted lines).

lowing the description of the structure base on a cut-off for the Sb–S distances of about 3.0 Å. Five of the six unique Sb atoms have bonds to 3 S atoms forming the well established trigonal SbS₃ pyramids and one Sb atom is bound to 4 S atoms yielding a SbS₄ unit (Fig. 2). These units may be called the primary building units (PBUs). Two different secondary building units (SBUs) are generated by the interconnection of the PBUs. A six-membered Sb₃S₃ ring is formed by three SbS₃ pyramids (Sb(1,2,6)), and a SbS₄ semi-cube is constructed by two SbS₃ groups and the SbS₄ unit (Sb(3,4,5)) (Fig. 2). In the semi-cube the Sb(3)S₄ and Sb(4)S₃ units are joined by a common edge whereas all other PBUs share common corners. The Sb₃S₃ rings and the Sb₃S₄ semi-cubes are joined by common S atoms to form the one-dimensional $\frac{1}{2}[Sb_6S_{10}]^{2-}$ chain anion which is directed along [001] (Fig. 3). The Sb–S bond lengths vary between 2.379(3) Å and 2.985(2) Å and S–Sb–S angles range from 84.92(6)° to 110.11(7)° (Table 2). We note that the long Sb(3)–S(7) distance is in *trans* position to the shorter Sb(3)–S(4) bond of 2.522(2) Å. All structural parameters are typical for the well known trigonal pyramidal SbS₃ unit and the SbS₄ moiety. All Sb atoms except the atom Sb(1) enhance their coordination spheres with S atoms at distances up to 3.8 Å (Table 3). The resulting polyhedra may be described as distorted SbS₆ octahedra (Sb(2,3,5,6)) and as a distorted SbS₅ rectangular pyramid (Sb(4)).

Two Novel Thioantimonates(III), $(C_6N_3H_{17})^2Sb_6S_{10}$ and $(C_7N_2H_{13})_3Sb_9S_{15}$ **Table 2** Selected interatomic distances/ \AA and angles/ $^\circ$ in the compound $(C_6N_3H_{17})^2Sb_6S_{10}$ (**I**). Estimated standard deviations are given in parentheses.

Sb(1)–S(1)	2.379(3)	Sb(4)–S(7)	2.393(2)
Sb(1)–S(2)	2.450(2)	Sb(4)–S(8)	2.470(2)
Sb(1)–S(10) ^[a]	2.512(2)	Sb(4)–S(5)	2.487(2)
Sb(2)–S(4)	2.457(2)	Sb(5)–S(8)	2.453(2)
Sb(2)–S(2)	2.476(2)	Sb(5)–S(6)	2.499(2)
Sb(2)–S(3)	2.510(2)	Sb(5)–S(9)	2.521(2)
Sb(3)–S(5)	2.452(2)	Sb(6)–S(10)	2.469(2)
Sb(3)–S(6)	2.488(2)	Sb(6)–S(9) ^[b]	2.512(2)
Sb(3)–S(4)	2.522(2)	Sb(6)–S(3) ^[b]	2.448(2)
Sb(3)–S(7)	2.985(2)		
S(1)–Sb(1)–S(2)	99.62(8)	S(8)–Sb(5)–S(9)	93.80(7)
S(1)–Sb(1)–S(10) ^[a]	93.54(8)	S(6)–Sb(5)–S(9)	92.34(6)
S(2)–Sb(1)–S(10)	100.22(8)	S(3)–Sb(6)–S(10)	98.18(8)
S(4)–Sb(2)–S(2)	90.72(8)	S(3)–Sb(6)–S(9) ^[b]	85.60(7)
S(4)–Sb(2)–S(3)	93.76(7)	S(10)–Sb(6)–S(9)	93.93(7)
S(2)–Sb(2)–S(3)	96.26(8)	Sb(1)–S(2)–Sb(2)	98.65(8)
S(4)–Sb(3)–S(7)	163.55(7)	Sb(6)–S(3)–Sb(2)	104.24(8)
S(5)–Sb(3)–S(6)	100.93(7)	Sb(2)–S(4)–Sb(3)	107.83(7)
S(5)–Sb(3)–S(4)	87.81(7)	Sb(3)–S(5)–Sb(4)	98.02(7)
S(6)–Sb(3)–S(4)	84.92(6)	Sb(3)–S(6)–Sb(5)	108.86(7)
S(7)–Sb(4)–S(8)	97.36(7)	Sb(3)–S(7)–Sb(4)	87.07(6)
S(7)–Sb(3)–S(6)	87.27(6)	Sb(5)–S(8)–Sb(4)	96.22(7)
S(7)–Sb(3)–S(5)	79.48(7)	Sb(6)–S(9)–Sb(5)	110.11(7)
S(7)–Sb(3)–S(6)	100.93(7)	Sb(6)–S(10)–Sb(1)	96.98(8)
S(7)–Sb(4)–S(5)	91.63(7)		
S(8)–Sb(4)–S(5)	98.13(8)		
S(8)–Sb(5)–S(6)	92.94(8)		

Symmetry codes: ^[a] x, y, -1+z; ^[b] x, y, 1+z;**Table 3** Long Sb–S distances/ \AA in $(C_6N_3H_{17})^2Sb_6S_{10}$ (**I**). Estimated standard deviations are given in parentheses.

Sb(2)–S(1)	3.262(3)	Sb(2)–S(2) ^[c]	3.654(3)
Sb(2)–S(7) ^[d]	3.167(2)	Sb(3)–S(3) ^[d]	3.396(3)
Sb(3)–S(5) ^[d]	3.694(3)	Sb(4)–S(2) ^[c]	3.524(3)
Sb(4)–S(6) ^[d]	3.557(3)	Sb(5)–S(7)	3.046(3)
Sb(6)–S(10)	3.670(3)		

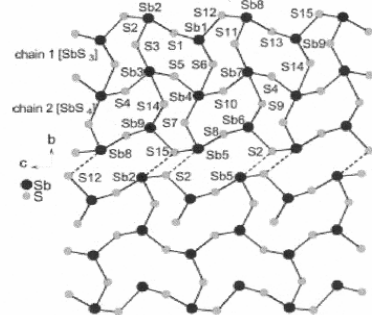
Symmetry codes: ^[c] 1+x, y, z; ^[d] -x, 0.5+y, 1-z; ^[e] -1+x, y, z;**Table 4** Intermolecular N–H···S contacts and angles/ \AA , $^\circ$ for $(C_6N_3H_{17})^2Sb_6S_{10}$ (**I**).

D–H	d(H···A)	<DHA	A
N2–H2C	2.483	152.92	S4
N2–H2C	2.752	120.72	S5
N3–H3C	2.454	157.11	S9 ^[a]
N3–H3D	2.891	141.46	S1 ^[a]
N3–H3E	2.545	156.47	S9 ^[b]
N3–H3E	2.954	119.42	S10 ^[b]

Symmetry codes: ^[a] 1-x, 0.5+y, 2-z; ^[b] 1+x, y, 1+z, ^[b] -x, y+0.5, -z+2; ^[b] -x, y+0.5, -z+2;

Along [010] neighbored chains are arranged in a way that pockets are formed which host the organic cations (Fig. 3). The cations are oriented towards the thioantimonate(III) anion in a way that optimal S···H bonding interactions are achieved. The H···S distances range from 2.454 \AA to 2.954 \AA with corresponding N–H···S angles between 119.42° and 157.11° (Table 4).

The shortest inter-chain Sb–S distances are 3.167(2) \AA along [010] and 3.558(2) \AA along [100]. Taking these Sb–S

**Fig. 4** The interconnection of the primary Sb_3S and Sb_4 units in $(C_7N_2H_{13}^+)_3Sb_9S_{15}$ (**II**) forming the $[\frac{1}{2}[Sb_9S_{15}]^{3-}]$ chains which are joined into layers via the long Sb–S bonds (dotted lines) together with atom labelling. The individual chains composed of Sb_3S pyramids and Sb_4S groups are denoted as chain 1 and 2.

contacts into account a three-dimensional network is formed with large cages accommodating the organic cations (Fig. 3). The cages are interconnected along [100] forming ellipsoidal tunnels with dimensions of about 7.1 · 7.6 \AA (measured from coordinate to coordinate). The opening of the cages consist of a puckered Sb_6S_6 heteroring.

The second new compound $(C_7N_2H_{13}^+)_3Sb_9S_{15}$ (**II**) crystallizes also as red needles (Fig. 1 right) in the monoclinic space group $P2_1/c$ with four formula units in the unit cell. All atoms are on general positions. Six Sb atoms (Sb(1, 2, 5, 6, 8, 9)) have bonds to three S atoms yielding the trigonal Sb_3S pyramids whereas the remaining Sb atoms form Sb_4S moieties (Fig. 4). In the $[Sb_9S_{15}]^{3-}$ anion individual chains may be identified that are formed by the interconnection of the PBUs. One chain is composed of the six alternating Sb_3S pyramids by vertex linkage (in Fig. 4 denoted as chain 1) and the second one is formed by corner sharing of the Sb_4S units (in Fig. 4 denoted as chain 2). Another chain is generated from the former chain by the n-glide plane. The two chains composed by the Sb_3S pyramids form the exterior of the $[Sb_9S_{15}]^{3-}$ ion and in the central part of the anion is located the chain which is constructed by the Sb_4S units (Sb(3,4,7)). The central chain is joined to the two other chains via common corners thus yielding the final $[\frac{1}{2}[Sb_9S_{15}]^{3-}]$ anion. The connection mode leads to the formation of Sb_4S_4 rings which are condensed along [001] (Fig. 4). The width of the thioantimonate(III) anion is determined by two Sb_4S_4 rings. The chains are stacked along [100] with an inter-chain separation of about 7 \AA . In the [010] direction the anions are lined-up with the shortest distance between neighbored anions of about 3.4 \AA (Fig. 5). The Sb–S bond lengths scatter over a large range from 2.372(2) to 2.943(2) \AA (Table 5). The long Sb–S distances are always found in the Sb_4S units and they are always located in *trans* position to a shorter Sb–S bond. The

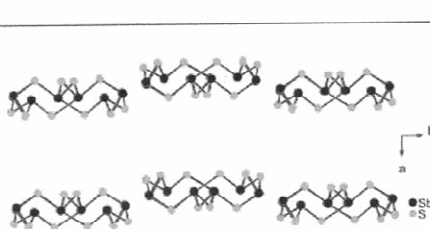


Fig. 5 Arrangement of the $[Sb_9S_{15}]^{3-}$ anion in $(C_7N_2H_{13}^+)_3Sb_9S_{15}$ (II) showing the large inter-chain separation along [100].

Table 5 Selected interatomic distances/ \AA and angles/ $^\circ$ in the compound $(C_7N_2H_{13}^+)_3Sb_9S_{15}$ (II). Estimated standard deviations are given in parentheses.

Sb(1)-S(1)	2.496(2)	Sb(1)-S(6)	2.381(2)
Sb(1)-S(12)	2.530(2)	Sb(2)-S(1)	2.470(2)
Sb(2)-S(2)	2.451(2)	Sb(2)-S(3)	2.423(2)
Sb(3)-S(3)	2.584(2)	Sb(3)-S(4)	2.456(2)
Sb(3)-S(5)	2.522(2)	Sb(4)-S(5)	2.458(2)
Sb(4)-S(6)	2.885(2)	Sb(4)-S(7)	2.641(2)
Sb(4)-S(10)	2.525(2)	Sb(5)-S(7)	2.419(2)
Sb(5)-S(8)	2.474(3)	Sb(5)-S(15)	2.445(2)
Sb(6)-S(2)	2.542(2)	Sb(6)-S(8)	2.494(2)
Sb(6)-S(9)	2.379(2)	Sb(7)-S(4) ^[a]	2.511(2)
Sb(7)-S(9)	2.855(2)	Sb(7)-S(10)	2.460(2)
Sb(7)-S(11)	2.655(2)	Sb(8)-S(11)	2.412(2)
Sb(8)-S(12)	2.451(2)	Sb(8)-S(13)	2.480(2)
Sb(9)-S(13)	2.497(2)	Sb(9)-S(14)	2.372(2)
Sb(9)-S(15)	2.544(2)	Sb(3)-S(14)	2.943(2)
S(6)-Sb(1)-S(1)	92.80(5)	S(6)-Sb(1)-S(12)	97.33(5)
S(1)-Sb(1)-S(12)	92.59(5)	S(3)-Sb(2)-S(2)	99.95(5)
S(3)-Sb(2)-S(1)	98.52(5)	S(2)-Sb(2)-S(1)	95.59(5)
S(3)-Sb(3)-S(14) ^[b]	174.75(5)	S(4)-Sb(3)-S(14) ^[b]	88.07(4)
S(4)-Sb(3)-S(5)	92.41(4)	S(4)-Sb(3)-S(3)	88.62(5)
S(5)-Sb(3)-S(3)	86.80(4)	S(5)-Sb(4)-S(10)	92.45(4)
S(5)-Sb(3)-S(14) ^[b]	90.08(4)	S(5)-Sb(4)-S(7)	88.07(4)
S(10)-Sb(4)-S(7)	87.15(4)	S(5)-Sb(4)-S(6)	87.80(4)
S(10)-Sb(4)-S(6)	89.80(4)	S(7)-Sb(4)-S(6)	174.76(4)
S(7)-Sb(5)-S(15) ^[a]	101.52(4)	S(7)-Sb(5)-S(8)	99.40(4)
S(15)-Sb(5)-S(8)	94.88(4)	S(9)-Sb(6)-S(8)	92.76(4)
S(9)-Sb(6)-S(2) ^[a]	95.16(5)	S(8)-Sb(6)-S(2) ^[a]	94.50(4)
S(10)-Sb(7)-S(4) ^[a]	91.49(4)	S(10)-Sb(7)-S(11)	89.10(5)
S(4) ^[a] -Sb(7)-S(11)	85.57(4)	S(10)-Sb(7)-S(9)	88.07(4)
S(4) ^[a] -Sb(7)-S(9)	90.08(4)	S(11)-Sb(7)-S(9)	174.75(4)
S(11)-Sb(8)-S(12)	100.91(5)	S(11)-Sb(8)-S(13)	99.88(4)
S(12)-Sb(8)-S(13)	96.29(5)	S(14)-Sb(9)-S(13)	93.07(5)
S(14)-Sb(9)-S(15)	98.20(4)	S(13)-Sb(9)-S(11)	94.07(4)
Sb(2)-S(1)-Sb(1)	100.62(5)	Sb(2)-S(2)-Sb(6) ^[a]	98.40(5)
Sb(2)-S(3)-Sb(3)	103.71(5)	Sb(3)-S(4)-Sb(7) ^[a]	100.68(5)
Sb(4)-S(5)-Sb(3)	101.52(4)	Sb(1)-S(6)-Sb(4)	101.94(4)
Sb(5)-S(7)-Sb(4)	103.30(4)	Sb(5)-S(8)-Sb(6)	100.01(5)
Sb(6)-S(9)-Sb(7)	103.23(4)	Sb(7)-S(10)-Sb(4)	101.60(5)
Sb(8)-S(11)-Sb(7)	105.09(5)	Sb(8)-S(12)-Sb(1)	98.71(5)
Sb(8)-S(13)-Sb(9)	97.75(5)	Sb(9)-S(14) ^[b] -Sb(3)	103.23(4)
Sb(9)-S(15)-Sb(5) ^[a]	99.27(4)		

Symmetry codes: ^[a] x, 0.5-y, -0.5+z; ^[b] x, 0.5-y, 0.5+z;

S-Sb-S angles between 86.80(4) $^\circ$ and 174.76(4) $^\circ$ are also distributed over a large range (Table 5). We note that both Sb-S bond lengths and the S-Sb-S angles are in the range observed in many other thioantimonates(III).

The Sb atoms enhance their coordination by S atoms located at longer distances (Table 6). The atoms Sb(2,5,8) have coordination numbers CN 4, Sb(1,6,9) CN = 5 and all Sb atoms of the SbS₄ units have CN = 6 forming distorted octahedra. Hence, the central part of the anion may be

V. Spetzler, R. Kiebach, C. Näther, W. Bensch

Sb(1)-S(5)	3.301(9)	Sb(1)-S(11)	3.346(6)
Sb(2)-S(15)	3.42(2) ^[c]	Sb(3)-S(1)	3.476(5)
Sb(3)-S(9)	3.153(8) ^[d]	Sb(4)-S(8)	3.493(5)
Sb(4)-S(14)	3.196(8) ^[d]	Sb(5)-S(2)	3.42(2) ^[d]
Sb(6)-S(3)	3.259(9) ^[c]	Sb(6)-S(10)	3.381(5)
Sb(7)-S(11)	3.611(5)	Sb(7)-S(6)	3.189(8)
Sb(8)-S(12)	3.50(2)	Sb(9)-S(4)	3.436(2) ^[d]
Sb(9)-S(7)	3.307(9)		

Symmetry codes: ^[c] 1-x, 1-y, 1-z; ^[d] x, 0.5-y, 0.5+z; ^[e] x, 0.5-y, 0.5+z; ^[f] 1-x, -0.5+y, 1.5-z

viewed as a chain of edge sharing SbS₆ octahedra. Whereas most of the long Sb-S contacts are within the thioantimonate(III) anion the atoms Sb(1,2,5,9) have such bonds to S atoms of neighbored chains. Considering the longer Sb-S distances as weak interactions the chains are interconnected into layers extending within the (100) plane (Fig. 5). The layers are separated by the organic amine cations and a sandwich-like arrangement of anions and cations is observed.

Optical spectroscopy

Charge compensation in the two compounds requires that the amine molecules are protonated. In I the H atoms could be located in the difference Fourier map. In the IR spectra the absorptions located at 1500, 2000, 2500 and 3500 cm⁻¹ are typical for R-NH₃ groups in I while II shows intensive bands of absorption at 1500, 1650, 2400 and 3200 cm⁻¹. In the Raman spectra (Fig. 6) a large number of intense bands are seen. The most intense resonances are located at 281.1 cm⁻¹, 292.9 cm⁻¹, 304.5 cm⁻¹, 318.5 cm⁻¹, 336.2 cm⁻¹, 348.9 cm⁻¹ (I) and 263.3 cm⁻¹, 289.3 cm⁻¹, 315.3 cm⁻¹, 340.3 cm⁻¹ and 361.1 cm⁻¹ (II). The bands between 362 cm⁻¹ and 339 cm⁻¹ are typical for SbS₃ units [29, 30]. We note that for the copper(I)-thioantimonates(III) the bands are observed at lower wave numbers, i.e. at 337 cm⁻¹ [31]. The strong absorptions at 281.3 cm⁻¹ and

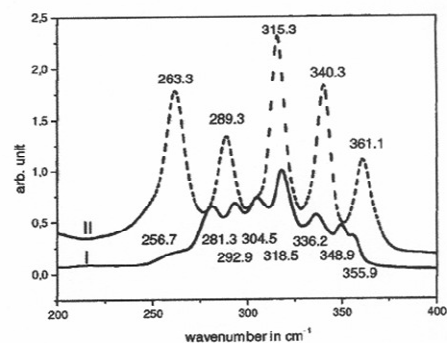


Fig. 6 Raman spectra of $(C_6N_3H_{17}^{2+})Sb_6S_{10}$ (I) (solid line) and $(C_7N_2H_{13}^+)_3Sb_9S_{15}$ (II) (dotted line).

Two Novel Thioantimonates(III), $(C_6N_3H_{17})_3Sb_6S_{10}$ and $(C_7N_2H_{13})_3Sb_9S_{15}$

318.5 cm^{-1} (**I**) respectively 289.3 cm^{-1} and 315.3 cm^{-1} (**II**) may be due to the SbS_x units with $x > 3$ [29]. Pfitzner et al. reported that a decrease of the bonding interactions between Sb and S atoms leads to a strong shift to lower wave numbers and the bands at 321 cm^{-1} and about 290 cm^{-1} are explained with SbS_5 units [29, 30]. In $MnSb_2S_4$ the resonances are at even lower wave numbers of 300 and 283 cm^{-1} which is due to the high coordination number of the Sb atoms [30].

UV-Vis diffuse reflectance measurements allowed the determination of the optical band gaps of the two compounds. For both thioantimonates E_g is about 2 eV demonstrating the semiconducting nature.

Thermal Investigations

The DTA-TG-DTG curves for compounds **I** and **II** are shown in Fig. 7. Compound (**I**) decomposes in one step ($T_{\text{onset}} = 238\text{ }^\circ\text{C}$) which is accompanied by an endothermic signal and a mass loss of 12.5% . The expected value for the emission of the organic ligand is 13.4% . The removal of the DBN molecule in (**II**) proceeds in two steps with two endothermic events at $T_p = 266\text{ }^\circ\text{C}$ and $T_p = 301\text{ }^\circ\text{C}$. The decomposition of this compound starts at a temperature $T_{\text{onset}} = 245\text{ }^\circ\text{C}$ and the total mass loss amounts to 20.1% .

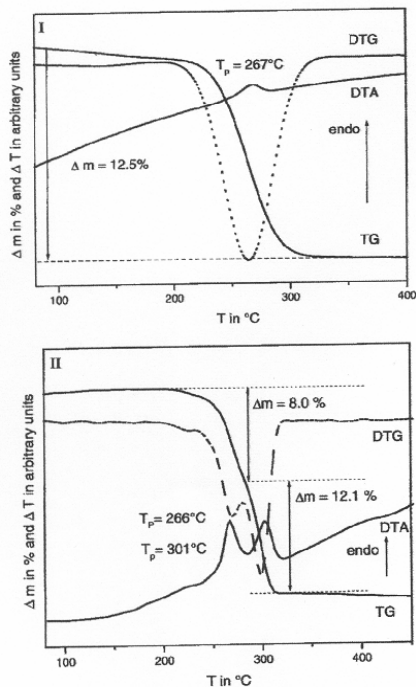


Fig. 7 DTA-TG-DTG curves for $(C_6N_3H_{17})_3Sb_6S_{10}$ (**I**) (top) and $(C_7N_2H_{13})_3Sb_9S_{15}$ (**II**) (bottom).

which is in good agreement with the emission of the organic part of the compound (calculated: 19.2%). The elemental analysis of the gray residues indicates only $0.13\% \text{ C}$ for **I** and $0.238\% \text{ N}$, $0.035\% \text{ H}$ and $0.795\% \text{ C}$ for **II**. In the X-ray powder pattern of the residues Stibnit Sb_2S_3 and Sb could be identified. The occurrence of elemental Sb suggests that a redox reaction takes place during the thermal reaction and due to the Sb:S ratio of the starting material it must be assumed that also sulfur is emitted.

Summary

We noted in the introduction that several structures of thioantimonates(III) were reported in the past which have an identical Sb : S ratio but a different network topology. The two new compounds belong to the group of thioantimonates(III) with a Sb:S ratio of $1:1.67$. The network topology of the anion in $(C_6N_3H_{17})_3Sb_6S_{10}$ (**I**) is different to all other compounds containing the $[Sb_6S_{10}]^{2-}$ anion. With the second new compound $(C_7N_2H_{13})_3Sb_9S_{15}$ (**II**) the series of thioantimonates(III) with the Sb:S ratio of $1:1.67$ covers now four different anions, i.e. $[Sb_3S_5]^{3-}$, $[Sb_6S_{10}]^{2-}$, $[Sb_9S_{15}]^{3-}$, and $[Sb_{12}S_{20}]^{4-}$. Using other amines in the syntheses it should be possible to synthesize other thioantimonates(III) with the Sb:S ratio of $1:1.67$. For a better understanding of the relation between the network topology, the dimensionality and the size, charge and shape of the structure directing organic molecule more compounds must be prepared.

Acknowledgements. The financial support by the State of Schleswig-Holstein and the Deutsche Forschungsgemeinschaft (DFG) is gratefully acknowledged.

References

- [1] H. A. Graf, H. Schäfer, *Z. Naturforsch.* **1972**, *27b*, 735.
- [2] G. Dittmar, H. Schäfer, *Z. Anorg. Allg. Chem.* **1977**, *437*, 183.
- [3] G. Dittmar, H. Schäfer, *Z. Anorg. Allg. Chem.* **1978**, *441*, 93.
- [4] G. Dittmar, H. Schäfer, *Z. Anorg. Allg. Chem.* **1978**, *441*, 98.
- [5] B. Eisenmann, H. Schäfer, *Z. Naturforsch.* **1979**, *34b*, 383.
- [6] G. Cordier, H. Schäfer, C. Schwidetzky, *Z. Naturforsch.* **1984**, *39b*, 131.
- [7] W. Bensch, M. Schur, *Z. Naturforsch.*, **1997** *52b*, 405.
- [8] W. S. Sheldrick, H.-J. Häusler, *Z. Anorg. Allg. Chem.* **1988**, *557*, 105.
- [9] M. Schur, W. Bensch, *Eur. J. Solid State Inorg. Chem.* **1997**, *34*, 457.
- [10] R. Stähler, C. Näther, W. Bensch, *J. Solid State Chem.* **2003**, *174*, 264.
- [11] K. Volk, P. Bickert, R. Kolmer, H. Schäfer, *Z. Naturforsch.* **1979**, *34b*, 380.
- [12] H. A. Graf, H. Schäfer, *Z. Anorg. Allg. Chem.* **1975**, *414*, 211.
- [13] G. Cordier, C. Schwidetzky, H. Schäfer, *J. Solid State Chem.* **1984**, *54*, 84.
- [14] R. Kiebach, F. Studt, C. Näther, W. Bensch, *Eur. J. Inorg. Chem.* **2004**, 2553.
- [15] T. J. McCarthy, M. G. Kanatzidis, *Inorg. Chem.* **1994**, *33*, 1205.
- [16] W. Bensch, C. Näther, R. Stähler, *Chem. Commun.* **2001**, 477.

V. Spetzler, R. Kiebach, C. Näther, W. Bensch

- [17] J. B. Parise, *Science* **1991**, *251*, 293.
[18] K. Volk, H. Schäfer, *Z. Naturforsch.* **1979**, *34b*, 172.
[19] J. B. Parise, Y.Ko, *Chem. Mater.* **1992**, *4*, 1446.
[20] M. Gostojic, W. Nowacki, P. Engel, *Z. Kristallogr.* **1982**, *159*, 217.
[21] L. Engelke, C. Näther, W. Bensch, *Eur. J. Inorg. Chem.* **2002**, 2936.
[22] J. Rijnberk, C. Näther, W. Bensch, *Monatsh. Chem.* **2000**, *131*, 721.
[23] R. Stähler, C. Näther, W. Bensch, *Eur. J. Chem.* **2001**, 1835.
[24] X. Wang, A. J. Jacobson, F. Liebau, *J. Solid State Chem.* **1998**, *140*, 387.
[25] W. S. Sheldrick, H.-J. Häusler, *Z. Anorg. Allgem. Chem.* **1988**, *561*, 149.
[26] J. B. Parise, *J. Chem. Soc., Chem. Commun.* **1990**, 1553.
[27] G. M. Sheldrick, SHELXS-97, Program for Crystal Structure Determination, University of Göttingen, Germany (1997)
[28] G. M. Sheldrick, SHELXL-97, Program for the Refinement of Crystal Structures, University of Göttingen, Germany (1997)
[29] A. Pfitzner, *Chem. Eur. J.* **1997**, *3*, 2032.
[30] A. Pfitzner, D. Kurowski, *Z. Kristallogr.* **2000**, *215*, 373.
[31] V. Spetzler, H. Rijnberk, C. Näther, W. Bensch, *Z. Anorg. Allg. Chem.* **2004**, *630*, 142.

3. 2 Synthese und Struktur von $(C_6N_2H_{18})Sb_4S_7$

Die Verbindung $(C_6N_2H_{18})Sb_4S_7$ gehört zur Gruppe der Thioantimonate(III) mit dem Verhältnis Sb:S = 1:1.75 [58-71]. Die Verbindung konnte mit den Edukten Sb und S im Molverhältnis 1:3 bei 140°C in 7 Tagen mit einer Ausbeute von 90% synthetisiert werden. Die **primären Baueinheiten** bilden eine trigonale SbS₃-Pyramide und drei SbS₄-Einheiten. Diese drei Einheiten sind zu der **sekundären Baueinheit** (SBE) Sb₃S₈ kondensiert (Abb. 3.2.1).

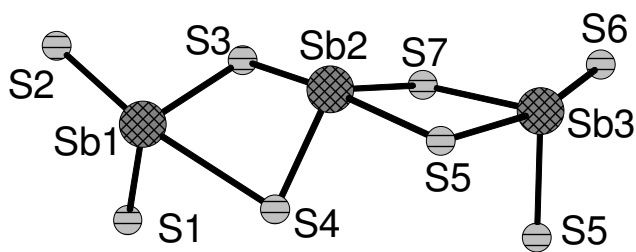


Abb. 3.2.1 SBE in der Struktur von $(C_6N_2H_{18})Sb_4S_7$

Eine weitere Verknüpfung der SBE über die trigonale SbS₃-Pyramide ergibt eine Kette aus alternierenden Sb₃S₈- und SbS₃-Einheiten. Die parallel verlaufenden **Ketten** werden über S(1)-Atome der Sb(4)S₃-Einheit zu **Schichten** verknüpft, die Sb₁₀S₁₀-Ringe mit den Abmessungen 7.98 Å · 13.54 Å (gemessen von Sb(4) zu Sb(1) und S(1) zu S(1)) als zentrales Strukturmotiv enthalten (Abb. 3.2.2).

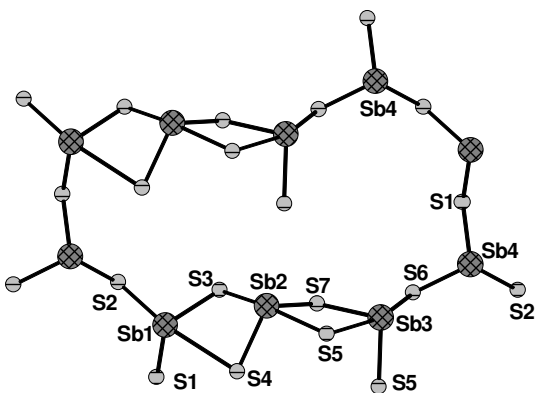


Abb. 3.2.2 Der Sb₁₀S₁₀-Ring in der Verbindung $(C_6N_2H_{18})Sb_4S_7$

Über S(5) werden **Doppelschichten** ausgebildet. Der Abstand zwischen den Doppelschichten beträgt 8.46 Å. Interessant ist dabei die zu den anionischen Schichten parallele Ausrichtung der paarweise angeordneten 1,6-Diaminohexanmoleküle (Abb. 3.2.3).

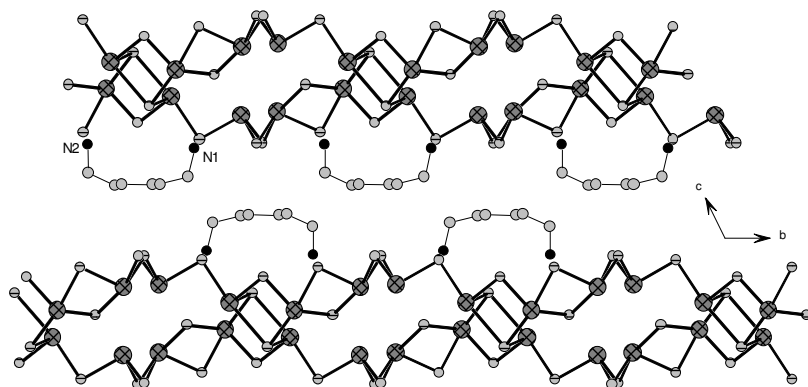


Abb. 3.2.3 Die parallele Anordnung des 1,6-Diaminohexans in der Struktur von $(C_6N_2H_{18})Sb_4S_7$

In dem **Ramanspektrum** treten Resonanzen zwischen 323.8 cm^{-1} und 361.0 cm^{-1} auf, welche charakteristisch für SbS_3 -Einheiten sind [90, 91]. Die Banden mit niedrigeren Wellenzahlen (289.7 cm^{-1} und 300.1 cm^{-1}) sind typische Indizien für das Vorhandensein von SbS_x -Gruppen mit $x > 3$. Die Verbindung ist ein optischer Halbleiter mit einer **Bandlücke** E_g von ungefähr 1.9 eV.

Die **thermische Zersetzung** der Verbindung $(C_6N_2H_{18})Sb_4S_7$ erfolgt in zwei Schritten ($T_{\text{onset}} = 196^\circ\text{C}$), welche von zwei endothermen Signalen begleitet ist ($T_p = 213^\circ\text{C}$, $T_p = 246^\circ\text{C}$). Der experimentell bestimmte Massenverlust stimmt nahezu mit dem berechneten Wert überein: $-\Delta m_{\text{theo.}} = 14.0\%$, $-\Delta m_{\text{exp.}} = 13.7\%$. Als Abbauprodukte konnten elementares Sb und Sb_2S_3 im Pulverdiffraktogramm identifiziert werden, was auf einen recht komplexen Abbauprozess hindeutet.

(C₆N₂H₁₈)Sb₄S₇ a Thioantimonate(III) with a Layered [Sb₄S₇]²⁻ Anion
in the Presence of a Diprotonated Amine as Structure Director

Volker Spetzler, Christian Näther, Wolfgang Bensch*

Institut für Anorganische Chemie, Christian-Albrechts-Universität Kiel, Olshausenstr. 40, D-
24098 Kiel, Germany

Reprint requests to Prof. Dr. Bensch. Fax: +49(0)431 880 1520; E-mail: wbensch@ac.uni-
kiel.de

Z. Naturforsch. **61b**,(2006); received February 1, 2006

Dedicated to Professor Wolfgang Jeitschko on the occasion of his 70th birthday

Abstract

The new thioantimonate(III) ($C_6N_2H_{18}Sb_4S_7$ ($C_6N_2H_{16}$ = 1,6-diaminohexane) was synthesized under solvothermal conditions using Sb, S and 1,6-diaminohexane (1,6-DAH). The compound crystallizes as orange needles in the triclinic space group $P\bar{1}$ with lattice parameters $a = 6.9834(5)$, $b = 11.8748(10)$, $c = 13.6588(12)$ Å, $\alpha = 115.248(9)$, $\beta = 100.165(9)$ and $\gamma = 92.568(14)^\circ$. A central SbS_4 group shares edges with two other SbS_4 moieties forming Sb_3S_8 units which are joined by SbS_3 pyramids sharing vertices to form a chain of alternating Sb_3S_8 and SbS_3 units. One S atom of the SbS_3 pyramid connects neighboring chains into sheets which contain large $Sb_{10}S_{10}$ heterorings. The sheets are then further connected into four atoms thick double sheets. Six edge-linked SbS_4 units are condensed yielding a complex Sb_6S_{14} building block. Layers of diprotonated amines and thioantimonate(III) layers are stacked along [001] in a sandwich-like fashion with an interlayer distance of 8.46 Å. The amine layer is two molecules thick with the amines being oriented parallel to the anionic layers. The title compound represents the first example for a layered $[Sb_4S_7]^{2-}$ anion with a diamine as structure director. The compound is an optical semiconductor with a band-gap of about 1.9 eV.

Keywords: Thioantimonate(III), Solvothermal Synthesis, Crystal Structure, Optical Properties

Introduction

Thioantimonates(III) exhibit several chemical and structural features resembling the chemistry of silicates or zeolites. Analogous to structures of silicates with isolated anions, anionic chains, layered anions and three-dimensional networks, also thioantimonates(III) are known which contain isolated ring anions, one-dimensional chains, two-dimensional layers and three-dimensional networks. In addition, silicates show a large range for the Si : O ratio and this phenomenon is also found in thioantimonates(III). The Sb : S ratio varies from 1:1.625 to 1:2 and examples are $[\text{Sb}_8\text{S}_{13}]^{2-}$ [1-5] for 1:1.625, $[\text{Sb}_3\text{S}_5]^-$ [6-10], $[\text{Sb}_6\text{S}_{10}]^{2-}$ [11, 12, 13], $[\text{Sb}_9\text{S}_{15}]^{3-}$ [13], $[\text{Sb}_{12}\text{S}_{20}]^{4-}$ [14] for 1:1.667, $[\text{Sb}_4\text{S}_7]^{2-}$ [15-28], and $[\text{Sb}_{12}\text{S}_{21}]^{6-}$ [26] for 1:1.75, $[\text{Sb}_5\text{S}_9]^{3-}$ [29], $[\text{Sb}_{10}\text{S}_{18}]^{6-}$ [30] for 1:1.8, and $[\text{Sb}\text{S}_2]^-$ [31, 32], $[\text{Sb}_2\text{S}_4]^{2-}$ [33], $[\text{Sb}_3\text{S}_6]^{3-}$ [34], $[\text{Sb}_4\text{S}_8]^{2-}$ [35], $[\text{Sb}_4\text{S}_8]^{4-}$ [36] for 1:2. But there are some remarkable differences between silicates and thioantimonates(III). Under normal conditions Si is always in a tetrahedral environment of O atoms, whereas Sb(III) can be surrounded by 3 to 6 S atoms. The Si-O bond is relatively rigid and shows only a small variation, whereas Sb-S bond lengths scatter over a large range from about 2.3 Å up to the sum of the van der Waals radii of about 3.8 Å. Finally, the Si-O-Si angle is flexible with values between 90 and 180 °, but Sb-S-Sb angles are distributed in a narrow range from about 90 to 110 °.

Anions with stoichiometry $[\text{Sb}_4\text{S}_7]^{2-}$ are particularly prevalent in thioantimonates(III) and examples include $\text{K}_2\text{Sb}_4\text{S}_7$ [15], $(\text{NH}_4)_2\text{Sb}_4\text{S}_7$ [16], $\text{Rb}_2\text{Sb}_4\text{S}_7 \cdot \text{H}_2\text{O}$ [17], $\text{Cs}_2\text{Sb}_4\text{S}_7$ [18], $\text{K}_2\text{Sb}_4\text{S}_7 \cdot \text{H}_2\text{O}$ [19], $\text{SrSb}_4\text{S}_7 \cdot 6\text{H}_2\text{O}$ [20], $\text{Rb}_2\text{Sb}_4\text{S}_7$ [21], $(\text{C}_4\text{N}_2\text{H}_8)\text{Sb}_4\text{S}_7$ [8], $[\text{M}(\text{C}_2\text{N}_2\text{H}_8)_3]\text{Sb}_4\text{S}_7$ ($\text{M} = \text{Mn, Fe, Co, Ni}$) [22, 23, 24], $(\text{C}_2\text{H}_5\text{NH}_3)_2\text{Sb}_4\text{S}_7$ [25], $[\text{Ni}(\text{C}_4\text{H}_{13}\text{N}_3)_2]\text{Sb}_4\text{S}_7 \cdot \text{H}_2\text{O}$ [26], $[\text{Mn}(\text{C}_4\text{H}_{13}\text{N}_3)_2]\text{Sb}_4\text{S}_7$ [27] and $(\text{C}_6\text{H}_{20}\text{N}_4)[\text{Sb}_4\text{S}_7]$ [24], $(\text{H}_3\text{N}(\text{CH}_2)_4\text{NH}_3)\text{Sb}_4\text{S}_7$, $(\text{CH}_3(\text{CH}_2)_2\text{NH}_3)_2\text{Sb}_4\text{S}_7$, $((\text{CH}_3)_2\text{CHNH}_3)_2\text{Sb}_4\text{S}_7$, $(\text{CH}_3(\text{CH}_2)_3\text{NH}_3)_2\text{Sb}_4\text{S}_7$, and $(\text{CH}_3(\text{CH}_2)_4\text{NH}_3)_2\text{Sb}_4\text{S}_7$ [28]. $(\text{C}_6\text{H}_{20}\text{N}_4)\text{Sb}_4\text{S}_7$ [24]. Of these, only $\text{K}_2\text{Sb}_4\text{S}_7$ [15] shows a three-dimensional $[\text{Sb}_4\text{S}_7]^{2-}$ anionic framework, and with increasing size of the cation, the dimensionality is reduced to two-dimensional layers and finally to one-dimensional chains [23, 37]. The compounds with organic amines as structure directors may be regarded as inorganic-organic hybrid materials, with the arrangements of the organic ammonium ions being often reminiscent of what is observed in layered clays. For instance, in vermiculites with a high layer charge, the alkyl-ammonium ions adopt a paraffin-like orientation. In addition, in many organically ‘templated’ thioantimonates(III) the $- \text{NH}_3^+$ groups adopt a special arrangement with respect to the S atoms of the thioantimonate network

[38, 39, 40, 10]. It can be assumed that this special orientation of the ammonium groups allows H···S bonding interactions. Furthermore, in the layered compounds the interlayer spacing covers a large range from for instance 6.56 Å for $(C_2H_5NH_3)_2Sb_4S_7$ [25] to 9.90 Å for $(CH_3(CH_2)_4NH_3)_2Sb_4S_7$ [28]. In our continuing work in the field of solvothermal syntheses of thioantimonates(III) we applied 1,6-diaminohexane as ‘template’ with the aim to prepare a layered thioantimonate(III) with the diamines acting like ‘pillars’. Here we present the crystal structure, and optical spectroscopy data for the compound $(C_6N_2H_{18})Sb_4S_7$.

Experimental Details

Synthesis

The compound $(C_6N_2H_{18})Sb_4S_7$ was prepared under solvothermal conditions in a Teflon-lined steel autoclave. A mixture of Sb (1 mmol) and S (3 mmol) was heated for 7 d in 4 ml of 1,6-diaminohexane. The product was collected by filtration and washed with deionized water and acetone and dried in vacuum. The compound crystallizes as orange needles and is stable on air. The yield of the product was about 90% based on Sb. $(C_6N_2H_{18})Sb_4S_7$ (829.5): calcd. C 8.4, H 3.2, N 2.0; found C 8.2, H 2.9, N 1.7.

X-ray structure determination

The X-ray intensity data were collected at 293 K using a STOE AED 4 with graphite monochromated Mo-K α radiation ($\lambda = 0.71073$ Å). The raw intensities were treated in the normal way applying a Lorentz polarization correction. The structure was solved using SHELXS-97 [41]. Crystal structure refinement was carried out against F² with SHELXL-97 [42]. All non-hydrogen atoms were refined with anisotropic displacement parameters. The hydrogen atoms were positioned with idealized geometry and refined with fixed isotropic displacement parameters using a riding model. Details of data collections and refinement results are summarized in Table 1. Bond lengths and angles are listed in Tables 2, 3, and 4. The crystal investigated was non-merohedrally twinned. Therefore, both individuals were indexed separately and integrated using the TWIN option in the STOE IPDS-1 software package. Crystallographic data (excluding structure factors) have been deposited with the Cambridge Crystallographic Data Center as supplementary publication no. CCDC- 296852.

Copies of the data can be obtained, free of charge, on application to CCDC, 12 Union Road, Cambridge data can be obtained, free of charge, on application to CCDC, 12 Union Road, Cambridge CB2 1 EZ, UK. (fax: +44-(0)1223-336033 or email: deposit@ccdc.cam.ac.uk).

Spectroscopy

The Raman spectrum was measured from 100 to 3500 cm⁻¹ with a Bruker IFS 66 Fourier transform Raman spectrometer (wavelength: 514.5 nm, T = 20 K).

Results and Discussion

The new compound ($C_6N_2H_{18}$)Sb₄S₇ crystallizes in the triclinic space group $P\bar{1}$ with all atoms located in general positions (Table 1). For the discussion of the structure Sb-S distances up to about 3.1 Å are considered as bonding contacts. But one should keep in mind that Sb-S distances scatter over a large range from about 2.3 to 4 Å and therefore, the assignment of the dimensionality is often arbitrary. The primary building units (PBUs) of ($C_6N_2H_{18}$)Sb₄S₇ are one trigonal SbS₃ pyramid and three SbS₄ units (Fig. 1). The Sb-S distances in SbS₃ groups scatter less (2.390(3) – 2.562(3) Å) than in the SbS₄ moieties (2.412(2) – 2.967(3) Å) (Table 2). In the SbS₄ groups the two long Sb-S bond lengths are in *trans* position and the angles S-Sb-S are about 165°. Sb-S bond lengths and angles are in the range observed in many other thioantimonates(III) [15-28]. All Sb atoms increase their coordination spheres with S atoms at distances up to 3.8 Å (Table 3) forming another SbS₄ group (Sb(1)) and three distorted SbS₅ rectangular pyramids.

The layered [Sb₄S₇]²⁻ anion is constructed in the following way. The Sb(2)S₄ group shares edges with two other SbS₄ moieties forming an Sb₃S₈ unit as a secondary building unit (SBU) (Fig. 1). These SBUs are then joined by SbS₃ pyramids sharing vertices yielding a chain of alternating Sb₃S₈ and SbS₃ units (Fig. 1). The S(1) atom of the SbS₃ pyramid connects neighboring chains to form sheets within the *ab* plane that contain relatively large Sb₁₀S₁₀ heterorings (Fig. 1). These sheets are then further connected through S(5) into four atoms thick double sheets (Fig. 2). The double sheets contain six edge-linked SbS₄ units yielding a complex Sb₆S₁₄ building block (Fig. 2). The individual layers are stacked along [001] with the diprotonated amine molecules lying in between (Fig. 3). The two N atoms of an amine molecule are directed towards S atoms of one thioantimonate(III) anion, i.e. the amines are

oriented parallel to the anionic layers. Along [010] the orientation of the amines is ...up-down-up-down... to form a two molecules thick organic layer (Fig. 3), and the shortest interlayer distance amounts to 8.46 Å. All H atoms bound to the two N atoms are involved in H···S bonding interactions with distances ranging from 2.369 to 2.997 Å with corresponding N-H···S angles between 120.46 and 167.32° (Table 4).

A short comparison with the hitherto known organically ‘templated’ compounds containing $[\text{Sb}_4\text{S}_7]^{2-}$ anions is given here. The topology of the anionic network of the title compound is very similar with that of $(\text{C}_2\text{H}_5\text{NH}_3)_2\text{Sb}_4\text{S}_7$ [25], $(\text{CH}_3(\text{CH}_2)_2\text{NH}_3)_2\text{Sb}_4\text{S}_7$, $(\text{CH}_3)_2\text{CHNH}_3)_2\text{Sb}_4\text{S}_7$, $(\text{CH}_3(\text{CH}_2)_3\text{NH}_3)_2\text{Sb}_4\text{S}_7$, and $(\text{CH}_3(\text{CH}_2)_4\text{NH}_3)_2\text{Sb}_4\text{S}_7$ [28], and only small differences are observed for Sb-S bond lengths and S-Sb-S angles. But in all these compounds the structure directors are mono-amines. The structures of the two compounds with diamines, $(\text{H}_3\text{N}(\text{CH}_2)_4\text{NH}_3)\text{Sb}_4\text{S}_7$ and $(\text{pipH}_2)\text{Sb}_4\text{S}_7$ as well as that of $(\text{C}_6\text{H}_{20}\text{N}_4)\text{Sb}_4\text{S}_7$ with a tetramine contain a thioantimonate(III) chain anion. Therefore, the title compound is the first example with a layered $[\text{Sb}_4\text{S}_7]^{2-}$ anion containing a diamine as structure director.

Optical Spectroscopy

Charge compensation requires that the amine molecules are diprotonated in $(\text{C}_6\text{N}_2\text{H}_{18})\text{Sb}_4\text{S}_7$. In the IR spectrum the absorptions located at 1068, 1473, 1552, 1635, 2858, 3108 and 3400 cm^{-1} are typical for R-NH $_3^+$ groups. In the Raman spectrum (Fig. 4) the most intense resonances are located at 323.8 and 361.0 cm^{-1} . Weak bands are observed at 289.7 and 300.1 cm^{-1} . The bands between 362 and 339 cm^{-1} are typical for SbS $_3$ units, while bands located at lower wave numbers are due to bonding interactions between Sb(III) and the next nearest S atoms. [43, 44]. Pfitzner et al. explained resonances at 321 cm^{-1} and about 290 cm^{-1} with SbS $_5$ units [43, 44]. In MnSb $_2$ S $_4$ the resonances are at even lower wave numbers of 300 and 283 cm^{-1} which is due to the high coordination number of the Sb atoms [44]. The optical band gap of the compound was determined from the transformed UV-Vis diffuse reflectance spectrum in the usual way (Kubelka-Munk relation). The optical band gap of about 1.9 eV indicates that the compound is an optical semiconductor.

Summary

The new compound $(C_6N_2H_{18})Sb_4S_7$ with diprotonated 1,6-diaminohexane molecules is a further example for the flexibility of thioantimonate(III) structures to adapt the size and charge requirements of the structure director. In the present compound the diamine molecules are parallel to the anionic layers with the NH_3 groups oriented towards S atoms to ensure optimal S...H bonding interactions. An interesting question is whether it is possible to synthesize a layered thioantimonate(III) with diamines which act as 'pillars' between neighboring layers. Syntheses with diamines with less conformational flexibility are under way to prove whether such thioantimonates(III) can be prepared.

References

- [1] K. Volk, H. Schäfer, Z. Naturforsch. **34b**, 1637 (1979).
- [2] X. Wang, F. Liebau, J. Solid State Chem. **111**, 385 (1994).
- [3] X. Wang, L. Liu, A. J. Jacobson, J. Solid State Chem. **155**, 409 (2000).
- [4] K. Tan, Y. Ko, J. B. Parise, Acta Crystallogr. **C50**, 1439 (1994).
- [5] Y. Ko, K. Tan, J. B. Parise, A. Darowsky, Chem. Mater. **8**, 493 (1996).
- [6] J. B. Parise, Science **251**, 293 (1991).
- [7] K. Volk, H. Schäfer, Z. Naturforsch. **34b**, 172 (1979).
- [8] J. B. Parise, Y. Ko, Chem. Mater. **4**, 1446 (1992).
- [9] M. Gostojic, W. Nowacki, P. Engel, Z. Kristallogr. **159**, 217 (1982).
- [10] L. Engelke, C. Näther, W. Bensch, Eur. J. Inorg. Chem., **2936** (2002).
- [11] J. Rijnberk, C. Näther, W. Bensch, Monatsh. Chem. **131**, 721 (2000).
- [12] R. Stähler, C. Näther, W. Bensch, Eur. J. Chem. **1835**, (2001).
- [13] V. Spetzler, R. Kiebach, C. Näther, W. Bensch, Z. Anorg. Allg. Chem. **630**, 2398 (2004).
- [14] X. Wang, A. J. Jacobson, F. Liebau, J. Solid State Chem. **140**, 387 (1998).
- [15] H. A. Graf, H. Schäfer, Z. Naturforsch. **27b**, 735 (1972).
- [16] G. Dittmar, H. Schäfer, Z. Anorg. Allg. Chem. **437**, 183 (1977).
- [17] G. Dittmar, H. Schäfer, Z. Anorg. Allg. Chem. **441**, 93 (1978).
- [18] G. Dittmar, H. Schäfer, Z. Anorg. Allg. Chem. **441**, **98 (1978)**.
- [19] B. Eisenmann, H. Schäfer, Z. Naturforsch. **34b**, 383 (1979).
- [20] G. Cordier, H. Schäfer, C. Schwidetzky, Z. Naturforsch. **39b**, 131 (1984).
- [21] W. S. Sheldrick, H.-J. Häusler, Z. Anorg. Allg. Chem. **557**, 105 (1988).
- [22] H.-O. Stephan, M. G. Kanatzidis, Inorg. Chem. **36**, 6050 (1997).
- [23] W. Bensch, M. Schur, Z. Naturforsch. **52b**, 405 (1997).
- [24] P. Vaqueiro, D. P. Darlow, A. M. Chippindale, A. V. Powell, Solid State Ionics **172**, 601 (2004).
- [25] M. Schur, W. Bensch, Eur. J. Solid State Inorg. Chem. **34**, 457 (1997).
- [26] R. Stähler, C. Näther, W. Bensch, J. Solid State Chem. **174**, 264 (2003).
- [27] M. Schaefer, D. Kurowski, A. Pfitzner, C. Näther, W. Bensch, Acta Crystallogr. **E60**, m183 (2004).

- [28] A. Puls, M. Schaefer, C. Näther, W. Bensch, A. V. Powell, S. Boissière, A. M. Chippindale, *J. Solid State Chem.* **178**, 1171 (2005).
- [29] W. S. Sheldrick, H.-J. Häusler, *Z. Anorg. Allg. Chem.* **561**, 149 (1988).
- [30] J. B. Parise, *J. Chem. Soc., Chem. Commun.* **1553** (1990).
- [31] K. Volk, P. Bickert, R. Kolmer, H. Schäfer, *Z. Naturforsch.* **34b**, 380 (1979).
- [32] H. A. Graf, H. Schäfer, *Z. Anorg. Allg. Chem.* **414**, 211 (1975).
- [33] G. Cordier, C. Schwidetzky, H. Schäfer, *J. Solid State Chem.* **54**, 84 (1984).
- [34] R. Kiebach, F. Studt, C. Näther, W. Bensch, *Eur. J. Inorg. Chem.* **2553** (2004).
- [35] T. J. McCarthy, M. G. Kanatzidis, *Inorg. Chem.* **33**, 1205 (1994).
- [36] W. Bensch, C. Näther, R. Stähler, *Chem. Commun.* **477** (2001).
- [37] W. S. Sheldrick, *J. Chem. Soc. Dalton Trans.* **3041** (2000).
- [38] M. Schur, W. Bensch, *Z. Naturforsch.* **57b**, 1 (2002).
- [39] V. Spetzler, H. Rijnberk, C. Näther, W. Bensch, *Z. Anorg. Allg. Chem.* **630**, 142 (2004).
- [40] M. Schur, A. Gruhl, C. Näther, I. Jess, W. Bensch, *Z. Naturforsch.* **54b**, 1524 (1999).
- [41] G. M. Sheldrick, *SHELXS-97, Program for Crystal Structure Determination*, University of Göttingen, Germany (1997).
- [42] G. M. Sheldrick, *SHELXL-97, Program for the Refinement of Crystal Structures*, University of Göttingen, Germany (1997).
- [43] A. Pfitzner, *Chem. Eur. J.* **3**, 2032 (1997).
- [44] A. Pfitzner, D. Kurowski, *Z. Kristallogr.* **215**, 373 (2000).

Table 1

Selected Crystallographic Data and Refinement Results for $(C_6N_2H_{18})Sb_4S_7$.

a (Å)	6.9834(5)
b (Å)	11.8748(10)
c (Å)	13.6588(12)
$\alpha/^\circ$	115.248(9)
$\beta/^\circ$	100.165(9)
$\gamma/^\circ$	92.568(9)
$V/\text{Å}^3$	999.18(14)
$d_{\text{calc}}/\text{g cm}^{-3}$	2.758
Crystal system	triclinic
Space group	$P\bar{1}$
$2\theta/\text{deg}$	6 - 56
hkl Range	$-8 \leq h \leq 8$ $-15 \leq k \leq 15$ $-18 \leq l \leq 18$
No. coll. Refl.	7421
No. unique refl:	3620
Refl. $F_o > 4\sigma(F_o)$	2669
No: par.	173
$R1 (F_o > 4\sigma(F_o))$	0.0462
$wR2 (F_o > 4\sigma(F_o))$	0.1154
$R1$ (all refl.)	0.0665
$wR2$ (all refl.)	0.1230
GOF	0.982
$\delta(F)/e \text{ Å}^{-3}$	-1.280/1.075

Table 2. Selected interatomic distances (\AA) and angles ($^\circ$) for $(\text{C}_6\text{N}_2\text{H}_{18})\text{Sb}_4\text{S}_7$. Estimated standard deviations are given in parentheses.

Sb(1)-S(3)	2.390(3)	S(3)-Sb(1)-S(1)	98.33(11)
Sb(1)-S(1)	2.460(3)	S(3)-Sb(1)-S(2)	88.12(9)
Sb(1)-S(2)	2.539(3)	S(1)-Sb(1)-S(2)	87.51(10)
Sb(2)-S(4)	2.415(3)	S(4)-Sb(2)-S(7) ^a	110.54(10)
Sb(2)-S(7) ^a	2.471(3)	S(7) ^a -Sb(2)-S(3)	81.38(9)
Sb(2)-S(3)	2.653(3)	S(4)-Sb(2)-S(3)	87.91(9)
Sb(2)-S(5)	2.775(3)	S(4)-Sb(2)-S(5)	88.38(8)
Sb(3)-S(5)	2.412(2)	S(7) ^a -Sb(2)-S(5)	86.70(8)
Sb(3)-S(7)	2.491(3)	S(3)-Sb(2)-S(5)	165.37(9)
Sb(3)-S(6)	2.562(3)	S(5)-Sb(3)-S(7)	91.58(9)
Sb(4)-S(2) ^b	2.409(3)	S(7)-Sb(3)-S(6)	85.15(9)
Sb(4)-S(1) ^c	2.475(3)	S(2) ^b -Sb(4)-S(1) ^c	93.32(10)
Sb(4)-S(6)	2.435(6)	S(6)-Sb(4)-S(1) ^c	90.11(9)
Sb(4) ^b -S(2)-Sb(1)	105.49(10)	Sb(4)-S(6)-Sb(3)	93.40(10)
Sb(3)-S(5)-Sb(2)	97.97(9)	Sb(2) ^a -S(7)-Sb(3)	104.09(10)
Sb(1)-S(1)-Sb(4) ^c	104.81(10)	Sb(1)-S(3)-Sb(2)	92.03(9)
Sb(2) ^[a] -S(7)-Sb(3)	104.09(10)		

Symmetry codes: ^a-x+3,-y+2,-z+1; ^b -x+2,-y+1,-z+1; ^c -x+3,-y+1,-z+1.

Table 3. Long Sb-S distances (\AA) in $(\text{C}_6\text{N}_2\text{H}_{18})\text{Sb}_4\text{S}_7$. Estimated standard deviations are given in parentheses.

Sb(1) – S(4)	3.089(2)
Sb(3) – S(4)	3.269(2) ^a
Sb(4) – S(4)	3.393(2) ^b
Sb(2) – S(5)	3.587(2) ^c
Sb(4) – S(4)	3.717(2)

Symmetry codes: ^a 2- x , 1- y , 1- z ; ^b -1+ x , y , z ; ^c 2- x , 2- y , 1- z ;

Table 4. N-H…S distances and angles [\AA , $^\circ$] for $(\text{C}_6\text{N}_2\text{H}_{18})\text{Sb}_4\text{S}_7$.

D-H	d(H…A)	<DHA	A
N1-H1A	2.618	159.28	S1 ^a
N1-H1B	2.997	155.89	S7 ^b
N1-H1C	2.689	160.96	S6 ^c
N2-H2A	2.824	120.46	S4 ^d
N2-H2A	2.954	121.95	S2 ^e
N2-H2B	2.369	167.32	S7 ^f
N2-H2C	2.563	160.16	S3 ^g

Symmetry codes: ^a - x +3, - y +1, - z +1; ^b - x +2, - y +1, - z +1, ^c - x +2, - y +1, - z +1; ^d x -1, y -1, z ; ^e x , y -1, z ; ^f - x +2, - y +1, - z +1; ^g - x , y -1, z .

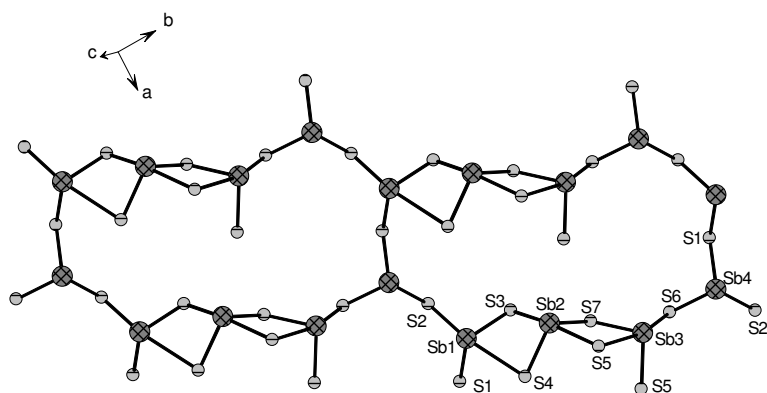


Fig. 1 The connectivity pattern of the Sb_4S_7 and Sb_3S_2 units in $(\text{C}_6\text{N}_2\text{H}_{18})\text{Sb}_4\text{S}_7$ with atom labelling.

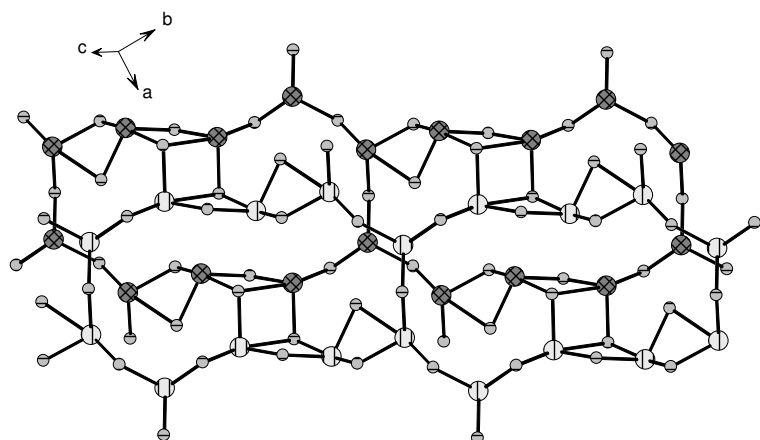


Fig. 2 The double layer in $(\text{C}_6\text{N}_2\text{H}_{18})\text{Sb}_4\text{S}_7$. Note that Sb atoms of the second sheet are drawn with a different shading.

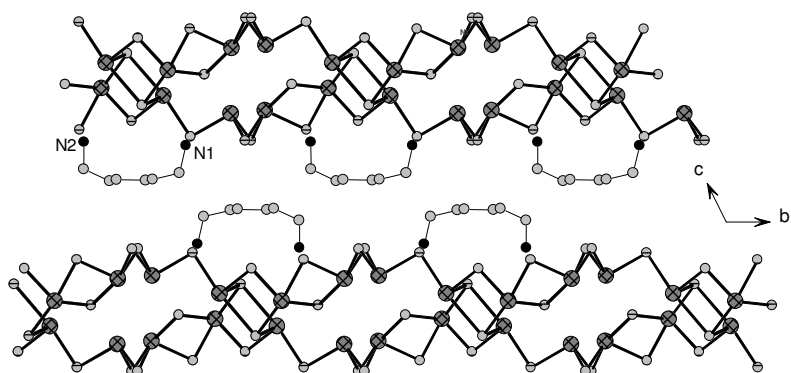


Fig. 3 The arrangement of the cations and anions in $(\text{C}_6\text{N}_2\text{H}_{18})\text{Sb}_4\text{S}_7$.

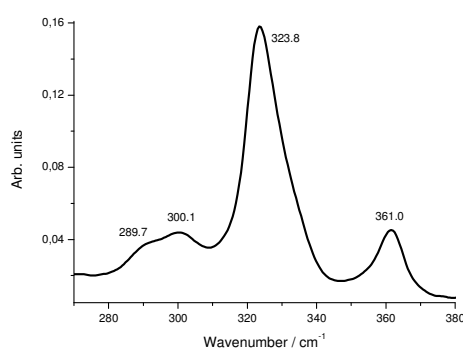


Fig. 4 Raman spectrum of $(\text{C}_6\text{N}_2\text{H}_{18})\text{Sb}_4\text{S}_7$.

3.3 Synthese und Struktur von Kupfer(I)-Thioantimonaten(III) mit der allgemeinen Formel RCu_2SbS_3 ($R = \text{Amin}$)

Die Verbindungen $(C_2N_2H_{10})_{0.5}Cu_2SbS_3$ (I) ($C_2N_2H_8$ = Ethyldiamin), $(C_3N_2H_{12})_{0.5}Cu_2SbS_3$ (II) ($C_3N_2H_{10}$ = 1,3-Diaminopropan) und $(C_4N_2H_{14})_{0.5}Cu_2SbS_3$ (III) ($C_4N_2H_{12}$ = 1,4-Diaminobutan) wurden mit den Edukten Sb_2S_3 , $CuCl_2 \cdot 2H_2O$ und S im Molverhältnis 2:2:5 in 5 mL der konzentrierten Aminlösungen Ethyldiamin (I), 1,3-Diaminopropan (II) und 1,4-Diaminobutan (III) bei 120 °C nach 6 Tagen erhalten. Die drei Verbindungen kristallisieren in der monoklinen Raumgruppe $P2_1/n$ und weisen alle die gleiche Topologie des Cu_2SbS_3 -Netzwerkes auf und können als anorganisch-organische Hybridverbindungen aufgefasst werden. Die Sb-S-, Cu-S-, Cu-Sb- und Cu-Cu-Abstände, sowie die entsprechenden Winkel unterscheiden sich nur geringfügig in den drei Verbindungen. Die Abstände zwischen den anorganischen Schichtanionen betragen 4.426(4) Å (I), 5.986(1) Å (II) und 5.931(1) Å (III). In Abbildung 3.3.1 ist ein SEM-Bild von Kristallen der Verbindung III dargestellt. Deutlich ist der schichtartige Charakter zu erkennen.

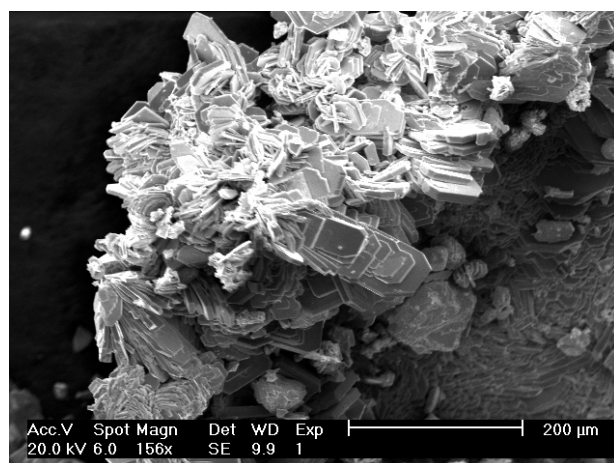


Abb. 3.3.1 SEM-Bild von Kristallen der Verbindung III

Die **primären Baueinheiten** des anorganischen Gerüstes bilden eine trigonal-pyramidale SbS_3 -Gruppe, ein verzerrtes CuS_3 -Dreieck und ein CuS_4 -Tetraeder.

Jede SbS_3 -Einheit ist mit 6 CuS_3 -Einheiten verknüpft, wobei jedes S-Atom an ein Sb-Atom und zwei Cu-Atome gebunden ist (Abb. 3.3.2).

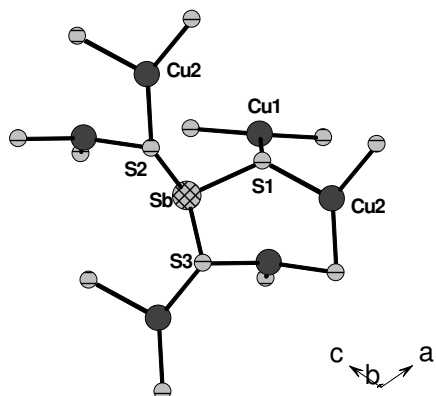


Abb. 3.3.2 Die SbS_3 -Pyramide und die CuS_3 -Einheiten in den Verbindungen I-III

Die weitere Verknüpfung führt zur Bildung 6-gliedriger Ringe (6 MR) der Formel Cu_2SbS_3 und 10-gliedriger Ringe (10 MR) der Formel $\text{Cu}_3\text{Sb}_2\text{S}_5$. Jeder der 10 MR ist mit vier weiteren 10 MR und vier 6 MR zu **Einfachschichten** in der (010)-Ebene verbunden. Zwei Einfachschichten bilden durch weitere Verknüpfung eine **Doppelschicht** und damit die $[\text{Cu}_2\text{SbS}_3]^-$ -Anionenschicht. Die protonierten Amine und anorganischen Schichten sind sandwichartig angeordnet (Abb. 3.3.3).

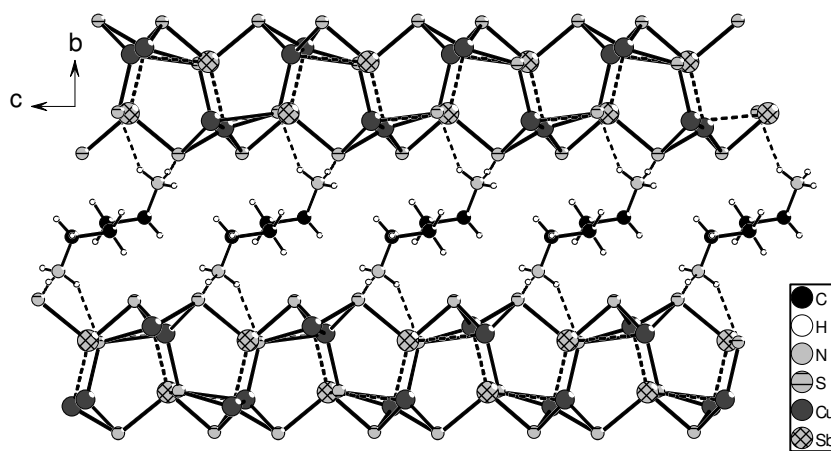


Abb. 3.3.3 Die sandwichartige Anordnung der anorganischen Schichten und der protonierten Amine in der Verbindung III

In den **Ramanspektren** werden Resonanzen im Bereich zwischen 293 und 338 cm⁻¹ beobachtet, welche den Moden der SbS_x-Einheiten zuzuordnen sind.

Der Beginn der **thermischen Zersetzung** liegt mit 135 °C für (enH₂)_{0.5}Cu₂SbS₃ (**I**) und 132 °C für (1,3-DAPH₂)_{0.5}Cu₂SbS₃ (**II**) bei relativ niedrigen Temperaturen, während die Verbindung (1,4-DABH₂)_{0.5}Cu₂SbS₃ (**III**) mit einer Zersetzungstemperatur von 200 °C stabiler ist. Der Massenabbau entspricht bei allen drei Verbindungen der Emission von 0.5 Aminmolekülen. Als Abbauprodukte konnten CuSbS₂ und Cu₃SbS₄ im Pulverdiffraktogramm identifiziert werden.

Zur Bestimmung der Oxidationszahl des Kupfers und zur Untersuchung weiterer physikalischer Eigenschaften wurden Messungen der **magnetischen Suszeptibilität** χ , **diffusen Reflexion** und **Impedanzspektroskopie** durchgeführt.

Die Temperaturabhängigkeit der **magnetische Suszeptibilität** der Verbindung **II** ist in der Abbildung 3.3.4 dargestellt.

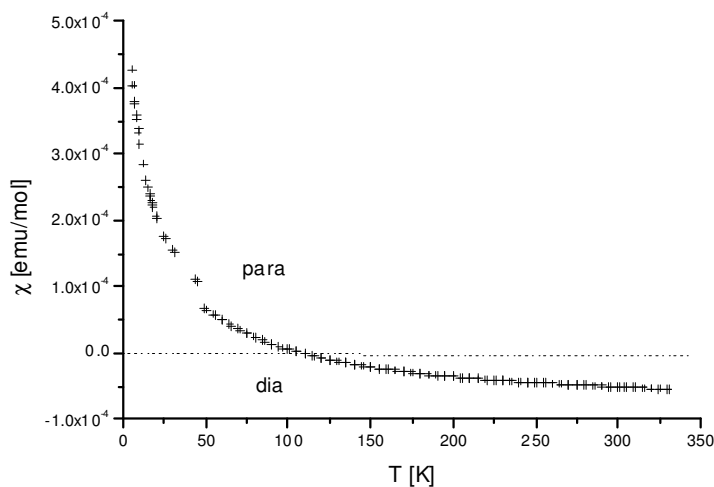


Abb. 3.3.4 Magnetische Suszeptibilität χ der Verbindung **II**

Oberhalb von 50 K ist die Substanz diamagnetisch, unterhalb von 50 K paramagnetisch, wobei das Signal sehr klein ist und auf eine geringe Kontamination zurückgeführt werden kann. Das Ergebnis der Messung der magnetischen Suszeptibilität belegt eindeutig, dass Cu¹ in der Verbindung vorliegt.

Mit der Messung der diffusen Reflexion konnte mit der Kubelka-Munk-Auswertung die **optische Bandlücke** zu etwa 1.9 eV bestimmt werden, wodurch der Halbleitercharakter belegt wird.

Mit **Impedanzspektroskopie** konnte für die Verbindung $(\text{en})_{0.5}\text{Cu}_2\text{SbS}_3$ (**I**) ein Ohm'scher Widerstand von $R = 1.9 \cdot 10^5 \Omega$ bei Raumtemperatur (RT) bestimmt werden (Abb. 3.3.5). Das ergibt einen spezifischen elektrischen Widerstand $\rho = 1.1 \cdot 10^6 \Omega\text{cm}$ und als spezifische elektrische Leitfähigkeit $\sigma = 9.1 \cdot 10^{-7} \Omega^{-1}\text{cm}^{-1}$.

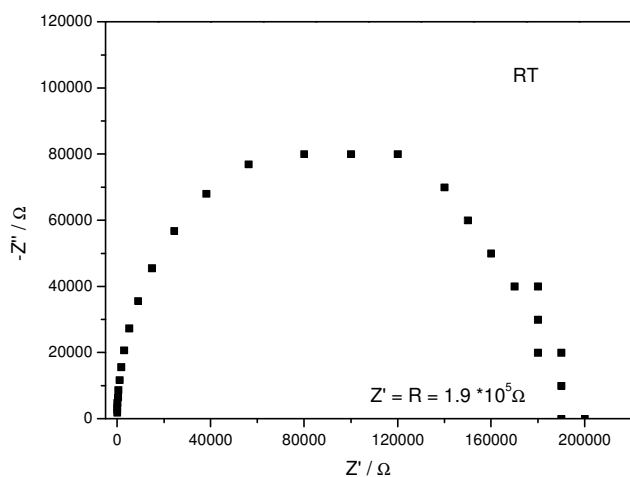


Abb. 3.3.5 Nyquistplot der Impedanzmessung bei RT für $(\text{en})_{0.5}\text{Cu}_2\text{SbS}_3$ (**I**)

Die Probe wurde schrittweise auf 90 °C erhitzt. Dabei verringert sich der Widerstand von $1.9 \cdot 10^5 \Omega$ bei Raumtemperatur auf $2 \cdot 10^4 \Omega$ bei 90 °C (Abb. 3.3.6).

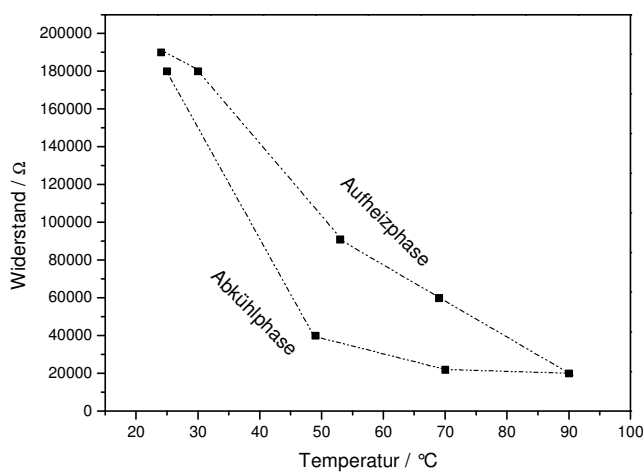


Abb. 3.3.6 Temperaturabhängigkeit des Ohm'schen Widerstandes von $(\text{en})_{0.5}\text{Cu}_2\text{SbS}_3$ (**I**)

Die Abkühlphase zeigt anfangs einen schwachen linearen Anstieg des elektrischen Widerstandes, um dann steiler auf $1.8 \cdot 10^5 \Omega$ wieder anzusteigen. Die Hysterese zwischen Aufheiz- und Abkühlkurven könnte auf eine partielle Degradation der Probe zurückzuführen sein (Abb. 3.3.6).

Mit der Arrhenius-Auftragung konnte die Aktivierungsenergie zu 0.52 eV berechnet werden (Abb. 3.3.7).

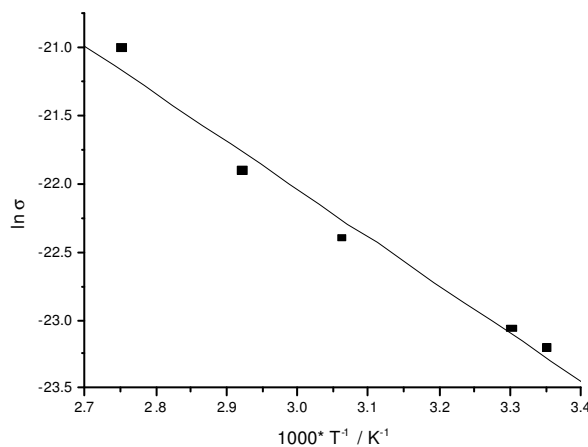


Abb. 3.3.7 Arrhenius-Auftragung mit Regression der Messwerte für $(en)_{0.5}Cu_2SbS_3$ (I)

Die unterschiedlichen Werte für die optische Bandlücke Eg = 1.9 eV und der Aktivierungsenergie E_A = 0.52 eV lassen sich durch die unterschiedlichen Leitfähigkeitsbereiche erklären (Abb. 3.3.8) [92].

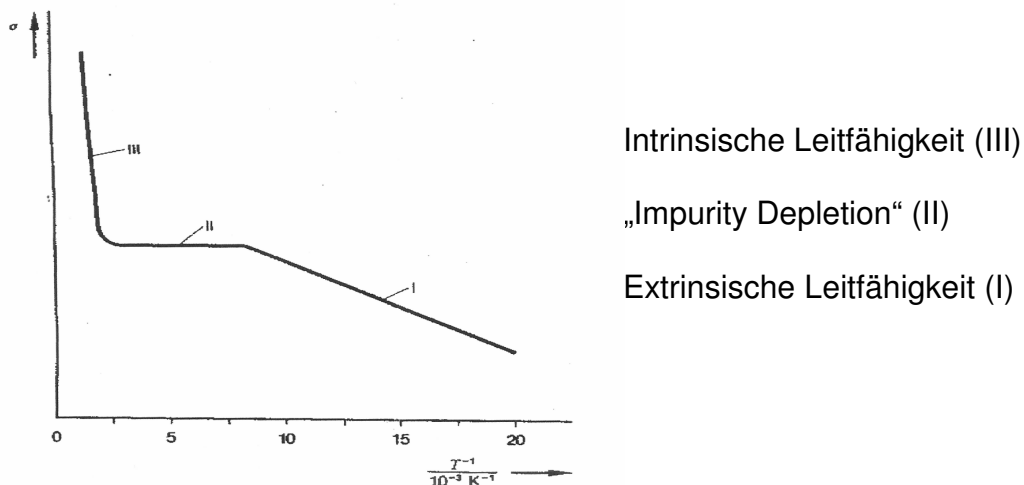


Abb. 3.3.8 Spezifische elektrische Leitfähigkeit σ als Funktion der reziproken Temperatur

Bei der spezifischen elektrischen Leitfähigkeit werden 3 Bereiche unterschieden (Abb.3.3.8):

- I) Extrinsische Leitfähigkeit bei "niedriger" Temperatur (ab 50 K): hierbei wirken "Verunreinigungen" als Ladungsträger und erhöhen σ , unterschieden werden hierbei der n- und der p-Typ.
- II) "Impurity Depletion" bei "mittlerer" Temperatur (ab 130 K): kein weiterer Anstieg von σ aufgrund von Verarmung an Verunreinigungen.
- III) Intrinsische Leitfähigkeit bei "höheren" Temperaturen (ab 293 K): der eigentliche Übergang von Ladungsträgern vom VB (Valenzband) in das LB (Leitungsband).

Der Messbereich bei der Impedanzspektroskopie liegt also im Bereich der intrinsischen Leitfähigkeit.

Novel Copper(I)-Thioantimonates(III): Solvothermal Synthesis, Crystal Structures, Thermal Stability and Magnetic Properties of $(C_2N_2H_{10})_{0.5}Cu_2SbS_3$, $(C_3N_2H_{12})_{0.5}Cu_2SbS_3$, and $(C_4N_2H_{14})_{0.5}Cu_2SbS_3$

Volker Spetzler, Herme Rijnberk, Christian Näther, and Wolfgang Bensch*

Kiel, Institut für Anorganische Chemie der Christian-Albrechts-Universität

Received August 1st, 2003.

Dedicated to Professor Klaus Range on the Occasion of his 65th Birthday

Abstract. The novel copper(I)-thioantimonates(III) $(enH_2^{2+})_{0.5}Cu_2SbS_3$ (**I**) (*en* = ethylenediamine), $(1,3-DAPH_2^{2+})_{0.5}Cu_2SbS_3$ (**II**) (1,3-DAP = 1,3-diaminopropane) and $(1,4-DABH_2^{2+})_{0.5}Cu_2SbS_3$ (**III**) (1,4-DAB = 1,4-diaminobutane) were synthesized under solvothermal conditions reacting Sb_2S_3 , $CuCl_2 \cdot 2H_2O$, S with the amines. The compounds crystallize in the monoclinic space group $P2_1/n$. The primary building units are a SbS_3 trigonal pyramid and two distorted CuS_3 units. In the structures the SbS_3 pyramid is connected to six CuS_3 moieties and every S atom has bonds to one Sb atom and to two Cu atoms. Further interconnection leads to the formation of ten-membered (10 MR) $Cu_3Sb_2S_5$ and six-membered (6 MR) Cu_2SbS_3 rings. Every 10 MR is condensed to four 10 MR and four 6 MR to form a single layer within the (010) plane. Two such single layers are connected to a

double layer thus forming the final $[Cu_2SbS_3]^-$ layered anion. The $[Cu_2SbS_3]^-$ protonated amines are located between the layers and the interlayer spacing depends on the size and orientation of these amines. Between the Sb atom and one Cu atom a remarkable short distance of about 2.7 Å is observed. At elevated temperatures the compounds decompose into $CuSbS_2$ and Cu_3SbS_4 suggesting a complex redox reaction. Diamagnetic susceptibilities indicate the copper(I) in the metal sulfide frameworks. All three compounds are semiconductors with intermediate band gaps of about 2 eV.

Keywords: Copper; Thioantimonates; Solvothermal synthesis; Crystal structure; Spectroscopy; Thermal investigations; Magnetic properties

Neue Kupfer(I)-Thioantimonate(III): Solvothermale Synthese, Kristallstrukturen, thermische und magnetische Eigenschaften von $(C_2N_2H_{10})_{0.5}Cu_2SbS_3$, $(C_3N_2H_{12})_{0.5}Cu_2SbS_3$ und $(C_4N_2H_{14})_{0.5}Cu_2SbS_3$

Inhaltsübersicht. Die neuen Kupfer(I)-Thioantimonate(III) $(enH_2^{2+})_{0.5}Cu_2SbS_3$ (**I**) (*en* = Ethylenediamin), $(1,3-DAPH_2^{2+})_{0.5}Cu_2SbS_3$ (**II**) (1,3-DAP = 1,3-Diaminopropan) und $(1,4-DABH_2^{2+})_{0.5}Cu_2SbS_3$ (**III**) (1,4-DAB = 1,4-Diaminobutan) wurden unter solvothermalen Bedingungen durch Reaktion von Sb_2S_3 , $CuCl_2 \cdot 2H_2O$ und S mit einer jeweils konzentrierten Lösung des Amins dargestellt. Die drei Verbindungen kristallisieren in der monoklinen Raumgruppe $P2_1/n$. Die primären Bildungseinheiten sind eine trigonal-pyramidal SbS_3 -Einheit und zwei verzerrte CuS_3 -Baugruppen. In den Strukturen ist die SbS_3 -Pyramide mit 6 CuS_3 -Baugruppen verknüpft und jedes S-Atom ist an ein Sb- und zwei Cu-Atome gebunden. Die weitere Verknüpfung führt zur Bildung von 10-gliedrigen (10 MR) $Cu_3Sb_2S_5$ - und 6-gliedrigen (6 MR) Cu_2SbS_3 -Ringen. Jeder der 10 MR ist mit vier weiteren

10 MR und vier 6 MR zu Einfachschichten in der (010)-Ebene verbunden. Zwei Einfachschichten bilden durch weitere Verknüpfung eine Doppelschicht und damit das schichtartig aufgebaute $[Cu_2SbS_3]^-$ -Anion. Die protonierten Aminmoleküle befinden sich $[Cu_2SbS_3]^-$ zwischen den Schichten und der Abstand zwischen benachbarten Schichten hängt von der Größe der Amine und deren Orientierung relativ zu den Anionenschichten ab. Zwischen dem Sb- und einem Cu-Atom wird ein bemerkenswert kurzer Abstand von etwa 2.7 Å beobachtet. Die Verbindungen zersetzen sich bei höheren Temperaturen in einer Disproportionierungsreaktion zu $CuSbS_2$ und Cu_3SbS_4 . Die Anwesenheit von Cu^I in den drei Titerverbindungen wird durch ihr diamagnetisches Verhalten unterstützt. Die optischen Bandlücken betragen etwa 2 eV und unterstreichen den Halbleitercharakter.

Introduction

A large number of thioantimonates(III) have been prepared by direct synthesis of the elements at relatively high tem-

peratures or by using solvothermal techniques with organic amines acting as structure directing agents [1–17]. Only few copper-based thioantimonates were described in the literature. Several of these compounds are of special interest because charge balancing is not always straightforward. The compound $CuSbS_2$ has a layered structure with the Sb^{III} atom having bonds to 3 S atoms forming a trigonal pyramidal geometry. The Cu^I atom is in a tetrahedral environment of 4 S atoms [18]. In tetrahedrite, $Cu_{12}Sb_4S_{13}$, two sorts of copper atoms are observed. The first Cu type is coordinated

* Prof. Dr. Wolfgang Bensch
Institut für Anorganische Chemie der Universität Kiel
Olshausenstraße 40
D-24098 Kiel, Germany
Fax: +49 (0)431/880 1520
email: wbensch@ac.uni-kiel.de

V. Spetzler, H. Rijnberk, C. Näther, W. Bensch

by four S atoms yielding a nearly regular CuS₄ tetrahedron. The second type has a triangular coordination with different distances to the S atoms. In this compound the oxidation state of the Cu atoms is not clear. From a formal point of view charge neutrality is achieved by two Cu^{II}, 10 Cu^I and 4 Sb^{III} atoms [19]. But it is well documented in the literature that Cu is always present as Cu^I in a sulfide matrix [20, 21].

In Cu₃SbS₃ the Cu^I atom is in a trigonal-planar environment with Cu–S distances between 2.239 and 2.359 Å typical for Cu^I [16]. The two compounds Cu₃SbS₄ and Cu₃SbSe₄ crystallize with a zinc-blende related structure (famatinite type) and the Sb atoms are pentavalent [22]. For the selenoantimonates(III) Cu₂SbSe₃·0.5en and Cu₂SbSe₃·en a mixed-valent state was postulated for Cu. In these compounds Cu₂SbSe₃ layers are formed which are separated by ethylenediamine molecules [23]. Recently, the synthesis of Cu₂SbS₃·0.5en containing Cu^I/Cu^{II} and a non-protonated ethylenediamine molecule was reported [24]. The occurrence of Cu^I/Cu^{II} was established by magnetic susceptibility data yielding an effective magnetic moment per copper atom of 0.94(6) μ_B [24]. On the other hand in the new thioantimonate(III) [C₄H₁₂N₂]_{0.5}[CuSb₆S₁₀] only Cu^I and a fully protonated amine were observed [25]. The valence state has been verified by the diamagnetic behavior of the compound. Bond valence sums are consistent with the presence of Sb^{III} and Cu^I, requiring complete protonation of the amine [25]. In Na₂CuSbS₃ distorted trigonal planar Cu^IS₃ units and SbS₃ pyramids are interconnected to form two-dimensional anionic layers. Charge compensation is achieved by the Na⁺ cations [26].

We further explored the Cu–Sb–S system to prepare new compounds under solvothermal conditions applying different amines as solvents and as structure directing agents. In the contribution the syntheses, crystal structures, thermal stability, magnetic properties, and optical spectroscopy data of the three compounds (enH₂²⁺)_{0.5}Cu₂SbS₃ (**I**), (1,3-DAPH₂²⁺)_{0.5}Cu₂SbS₃ (**II**) and (1,4-DABH₂²⁺)_{0.5}Cu₂SbS₃ (**III**) are presented. The structure of the compound with ethylenediamine (en) which was published earlier [24] was re-determined in order to locate the hydrogen atoms at the organic cation.

Results and Discussion

The three compounds (enH₂²⁺)_{0.5}Cu₂SbS₃ (**I**), (1,3-DAPH₂²⁺)_{0.5}Cu₂SbS₃ (**II**) and (1,4-DABH₂²⁺)_{0.5}Cu₂SbS₃

(**III**) crystallize in the monoclinic space group P2₁/n with four formula units in the unit cell. In all compounds two crystallographically independent Cu atoms, one Sb atom and three S atoms are found which are all on general positions. The structures are composed of negatively charged [Cu₂SbS₃]⁻ layers separated by protonated amine molecules. The description of the structure base on compound **III** and can be applied to the other compounds because they all contain an identical topology of the CuSbS framework. The Cu(1) atom is trigonal coordinated by 3 S atoms with Cu–S distances between 2.276(2) Å and 2.328(2) Å and S–Cu(1)–S angles in the range from 114.15(6) $^\circ$ to 121.04(6) $^\circ$ (see Fig. 1: left). The Cu(1) atom is 0.266 Å (compound **I**: 0.156 Å; **II**: 0.167 Å) above the plane formed by the three S atoms in the Cu(1)S₃ moiety. At a far longer distance Cu(1) has another S(1) neighbor at 2.974(2) Å. Taking the long Cu–S distance into account a strongly distorted CuS₄ tetrahedron is formed. We note that the CuS₄ tetrahedra in Cu₁₂Sb₄S₁₃ are regular [19]. The environment of Cu(1) is completed by a Sb atom at a distance of 3.085(1) Å which is significantly larger than the Cu(2)–Sb separation (see below and Fig. 1). Such Cu–Sb contacts were also observed in Cu₂SbSe₃ [23]. The Cu(2) atom is also trigonal coordinated by S(1), S(2) and S(3) and is situated 0.547 Å (compound **I**: 0.588 Å; **II**: 0.533 Å) above the plane formed by the S atoms (Fig. 1: middle). The Cu(2)–S distances are in the range from 2.320(2) Å to 2.358(2) Å and the angles are between 104.07(6) $^\circ$ and 123.18(5) $^\circ$. We note that the Cu–S distances and the angles are both in close agreement with data published for Cu₂SbS₃, Cu₂SbS₃·0.5en and Cu₁₂Sb₄S₁₃ [16, 23, 19]. The Cu(2) atom has a short contact to the Sb atom of 2.701(9) Å and a short distance to Cu(1) of 2.638(1) Å, which is slightly longer than in Cu metal (2.556 Å). The Cu(1)–Cu(2) distance is longer than in other sulfides or selenides for which d¹⁰–d¹⁰ interactions were discussed [27].

Assuming that the electron lone pair of Sb^{III} is located opposite to the plane of the 3 S atoms which forms the base of the SbS₃ trigonal pyramid it points towards the Cu(1) atom. The Cu(2)–Sb distance is comparable with the Cu–Sb separations found in the alloys Cu₂Sb (2.625 – 2.835 Å) [28] and Cu₃Sb (2.731 – 2.919 Å) [29] as well as with Cu–Sb separations in Na₂CuSbS₃ of 2.808 Å [26] and in Cu₂SbS₃·0.5en [23]. With the Cu(1)–Cu(2) and Cu(2)–Sb contacts a Cu(1,2)SbS₃ unit may be identified which can be described as a distorted rectangular pyramid

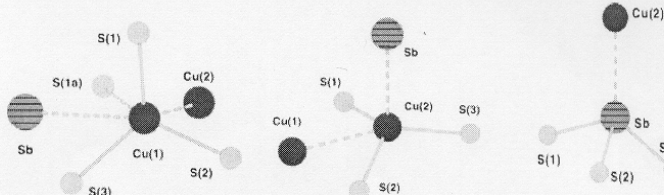


Fig. 1 Environment of Cu(1) (left), Cu(2) (middle) and Sb (right) with labelling. Dotted lines indicate long contacts.

Novel Copper(I)-Thioantimonates(III)

Table 1 Selected interatomic distances (in Å) and angles (in °) in the three compounds (enH_2^{2+})_{0.5} Cu_3Sb_3 (I), (1,3-DAPH₂₊)_{0.5} Cu_3Sb_3 (II) and (1,4-DABH₂₊)_{0.5} Cu_3Sb_3 (III). Estimated standard deviations are given in parentheses.

	I	II	III
Cu(1)			
$\text{Cu}(1)-\text{S}(1)^{[d]}$	2.266(1)	2.268(1)	2.276(2)
$\text{Cu}(1)-\text{S}(2)^{[e]}$	2.296(1)	2.303(1)	2.313(2)
$\text{Cu}(1)-\text{S}(3)$	2.317(1)	2.324(1)	2.328(2)
average	2.293	2.298	2.306
$\text{Cu}(1)-\text{Sb}$	3.096(1)	3.108(8)	3.085(1)
$\text{Cu}(1)-\text{S}(1a)$	3.094(2)	3.080(1)	2.974(2)
Cu(2)			
$\text{Cu}(2)-\text{S}(1)^{[b]}$	2.359(1)	2.351(1)	2.358(2)
$\text{Cu}(2)-\text{S}(2)^{[d]}$	2.320(1)	2.321(1)	2.320(2)
$\text{Cu}(2)-\text{S}(3)^{[a]}$	2.333(1)	2.329(1)	2.322(2)
Average	2.337	2.334	2.333
$\text{Cu}(2)-\text{Cu}(1)^{[b]}$	2.666(1)	2.643(1)	2.638(1)
$\text{Cu}(2)-\text{Sb}$	2.706(9)	2.741(7)	2.701(9)
Sb			
$\text{Sb}-\text{S}(1)$	2.445(1)	2.443(1)	2.437(1)
$\text{Sb}-\text{S}(2)$	2.450(1)	2.454(1)	2.463(1)
$\text{Sb}-\text{S}(3)$	2.425(1)	2.429(1)	2.430(1)
Average	2.440	2.442	2.443
S(1)			
$\text{S}(1)^{[d]}-\text{Cu}(1)-\text{S}(2)^{[e]}$	124.61(4)	122.96(4)	120.86(6)
$\text{S}(1)^{[d]}-\text{Cu}(1)-\text{S}(3)$	121.52(4)	122.66(4)	121.04(6)
$\text{S}(2)^{[e]}-\text{Cu}(1)-\text{S}(3)$	112.48(4)	112.79(4)	114.15(6)
$\text{S}(1)^{[d]}-\text{Cu}(1)-\text{Cu}(2)^{[e]}$	103.68(3)	104.65(4)	106.99(5)
$\text{S}(2)^{[e]}-\text{Cu}(1)-\text{Cu}(2)^{[e]}$	55.15(3)	55.47(3)	55.42(4)
$\text{S}(2)^{[d]}-\text{Cu}(2)-\text{S}(3)^{[a]}$	113.00(4)	114.14(4)	116.51(6)
$\text{S}(2)^{[d]}-\text{Cu}(2)-\text{S}(1)^{[b]}$	123.25(4)	125.11(4)	123.18(5)
$\text{S}(3)^{[a]}-\text{Cu}(2)-\text{S}(1)^{[b]}$	105.11(4)	105.28(4)	104.07(6)
$\text{S}(2)^{[d]}-\text{Cu}(2)-\text{Cu}(1)^{[b]}$	54.29(3)	54.82(3)	55.16(4)
$\text{S}(3)^{[a]}-\text{Cu}(2)-\text{Cu}(1)^{[b]}$	159.59(4)	161.33(4)	159.65(5)
$\text{S}(1)^{[b]}-\text{Cu}(2)-\text{Cu}(1)^{[b]}$	75.74(3)	75.90(3)	72.81(5)
$\text{S}(3)-\text{Sb}-\text{S}(1)$	101.00(4)	99.84(3)	100.16(5)
$\text{S}(3)-\text{Sb}-\text{S}(2)$	98.96(4)	98.21(4)	98.93(5)
$\text{S}(1)-\text{Sb}-\text{S}(2)$	99.09(4)	99.39(3)	99.50(5)
$\text{S}(3)-\text{Sb}-\text{Cu}(2)$	130.21(3)	131.77(3)	130.78(4)
$\text{S}(2)-\text{Sb}-\text{Cu}(2)$	112.11(3)	111.56(3)	114.09(4)
$\text{S}(1)-\text{Sb}-\text{Cu}(2)$	110.78(3)	111.07(3)	108.62(4)

Symmetry codes: ^[a] 0.5+x, 1.5-y, 0.5+z; ^[b] -0.5+x, 1.5-y, 0.5 + z; ^[c] 0.5+x, 1.5-y, -0.5+z; ^[d] 0.5+x, 1.5-y, -0.5+z; ^[e] x, y, -1 + z.

with S(1–3) and Cu(1) forming the basal plane (see Fig. 1: middle).

The Sb atom is surrounded by 3 S atoms with Sb–S bond lengths between 2.430(1) Å and 2.463(1) Å and S–Sb–S angles ranging from 98.93(5)° to 100.16(5)° (Fig. 1: right). These values are typical for the well known trigonal pyramidal SbS₃ units and demonstrate the presence of the stereochemically active lone pair [18, 22, 23, 24, 30]. The environment of Sb is completed by the contact to Cu(2) yielding a distorted tetrahedron (see above and Fig. 1: right).

The SbS₃ unit is connected to six CuS₃ moieties (3 × Cu(1) and 3 × Cu(2)) and every S atom has bonds to one Sb atom and to two Cu atoms (Fig. 2). Further interconnection leads to the formation of ten-membered (10 MR) Cu₃Sb₂S₃ and six-membered (6 MR) Cu₂SbS₃ rings. Every 10 MR is condensed to four 10 MR and four 6 MR to form a single layer within the (010) plane (Fig. 3: left). Two such single layers are connected into the final [Cu₂SbS₃]⁻ layered anion and due to the 2₁ screw axis and the n glide plane

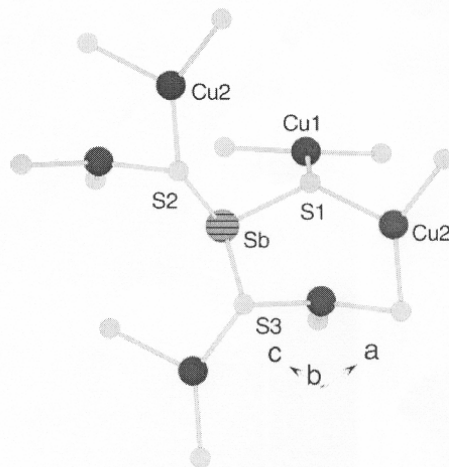


Fig. 2 The SbS₃ pyramid connecting the CuS₃ moieties.

the 6 MR are above and below the 10 MR (Fig. 3: right). In the description of the interconnection of the SbS₃ pyramids and the CuS₃ units Cu–Cu and Cu–Sb contacts were neglected. The anionic layers are stacked perpendicular to the crystallographic b-axis (Fig. 4).

Charge compensation requires that the amine molecules are diprotonated. The H atoms in I could be located in a difference Fourier map whereas for II and III the partial disorder of the organic molecules prevented the localization of the H atoms. However, in the IR spectra the absorptions located at 1555, 2000 and 2500 cm⁻¹ are typical for R-NH₃⁺ species. The cations are located between the layers and N–S distances are indicative for N–H···S hydrogen bonds (see Fig. 4 and Table 2). In the three compounds the protonated amines are not parallel to the anionic layers and a sandwich-like arrangement is formed (Fig. 4). The shortest interlayer separations amount to 4.426(4) Å, 5.986(1) Å, and 5.931(1) Å for I, II and III respectively. Despite the larger number of C atoms of the amine in III the interlayer distances is shorter than in II. Analyzing the orientation of the NH₃ groups with respect to the inorganic layers the N atoms sit above a triangle of S atoms which are members the 10 MR. This arrangement seems to favor the formation of N–H···S bonds. We note that the decrease of the interlayer spacing going from II to III is accompanied by a shortening of the crystallographic b axis and the monoclinic angle becomes less obtuse (Table 4). For many host lattices like TaS₂ or vermiculites the layer expansion is independent from the number of C atoms for alkyl chains with less than 6 C atoms [31].

The interlayer distances for Cu₂SbSe₃·0.5en, Cu₂SbSe₃·en and Cu₂SbSe₃·0.5en are about 5 Å, 6.8 Å and approximately 5 Å respectively [23, 24]. Interestingly, in Cu₂SbSe₃·en the

V. Spetzler, H. Rijnberk, C. Näther, W. Bensch

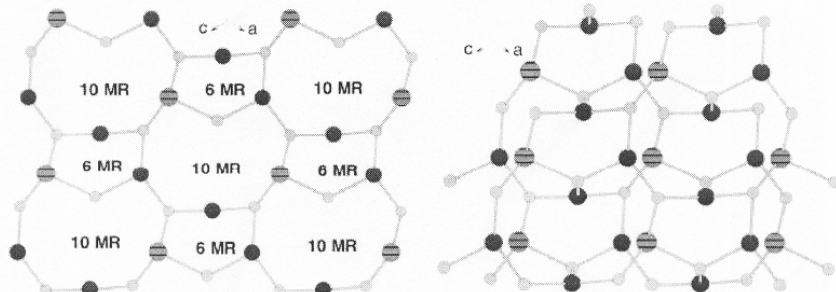
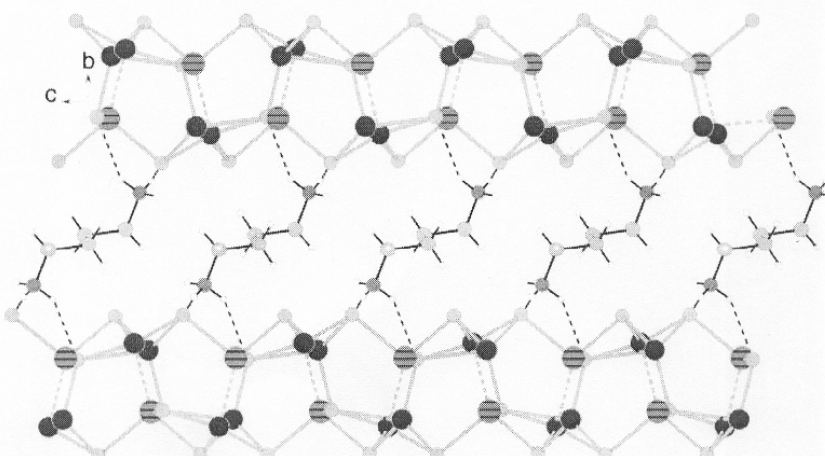


Fig. 3 Formation of the six (6 MR) and ten (10 MR) membered heterorings (left) and location of the 6 MR above the 10 MR (right).

Fig. 4 Arrangement of the $(\text{Cu}_2\text{SbS}_3)^-$ layers and the $(1,4\text{-DABH}_2^{2+})$ cations in the crystal structure of $(1,4\text{-DABH}_2^{2+})_{0.5}\text{Cu}_2\text{SbS}_3$ (III) (Possible hydrogen bonds are indicated as dotted lines; disorder of the organic cations is deleted for clarity).**Table 2** Intermolecular N···S distances (in Å) in $(\text{enH}_2^{2+})_{0.5}\text{Cu}_2\text{SbS}_3$ (**I**), $(1,3\text{-DAPH}_2^{2+})_{0.5}\text{Cu}_2\text{SbS}_3$ (**II**) and $(1,4\text{-DABH}_2^{2+})_{0.5}\text{Cu}_2\text{SbS}_3$ (**III**).

	I	II	III
N···S	3.262 (S1)	3.332 (S2)	3.367 (S2)
	3.340 (S3)	3.471 (S2)	3.159 (S1)
	3.334 (S2)	3.377 (S3)	3.343 (S2)
			3.402 (S3)

Table 3 Long Sb–S distances (in Å) in $(\text{enH}_2^{2+})_{0.5}\text{Cu}_2\text{SbS}_3$ (**I**), $(1,3\text{-DAPH}_2^{2+})_{0.5}\text{Cu}_2\text{SbS}_3$ (**II**) and $(1,4\text{-DABH}_2^{2+})_{0.5}\text{Cu}_2\text{SbS}_3$ (**III**). Estimated standard deviations are given in parentheses.

	I	II	III
Sb–S(1a) ^[d]	3.754(2)	3.720(1)	3.780(1)
Sb–S(1b) ^[b]	3.868(1)	3.863(1)	3.755(2)
Sb–S(1c) ^[c]	3.882(1)	3.909(1)	3.979(2)
Sb–S(3a) ^[a]	3.852(1)	3.866(1)	3.883(2)

Symmetry codes: ^[a] 0.5+x, 1.5-y, 0.5+z; ^[b] -0.5+x, 1.5-y, 0.5+z; ^[c] 0.5+x, 1.5-y, -0.5+z (see Table 1) and ^[d] -1+x, y, z;

en molecules are approximately perpendicular to the layers leading to the large interlayer distance [23]. The Sb^{III} atom has four next-nearest S neighbors (Table 3) with Sb–S distances between about 3.7 and 4 Å. These Sb–S separations are just in the range for the sum of the van der Waals radii of Sb^{III} and S²⁻.

A comparison of the geometrical parameters of the three compounds reveals small differences suggesting that the or-

ganic structure directing molecules have a moderately influence onto the bonding properties within the inorganic layers and the inorganic part is flexible enough to accommodate the requirements of the amines (see data in Table 1). Some tendencies should be shortly highlighted. The average <Cu(1)–S> bond length increases from en **I** to the

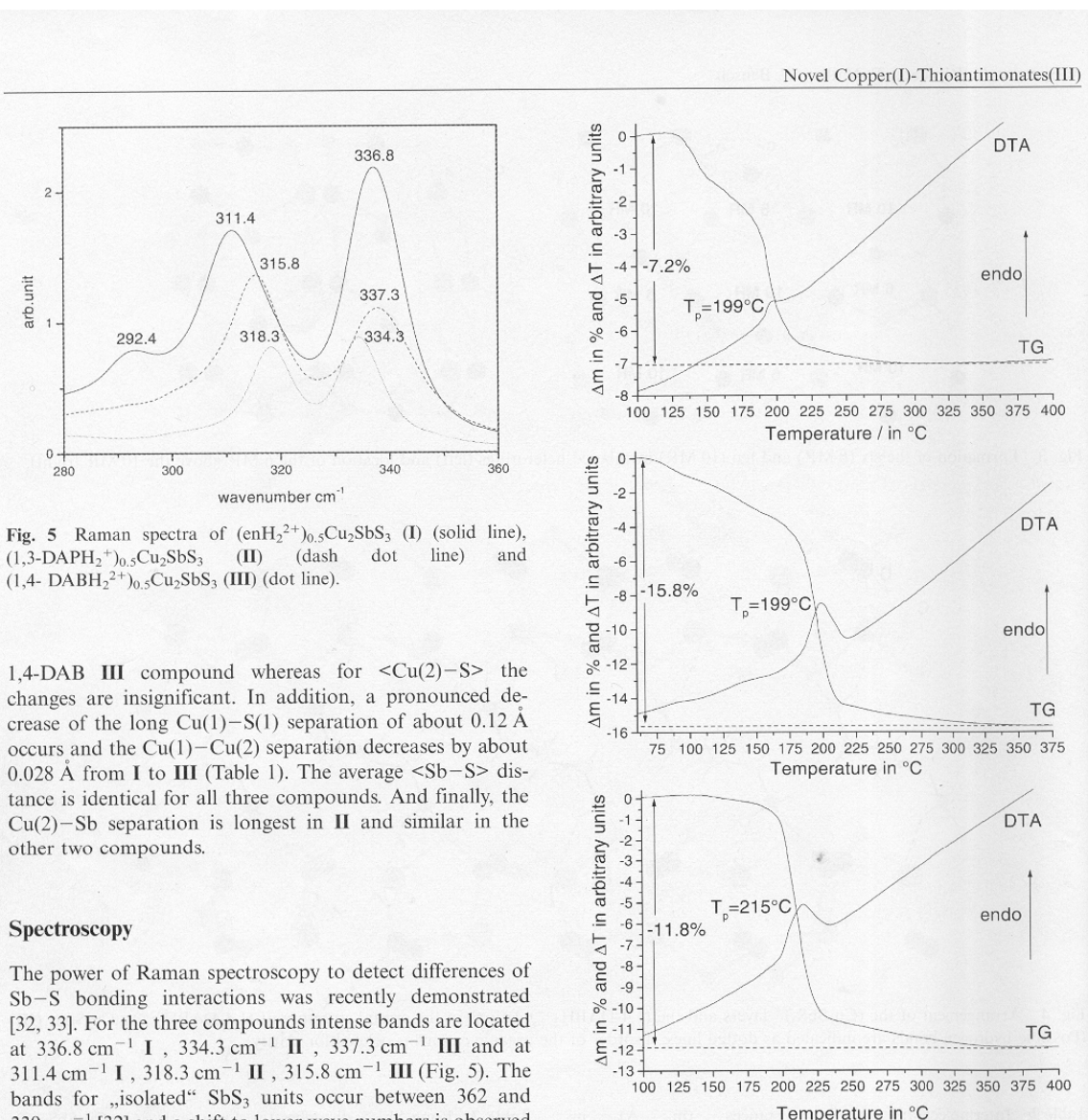


Fig. 5 Raman spectra of $(\text{enH}_2^{2+})_{0.5}\text{Cu}_2\text{SbS}_3$ (**I**) (solid line), $(1,3\text{-DAPH}_2^{+})_{0.5}\text{Cu}_2\text{SbS}_3$ (**II**) (dash dot line) and $(1,4\text{-DABH}_2^{+})_{0.5}\text{Cu}_2\text{SbS}_3$ (**III**) (dot line).

1,4-DAB **III** compound whereas for $\langle \text{Cu}(2)\text{--S} \rangle$ the changes are insignificant. In addition, a pronounced decrease of the long Cu(1)–S(1) separation of about 0.12 \AA occurs and the Cu(1)–Cu(2) separation decreases by about 0.028 \AA from **I** to **III** (Table 1). The average $\langle \text{Sb--S} \rangle$ distance is identical for all three compounds. And finally, the Cu(2)–Sb separation is longest in **II** and similar in the other two compounds.

Spectroscopy

The power of Raman spectroscopy to detect differences of Sb–S bonding interactions was recently demonstrated [32, 33]. For the three compounds intense bands are located at 336.8 cm^{-1} **I**, 334.3 cm^{-1} **II**, 337.3 cm^{-1} **III** and at 311.4 cm^{-1} **I**, 318.3 cm^{-1} **II**, 315.8 cm^{-1} **III** (Fig. 5). The bands for „isolated“ SbS_3 units occur between 362 and 339 cm^{-1} [32] and a shift to lower wave numbers is observed due to bonding interactions between Sb^{III} and the next nearest S atoms [32, 33]. In the present compounds the Sb^{III} atom has a 3+4 environment and the resonances are shifted to about 335 and 315 cm^{-1} . The Sb–S modes occur at different frequencies for compounds **I** to **III** reflecting the slightly different Sb–S bonding interaction in the three compounds. We note that for Cu_3SbS_3 with Sb in a 3+5 environment of S atoms the bands are observed at even lower wave numbers, i.e. at 321 and 290 cm^{-1} [32] and in MnSb_2S_4 the resonances are at 300 and 283 cm^{-1} [33]. In the latter compound the coordination of the two crystallographically distinct Sb^{III} atoms were described as 3+2+1 and 3+2+2 [33].

The optical band gaps were determined from transformed UV-VIS spectra in the usual way. The values of 1.9 eV **I**, 2.1 eV **II** and 1.9 eV **III** confirm the semiconducting nature of the three compounds.

Thermal Investigations

The thermal stability was investigated with differential thermal analysis (DTA) and thermogravimetry (TG). The DTA-TG curves are shown in Figure 6. The compounds **I** and **II** start to decompose at relatively low temperatures ($T_{\text{onset}} = 135\text{ }^\circ\text{C}$ **I** and $132\text{ }^\circ\text{C}$ **II**) with weight losses proceeding in two not well resolved steps. Endothermic signals occur at $T_p = 199\text{ }^\circ\text{C}$ for **I** and (see Fig. 6: top). The total mass loss at the end of the experiment ($T = 350\text{ }^\circ\text{C}$) is 7.2% for **I** being in rough agreement with the removal of 0.5 en molecules (calculated: 7.6%). The elemental analysis of the gray residue shows that C and N are still present (C: 1.3% , N: 0.4%). In the X-ray powder pattern of the residue,

V. Spetzler, H. Rijnberk, C. Näther, W. Bensch

CuSbS_2 and Cu_3SbS_4 could be identified. In a second run the thermal decomposition was stopped at 170 °C. Interestingly, in the X-ray powder pattern of this decomposition product only reflections of elemental Sb could be identified. The strong modulation of the background is due to the presence of an amorphous intermediate. When the reaction was stopped at 210 °C reflections of the two compounds CuSbS_2 and Cu_3SbS_4 are seen. No changes occur in the powder pattern when the temperature is raised to 350 °C.

For **II** the experimental mass loss of 15.8 % is about 2 % lower than expected for the complete removal of 1,3-diaminopropane (calculated: 17.8 %) (Fig. 6: middle). In the dark gray residue only small amounts of C and N are found (C: 0.5 %, N: 0.1 %). In the X-ray powder pattern of the thermal decomposition product again reflections of CuSbS_2 and Cu_3SbS_4 were seen. Compound **III** seems to be more stable because decomposition starts at a higher temperature of $T_{\text{onset}} = 200$ °C (Fig. 6: bottom) and only one endothermic event at $T_p = 215$ °C is seen. Until 350 °C the mass loss is 11.8 % which is larger than calculated for the removal of 0.5 1,4-diaminobutane molecules (calculated: 10.4 %). In the dark gray residue no C, N and H could be detected. The X-ray powder pattern shows the same products as found in the decomposition product of compound **II**.

The results of the thermal decomposition reactions are of special interest. In the residues of all three compounds Sb is in the oxidation states +III and +V. An amorphous intermediate together with elemental Sb occur when the reaction is stopped after the first event, at least for compound **I**. Hence, even in the first step a redox reaction leads to the formation of elemental Sb. Raising the temperature another redox reaction must occur yielding the two final products CuSbS_2 and Cu_3SbS_4 .

Magnetic properties

The temperature dependence of the magnetic susceptibilities of compounds **I** and **II** are displayed in Fig. 7. Down to about 40 K both compounds are diamagnetic and the paramagnetic tail at the lowest temperatures may be caused by impurities which could not be detected in the X-ray powder patterns of the samples. The diamagnetic behavior is a good hint that the Cu atoms are monovalent in the two compounds.

Summary

In the copper(I)-thioantimonate(III) compounds double layers are formed by the interconnection of SbS_3 pyramids and CuS_3 entities. The protonated amines are sandwiched by the double layers and the compounds may be regarded as inorganic-organic hybrids. Within the double layers short Cu–Cu and Cu–Sb separations are remarkable which may play an important role for the stability of the compounds. The amines only slightly influence the bonding interactions within the inorganic framework. The interlayer separation is not a linear function of the size/chain length of the amine

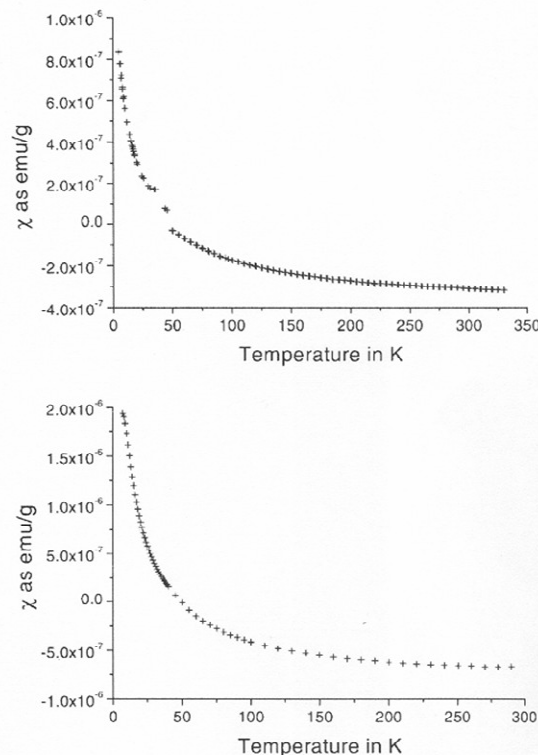


Fig. 7 Magnetic susceptibilities of $(1,3\text{-DAPH}_2^+)_0.5\text{Cu}_2\text{SbS}_3$ (**II**) (top) and of $(\text{enH}_2^+)_0.5\text{Cu}_2\text{SbS}_3$ (**I**) (bottom).

but is also determined by the relative orientation of the amine molecules with respect to the inorganic layers. Syntheses with amines having more than 4 C atoms are under way to prepare compounds which may be described as “pillared” inorganic-organic hybrids. Further theoretical studies should help to understand how the short distances must be interpreted in terms of chemical bonding.

Experimental

Synthesis and characterization

The three compounds $(\text{enH}_2^{2+})_0.5\text{Cu}_2\text{SbS}_3$ (**I**), $(1,3\text{-DAPH}_2^+)_0.5\text{Cu}_2\text{SbS}_3$ (**II**) and $(1,4\text{-DABH}_2^{2+})_0.5\text{Cu}_2\text{SbS}_3$ (**III**) were prepared under solvothermal conditions in a Teflon-lined steel autoclave. For **I** a mixture of $\text{CuCl}_2 \cdot 2\text{H}_2\text{O}$ (2 mmol), Sb_2S_3 (2 mmol), S (5 mmol) and 5 ml ethylenediamine was heated at 393 K for 6 days followed by cooling to room temperature. The same molar ratio was applied for the other two compounds applying 5 ml 1,3-diaminopropane respectively 5 ml 1,4-diaminobutane. The products were collected by filtration and washed with deionised water and ethanol. The yield of all products was between 80 and 90 % based on Cu. Compounds **I** and **II** consist of orange needle-like crystals, whereas **III**

Novel Copper(I)-Thioantimonates(III)

Table 4 Details of the data collections and selected refinement results for $(\text{enH}_2^{2+})_{0.5}\text{Cu}_2\text{SbS}_3$ (**I**), $(1,3\text{-DAPH}_2^{2+})_{0.5}\text{Cu}_2\text{SbS}_3$ (**II**) and $(1,4\text{-DABH}_2^{2+})_{0.5}\text{Cu}_2\text{SbS}_3$ (**III**).

	I	II	III
a / Å	6.173(2)	6.131(2)	6.159(2)
b / Å	18.657(5)	21.504(4)	21.254(3)
c / Å	6.502(2)	6.558(2)	6.544(2)
β / °	113.05(2)	113.01(1)	111.50(3)
V / Å ³	689.0(3)	795.9(2)	797.0(3)
Z	4	4	4
μ / mm ⁻¹	10.80	9.36	9.35
MW / g mol ⁻¹	375.59	382.61	389.62
Space group	P2 ₁ /n	P2 ₁ /n	P2 ₁ /n
ρ_{calc} / g cm ⁻³	3.621	3.193	3.247
2θ range / °	3-56	3-60	3-60
Data collected	2127	4183	4964
unique data	1666	2321	2297
R _{int}	0.0154	0.0213	0.0506
Data F ₀ > 4σ(F ₀)	1439	2034	1674
R1 for F ₀ > 4σ(F ₀)	0.0220	0.0277	0.0304
wR2 all reflections	0.0567	0.0796	0.0772
wR2 for F ₀ > 4σ(F ₀)	0.0549	0.0769	0.0683
δF(eÅ ⁻³)	0.78/-0.88	2.48/-0.83	1.31/-1.35

was obtained as brown tiny crystals. Elemental analysis: **I** found: C 32.5, H 0.98, N 2.89 %; calc.: C 2.99, H 0.98, N 3.38 %. **II** found: C 7.1; H 2.7; N 5.1; calc.: C 8.5, H 2.7, N 6.7 %. **III** found: C 6.0; H 1.6; N 3.3%; calc.: C 5.6, H 1.4, N 3.3 %.

Thermogravimetry analyses were performed using a Netzsch STA 429 DTA-TG device. The samples were heated in Al₂O₃ crucibles at a rate of 4 K min⁻¹ to 400 °C under a flow of argon of approximately 100 ml min⁻¹.

The Raman spectra were measured from 100 to 500 cm⁻¹ with a Bruker IFS 66 Fourier transform Raman spectrometer (wavelength: 514.5 nm, T = 20 K).

The X-ray intensity data were collected at 293 K using a Phillips PW 1100 (**I**), STOE AED 4 (**II**) and a NONIUS CAD4 (**III**) diffractometer with graphite monochromated MoK α radiation (λ = 0.71073 Å). The raw intensities were corrected for absorption effects. The structures were solved using SHELXS-97 [34]. Crystal structure refinements were done against F² with SHELXL-97 [35]. All non-hydrogen atoms were refined with anisotropic displacement parameters. The hydrogen atoms were positioned with idealized geometry and refined with fixed isotropic displacement parameters using a riding model. The amine molecules are partially disordered around the center of inversion and were refined using a split model. The site occupation factors were refined to 50:50 (C1:C1', C2:C2', and C3:C3') for **II** and to 26:74 (C2:C2') for **III**. We note that the lattice parameters of **I** are similar to that published in (24). Details of the data collections and refinement results are summarized in Table 4. Bond lengths and angles for all compounds are listed in Table 1.

Magnetic susceptibility measurements were performed on a MPMS SQUID (Quantum Design) and on a PPMS (Quantum Design) applying H = 1 T. For the diffuse reflectance measurements a Cary 5 Varian Techtron Pty. Darmstadt was used. Data were collected in the wavelength range 250 – 2000 nm. BaSO₄ was applied as a standard of 100 % reflectance.

Crystallographic data (excluding structure factors) for the structure reported in this paper have been deposited with the Cambridge Crystallographic Data Center as supplementary publication CCDC no. 216549, 216550, 216551. Copies of the data can be obtained free of charge on application to CCDC, 12 Union Road, Cam-

bridge CB2 1EZ, UK [Fax: +44-(0)1223-336-033 or email: deposit@ccdc.cam.ac.uk].

Acknowledgements. The financial support by the State of Schleswig-Holstein and the Deutsche Forschungsgemeinschaft (DFG) is gratefully acknowledged.

References

- [1] G. Dittmar, H. Schäfer, *Z. Anorg. Allg. Chem.* **1977**, *437*, 183.
- [2] H. A. Graf, H. Schäfer, *Z. Anorg. Allg. Chem.* **1975**, *414*, 220.
- [3] G. Dittmar, H. Schäfer, *Z. Anorg. Allg. Chem.* **1978**, *441*, 98.
- [4] B. Eisenmann, H. Schäfer, *Z. Naturforsch.* **1979**, *34b*, 383.
- [5] G. Cordier, H. Schäfer, C. Schwidetzky, *Z. Naturforsch.* **1984**, *39b*, 131.
- [6] K. Volk, P. Bickert, R. Kolmer, H. Schäfer, *Z. Naturforsch.* **1979**, *34b*, 380.
- [7] U. Müller, A. T. Mohammed, *Z. Anorg. Allg. Chem.* **1986**, *533*, 65.
- [8] B. F. Hoskins, E. R. T. Tiekkink, G. Winter, *Inorg. Chim. Acta* **1985**, *99*, 177.
- [9] M. Schur, W. Bensch, *Z. Anorg. Allg. Chem.* **1998**, *624*, 310.
- [10] H. Rijnberk, C. Näther, M. Schur, I. Jeß, W. Bensch, *Acta Crystallogr.* **1998**, *C54*, 920.
- [11] G. L. Schimek, J. W. Kolis, *Inorg. Chem.* **1997**, *36*, 1689.
- [12] K. Volk, H. Schäfer, *Z. Naturforsch.* **1979**, *34b*, 172.
- [13] J. B. Parise, *Science* **1991**, *251*, 293.
- [14] J. B. Parise, Y. Ko, *Chem. Mater.* **1992**, *4*, 1446.
- [15] R. M. Imamov, Z. G. Pinsker, A. I. Ivchenko, *Kristallografiya* **1964**, *9*, 853.
- [16] A. Pfitzner, *Z. Anorg. Allg. Chem.* **1994**, *620*, 1992.
- [17] A. Pfitzner, *Z. Kristallogr.* **1994**, *209*, 685.
- [18] A. F. Wells, *Structural Inorganic Chemistry*, 4. Auflage, Oxford University Press, London, **1975**, p.633.
- [19] B. J. Wuensch, *Z. Kristallogr.* **1964**, *119*, 437.
- [20] J. C. W. Folmer, F. Jellinek, *J. Less-common Met.* **1980**, *76*, 153.
- [21] J. C. W. Folmer, F. Jellinek, G. H. M. Calis, *J. Solid State Chem.* **1988**, *72*, 137.
- [22] J. Garin, E. Parthe, *Acta Crystallogr.* **1972**, *B28*, 3672.
- [23] Zh. Chen, R. E. Dillks, R.-J. Wang, J. Y. Lu, J. Li, *Chem. Mater.* **1998**, *10*, 3184.
- [24] A. V. Powell, S. Boissiere, A. M. Chippindale, *J. Chem. Soc., Dalton Trans.* **2000**, 4192.
- [25] A. V. Powell, R. Paniagua, P. Vaqueiro, A. M. Chippindale, *Chem. Mater.* **2002**, *14*, 1220.
- [26] E. Jerome, G. L. Schimek, G. W. Drake, J. W. Kolis, *Eur. J. Solid State Inorg. Chem.* **1996**, *33*, 765.
- [27] M. Jansen, *Angew. Chemie* **1987**, *99*, 1136; *Angew. Chem. Int. Ed. Engl.* **1987**, *26*, 1098.
- [28] W. B. Pearson, *Z. Kristallogr.* **1985**, *171*, 23.
- [29] E. Guenzel, K. Schubert, *Z. Metallk.* **1958**, *49*, 124.
- [30] H.-O. Stephan, M. G. Kanatzidis, *Inorg. Chem.* **1997**, *36*, 6050.
- [31] Intercalated Layered Materials, ed. F. A. Lévy, D. Reidel Publishing, Dordrecht, Boston, London, **1979**; A. Lerf in „Handbook of Nanostructured Materials and Nanotechnology“, ed. H. S. Nalaw, Vol. 5, Academic Press, **2000**.
- [32] A. Pfitzner, *Chem. Eur. J.* **1997**, *3*, 2032.
- [33] A. Pfitzner, D. Kurowski, *Z. Kristallogr.* **2000**, *215*, 373.
- [34] G. M. Sheldrick, *SHELXS-97*, Program for Crystal Structure Determination, University of Göttingen, Germany **1997**.
- [35] G. M. Sheldrick, *SHELXL-97*, Program for the Refinement of Crystal Structures, University of Göttingen, Germany **1997**.

3.4 Synthese und Struktur von Kupfer(I)-Thioantimonaten(III) mit den allgemeinen Formeln RCu_2SbS_3 und $\text{RCu}_3\text{Sb}_2\text{S}_5$ ($\text{R} = \text{Amin}$)

Die fünf Verbindungen $(\text{C}_6\text{N}_2\text{H}_{18})_{0.5}\text{Cu}_2\text{SbS}_3$ (**I**) [$\text{C}_6\text{N}_2\text{H}_{16}$ = 1,6-Diaminohexan], $(\text{C}_4\text{N}_3\text{H}_{15})_{0.5}\text{Cu}_2\text{SbS}_3$ (**II**) [$\text{C}_4\text{N}_3\text{H}_{13}$ = Diethylentriamin], $(\text{C}_8\text{N}_4\text{H}_{22})_{0.5}\text{Cu}_2\text{SbS}_3$ (**III**) [$\text{C}_8\text{N}_4\text{H}_{20}$ = 1,4-bis(2-aminoethyl)-Piperazin], $(\text{C}_4\text{N}_3\text{H}_{14})\text{Cu}_3\text{Sb}_2\text{S}_5$ (**IV**) [$\text{C}_4\text{N}_3\text{H}_{13}$ = Diethylentriamin] und $(\text{C}_6\text{N}_4\text{H}_{20})_{0.5}\text{Cu}_3\text{Sb}_2\text{S}_5$ (**V**) [$\text{C}_6\text{N}_4\text{H}_{18}$ = Triethylentetramin] wurden mit den Edukten Cu, Sb und S im Molverhältnis 2:2:5 in 5 mL (**V**: 4 mL) des entsprechenden Amins bei 140 °C nach 7 (**V**: 9) Tagen erhalten. Die Verbindungen RCu_2SbS_3 (**I-III**) kristallisieren als orange nadelförmige Kristalle in der Raumgruppe $\text{P}2_1/n$ und sind „isostrukturell“ zu den Verbindungen $(\text{enH}_2)_{0.5}\text{Cu}_2\text{SbS}_3$ ($\text{en} = \text{Ethylendiamin}$), $(1,3-\text{DAPH}_2)_{0.5}\text{Cu}_2\text{SbS}_3$ ($1,3-\text{DAP} = 1,3\text{-Diaminopropan}$) und $(1,4-\text{DABH}_2)_{0.5}\text{Cu}_2\text{SbS}_3$ ($1,4-\text{DAB} = 1,4\text{-Diaminobutan}$).

Interessant ist, dass während der solvothermalen Synthese der Verbindung **III** Triethylentetramin (TETN) zum **1,4-bis(2-aminoethyl)-Piperazin** cyclisiert, wobei das im TETN zu 30% enthaltene TREN [tris(2-aminoethyl)amin = $\text{C}_6\text{N}_4\text{H}_{18}$] für diese Ringbildung verantwortlich sein könnte (Abb. 3.4.1).

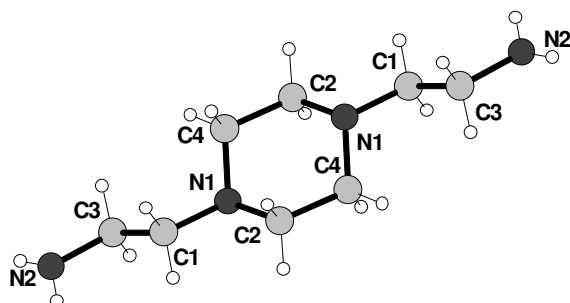


Abb. 3.4.1 1,4-bis(2-aminoethyl)-Piperazin

Die Verbindungen $\text{RCu}_3\text{Sb}_2\text{S}_5$ kristallisieren als rote Nadeln in der monoklinen bzw. triklinen Raumgruppe C2/c (**IV**) bzw. $\text{P}\bar{1}$ (**V**).

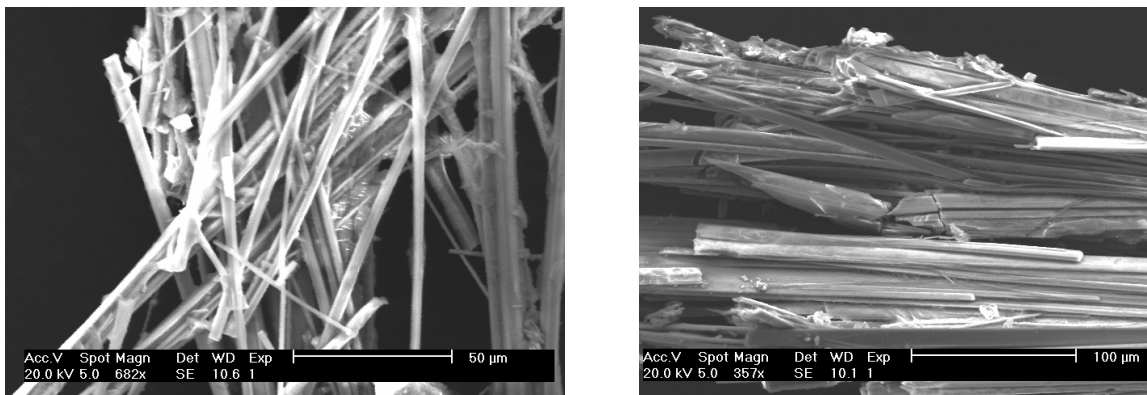


Abb. 3.4.2 SEM-Bilder von Kristallen der Verbindung **IV** (links) und **V** (rechts)

Für die beiden Verbindungen wird ein identisches Cu:Sb:S-Verhältnis gefunden, die Strukturen sind jedoch völlig verschiedenartig. In der Struktur von Verbindung **IV** werden als **primäre Baueinheiten** eine trigonal-pyramidal SbS₃- und eine SbS₄-Einheit, sowie ein CuS₄-Tetraeder und zwei trigonale CuS₃-Baugruppen gefunden. Die Struktur von Verbindung **V** wird von zwei trigonal-pyramidalen SbS₃- und zwei trigonalen CuS₃-Einheiten sowie einem CuS₄-Tetraeder aufgebaut (Abb. 3.4.3).

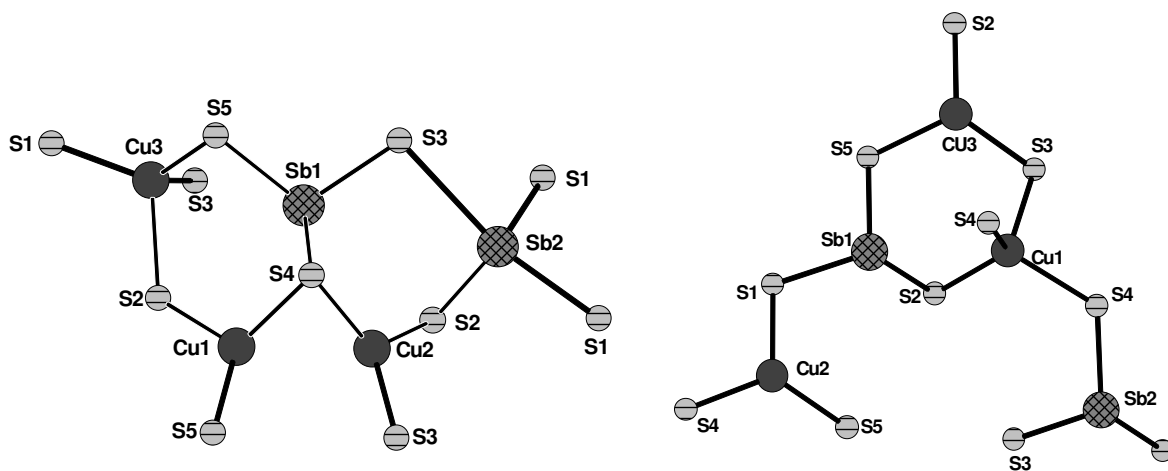


Abb. 3.4.3 Die primären Baueinheiten in den Strukturen der Verbindungen **IV** (links) und **V** (rechts)

In der Struktur von $(C_4N_3H_{14})Cu_3Sb_2S_5$ (**IV**) führt die Verknüpfung der primären Baueinheiten zur Bildung von vier verschiedenen Sechsringen (6 MR, A, B, C, D) und einem Zehnerring (10 MR). Diese 6 MR und 10 MR sind aneinander kondensiert und bilden eine wellenartige $(Cu_3Sb_2S_5^-)$ -**Einfachschicht**. Entlang [010] wird für diese Ringe die Abfolge ...A – B – C – D – 10 MR – 10 MR – A – B – C – D... beobachtet. In der Richtung [001] sind die 10 MR aneinander gebunden und die 6 MR weisen in diese Richtung die Sequenz ...A – D – A – D... und ...B – C – B – C... auf. Die Einfachschicht wird über ein S-Atom des CuS₄-Tetraeders zu einer **Doppelschicht** verknüpft, wobei aus dem 10 MR ein neuer 6 MR und ein 4 MR generiert werden. Zwischen den Schichten in der (001)-Ebene befinden sich die organischen Kationen und der Interschichtabstand beträgt 6.184 Å.

Die Verknüpfung der **primären Baueinheiten** in der Verbindung **V** führt ausschließlich zu 6 MR, wobei die **Einfachschicht** aus fünf verschiedenen kondensierten Sechsringen in der Abfolge ...A – B – C – D – E – A... gebildet wird. Zwei solcher Schichten sind über Cu(1)-S(4)-Bindungen zu **Doppelschichten** verknüpft. Da in den Schichten nur Sechsringe vorliegen, können diese als anorganische graphitähnliche oder 6³-Netze beschrieben werden.

Auch bei dieser Verbindung liegt eine sandwichartige Abfolge von anionischen Schichten und Kationen vor, und der kürzeste Interschichtabstand beträgt 6.44 Å.

In den **Ramanspektren** sind Resonanzen zwischen 309 und 340 cm⁻¹ zu beobachten, welche den Moden der SbS-Einheiten zuzuordnen sind.

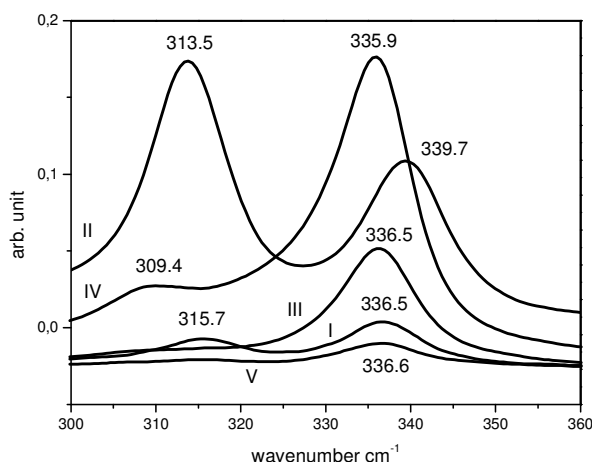


Abb. 3.4.4 Ramanspektren der Verbindungen I-V

Dabei liegen die Resonanzen für die trigonalen SbS_3 -Pyramiden zwischen 362 cm^{-1} und 339 cm^{-1} , während die Banden mit niedrigerer Wellenzahl auf sekundäre Bindung von Sb(III) zu den nächsten S-Nachbarn hinweisen [90, 91] (Abb. 3.4.4).

Die **thermische Zersetzung** der Verbindungen I–V beginnt bei unterschiedlichen Temperaturen, was vorsichtige Rückschlüsse auf die Stabilität der einzelnen Verbindungen zulässt. Verbindung I scheint mit der Zersetzungstemperatur von 201°C am stabilsten zu sein. Der experimentell bestimmte Massenverlust liegt um 1% höher als der theoretisch berechnete Wert ($-\Delta m_{\text{exp.}} = 15.9\%$, $-\Delta m_{\text{theo.}} = 14.9\%$) und erfolgt in einem Schritt (Abb. 3.4.5).

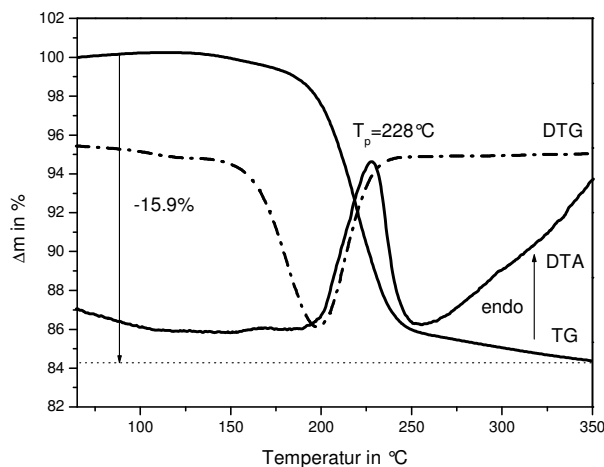


Abb. 3.4.5 TG-DTG-DTA-Kurven der Verbindung $(\text{C}_6\text{N}_2\text{H}_{18})_{0.5}\text{Cu}_2\text{SbS}_3$ (I)

Die TG-DTG-DTA-Kurven der Verbindungen II und III weisen auf wesentlich kompliziertere Zersetzungsreaktionen hin. Die Emission des Amins erfolgt jeweils in zwei Schritten ab 100 (II) bzw. 60 °C (III), was auf eine geringere thermische Stabilität der Verbindungen hinweist. Die experimentell bestimmten Massenverluste entsprechen annähernd den berechneten Werten II ($-\Delta m_{\text{exp.}} = 15.1\%$, $-\Delta m_{\text{theo.}} = 14.8\%$), III ($-\Delta m_{\text{exp.}} = 10.4\%$, $-\Delta m_{\text{theo.}} = 11.6\%$) (Abb. 3.4.6).

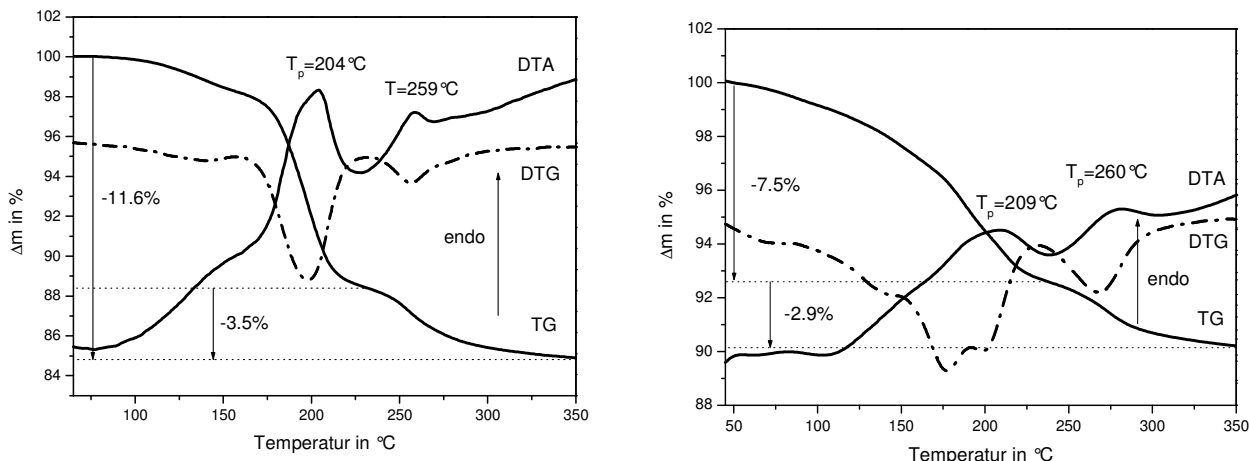


Abb. 3.4.6 TG-DTG-DTA-Kurven der Verbindungen $(C_4N_3H_{15})_{0.5}Cu_2SbS_3$ (II) (links) und $(C_8N_4H_{22})_{0.5}Cu_2SbS_3$ (III) (rechts)

Die thermische Zersetzung von **IV** beginnt bei 80°C und die von **V** bei 150°C (Abb. 3.4.7) und der Prozeß ist jeweils erst bei ca. 450°C abgeschlossen. In Verbindung **V** zeigt die DTG-Kurve zwei Schritte für den Massenverlust an, während die Situation für **IV** weniger deutlich ist. Die experimentell bestimmten Werte für die Emission der Amine entsprechen nahezu den berechneten Werten **IV** ($-\Delta m_{\text{exp.}} = 13.7\%$, $-\Delta m_{\text{theo.}} = 15.1\%$), **V** ($-\Delta m_{\text{exp.}} = 11.5\%$, $-\Delta m_{\text{theo.}} = 10.3\%$).

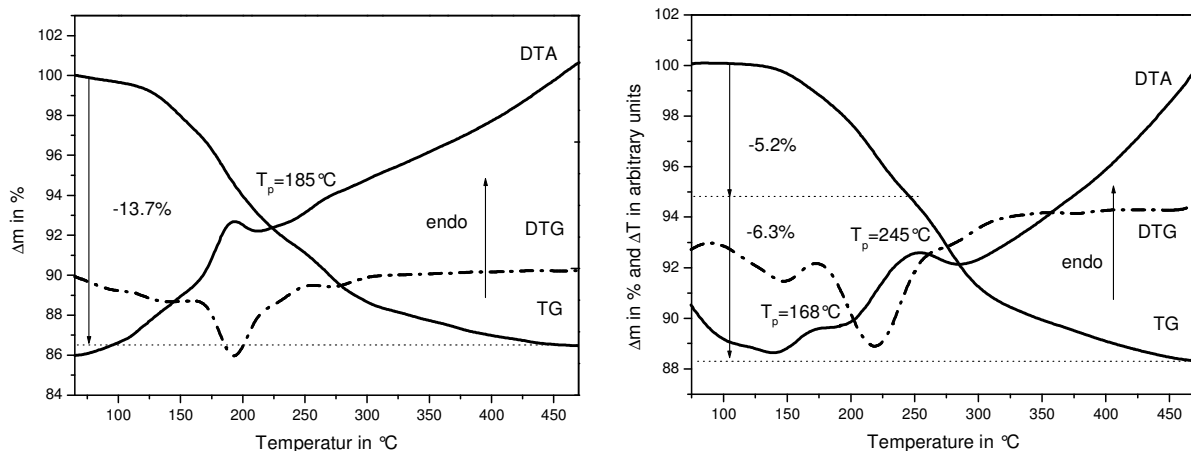


Abb. 3.4.7 TG-DTG-DTA-Kurven der Verbindungen $(C_4N_3H_{14})Cu_3Sb_2S_5$ (IV) (links) und $(C_6N_4H_{20})_{0.5}Cu_3Sb_2S_5$ (V) (rechts)

Als **Abbauprodukte** konnten CuSbS_2 und Cu_3SbS_4 (**I-III**) sowie CuSbS_2 und Cu_3SbS_3 (**IV, V**) in dem Pulverdiffraktogramm identifiziert werden.

Inorg. Chem. 2005, 44, 5805–5812



Template-Assisted Solvothermal Synthesis of Five Copper(I)–Thioantimonate(III) Composites: Crystal Structures and Optical and Thermal Properties of $(C_6N_2H_{18})_{0.5}Cu_2SbS_3$, $(C_4N_3H_{15})_{0.5}Cu_2SbS_3$, $(C_8N_4H_{22})_{0.5}Cu_2SbS_3$, $(C_4N_3H_{14})Cu_3Sb_2S_5$, and $(C_6N_4H_{20})_{0.5}Cu_3Sb_2S_5$

V. Spetzler, C. Näther, and W. Bensch*

Institut für Anorganische Chemie, Christian-Albrechts-Universität Kiel, Olshausenstrasse 40, D-24098 Kiel, Germany

Received February 4, 2005

The novel copper(I)–thioantimonates(III) $(C_6N_2H_{18})_{0.5}Cu_2SbS_3$ (I) ($C_6N_2H_{18}$ = 1,6-diaminohexane), $(C_4N_3H_{15})_{0.5}Cu_2SbS_3$ (II) ($C_4N_3H_{15}$ = diethylenetriamine), $(C_8N_4H_{22})_{0.5}Cu_2SbS_3$ (III) ($C_8N_4H_{22}$ = 1,4-bis(2-aminoethyl)piperazine), $(C_4N_3H_{14})Cu_3Sb_2S_5$ (IV) ($C_4N_3H_{14}$ = diethylenetriamine), and $(C_6N_4H_{20})_{0.5}Cu_3Sb_2S_5$ (V) ($C_6N_4H_{20}$ = triethylenetetramine) were synthesized under solvothermal conditions reacting Sb, Cu, and S with the amines. The compounds I–III belong to the RCu_2SbS_3 structure family (R = amine) and are built up of trigonal SbS_3 pyramids and two CuS_3 moieties forming 6-membered (6 MR) and 10-membered (10 MR) rings. The rings are condensed yielding single layers which are joined into $[Cu_2SbS_3]^-$ double layers via Cu–S bonds. The organic ions are located between the anionic layers, and the shortest interlayer distances are 7.8 Å (I), 7.4 Å (II), and 8.8 Å (III). The structure of the novel inorganic–organic hybrid compound IV contains one SbS_3 group, one SbS_4 unit, two CuS_3 triangles, and one CuS_4 tetrahedron. These units are joined into four-membered (4 MR) and six-membered rings (6 MR) forming a hitherto unknown strong undulated layered $(Cu_3Sb_2S_5)^-$ anion. Anions and cations are arranged in a sandwichlike manner with an interlayer distance of 6.184 Å. The new composite V contains an anion with the same chemical composition as compound IV, but the structure exhibits a unique and different network topology which is constructed by two SbS_3 pyramids, two CuS_3 triangles, and one CuS_4 tetrahedron. These units are joined into 6 MR which may be described as an inorganic graphene-like layer or as a 6^3 net. Two such layers are connected via Cu–S bonds into the final double layer. The interlayer distance amounts to 6.44 Å. All compounds decompose in a more or less complex manner when heated in an inert atmosphere.

Introduction

During the past decades a large number of thioantimonates(III) were synthesized under solvothermal conditions,^{1–17}

* Author to whom correspondence should be addressed. E-mail: wbensch@ac.uni-kiel.de.

- (1) Dittmar, G.; Schäfer, H. Z. Anorg. Allg. Chem. 1977, 437, 183–187.
- (2) Graf, H. A.; Schäfer, H. Z. Anorg. Allg. Chem. 1975, 414, 220–230.
- (3) Dittmar, G.; Schäfer, H. Z. Anorg. Allg. Chem. 1978, 441, 93–97.
- (4) Eisenmann, B.; Schäfer, H. Z. Naturforsch. 1979, 34b, 383–385.
- (5) Cordier, G.; Schäfer, H.; Schwidetzky, C. Z. Naturforsch. 1984, 39b, 131–134.
- (6) Volk, K.; Bickert, P.; Kolmer, R.; Schäfer, H. Z. Naturforsch. 1979, 34b, 380–382.
- (7) Wang, X.; Liebau, F. J. Solid State Chem. 1994, 111, 385–389.
- (8) Wang, X. Eur. J. Solid State Inorg. Chem. 1995, 32, 303–312.
- (9) Schur, M.; Bensch, W. Z. Anorg. Allg. Chem. 1998, 624, 310–314.

and in several compounds a transition metal ion (TM^{n+}) is part of the SbS_x network.^{18–33} The latter compounds exhibit

- (10) Rijnberk, H.; Näther, C.; Sciur, M.; Jess, I.; Bensch, W. Acta Crystallogr. 1998, C54, 920–923.
- (11) Schimek, G. L.; Kolis, J. W. Inorg. Chem. 1997, 36, 1689–1693.
- (12) Volk, K.; Schäfer, H. Z. Naturforsch. 1979, 34b, 172–175.
- (13) Parise, J. B. Science 1991, 251, 293–294.
- (14) Parise, J. B.; Ko, Y. Chem. Mater. 1992, 4, 1446–1450.
- (15) Wang, X.; Jacobson, A. J.; Liebau, F. J. Solid State Chem. 1998, 140, 387–395.
- (16) Wang, X.; Liu, L.; Jacobson, A. J. J. Solid State Chem. 2000, 155, 409–416.
- (17) Ko, Y.; Tan, K.; Parise, J. B.; Darovsky, A. Chem. Mater. 1996, 8, 493–496.
- (18) Stephan, H.-O.; Kanatzidis, M. G. Inorg. Chem. 1997, 36, 6050–6057.
- (19) Bensch, W.; Schur, M. Z. Naturforsch. 1997, 52b, 405–409.

Spetzler et al.

new network topologies and show different physical properties which are significantly different from the TM^{n+} free materials. A series of isostructural manganese thioantimonates(III) $\text{Mn}_2\text{Sb}_2\text{S}_5 \cdot \text{L}$ (L = methylamine, ethylamine, 1,3-diaminopropane, *N*-methyl-1,3-diaminopropane, diethylenetriamine) were synthesized and characterized in our group with Mn^{2+} being a part of the thioantimonate(III) network.^{25,31,32} Further examples are $[\text{Co}(\text{C}_6\text{H}_{18}\text{N}_4)]_2\text{Sb}_2\text{S}_8$ and $[\text{Co}(\text{C}_6\text{H}_{18}\text{N}_4)]_2\text{Sb}_2\text{S}_5$ with the anions bridging the $[\text{TML}_n]^{n+}$ (L = ligand) complexes.^{26,33} Copper–chalcogeno–antimonates(III) were reported in the past containing protonated or nonprotonated amines.^{27–30} In $\text{Cu}_2\text{SbS}_3 \cdot 0.5\text{en}$ (en = ethylenediamine),²⁷ $\text{Cu}_2\text{SbSe}_3 \cdot 0.5\text{en}$, and $\text{Cu}_2\text{SbSe}_3 \cdot \text{en}$ the existence of mixed-valent $\text{Cu}^{I/\text{II}}$ and nonprotonated ethylenediamine was postulated.²⁸ In $(\text{C}_4\text{H}_{12}\text{N}_2)_{0.5}\text{CuSb}_2\text{S}_{10}$,²⁹ ($\text{enH}_2\right)_{0.5}\text{Cu}_2\text{SbS}_3$, (1,3-DAPH₂)_{0.5} Cu_2SbS_3 (1,3-DAP = 1,3-diaminopropane), and (1,4-DABH₂)_{0.5} Cu_2SbS_3 (1,4-DAB = 1,4-diaminobutane) $\text{Cu}(\text{I})$ fully protonated amines are present.³⁰ In these compounds the anionic layers are separated by the amines. The interlayer separations depend on the size and packing of the different amines. Most of these inorganic–organic hybrid compounds show layered structures with a sandwichlike arrangement, which may be regarded as nanostructures.³⁴

In our continuing work we prepared new copper thioantimonates under solvothermal conditions applying different amines as solvents and as structure-directing agents. In this contribution the syntheses, crystal structures, thermal stability, and optical spectroscopy data for the compounds $(\text{C}_6\text{N}_2\text{H}_{18})_{0.5}\text{Cu}_2\text{SbS}_3$ (**I**), $(\text{C}_4\text{N}_3\text{H}_{15})_{0.5}\text{Cu}_2\text{SbS}_3$ (**II**), $(\text{C}_8\text{N}_4\text{H}_{22})_{0.5}\text{Cu}_2\text{SbS}_3$ (**III**), $(\text{C}_4\text{N}_3\text{H}_{14})\text{Cu}_3\text{Sb}_2\text{S}_5$ (**IV**), and $(\text{C}_6\text{N}_4\text{H}_{20})_{0.5}\text{Cu}_3\text{Sb}_2\text{S}_5$ (**V**) are presented. In addition, the structural and spectroscopic properties of compounds **I**–**III** are compared with those of the previously reported compounds ($\text{enH}_2\right)_{0.5}\text{Cu}_2\text{SbS}_3$ (**1**), (1,3-DAPH₂)_{0.5} Cu_2SbS_3 (1,3-DAP = 1,3-

diaminopropane) (**2**), and (1,4-DABH₂)_{0.5} Cu_2SbS_3 (**3**) (1,4-DAB = 1,4-diaminobutane).³⁰

Experimental Details

Syntheses. The five compounds $(\text{C}_6\text{N}_2\text{H}_{18})_{0.5}\text{Cu}_2\text{SbS}_3$ (**I**), $(\text{C}_4\text{N}_3\text{H}_{15})_{0.5}\text{Cu}_2\text{SbS}_3$ (**II**), $(\text{C}_8\text{N}_4\text{H}_{22})_{0.5}\text{Cu}_2\text{SbS}_3$ (**III**), $(\text{C}_4\text{N}_3\text{H}_{14})\text{Cu}_3\text{Sb}_2\text{S}_5$ (**IV**), and $(\text{C}_6\text{N}_4\text{H}_{20})_{0.5}\text{Cu}_3\text{Sb}_2\text{S}_5$ (**V**) were prepared under solvothermal conditions in Teflon-lined steel autoclaves. For **I**–**IV** a mixture of Cu (2 mmol), Sb (2 mmol), S (5 mmol), and 5 mL of 1,6-diaminohexane (**I**), 5 mL of diethylenetriamine (**II** and **IV**), and 5 mL of triethylenetetramine (70%) (**III**), respectively, was heated at 140 °C for 7 days followed by cooling to room temperature. For the synthesis of compound **V** the same mixture of elements was heated with 4 mL of triethylenetetramine (97%) at 140 °C for 9 days. The products were filtered off and washed with deionized water and dry acetone. Crystals were obtained with a yield of about 60% (**I**, **II**) and 30% (**III**) based on Cu. Compound **II** occurred always together with **IV** (<30%). The yield of compound **V** was between 50 and 60% based on Cu. In the product of **III** red needles were identified as $(\text{C}_6\text{N}_4\text{H}_{20})\text{Sb}_4\text{S}_7$ ($\text{C}_6\text{N}_4\text{H}_{20} =$ double protonated tris(2-aminoethyl)amine). Anal. Found (%) for **I**: C, 8.2; H, 2.04; N, 3.2. Calcd: C, 7.8; H, 1.9; N, 3.0. Found for **II**: C, 5.2; H, 1.4; N, 4.3. Calcd: C, 5.5; H, 1.5; N, 4.6. Found for **III**: C, 3.9; H, 0.91; N, 2.9. Calcd: C, 4.2; H, 1.1; N, 3.2. Found for **IV**: C, 6.6; H, 1.9; N, 5.7. Calcd: C, 6.9; H, 2.1; N, 5.9. Found for **V**: C, 4.8; H, 1.2; N, 3.6. Calcd: C, 4.9; H, 1.3; N, 4.0.

X-ray Scattering Studies. The X-ray intensity data were collected at 293 K using a NONIUS CAD4 for **I** and a STOE AED 4 diffractometer for **II**–**V** with graphite-monochromated Mo K α radiation ($\lambda = 0.710\text{73}\text{\AA}$). The raw intensities were treated in the normal way by applying a Lorentz–polarization correction. The data were also corrected for absorption effects. The structures were solved using SHELXS-97.³⁵ Crystal structure refinements were done against F^2 with SHELXL-97.³⁶ All non-hydrogen atoms were refined with anisotropic displacement parameters. The hydrogen atoms were positioned with idealized geometry and refined with fixed isotropic displacement parameters using a riding model. The amine molecules in **I** and **II** are partially disordered around a center of inversion and were refined using a split model. The site occupation factors were refined to 50:50 (C3:C3') for **I** and to 60:40 (C1:C1', C2:C2', N1:N1', and N2:N2') for **II**. In compounds **IV** and **V** the strong disorder of the amines prevented a successful refinement. Hence, the SQUEEZE option in the program package Platon was used to correct the structure factors.³⁷ Details of the data collections and refinement results are summarized in Table 1. Bond lengths and angles for all compounds are listed in Tables 2, 4, and 5.

Spectroscopy. The Raman spectra were measured from 100 to 500 cm^{-1} with a Bruker IFS 66 Fourier transform Raman spectrometer (wavelength, 514.5 nm; $T = 20$ K).

Thermoanalytical Investigations. Thermogravimetry analyses were performed using a Netzsch STA 429 DTA-TG device. The samples were heated in Al_2O_3 crucibles at a rate of 4 $\text{K} \cdot \text{min}^{-1}$ to 400 °C under a flow of argon of 100 mL min⁻¹.

Results and Discussion

The three compounds $(\text{C}_6\text{N}_2\text{H}_{18})_{0.5}\text{Cu}_2\text{SbS}_3$ (**I**) ($\text{C}_4\text{N}_3\text{H}_{15})_{0.5}\text{Cu}_2\text{SbS}_3$ (**II**), and $(\text{C}_8\text{N}_4\text{H}_{22})_{0.5}\text{Cu}_2\text{SbS}_3$ (**III**) crystallize in

(35) Sheldrick, G. M. *SHELXS-97, Program for Crystal Structure Solution*; University of Göttingen: Göttingen, Germany, 1997.

(36) Sheldrick, G. M. *SHELXL-97, Program for the Refinement of Crystal Structures*; University of Göttingen: Göttingen, Germany, 1997.

(37) Spek, A. L. *Platon for Windows*; Utrecht University: Utrecht, The Netherlands, 2000.

- (20) Kiebach, R.; Näther, C.; Bensch, W. *Z. Anorg. Allg. Chem.* **2002**, *628*, 2176–2181.
- (21) Stähler, R.; Bensch, W. *Eur. J. Inorg. Chem.* **2001**, *3073*–3078.
- (22) Stähler, R.; Näther, C.; Bensch, W. *Acta Crystallogr.* **2001**, *C57*, 26–27.
- (23) Stähler, R.; Bensch, W. *Z. Anorg. Allg. Chem.* **2002**, *628*, 1657–1662.
- (24) Schäfer, M.; Näther, N.; Bensch, W. *Solid State Sci.* **2003**, *5*, 1135–1139.
- (25) Engelke, L.; Stähler, R.; Schur, M.; Näther, C.; Bensch, W.; Pöttgen, R.; Möller, M. H. Z. *Naturforsch.* **2004**, *59b*, 869–876.
- (26) Schäfer, M.; Stähler, R.; Kiebach, W.-R.; Näther, C.; Bensch, W. *Z. Anorg. Allg. Chem.* **2004**, *630*, 1816–1822.
- (27) Powell, A. V.; Boissiere, S.; Chippindale, A. M. *J. Chem. Soc., Dalton Trans.* **2000**, 4192–4195.
- (28) Chen, Zh.; Dillks, R. E.; Wang, R.-J.; Lu, J. Y.; Li, J. *Chem. Mater.* **1998**, *10*, 3184–3188.
- (29) Powell, A. V.; Paniagua, R.; Vaqueiro, P.; Chippindale, A. M. *Chem. Mater.* **2002**, *14*, 1220–1224.
- (30) Spetzler, V.; Rijnberk, H.; Näther, C.; Bensch, W. *Z. Anorg. Allg. Chem.* **2004**, *630*, 142–148.
- (31) Bensch, W.; Schur, M. *Eur. J. Solid State Inorg. Chem.* **1996**, *33*, 1149–1160.
- (32) Schur, M.; Näther, C.; Bensch, W. *Z. Naturforsch.* **2001**, *56b*, 79–84.
- (33) Stähler, R.; Bensch, W. *J. Chem. Soc., Dalton Trans.* **2001**, 2518–2522.
- (34) Lerf, A. In *Handbook of Nanostructured Materials and Nanotechnology*; Nalwa, H. S., Ed.; Academic Press: New York, 2000; Vol. 5. Lerf, A. In *Intercalated Layered Materials*; Lévy, F. A., Ed.; D. Reidel Publishing: Dordrecht, Boston, London, 1979.

Copper(I)–Thioantimonate(III) Composites**Table 1.** Selected Crystallographic Data and Refinement Results for $(C_6N_2H_{18})_{0.5}Cu_2SbS_3$ (**I**), $(C_4N_3H_{15})_{0.5}Cu_2SbS_3$ (**II**), $(C_8N_4H_{22})_{0.5}Cu_2SbS_3$ (**III**), $(C_4N_3H_{14})Cu_3Sb_2S_5$ (**IV**), and $(C_6N_4H_{20})_{0.5}Cu_3Sb_2S_5$ (**V**)

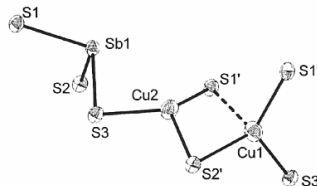
param	I	II	III	IV	V
$a/\text{\AA}$	6.1401(12)	6.1962(4)	6.1594(12)	23.6408(16)	6.3188(8)
$b/\text{\AA}$	24.7704(5)	22.4696(18)	27.4803(6)	20.4108(15)	9.9523(13)
$c/\text{\AA}$	6.5545(13)	6.5461(4)	6.5491(13)	6.4599(7)	11.3630(13)
α/deg					103.376(14)
β/deg	112.530(10)	112.47(6)	112.24(3)	100.153(7)	91.420(14)
γ/deg					108.340(14)
$V/\text{\AA}^3$	919.0 (2)	842.20(10)	1026.01(4)	3068.3(2)	656.19(14)
$d_{\text{calc}}/\text{g cm}^{-3}$	2.921	3.136	2.791		
cryst system	monoclinic	monoclinic	monoclinic	monoclinic	triclinic
space group	$P2_1/n$	$P2_1/n$	$P2_1/n$	$C2/c$	$P\bar{1}$
$2\theta/\text{deg}$	3–60	4–56	3–52	5–56	4–60
hkl range	$0 \leq h \leq 8$ $-32 \leq k \leq 32$ $-8 \leq l \leq 7$	$-8 \leq h \leq 8$ $-29 \leq k \leq 29$ $-8 \leq l \leq 8$	$-7 \leq h \leq 7$ $-33 \leq k \leq 33$ $-8 \leq l \leq 8$	$-31 \leq h \leq 31$ $-26 \leq k \leq 26$ $-8 \leq l \leq 8$	$-7 \leq h \leq 7$ $-11 \leq k \leq 10$ $-13 \leq l \leq 12$
no. colld reflens	4745	7739	7806	14 656	3714
no. unique reflens	2215	1954	1957	3587	2173
reflens $F_o > 4\sigma(F_o)$	2062	1691	1753	2624	1485
params	92	108	117	92	91
R1 ($F_o > 4\sigma(F_o)$)	0.0161	0.0299	0.0280	0.0407	0.0639
wR2 ($F_o > 4\sigma(F_o)$)	0.0395	0.0736	0.0689	0.0944	0.1623
R1 (all reflens)	0.0190	0.0371	0.0343	0.0609	0.0863
wR2 (all reflens)	0.0401	0.0766	0.0713	0.1002	0.1691
GOF	1.129	1.036	1.032	0.925	0.961
$\delta(F)/e \text{\AA}^{-3}$	0.532/–0.529	0.832/–1.839	0.73/–1.44	1.063/–1.272	2.448/–2.630

Table 2. Ranges of Interatomic Distances (Å) and Angles (deg) for $(C_6N_2H_{18})_{0.5}Cu_2SbS_3$ (**I**), $(C_4N_3H_{15})_{0.5}Cu_2SbS_3$ (**II**), and $(C_8N_4H_{22})_{0.5}Cu_2SbS_3$ (**III**) with Estimated Standard Deviations in Parentheses

	I	II	III
Cu(1)–S	2.271(1)–2.327(1)	2.280(1)–2.338(1)	2.277(1)–2.332(1)
Cu(2)–S	2.316(1)–2.367(1)	2.315(1)–2.361(1)	2.313(1)–2.358(1)
Sb–S	2.422(1)–2.450(1)	2.435(1)–2.459(1)	2.427(1)–2.454(1)
Cu–Sb	2.726(1)–3.075(1)	2.737(1)–3.094(1)	2.726(1)–3.086(1)
Cu(1)–S(1a)	2.954(2)	2.989(1)	2.977(1)
Cu(2)–Cu(1)	2.633(1)	2.646(1)	2.635(1)
S–Cu(1)–S	113.46(3)–122.32(2)	113.65(4)–122.19(5)	114.02(5)–121.25(5)
S–Cu(2)–S	105.33(2)–122.88(3)	105.83(5)–123.31(4)	105.41(5)–123.65(5)
S–Sb–S	98.08(2)–100.77(2)	98.24(4)–99.70(4)	98.69(4)–99.79(4)

the monoclinic space group $P2_1/n$ with four formula units in the unit cell, and they are isostructural with $(enH_2)_{0.5}Cu_2SbS_3$ (**I**), $(1,3\text{-DAPH}_2)_{0.5}Cu_2SbS_3$ ($1,3\text{-DAP} = 1,3\text{-diaminopropane}$) (**2**), and $(1,4\text{-DABH}_2)_{0.5}Cu_2SbS_3$ (**3**) ($1,4\text{-DAB} = 1,4\text{-diaminobutane}$).³⁰ Hence, the structure is only briefly discussed. In many thioantimonates(**III**) the Sb–S distances scatter from about 2.4 to 3.8 Å and a consistent assignment of the dimensionality depends on the cutoff chosen. In the present contribution the description of the structures is restricted to a cutoff for the Sb–S distances of about 3.1 Å. The primary building units (PBUs) in **I**–**III** are one trigonal SbS₃ pyramid and two CuS₃ moieties (Figure 1). The Sb–S bond lengths and S–Sb–S angles (see Table 2) are in the range found in many other thioantimonates(**III**).^{18–33} The Sb atom has a Cu(2) atom as the next-nearest neighbor (Table

2), and with this atom a distorted SbS₃Cu(2) tetrahedron is formed. The Cu(1) atom is located at the apex of a flat trigonal pyramid with 3 S atoms forming the basis of the pyramid (Figure 1) and is 0.2589 Å (**II**, 0.2447 Å; **III**, 0.2523 Å) above this plane. The Cu(1)–S bond lengths and S–Cu(1)–S angles (Table 2) are similar to the values observed for the other three isostructural compounds.³⁰ In **I**–**III** the Cu(1) atoms have an additional relatively long contact expanding the pyramid into a strongly distorted Cu(1)S₄ tetrahedron (Table 2, Figure 1). If the Sb atom is considered as another neighbor, a distorted rectangular Cu(1)SbS₄ pyramid may be identified (Figure 1). The Cu(2) atom is also in a trigonal environment of three S atoms and is situated 0.5405 Å (**I**) above the plane formed by the S atoms (0.5220 Å (**II**), 0.5281 Å (**III**)). The Cu(2)–S distances and the S–Cu(2)–S angles are in close agreement with data published for the compounds (**1**–**3**).³⁰ Cu(2) has an Sb and Cu(1) as next neighbors with a Cu–Cu distance which is slightly longer than in Cu metal (2.556 Å) or in other sulfides and selenides for which a d¹⁰–d¹⁰ interaction was discussed^{38,39} (see Figure 1 and Table 2). The Cu–Cu distances in oligomers and polymers are in some compounds about 0.2 Å shorter than in metallic Cu which was explained

**Figure 1.** Environment of Sb1, Cu1, and Cu2 in the crystal structure of compound **I**. (Dotted line indicates a long bond.) Displacement ellipsoids are drawn at the 60% probability level.

(38) Jansen, M. *Angew. Chem.* 1987, 99, 1136–1149.

(39) Merz, K. M.; Hoffmann, R., Jr. *Inorg. Chem.* 1988, 27, 2120–2127.

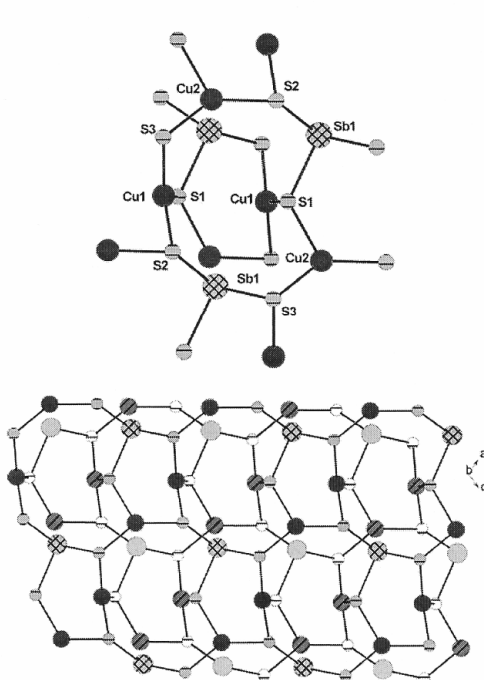


Figure 2. 10-membered ring 10 MR and the 6-membered ring 6 MR below the 10 MR in compounds **I–III** (top) and the interconnection of 10 MR and 6 MR into the final $[\text{CuSbS}_3]^-$ layer (bottom). Note that the Sb and S atoms of neighbored layers have a different color/shading.

by a mixing of 4s and 4p orbitals into 3d orbitals, converting repulsive d^{10} – d^{10} interactions into partial bonding.³⁹ A comparison of the geometrical parameters of the three compounds reveals only small differences (Table 2).

The connection of SbS_3 , $\text{Cu}(1)\text{S}_3$, and $\text{Cu}(2)\text{S}_3$ units yields 6-membered (6 MR) Cu_2SbS_3 rings and 10-membered rings (10 MR) $\text{Cu}_3\text{Sb}_2\text{S}_5$ (Figure 2, top). Every 10 MR is condensed to four 10 MR and four 6 MR to form a single layer within the (010) plane (Figure 2, bottom). Two such single layers are connected into the final $[\text{CuSbS}_3]^-$ layered anion, and due to the 2_1 screw axis and the n glide plane the 6 MR are above and below the 10 MR (Figure 2, bottom). In the description of the interconnection of the SbS_3 pyramids and the CuS_3 units Cu–Cu and Cu–Sb contacts were neglected. The Sb atom has four next-nearest S neighbors at distances in the range for the sum of the van der Waals radii of Sb and S.

The amines are located between successive anionic layers yielding a sandwichlike arrangement (Figure 3). Similar to the previously reported isostructural compounds (**1–3**) the NH_3 groups are oriented toward the $[\text{CuSbS}_3]^-$ layers achieving optimal S···H interactions (Table 3).

The interlayer distances are determined by the lengths of the amine molecules and their relative orientation with respect to the anionic layers. For $\text{Cu}_2\text{SbS}_3 \cdot 0.5\text{en}$ the separa-

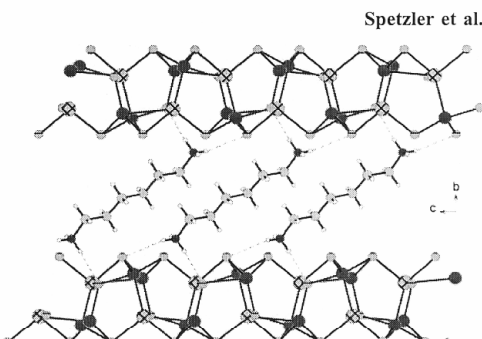


Figure 3. Crystal structure of compound **I** with view along the a -axis. (Intermolecular S–H bonds are indicated as dotted lines.)

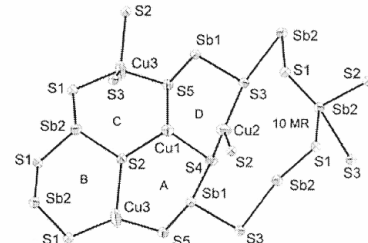


Figure 4. Crystal structure of compound **IV** with labeling showing the displacement ellipsoids are drawn on the 50% probability level. The letters identify the different heterorings discussed in the text.

Table 3. N···S Distances (Å) in $(\text{C}_6\text{N}_2\text{H}_{18})_{0.5}\text{Cu}_2\text{SbS}_3$ (**I**), $(\text{C}_6\text{N}_3\text{H}_{15})_{0.5}\text{Cu}_2\text{SbS}_3$ (**II**), and $(\text{C}_8\text{N}_4\text{H}_{22})_{0.5}\text{Cu}_2\text{SbS}_3$ (**III**)

	I	II	III
3.161 (S1)	3.158 (S1)	3.178 (S1)	
3.286 (S2)	3.329 (S2)	3.292 (S2)	
3.301 (S3)	3.401 (S3)	3.337 (S3)	

tion amounts to 5 Å.²⁷ For compounds (**1–3**) the values are 4.426(4), 5.986(1), and 5.931(1) Å, respectively.³⁰ In **I–III** the interlayer distances are 7.441(1), 7.446(2), and 8.842(5) Å. The increase of the interlayer spacing going from **I** to **III** is accompanied by a longer crystallographic b axis. The thickness of inorganic host lattices is often in the range from 3 to 10 Å, and the layer separations caused by intercalated species can vary from 3 to 50 Å. For instance, an interlayer distance of 56.1 Å was reported for $(\text{octadecylamine})_x\text{TaS}_2$. Such compounds belong to the so-called “nanostructured systems”,³⁴ and consequently, compounds **I–III** belong also to this type of materials.

An interesting observation is that triethylenetetramine (TETN) (**III**) cyclizes under the solvothermal conditions forming the protonated 1,4-bis(2-ammoniomethyl)piperazine cation. It is known that TETN decomposes under special synthetic conditions to form ethylenediamine and cyclized amines, including piperazine (pip).⁴⁰ Parise et al. reported the synthesis of $\text{Sb}_4\text{S}_7\text{N}_2\text{C}_4\text{H}_8$ with a piperazinium cation formed in-situ by applying TETN as solvent.⁴⁰ It is known that under pyrolytic conditions amines cyclize and form

(40) Parise, J. B. *Chem. Mater.* 1992, 4, 1446–1450.

Copper(I)–Thioantimonate(III) Composites**Table 4.** Ranges of Interatomic Distances (Å) and Angles (deg) for $(C_6N_3H_{14})Cu_3Sb_2S_5$ (**IV**) with Estimated Standard Deviations in Parentheses

Sb(1)–S	2.416(2)–2.450(2)
Sb(1)–Cu	2.927(1)–3.016(1)
Sb(2)–S	2.434(2)–3.037(1)
Cu(1)–S	2.290(2)–2.320(2)
Cu(2)–S	2.278(2)–2.336(2)
Cu(3)–S	2.290(2)–2.395(2)
Cu–Cu	2.622(1)–2.857(2)
S–Sb(1)–S	99.35(6)–104.11(6)
S–Sb(2)–S	87.73(5)–168.12(5)
S–Cu(1)–S	112.66(7)–120.84(7)
S–Cu(2)–S	113.92(8)–121.88(8)
S–Cu(3)–S	95.83(7)–124.39(8)

amines such as 1,4-bis(2-aminoethyl)piperazine.⁴⁰ We note that our TETN (70%) solution was a mixture with about 30% tris(2-aminoethyl)amine ($C_6N_4H_{18}$), which can be responsible for the ring formation too.

The new compound $(C_6N_3H_{14})Cu_3Sb_2S_5$ (**IV**) crystallizes in the monoclinic space group $C2/c$ with two unique Sb atoms, three independent Cu atoms, and 5 unique S atoms. Sb(1) is in a trigonal pyramidal environment of 3 S atoms, and Sb(2) is coordinated by four S atoms with two long and two short bonds (Figure 4, Table 4). The Sb(2) S_4 moiety may be described as trigonal bipyramidal considering the electron lone pair as a coordination site. In such Sb S_4 units the long Sb–S bonds are in trans position. Up to the sum of the van der Waals radii of Sb and S of about 3.80 Å Sb(1) has two additional S atoms and Sb(2) one S atom as neighbors. Cu(1) is surrounded by three S atoms and is situated 0.304 Å above the S_3 plane forming a trigonal Cu(1) S_3 moiety (Figure 4, Table 4). Two additional contacts to Sb(1) and Cu(2) are observed (Table 4), and the resulting coordination polyhedron may be described as a distorted rectangular pyramid like in the other compounds (see above³⁰). Cu(2) is also coordinated by three S atoms (Figure 4), but the Cu(2) S_3 group is more flat than Cu(1) S_3 with Cu(2) being 0.1858 Å above the plane formed by the three S atoms. There are additional contacts to Cu(1), Cu(3), and Sb(1) with a Cu(2)–Cu(3) distance which is shorter than the Cu–Cu separations in compounds **I**–**III** (compare Tables 2 and 4) but slightly longer than in Cu metal (2.556 Å).^{38,39} Cu(3) has bonds to 4 S atoms within an distorted tetrahedron (Figure 4).

The PBUs are joined to form different puckered heterorings: Sb(1)Cu(1)Cu(3) S_3 (6 MR A), Sb(2) S_2 Cu(3) S_3 (6 MR B), Sb(2)Cu(1)Cu(3) S_3 (6 MR C), Sb(1)Cu(1)Cu(2) S_3 (6 MR D), (Sb(1)Sb(2)) S_2 Cu(2) S_5 (10 MR) (Figure 5, top). These SBUs are then condensed to form a single layer. Along [010] the sequence of the different rings is ...A–B–C–D–10 MR–10 MR–A–B–C–D... (Figure 5, top). The 10 MR are condensed along [001], and the 6 MR show the sequence ...A–D–A–D... and ...B–C–B–C... (Figure 5, top). (Figure 5, top). Further interconnection of the single layer proceeds via an A ring containing the Cu(3) S_4 tetrahedron and which is located above (below) each D ring. The Cu(3) atom of the A ring is bound to S(3) of the D ring, and Cu(2) of the D ring has a bond to S(2) of the A ring. Furthermore, the atoms of the A (D) ring above (below) have bonds to

atoms of the 10 MR yielding a 6 MR type E ring (Sb(1)Sb(2)Cu(2) S_3) and two 4 MR (Sb(2)Cu(3) S_2 , Cu(2)Cu(3) S_2). Interestingly, the Sb(2) atom of the 6 MR type C is involved in a 6 MR of type E, which is below (above) the 6 MR C. The interconnection mode generates a double-layer thick central part of the undulated anion (Figure 5, bottom). The layers within the (001) plane are separated by the organic amine cations, and a sandwichlike arrangement of anions and cations is observed. The shortest interlayer S–S distance is 6.184 Å (measured from coordinate to coordinate).

The novel compound $(C_6N_4H_{20})_{0.5}Cu_3Sb_2S_5$ (**V**) crystallizes in the triclinic space group $P\bar{1}$ with two formula units in the unit cell. All atoms are on general positions. Two trigonal Sb S_3 pyramids, two Cu S_3 moieties, and one Cu S_4 tetrahedron are the PBUs (Figure 6). The Sb–S bond lengths and angles are in the normal range (Table 5). Each Sb atom has one S atom at a longer distance of about 3.5 Å. Cu(1) is tetrahedrally coordinated by 4 S atoms, and the distortion of the Cu(1) S_4 tetrahedron is less pronounced than that of the Cu(3) S_4 tetrahedron in **IV** (Table 5). The distance Cu(1)–Cu(1a) of 2.715(5) Å is longer than in the compounds presented above. The two other Cu atoms are trigonally coordinated by three S atoms with Cu–S distances and angles in the range observed in the other compounds (Table 5). The S–Cu–S angles indicate a different degree of distortion, which is also evident by the position of the Cu atoms above the planes formed by the three S atoms: Cu(2), 0.3783 Å; Cu(3), 0.5113 Å. As in the other compounds relatively short Cu–Sb contacts are observed which are shorter than in compounds **I**–**III** and **I**–**IV** (see above and Table 5).

The layered anion (Figure 7) contains only 6 MR: Sb(1)Cu(2)Cu(3) S_3 (6 MR A); Sb(1)Cu(1)Cu(3) S_3 (6 MR B); Sb(2)Cu(1)Cu(3) S_3 (6 MR C); Sb(2)Cu(1)Cu(2) S_3 (6 MR D); Sb(1)Sb(2)Cu(2) S_3 (6 MR E). These rings are condensed with the sequence ...A–B–C–D–E–A... (Figure 7) forming a single layer within the (001) plane. The single layer may be viewed as an undulated distorted graphene layer with the C atoms replaced by Cu, Sb, and S atoms. Also the layer can be described as a distorted 6^3 net. Two adjacent layers are joined via Cu(1)–S(4) bonds (Figure 8) yielding a double layer and Cu(2) S_2 rings. The double layers are stacked along [001] with the disordered amine molecules between the inorganic layers (Figure 8). The shortest interlayer separation amounts to 6.44 Å.

Spectroscopy. In the IR spectra of all compounds show bands which are typical for $R-NH_3^+$ cations, and charge compensation requires that the amines are protonated.

The power of Raman spectroscopy to probe differing Sb–S bonding interactions (see Tables 2, 4, and 5) is well-known.^{41,42} The bands of the five compounds are located at 315.7 cm⁻¹ (**I**), 313.5 cm⁻¹ (**III**), 309.4 cm⁻¹ (**IV**), 315.0 cm⁻¹ (**V**) and 339.7 cm⁻¹ (**II**), 335.9 cm⁻¹ (**IV**), 336.5 cm⁻¹ (**I** and **III**), 336.6 cm⁻¹ (**V**). The resonances for the Sb S_3

(41) Pfitzner, A. *Chem.–Eur. J.* **1997**, *3*, 2032–2038.

(42) Pfitzner, A.; Kurowski, D. Z. *Kristallogr.* **2000**, *215*, 373–376.

Spetzler et al.

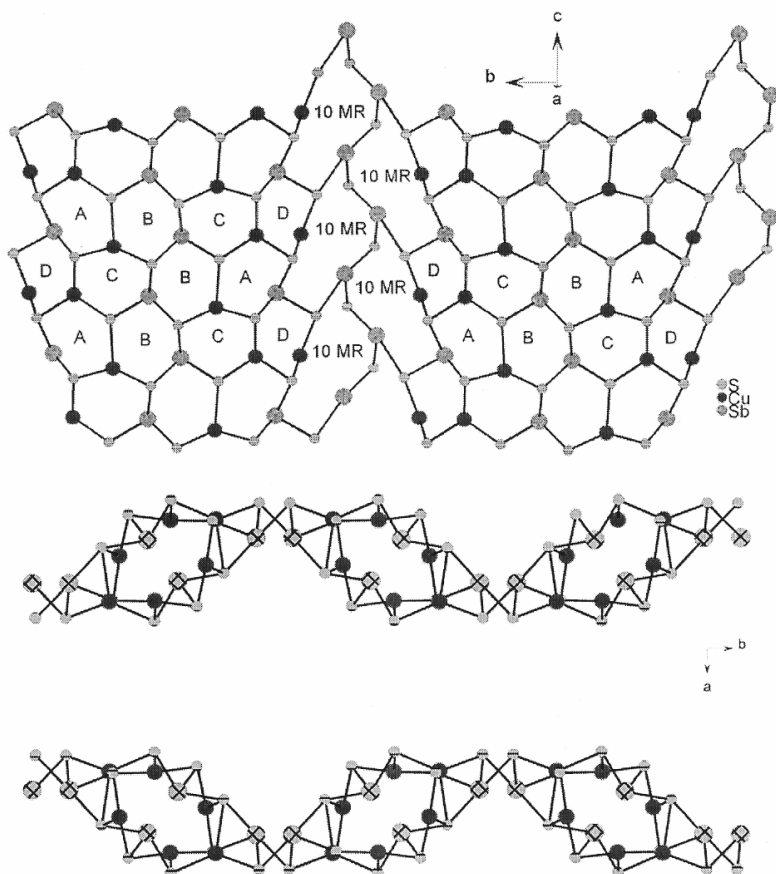


Figure 5. Condensation of the different heterorings in compound **IV** forming one layer (top). The letters identify the types of the rings (see text). View along [001] showing the packing of the undulated layers (bottom). (Note: the amine ligands which were not located are arranged between the layers.)

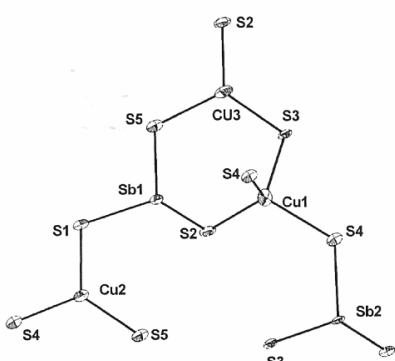


Figure 6. Crystal structure of compound **V** with labeling showing the connection of the primary building units. The displacement ellipsoids are drawn on the 50% probability level.

pyramids are observed between 362 and 339 cm^{-1} , while bands located at lower wavenumbers characterize the bonding interactions between Sb(III) and the next nearest S atoms.⁴²

Table 5. Ranges of Interatomic Distances (\AA) and Angles (deg) for $(\text{C}_6\text{N}_4\text{H}_{20})_{0.5}\text{Cu}_3\text{Sb}_2\text{S}_3$ (**V**) with Estimated Standard Deviations in Parentheses

Sb(1)–S	2.406(4)–2.547(4)
Sb(1)–Cu(2)	2.869(3)
Sb(2)–S	2.398(5)–2.522(4)
Sb(2)–Cu(3)	2.683(3)
Cu(1)–S	2.340(5)–2.482(5)
Cu(2)–S	2.262(4)–2.348(4)
Cu(3)–S	2.284(4)–2.301(4)
Cu(1)–Cu(1a)	2.715(5)
S–Sb(1)–S	95.89(15)–101.45(14)
S–Sb(2)–S	93.00(15)–106.21(13)
S–Cu(1)–S	98.57(17)–119.04(18)
S–Cu(2)–S	109.77(17)–127.62(16)
S–Cu(3)–S	112.76(17)–117.39(17)

The spectra of **I**–**III** are similar to those reported for **1**–**3**.³⁰ In the three new as well as in the previously reported compounds the Sb(III) atom has 3 short and 2 significantly longer contacts to S atoms giving rise to the resonances at about 335 and 315 cm^{-1} . We note that for $\text{Cu}_3\text{Sb}_2\text{S}_3$ with Sb(III) in a 3 + 5 surrounding of S atoms the bands are observed at even lower wavenumbers, i.e., at 321 and 290

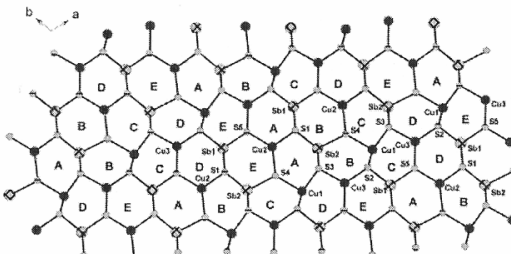
Copper(I)–Thioantimonate(III) Composites

Figure 7. Crystal structure of compound V with labeling and view along [001] showing the sequences of the different rings.

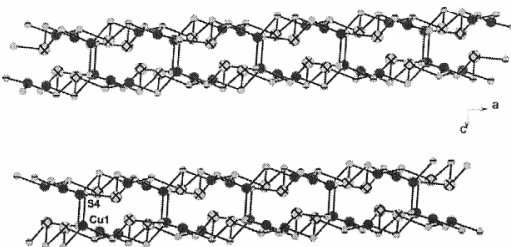


Figure 8. Crystal structure of compound V with view along [010] showing the interconnection of the layers into double layers via the Cu(1)–S(4) bonds.

cm^{-1} , and in MnSb_2S_4 with $3 + 2 + 1$ and $3 + 2 + 2$ environments for the two unique Sb(III) atoms the resonances are at 300 and 283 cm^{-1} .⁴²

Thermal Investigations. Compound I starts to decompose at $T_{\text{onset}} = 201^\circ\text{C}$. A weight loss of 15.9% occurs in one step being accompanied by an endothermic signal at a peak temperature $T_p = 228^\circ\text{C}$. The mass loss is 1% larger than expected for the removal of 1,6-diaminohexane ($-\Delta m = 14.9\%$). In the decomposition product the reflections of CuSb_2S_2 and $\text{Cu}_3\text{Sb}_2\text{S}_4$ are identified in the X-ray powder pattern.

For compounds II and III the decomposition reactions are more complex. The two compounds seem to be less stable because decomposition starts at significantly lower temperatures. For II the mass starts to decrease just above 100°C and the thermal decomposition reaction is accompanied by two endothermic peaks at $T_p = 204^\circ\text{C}$ and $T_p = 259^\circ\text{C}$. Compound III is even less stable, and the decomposition starting above about 60°C proceeds over a large temperature range. The first very broad DTA peak has $T_p = 209^\circ\text{C}$, and the second, $T_p = 260^\circ\text{C}$. The total weight losses of 15.1% for II (calcd 14.8%) and 10.4% for III (calcd 11.6%) are in rough agreement with the removal of the amine molecules. In the dark gray residue of II about 0.5% C, H, and N were found, and for III the C, H, and N content in the decomposition product is 1.3%. Again, the reflections of CuSb_2S_2 and $\text{Cu}_3\text{Sb}_2\text{S}_4$ occur in the powder patterns of the residues.

For compound IV the curves indicate a low stability because decomposition starts as low as about 80°C . Up to 450°C the mass loss is 13.7% (calcd 15.1%). In the DTA curve only one pronounced signal is observed ($T_p = 185^\circ\text{C}$). The gray residue contains about 1.5% C, H, and N, and

only the two compounds $\text{Cu}_3\text{Sb}_2\text{S}_3$ and CuSb_2S_2 could be identified in the powder pattern. Finally, compound V shows a complex thermal behavior with a beginning of decomposition at about 150°C . A not well-resolved endothermic event occurs at $T_p = 168^\circ\text{C}$, and a second one, at $T_p = 245^\circ\text{C}$. The total weight change of 11.5% is in rough agreement with the removal of the tetn molecules (calcd: 10.3%). Again, the gray decomposition product was contaminated with C, H, and N (2.5%) and in the X-ray powder pattern residues only reflections of $\text{Cu}_3\text{Sb}_2\text{S}_3$ and CuSb_2S_2 were seen.

Summary

Several features of the new inorganic–organic hybrid compounds will shortly highlighted. Compounds I–III are new members of the copper thioantimonate family with the general formula RCu_2Sb_3 , with R being an amine of different size and shape.^{27,30} The space between the anionic layers is determined by the size, packing, and orientation of the structure directing molecules. For the seven compounds with the layered $[\text{Cu}_2\text{Sb}_3]^-$ anion the interlayer separation reaches from 4.43 to 8.44 Å. Applying suitable templates, it should be possible to increase the space between the anionic layers generating new inorganic–organic hybrid materials. In the structures of all compounds the orientation of the protonated amines toward the anionic layers suggests that N–H···S bonds cannot be neglected.

In I–III as well as in compounds I–III³⁰ only Sb_3 and CuS_3 moieties are present, which are joined to form Cu_2Sb_3 (6 MR) and $\text{Cu}_3\text{Sb}_2\text{S}_5$ (10 MR) rings. In IV CuS₄ tetrahedra and Sb₂S₄ units are present yielding a complex undulated anionic layer with 4 MR and 6 MR. The anionic layer in compound V is constructed by condensation of 6 MR. The tetrahedrally coordinated Cu(1) atom has one S atom in the adjacent layer yielding finally a double layer. The anions in compounds IV and V have the same chemical composition but very different structures due to the presence of different PBUs. Relatively short Cu–Cu distances are found in IV but only long Cu–Sb separations. In V the situation is opposite; i.e., short Cu–Sb distances are present but only one medium-sized Cu–Cu separation (compare Tables 4 and 5). A short Cu(2)–Cu(3) distance of 2.622(1) Å in IV leads to a stronger distortion of the Cu(3)S₄ tetrahedron compared to the Cu(1)S₄ tetrahedron in V with a longer Cu(1)–Cu(1a) separation of 2.715(5) Å (see Tables 4 and 5).

Interesting features of all compounds are short Cu–Sb separations ranging from 2.683(3) Å in V to about 3.1 Å in I–III (compare Tables 2, 4, and 5) and the orientation of the Sb(III) 5s² lone pair which always points toward the Cu(I) centers. In all cases the distances are in the range found in binary or ternary antimonides.^{43–45} Whether there are Cu–Sb bonding interactions in the title compounds cannot be decided on the basis of the interatomic separations.

(43) Nuss, J.; Jansen, M. Z. *Anorg. Allg. Chem.* 2002, 628, 1152–1157.

(44) Koblyuk, N. D.; Melnyk, G. A.; Romaka, L. P.; Bodak, O. I.; Fruchart, D. *J. Alloys Compd.* 2001, 317, 284–286.

(45) Jandali, M. Z.; Rajasekharan, T.; Schubert, K. Z. *Metallk.* 1982, 73, 354–359.

Spetzler et al.

Calculations of the band structures are necessary to gain further insight into the bonding properties in the new copper thioantimonates.

Using the SOLV option in Platon,³⁷ the volume of the extraframework molecules in the interlayer galleries can be calculated. The values range from about 35.7% in **V** to 45.6% for **IV** (**I**, 45%; **II**, 39.4%; **III**, 37%).

As pointed out above, the anionic layered structures are constructed by condensation of Cu–Sb–S heterorings. Considering only the 6 MR, two different situations can be distinguished: Cu₂Sb₃ and CuSb₂S₃. If only 6 MR are present, the ratio of these two different ring types determines the chemical composition of the anionic network. In **V** the ratio is 4:1 and the chemical formula is then Cu₉Sb₆S₁₅, which corresponds to Cu₃Sb₂S₅. Many more combinations of these 6 MR can be envisaged yielding other networks with a different chemical composition and new network topologies. One interesting example with Ag instead of Cu was recently published. In the [Ag₅Sb₃S₈]²⁻ anion AgSb₂S₃

and Ag₂SbS₃ rings occur in a 1:7 ratio giving the overall stoichiometry of the anion.⁴⁶

The structural diversity is significantly enhanced taking also the 10 MR into account which are observed in compounds **I**–**III**. In the structure of **I**–**III** only one 6 MR type and one 10 MR type occur. Obviously, a large number of combinations of such rings are possible generating compounds with different Cu:Sb:S ratios and new network topologies. Solvothermal syntheses under different conditions are under way to further explore the Cu–Sb–S system.

Acknowledgment. The financial support by the State of Schleswig-Holstein and the Deutsche Forschungsgemeinschaft (DFG) is gratefully acknowledged.

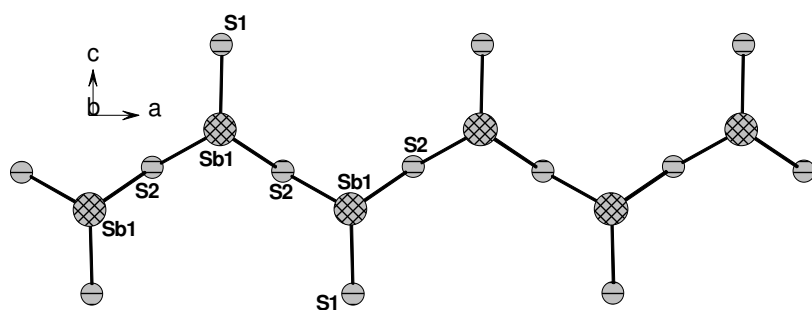
IC050196+

(46) Vaqueiro, P.; Chippindale, A. N.; Cowley, A. R.; Powell, A. V. *Inorg. Chem.* 2003, 42, 7846–7851.

3.5 Synthese und Struktur von $(C_4N_2H_{14})Ag_3Sb_3S_7$ und $(C_2N_2H_9)_2Ag_5Sb_3S_8$

Die Verbindungen $(C_4N_2H_{14})Ag_3Sb_3S_7$ (**I**) ($C_4N_2H_{12}$ = 1,4-Diaminobutan) und $(C_2N_2H_9)_2Ag_5Sb_3S_8$ (**II**) ($C_2N_2H_8$ = Ethylendiamin) wurden unter solvothermalen Bedingungen mit $AgNO_3$, Sb und S im Molverhältnis 2:2:4 (**I**) und 2:2:5 (**II**) und dem jeweiligen Amin bei 140 °C nach 7 (**I**) bzw. 5 Tagen (**II**) erhalten. Verbindung **I** kristallisiert in der orthorhombischen Raumgruppe Pnma und **II** in der monoklinen Raumgruppe P2₁/n.

In der Verbindung $(C_4N_2H_{14})Ag_3Sb_3S_7$ (**I**) bilden zwei leicht pyramidale AgS_3 -Dreiecke (Ag-S-Abstände: 2.390(3)-2.647(2) Å) und zwei trigonale SbS_3 -Pyramiden die **primären Baueinheiten** (PBE). Unter Berücksichtigung einer langen Ag-S-Bindung von 2.944(4) Å wird aus einer AgS_3 -Gruppe ein stark verzerrter AgS_4 -Tetraeder gebildet. Das Ag(1)-Atom liegt 0.0991 Å oberhalb der von den drei S-Atomen aufgespannten Ebene der Ag(1) S_3 -Einheit. Die Ag-Ag-Abstände sind mit 3.182(2), 3.287(2) und 3.334(4) Å länger als im Silbermetall (Ag-Ag-Abstand 2.89 Å). Die Bildung des zweidimensionalen $[Ag_3Sb_3S_7]^{2-}$ -Anions erfolgt durch die Kondensation zweier verschiedener Ketten. Die trigonalen SbS_3 -Pyramiden bilden eine **eindimensionale $[Sb_2S_5]$ -Kette** und die Verknüpfung von Ag(1) S_3 , Ag(2) S_4 und SbS_3 führt zu einer zweiten Kette mit einer Ag_3SbS_5 -Gruppe. Das Zentralmotiv ist ein verzerrter Ag_3SbS_3 -Halbwürfel. Die Ag_3SbS_5 -Einheiten sind über drei S(4)-Atome zu einer **Zentralkette** verbunden (Abb 3.5.1).



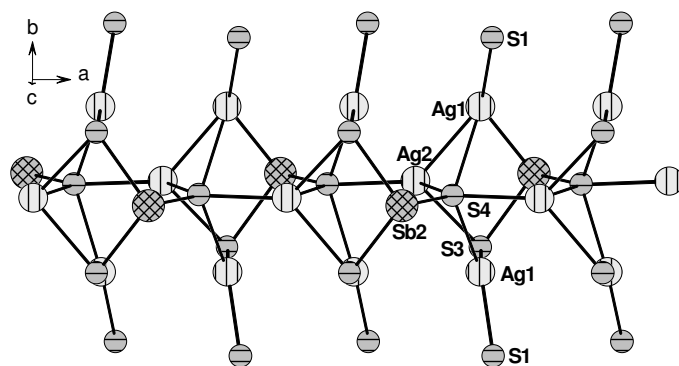


Abb. 3.5.1 Die $[Sb_2S_5]$ -Kette (oben) und die Zentralkette aus $Ag_3Sb_3S_5$ -Einheiten (unten) in der Verbindung I

Die Zentralkette ist über gemeinsame S-Atome mit den $[Sb_2S_5]$ -Ketten zu dem **$[Ag_3Sb_3S_7]^{2-}$ -Schichtanion** verknüpft. Zwischen den Schichtanionen ist das protonierte Amin sandwichartig angeordnet (Schichtabstand: 7.355 Å) (Abb. 3.5.2).

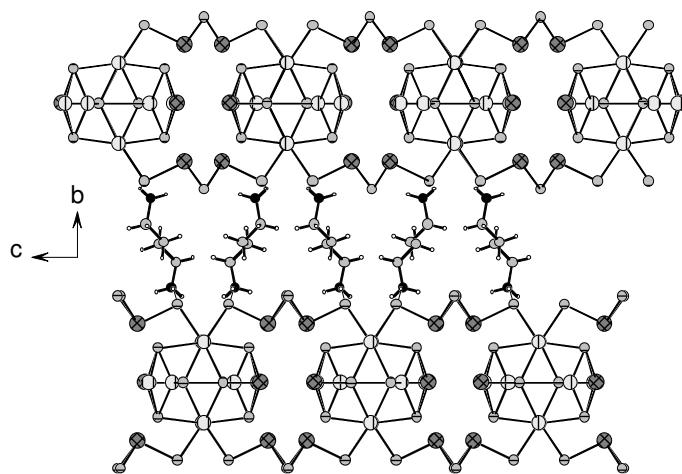


Abb. 3.5.2 Die sandwichartige Anordnung der Anionenschichten und Kationen in Verbindung I

Die Struktur der Verbindung II besteht aus zwei trigonalen AgS_3 -Einheiten, drei AgS_4 -Tetraedern und drei trigonalen SbS_3 -Pyramiden als **primäre Baueinheiten** (PBE).

Die Ag-S-Abstände von 2.497(2) bis 2.813(2) Å sind typisch und analoge Werte werden auch in den Verbindungen Stephanit Ag_5SbS_4 [39], $\text{M}\text{Ag}_2\text{SbS}_4$ und M_2AgAbS_4 ($\text{M} = \text{K}, \text{Rb}$) gefunden [40]. Die Ag-Atome liegen 0.6224 Å (Ag1) bzw. 0.4259 Å (Ag2) oberhalb der von S-Atomen aufgespannten Ebene der AgS_3 -Einheiten. Wie bei den Kupfer(I)-Thioantimonaten(III) ist in Verbindung **II** das Lone-pair des Antimonatoms auf das Silberatom ausgerichtet und der kürzeste Ag-Sb-Abstand beträgt 3.029(7) Å (Cu-Sb-Abstände: 2.726(1)-3.094(1) Å). Der kürzeste Ag-Ag-Abstand ist mit 3.071(1) Å länger als im Metall (2.89 Å), dennoch kann von einer d^{10} - d^{10} -Wechselwirkung für Ag-Ag-Abstände < 3.3 Å ausgegangen werden. Die primären Baueinheiten sind zu einer **Einfachschicht** mit acht verschiedenen sechsgliedrigen Ringen verbunden. Sieben dieser Ringe sind aus zwei Ag-, einem Sb- und drei S-Atomen zusammengesetzt, während der achte Ring aus einem Ag-, zwei Sb- und drei S-Atomen besteht. Die erste Schicht ist über Ag-S-Bindungen zu einer **Doppelschicht** verknüpft (Abb. 3.5.3).

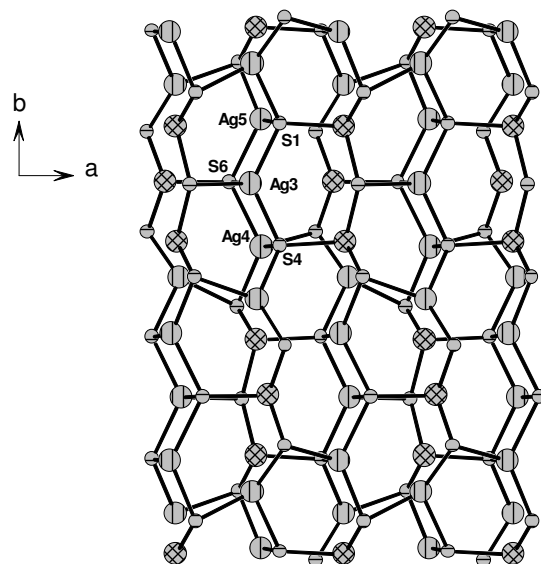


Abb. 3.5.3 Doppelschicht in der Verbindung $(\text{C}_2\text{N}_2\text{H}_9)_2\text{Ag}_5\text{Sb}_3\text{S}_8$ (**II**)

Diese Doppelschichten bilden mit dem paarweise auftretenen protonierten Ethylendiamin eine sandwichartige Anordnung. Der kürzeste Interschichtabstand der Verbindung beträgt ca. 5.4 Å.

In den **Ramanspektren** sind Resonanzen zwischen 362 und 339 cm⁻¹ zu beobachten, welche charakteristisch für SbS₃-Einheiten sind. Banden mit geringerer Wellenzahl deuten auf Bindungen zwischen Sb(III) und den nächsten S-Nachbarn hin. So werden beispielsweise Resonanzen bei 321 und 290 cm⁻¹ einer SbS₅-Einheit zugeordnet. Allerdings sind in Verbindung II keine so genannten sekundären Sb-S-Bindungen vorhanden, so dass diese Zuordnung nicht zulässig ist.

Die beiden Verbindungen sind aufgrund ihrer **optischen Bandlücken** von ungefähr 1.9 eV als Halbleiter einzustufen.

Mit Hilfe der **Impedanzspektroskopie** wurde der Widerstand R zu $4.2 \cdot 10^5 \Omega$ bestimmt, der spezifische elektrische Widerstand ρ ist $1.3 \cdot 10^6 \Omega \text{cm}$. Die spezifische elektrische Leitfähigkeit σ beträgt $7.6 \cdot 10^{-7} \Omega^{-1} \text{cm}^{-1}$ und die Kapazität C = 0.1 nF. Die Aktivierungsenergie E_A = 0.7 eV konnte mit einem Arrheniusplot ermittelt werden.

Bei der **thermischen Zersetzung** stimmen die experimentell bestimmten Massenverluste der Verbindungen I und II nahezu mit den berechneten Werten überein: I: $-\Delta m_{\text{theo}} = 12.4\%$, $-\Delta m_{\text{exp.}} = 12.1\%$, II: $-\Delta m_{\text{theo}} = 9.6\%$, $-\Delta m_{\text{exp.}} = 8.9\%$. Die Zersetzungstemperaturen von T_{onset} = 196 °C (I) und T_{onset} = 147 °C (II) deuten darauf hin, dass I die stabilere Verbindung ist. Als Abbauprodukt konnte jeweils AgSbS₂ im Pulverdiffraktogramm identifiziert werden.

The new silver(I)thioantimonate(III) $[C_4N_2H_{14}][Ag_3Sb_3S_7]$ and a new structural variant of the silver(I)thioantimonate(III) $[C_2N_2H_9)_2[Ag_5Sb_3S_8]$ both synthesized under solvothermal conditions

V. Spetzler, C. Näther, W. Bensch *

Institut für Anorganische Chemie, Christian-Albrechts-Universität Kiel, Olshausenstr. 40, D-24098 Kiel, Germany

Abstract

The novel silver(I)thioantimonates(III) $[C_4N_2H_{14}][Ag_3Sb_3S_7]$ (**I**) ($C_4N_2H_{12}$ = 1,4-diaminobutane) and $[C_2N_2H_9)_2[Ag_5Sb_3S_8]$ (**II**) ($C_2N_2H_8$ = ethylenediamine) were synthesized under solvothermal conditions using $AgNO_3$, Sb, S and the amines as structure directing molecules. In both compounds the primary building units are trigonal SbS_3 pyramids, AgS_3 triangles and AgS_4 tetrahedra. In **I** the layered $[Ag_3Sb_3S_7]^{2-}$ anion is constructed by two different chains. An $[Sb_2S_5]$ chain running along [100] is formed by vertex sharing of SbS_3 pyramids. The second chain contains a Ag_3SbS_5 group composed of the AgS_4 tetrahedron, two AgS_3 units and one SbS_3 pyramid. The Ag_3SbS_5 units are joined via S atoms to form the second chain which is also directed along [100]. The layered anion is then obtained by condensation of the two individual chains. The organic structure director is sandwiched by the inorganic layers and the shortest inter-layer distance is about 6.4 Å. In **II** the primary building units are linked into different six-membered rings which form a honeycomb-like layer. Two such layers are connected via Ag-S bonds of the AgS_4 tetrahedra giving the final undulated double layer anion. The structure directing ethylenediamine cations are located in pairs between the layers and a sandwich-like arrangement of alternating anionic layers and organic cations is observed. The inter-layer separation is about 5.4 Å. Both compounds decompose in a more or less complex manner when heated in an argon atmosphere. The optical band gaps of about 1.9 eV for the two compounds proof the semiconducting behavior. For **II** the conductivity was determined yielding $\sigma_{295K} = 7.6 \cdot 10^{-7} \Omega^{-1} cm^{-1}$. At 80°C the conductivity is significantly larger by one order of magnitude.

Keywords: Thioantimonates; Solvothermal synthesis; Crystal structures; Thermoanalytical measurements, Optical properties, Impedance spectroscopy.

Introduction

During the last few years the number of thioantimonates(III) containing a transition metal ion (TM^{n+}) as a part of the SbS_x network increased steadily [1-17]. One of the first groups of such compounds were the series of isostructural thioantimonates(III) $\text{Mn}_2\text{Sb}_2\text{S}_5 \cdot \text{L}$ (L = methyleamine, ethylamine, 1,3-diaminopropane, diethylenetriamine, N-methyl-1,3-diaminopropane) and copper-thioantimonates(III) $(\text{L})\text{Cu}_2\text{SbS}_3$ (L = ethylendiamine, 1,3-DAP = 1,3-diaminopropane, 1,4-DAB = 1,4-diaminobutane, 1,6-diaminohexane, 1,4-di-(2-aminoethyl)-piperazine, diethylenetriamine) [8, 13, 14]. Another series of Cu(I)thioantimonates(III) with composition $(\text{L})\text{Cu}_3\text{Sb}_2\text{S}_5$ (L = $\text{C}_4\text{N}_3\text{H}_{13}$ =; $\text{C}_6\text{N}_4\text{H}_{18}$ = triethylenetetramine) were reported very recently [14]. In all the Cu compounds protonated amines act as structure directors and they are arranged in the galleries between the anionic layers. Hence, these compounds may be regarded as inorganic/organic composite materials. There are some examples with silver like the minerals Miargyrite AgSbS_2 [18], Pyrargyrite Ag_3SbS_3 [19], and Stephanite Ag_5SbS_4 [20]. Silver is incorporated into anionic frameworks in $\text{RbAg}_2\text{SbS}_4$, $\text{Rb}_2\text{AgSbS}_4$, KAg_2SbS_4 , K_2AgSbS_4 [21], $[\text{C}_2\text{H}_9\text{N}_2]_2[\text{Ag}_2\text{SbS}_3]$, $[\text{C}_2\text{H}_9\text{N}_2]_2[\text{Ag}_5\text{Sb}_3\text{S}_8]$ [22] and $[\text{C}_6\text{H}_{20}\text{N}_4][\text{Ag}_5\text{Sb}_3\text{S}_8]$ [23]. In many of these inorganic/organic hybrid compounds the anionic part is layered with the amines being sandwiched by the anions. In the present contribution the crystal structures, thermal stability and optical spectroscopy data for the compounds $[\text{C}_4\text{N}_2\text{H}_{14}][\text{Ag}_3\text{Sb}_3\text{S}_7]$ (**I**) and $[\text{C}_2\text{N}_2\text{H}_9]_2[\text{Ag}_5\text{Sb}_3\text{S}_8]$ (**II**) are presented. In addition, we present results of the impedance spectroscopy of compound **II**.

Experimental Details

Syntheses

The two compounds $[C_4N_2H_{14}][Ag_3Sb_3S_7]$ (**I**) and $[C_2N_2H_9]_2[Ag_5Sb_3S_8]$ (**II**) were prepared under solvothermal conditions in Teflon-lined steel autoclaves. For **I** a mixture of $AgNO_3$ (2 mmol), Sb (2 mmol), S (5 mmol) and 4 mL 1,4-diaminobutane was heated at 140°C for 7 days. Compound **II** was synthesized applying a mixture of $AgNO_3$ (2 mmol), Sb (2 mmol), S (4 mmol) and 4 mL ethylenediamine. The slurry was heated at 140°C for 5 days followed by cooling to room temperature. The products were collected by filtration and washed with deionized water, acetone and dried in vacuum. Both compounds crystallized as orange needles. The yield was about 80% for **I** and 60% for **II** based on Ag. The compounds are stable on air. Anal. found for **I**: C:5.0%, H: 1.3%, N: 3.0%; Calcd.: C: 4.8%, H: 1.2%, N: 2.8%. **II**: C: 2.7%, H: 0.9%, N. 2.7%; Calcd.: C: 2.1%, H:0.7%, N: 2.3%;

X-ray Scattering Studies

The X-ray intensity data were collected at 293 K using a STOE AED 4 equipped with a graphite monochromator using $MoK\alpha$ radiation ($\lambda = 0.71073 \text{ \AA}$). The raw intensities were treated in the normal way applying a Lorentz, polarization correction. The data were also corrected for absorption effects. The structures were solved using SHELXS-97 [24]. Crystal structure refinements were done against F^2 with SHELXL-97 [25]. All non-hydrogen atoms were refined with anisotropic displacement parameters. The hydrogen atoms were positioned with idealized geometry and refined with fixed isotropic displacement parameters using a riding model. One of the two independent Ag atoms in **I** is partially disordered and the two positions were refined using a split model yielding site occupation factors of 90%:10% (Ag2:Ag2'). Details of data collections and refinement results are summarized in Table 1. Bond lengths and angles are listed in Tables 2, 3, and 4.

Spectroscopy

The Raman spectra were measured from 100 to 3500 cm^{-1} with a Bruker IFS 66 Fourier transform Raman spectrometer (wavelength: 514.5 nm, T = 20 K).

The impedance were measured with a Kieler Zelle and a HP 4192 Impedance-Analizer at 5Hz –13MHz. For the temperature-program we need a Cr/CrNi thermocouple.

Thermoanalytical Investigations

Thermogravimetric analyses were performed using a Netzsch STA 429 DTA-TG device. The samples were heated in Al_2O_3 crucibles at a rate of $4 \text{ K}\cdot\text{min}^{-1}$ to 400°C under a flow of argon of 100 ml min^{-1} .

Impedance Spectroscopy

The measurements were done with the so-called Kieler cell in an argon atmosphere using a HP 4192 Impedance-Analizer at 5 Hz–13 MHz with gold electrodes. The temperature was controlled with a Cr/CrNi thermocouple. Non-blocking interfaces/electrodes behave like a resistance (R) and capacitance (C) in parallel. This leads to a semicircle in the so called Nyquisplot which has a high frequency limit at the origin and a low frequency limit at $Z' = R$. At the maximum of the semicircle the capacitance can be evaluated. Additionally, the interface impedance has a Warburg impedance W in series with R [26-28]. For compound **II** a non blocking effect was observed with the slow diffusion of the species (Ag^+) crossing the interface indicated by a Nyquist-diagram with the Warburg impedance. The Warburg impedance (W) arises from the fact that the concentration of a species at an electrode surface is out of phase by 45° with the flux of the same species across the surface [26-28].

Results and Discussion

The new compound $[\text{C}_4\text{N}_2\text{H}_{14}][\text{Ag}_3\text{Sb}_3\text{S}_7]$ (**I**) crystallizes in the orthorhombic space group Pnma with four formula units in the unit cell (Table 1). The atoms Sb(2), Ag(2) and S(4) are located on general positions whereas all other unique atoms are on general positions. The two Ag atoms are surrounded by 3 S atoms to form AgS_3 triangles with Ag-S bonds ranging from 2.390(3) to 2.647(2) Å. The corresponding S-Ag-S angles are between 90.43(8) and 133.73(4)°. The geometrical parameters are in the range reported for AgSbS_2 [18], Ag_3SbS_3 [19], Ag_5SbS_4 [20], or $[\text{C}_2\text{N}_2\text{H}_9]_2[\text{Ag}_5\text{Sb}_3\text{S}_8]$ [22]. Ag(2) has another S atom at the long distance of 2.944(4) Å and taking this atom into account the environment is a strongly distorted tetrahedron (Fig. 1, Table 2).

The Ag(1) atom is situated 0.0991 Å above the plane formed by the three S atoms. The Ag-Ag separations (3.182(2) and 3.334(4) Å) are significantly larger than in metallic Ag. The Sb-S bond lengths and S-Sb-S angles in the two unique trigonal SbS_3 pyramids are in the typical

range observed for this environment (Table 5) [1-17]. The two-dimensional $[Ag_3Sb_3S_7]^{2-}$ anion is constructed by condensation of two different chains. The Sb(1)S₃ units form a one-dimensional [Sb₂S₅] chain by vertex sharing running along [100] (Fig. 2, top). Another chain is formed by interconnection of the Ag(1)S₃, Ag(2)S₄ and Sb(2)S₃ moieties. The AgS₄ unit shares two edges with two AgS₃ triangles and one edge with SbS₃ yielding an Ag₃SbS₅ group with a distorted Ag₃SbS₃ semi-cube as central motif (Fig. 2, bottom). The Ag₃SbS₅ units are joined by three S(4) atoms to form a chain directed along [100].

This central chain is bridged by the [Sb₂S₅] chain forming the final layered $[Ag_3Sb_3S_7]^{2-}$ anion extending in the (010) plane (Fig. 3). An interesting structural detail is the unusual bind mode of S(4) which has bonds to 4 Ag and 1 Sb atoms (see Fig. 2, bottom).

In contrast to compound **II** where no so called secondary Sb-S bonds are found the Sb(1) atom in **I** has two such contacts at 3.399 and 3.423 Å. The amine cations are located in pairs between the layers and the two NH₃ groups of the amines are oriented toward the networks forming a sandwich-like arrangement with an interlayer distance of 7.355 Å (Fig. 3, top). The short intermolecular N–H … S distances with H…S separations ranging from 2.403 Å to 2.994 Å indicate hydrogen bonding interactions between the anionic layers and the structure directing ammonium ions (Table 3).

The compound $[C_2N_2H_9]_2[Ag_5Sb_3S_8]$ (**II**) crystallizes in the monoclinic space group P2₁/n with four formula units in the unit cell (Table 1). Five crystallographically independent Ag atoms, three Sb and eight S atoms are found in **II**. Two trigonal AgS₃ units (Ag(1), Ag(2)), three AgS₄ tetrahedra (Ag(3), Ag(4), Ag(5)) and three trigonal SbS₃ pyramids are the primary building units (PBUs) (Fig. 4).

The Ag-S distances in the AgS₃ groups are between 2.497(2) and 2.672(2) Å with S-Ag-S angles ranging from 96.23(5)° to 134.66(6)° (Table 4). The Ag-S bonds are longer than in minerals like Miargyrite AgSbS₂ (Ag–S: 2.36 to 2.58 Å) [18] or Pyrargyrite Ag₃SbS₃ (Ag–S average: 2.40 Å) [19], but they match well with data for Stephanite Ag₅SbS₄ [20], MAg₂SbS₄, and M₂AgSbS₄ (M = K, Rb) [21], $(C_2N_2H_9)_2Ag_5Sb_3S_8$ [22] or $[C_6H_{20}N_4][Ag_5Sb_3S_8]$ [23]. The Ag atoms are situated 0.6224 Å (Ag(1)) and 0.4259 Å (Ag(2)) above the planes formed by the three S atoms. Ag(1) has Sb(2) at a distance of 3.029(7) Å as next nearest neighbor. Assuming that the electron lone pair of Sb(2) is located opposite to the plane of the three S atoms in the Sb(2)S₃ pyramid it points towards the Ag(1) atom, similar to what was observed in copper-thioantimonates [13,14]. The Ag(3,4,5)S₄ tetrahedra are severely distorted with Ag-

S bonds from 2.551(2) Å to 2.976(2) Å and corresponding angles between 89.23(5)° and 126.58(6)°. The Sb-S bond lengths (Table 2) are typical for the well known trigonal pyramidal SbS₃ unit [1-17]. The Ag(3) and Ag(5) atoms are 3.250(1) Å apart, which is longer than in Ag metal (2.89 Å), while Ag-Ag distances in Ag₅SbS₄ [20] and (C₂H₉N₂)₂[Ag₂SbS₃] [22] are with 2.91 Å shorter than in **II**, suggesting weak d¹⁰- d¹⁰ interactions which are significant for Ag-Ag distances < 3.3 Å [29]. The next-nearest S atoms of Sb are at distances larger than the sum of the van der Waals radii of 3.80 Å.

The first layer shows a honeycomb like arrangement of eight different condensed six-membered rings: Ag(1,4)Sb(3)S₃, Ag(1,4)Sb(1)S₃, Ag(1,3)Sb(1)S₃, Ag(3)Sb(1,2)S₃, Ag(2,3)Sb(2)S₃, Ag(2,5)Sb(2)S₃, Ag(2,5)Sb(3)S₃, and Ag(4,5)Sb(3)S₃ (Fig.2). Seven of these rings are composed of two Ag, one Sb and three S atoms and the eighth ring contains one Ag, two Sb and three S atoms (Fig. 5).

The layer is connected to a symmetry related layer via Ag(3,4,5)-S bonds to form a buckled double layer extending in the (001) plane, and due to the 2₁ screw axes and the n glide plane the different rings are located above and/or below each other (see Fig. 6).

The cations are located in pairs between the layers and a sandwich-like arrangement is observed (Fig. 6), similar to what was previously observed in other thioantimonates(III) [13, 14]. Relatively short H···S distances ranging from 2.536 Å to 3.004 Å indicate hydrogen bonding interactions (Table 3). The shortest interlayer distance amounts to 5.4 Å.

We note that two compounds with the [Ag₅Sb₃S₈]²⁻ anion were reported recently. Both compounds were prepared under solvothermal conditions in the presence of ethylenediamine as structure director [22, 23], and the first is denoted as **III**. This compound crystallizes in space group Pm and the layered anion is constructed by interconnection of four SbS₃ pyramids, three AgS₄ tetrahedra, two AgS₃ triangles and one bend AgS₂ group. The Ag atom of this latter unit has a S atom at a large distance of about 3.17 Å. Like in **II** honeycomb sheets are produced by fused six-membered rings (seven Ag₂SbS₃ and one AgSb₂S₃ rings), and buckled double layers are formed. A remarkable difference between the two compounds are the short Ag-Sb separations of 2.868 and 2.985 Å in **III** compared to the shortest distances of 3.029 and 3.156 Å in **III**. The arrangement of the cations is also different in the two compounds. In **III** the en molecules occur in pairs with short N···N separations of 2.40 – 2.63 Å whereas the shortest N···N distances in **II** are 2.828 and 2.778 Å. Furthermore, the

interlayer distance is about 0.6 Å larger in **III** than in **II**. The other thioantimonate(III) with the $[\text{Ag}_5\text{Sb}_3\text{S}_8]^{2-}$ ion was prepared with triethylenetetramine (TETN) as structure director [23], and is denoted as **IV**. The compound crystallizes in $\text{P}2_1/\text{m}$ with two SbS_3 units, two AgS_4 tetrahedra and one AgS_3 moiety. Again, six-membered rings are formed by vertex linking of these building units to form honeycomb like double layers. The bond lengths in the AgS_3 groups and AgS_4 tetrahedra are in a narrower range than in **II**. The TETN molecule adopts a C shaped geometry and the shortest interlayer separation is about 6.3 Å. All three compounds crystallize in monoclinic space groups with very similar a and b axes, but very different values for the c axis and the monoclinic angle β.

Optical Spectroscopy

Charge compensation requires that the amine molecules are monoprotonated in **I** and diprotonated in **II**. In the IR spectra the absorptions located at 1100, 1400, 1600, 2400 and 3400 cm⁻¹ are typical for R-NH₃⁺ groups. In the Raman spectra (Fig. 7) the most intense resonances are located at 354.9 cm⁻¹, 326.2 cm⁻¹ and 277.4 cm⁻¹ for **I** and at 331.3 cm⁻¹ and 321.8 cm⁻¹ for **II**. Weak bands are observed at 312.3 cm⁻¹ for **I** and at 276.3 cm⁻¹, 284.9 cm⁻¹, 301.5 cm⁻¹, 350.2 cm⁻¹ and 373.1 cm⁻¹ for **II**. The bands between 362 cm⁻¹ and 339 cm⁻¹ are typical for SbS_3 units [31, 32]. The optical band gaps of both compounds were determined from transformed UV-Vis diffuse reflectance spectra in the usual way (Kubelka-Munk). The optical band gaps of about 1.9 eV indicate that the compounds are semiconductors. This value are similar to values obtained for copper thioantimonates [13, 14, 30].

Impedance Spectroscopy

Impedance spectroscopy was performed using a pressed pellet of **II**. From the Nyquist plot (Fig. 8) the resistance at room temperature was estimated as $R_{\text{RT}} = 4.2 \cdot 10^5 \Omega$, the conductivity $\sigma_{\text{RT}} = 7.6 \cdot 10^{-7} \Omega^{-1} \text{ cm}^{-1}$ and the capacitance $C_{\text{RT}} = 0.1 \text{ nF}$. With increasing temperature the resistance decreases reaching $5.3 \cdot 10^4 \Omega$ at 80 °C (Fig. 8). The activation energy $E_A = 0.7 \text{ eV}$ was estimated applying the Arrhenius equation, but for Ag ion conductivity one would expect a lower value.

The difference between the optical band gap ($E_g = 1.9 \text{ eV}$) and the activation energy E_A (0.7 eV) can be explained by impurities or point defects in the material [26-28]. The impurities lead to an impurity level below the conduction band (donor level) and an impurity level above

the valence band (acceptor level). At lower temperatures such impurities dominate the conductivity and at higher temperatures the intrinsic conduction mainly contributes to the electrical conductivity. In the present case the temperature regime covers the range where the intrinsic properties are measured. It is not unusual that the activation energy E_A differs from the optical band gap.

Thermal Investigation

The DTA-TG-DTG curves are shown in Figure 9. Compound **I** starts to decompose at $T_{\text{onset}} = 196^\circ\text{C}$ with a strong endothermic signal at $T_p = 213^\circ\text{C}$. The total weight loss of 12.1% is in good agreement with the calculated value ($-\Delta m_{\text{theo}} = 12.4\%$). In the dark gray residue only minute amounts of CHN are present. The second endothermic event at $T_p = 384^\circ\text{C}$ is not accompanied by a mass change and it can be assumed that the decomposition product melts. In the X-ray powder pattern of the residue AgSbS_2 could be identified. Compound **II** seems to be less stable than **I** and decomposes in one step ($T_{\text{onset}} = 147^\circ\text{C}$) which is accompanied by an endothermic signal with a peak temperature $T_p = 169^\circ\text{C}$ and a weight loss of 8.9%. The expected value for the emission of two ethylenediamine molecules is 9.6%. A small thermal event occurs at $T_p = 376^\circ\text{C}$ which is not accompanied by a weight change and may be due to melting of an intermediately formed compound. The C, H, N elemental analysis of the gray residue yields a very low level of 0.56% for CHN. In the decomposition product the reflections of Ag_3SbS_3 and AgSbS_2 are identified in the X-ray powder pattern.

Summary

Compared to the relatively large number of copper(I)thioantimonates(III) obtained under solvothermal conditions using organic cations as structure directors the number of silver(I)thioantimonates(III) is relatively low. In the two compounds **I** and **II** layers are formed by the interconnection of trigonal SbS_3 pyramids, AgS_4 tetrahedra and AgS_3 units. The network topologies are quite different reflecting the flexibility to adopt the requirements of the organic structure directing molecules. The protonated amines are sandwiched by the anionic layers and the compounds may be regarded as inorganic-organic hybrids with interlayer separations of 6.4 Å (**I**) and 5.4 Å (**II**). A larger range for such layer separations was observed for copper(I)thioantimonates(III) with values ranging from 4.43 to 8.44 Å [14]. For many host lattices like TaS_2 or vermiculites the interlayer expansion is independent from

the number of C atoms for alkyl chains with less than 6 C atoms [33]. The same observation is made for the layered coin metal thioantimonate compounds. In all these compounds the ammonium groups of the organic molecules are oriented towards the anionic layers ensuring optimal S···H bonding interactions. Another interesting aspect of the Ag thioantimonate chemistry is the occurrence of three topologically very similar $[\text{Ag}_5\text{Sb}_3\text{S}_8]^{2-}$ anions which were synthesized under different conditions. The difference between the two materials containing the en cation are different antimony sources, different Sb:Ag:S ratios and different temperatures. The previously reported compound [22] was obtained with a molar composition $\text{Sb}_2\text{S}_3:\text{AgNO}_3:\text{S} = 1:1:2.5$ ($\text{Sb:Ag:S} = 2:1:5.5$) at 190°C whereas the title compound crystallized from a mixture with molar ratio $\text{Sb:AgNO}_3:\text{S} = 1:1:2$ at 140°C . The observation that the two compounds are obtained under very different conditions may suggest that in solution the same building units exist.

References

- [1] H.-O. Stephan, M. G. Kanatzidis, Inorg. Chem. 36 (1997) 6050-6057.
- [2] W. Bensch, M. Schur, Z. Naturforsch. 52b (1997) 405-409.
- [3] R. Kiebach, C. Näther, W. Bensch, Z. Anorg. Allg. Chem. 628 (2002) 2176-2181.
- [4] R. Stähler, W. Bensch, Eur. J. Inorg. Chem. (2001) 3073-3078.
- [5] R. Stähler, C. Näther, W. Bensch, Acta Cryst. C57 (2001) 26-27.
- [6] R. Stähler, W. Bensch, Z. Anorg. Allg. Chem. 628 (2002) 1657-1662.
- [7] M. Schäfer, C. Näther, W. Bensch, Solid State Sci. 5 (2003) 1135-1139.
- [8] L. Engelke, R. Stähler, M. Schur, C. Näther, W. Bensch, C. Pöttgen, R. Möller, M. H. Z. Naturforsch. 59b (2004) 869-876.
- [9] M. Schäfer, R. Stähler, R. Kiebach, C. Näther, C. Bensch, W. Z. Anorg. Allg. Chem. 630 (2004) 1816-1822.
- [10] A. V. Powell, S. Boissiere, A. M. Chippindale, J. Chem. Soc., Dalton Trans. (2000) 4192-4195.
- [11] Zh. Chen, R. E. Dillks, R.-J. Wang, J. Y. Lu, J. Li, Chem. Mater. 10 (1998) 3184-3188.
- [12] A. V. Powell, R. Paniagua, P. Vaqueiro, A. M. Chippindale, Chem. Mater. 14 (2002) 1220-1224.
- [13] V. Spetzler, H. Rijnberk, C. Näther, W. Bensch, Z. Anorg. Allg. Chem. 630 (2004) 142-148.
- [14] V. Spetzler, C. Näther, W. Bensch, Inorg. Chem. 44 (2005) 5805-5812.
- [15] W. Bensch, M. Schur, Eur. J. Solid State Inorg. Chem. 33 (1996) 1149-1160.
- [16] M. Schur, C. Näther, W. Bensch, Z. Naturforsch. 56b (2001) 79-84.
- [17] R. Stähler, W. Bensch, J. Chem. Soc., Dalton Trans. (2001) 2518-2522.
- [18] C. R. Knowles, Acta Crystallogr. 17 (1964) 847-851.
- [19] D. Harker, J. Chem. Phys. 4 (1936) 381-390.
- [20] B. Ribar, W. Nowacki, Acta Crystallogr. B 26 (1970) 201-207.
- [21] G. L. Schimek, W. T. Pennington, P. T. Wood, J. W. Kolis, J. Solid State Chem. 123 (1996) 277-284.
- [22] P. Vaqueiro, A. M. Chippindale, A. R. Cowley, A. V. Powell, Inorg. Chem. 42 No. 24 (2003) 7846-7851.
- [23] A. V. Powell, J. Thun, A. M. Chippindale, J. Solid State Chem. 178 (2005) 3414-3419.

- [24] G. M. Sheldrick, SHELXS-97, Program for Crystal Structure Determination, University of Göttingen, Germany 1997.
- [25] G. M. Sheldrick, SHELXL-97, Program for the Refinement of Crystal Structures, University of Göttingen, Germany 1997.
- [26] R. D. Armstrong, T. Dickensen, P. M. Willis, Electroan. Chem. Interf. Electrochem. 53 (1974) 389-397.
- [27] F. Sauerwald, Dissertation, Geowissenschaften der Philipps-Universität Marburg 2005.
- [28] C. J. Wen, C. Ho, B. A. Boukamp, I. D. Raistrick, W. Weppner, and R. A. Huggens, International Metals Reviews 5 (1981) 253-259.
- [29] M. Jansen, Angew. Chem. 99 (1987) 1136-1149.
- [30] V. Spetzler, R. Kiebach, C. Näther, and W. Bensch, Z. Anorg. Allg. Chem. 630 (2004) 2398-2404.
- [31] A. Pfitzner, Chem. Eur. J. 3 (1997) 2032-2038.
- [32] A. Pfitzner, D. Kurowski, Z. Kristallogr. 215 (2000) 373-376.
- [33] Lerf, A. in “Handbook of Nanostructured Materials and Nanotechnology”, ed. H. S. Nalwa, Academic Press 2000 Vol. 5.; Intercalated Layered Materials, ed. F. A. Lévy, D. Reidel Publishing, Dordrecht, Boston, London, 1979. D. Reidel Publishing, Dordrecht, Boston, London, 1979.

Table 1

Selected Crystallographic Data and Refinement Results for $[C_4N_2H_{14}][Ag_3Sb_3S_7]$ (**I**) and $[C_2N_2H_9]_2[Ag_5Sb_3S_8]$ (**II**)

	I	II
a (Å)	6.6689(9)	6.2712(4)
b (Å)	30.440(3)	15.9008(13)
c (Å)	9.1538(8)	23.0119(7)
$\beta/^\circ$		95.371(6)
$V/\text{Å}^3$	1858.2(3)	2290.7(3)
$d_{\text{calc}}/\text{g cm}^{-3}$	3.587	3.715
crystal system	orthorhombic	monoclinic
space group	Pnma	P2 ₁ /n
$2\theta/\text{deg}$	4 – 56	4 – 56
hkl range	$-7 \leq h \leq 7$ $-35 \leq k \leq 36$ $-10 \leq l \leq 10$	$-8 \leq h \leq 8$ $-21 \leq k \leq 21$ $-30 \leq l \leq 30$
no. coll refl	12238	22614
no. unique refl.	1648	5303
refl $F_o > 4\sigma(F_o)$	4202	1536
params	98	215
R1 ($F_o > 4\sigma(F_o)$)	0.0346	0.0332
wR2 ($F_o > 4\sigma(F_o)$)	0.0888	0.0768
R1 (all refl)	0.0371	0.0471
wR2 (all refl)	0.0909	0.0815
GOF	1.082	1.025
$\delta(F)/e \text{ Å}^{-3}$	-2.272/2.245	-2.78/3.55

Table 2. Selected interatomic distances (\AA) and angles ($^\circ$) for $[\text{C}_4\text{N}_2\text{H}_{14}][\text{Ag}_3\text{Sb}_3\text{S}_7]$ (**I**). Estimated standard deviations are given in parentheses.

Sb(1)-S(1)	2.4050(16)	Ag(1)-Ag(1) ^[c]	3.3349(4)
Sb(1)-S(2)A ^[a]	2.4616(15)	Ag(1)-Ag(2)	3.2874(14)
Sb(1)-S(2)	2.4859(15)	Ag(2)-S(4) ^[e]	2.390(3)
Sb(2)-S(4)	2.421(3)	Ag(2)-S(3)A ^[b]	2.647(2)
Sb(2)-S(3)	2.4240(16)	Ag(2)-S(3)	2.647(2)
Sb(2)-S(3)A ^[b]	2.4240(17)	Ag(2)-S(4)A ^[c]	2.944(4)
Ag(1)-S(1)	2.4658(17)	Ag(2)-Ag(1) ^[c]	3.1821(13)
Ag(1)-S(3)	2.5322(17)		
Ag(1)-S(4) ^[c]	2.5484(14)		
S(1)-Sb(1)-S(2) ^[a]	96.69(5)	S(2) ^[a] -Sb(1)-S(2)	84.82(4)
S(4)-Sb(2)-S(3)	94.39(6)	S(3)-Sb(2)-S(3) ^[b]	101.60(9)
S(1)-Ag(1)-S(3)	131.01(6)	S(1)-Ag(1)-S(4) ^[c]	121.50(7)
S(3)-Ag(1)-S(4) ^[c]	107.01(7)	S(4) ^[e] -Ag(2)-S(3)	133.73(4)
S(3) ^[b] -Ag(2)-S(3)	90.43(8)	S(4) ^[e] -Ag(2)-S(4) ^[c]	95.80(9)
S(3) ^[b] -Ag(2)-S(4) ^[c]	93.71(6)		

Symmetry codes:

^[a] $x+0.5, y, -z+0.5$; ^[b] $x, -y+1.5, z$; ^[c] $x-0.5, y, -z+1.5$; ^[d] $x+0.5, y, -z+1.5$; ^[e] $x-1, y, z$;

Table 3. Intermolecular N .. S distances (\AA) in $[\text{C}_4\text{N}_2\text{H}_{14}][\text{Ag}_3\text{Sb}_3\text{S}_7]$ (**I**) and $[\text{C}_2\text{N}_2\text{H}_9]_2[\text{Ag}_5\text{Sb}_3\text{S}_8]$ (**II**)

	II	I
N .. S	2.536 (S8) 2.556 (S7) 2.827 (S2) 2.790 (S7) 3.004 (S2)	2.403 (S2) 2.561 (S1) 2.599 (S1) 2.876 (S2) 2.994 (S1)

Table 4. Selected interatomic distances (\AA) and angles ($^\circ$) for $[\text{C}_2\text{N}_2\text{H}_9]_2[\text{Ag}_5\text{Sb}_3\text{S}_8]$ (II).

Estimated standard deviations are given in parentheses.

Sb(1)-S(1)	2.4241(18)	Ag(3)-S(2) ^[f]	2.8132(18)
Sb(1)-S(2)	2.5100(15)	Ag(3)-S(4)	2.5440(16)
Sb(1)-S(3)	2.4085(15)	Ag(3)-S(6)	2.6993(17)
Sb(2)-S(2) ^[a]	2.5243(15)	Ag(4)-S(3)	2.5546(16)
Sb(2)-S(4)	2.4290(17)	Ag(4)-S(4)	2.6678(17)
Sb(2)-S(5)	2.3887(15)	Ag(4)-S(6)	2.6785(16)
Sb(3)-S(6)	2.4348(17)	Ag(4)-S(7) ^[b]	2.6621(17)
Sb(3)-S(7)	2.4127(15)	Ag(5)-S(1) ^[a]	2.6032(19)
Sb(3)-S(8)	2.4184(15)	Ag(5)-S(5) ^[a]	2.5122(17)
Sb(1)-Ag(2)	3.1559(7)	Ag(5)-S(6)	2.6719(16)
Sb(2)-Ag(1)	3.0293(7)	Ag(1)-Ag(4) ^[e]	3.2499(10)
Ag(1)-S(1)	2.6376(16)	Ag(3)-Ag(4)	3.3659(9)
Ag(1)-S(3) ^[b]	2.5407(17)	Ag(3)-Ag(5)	3.0708(9)
Ag(1)-S(7) ^[b]	2.5007(16)	Ag(2)-S(4)	2.5349(16)
Ag(2)-S(5) ^[e]	2.5903(18)	Ag(2)-S(8) ^[d]	2.4968(17)
Ag(3)-S(1) ^[a]	2.5512(16)		

S(1)-Sb(1)-S(2)	100.52(6)	S(4)-Ag(4)-S(6)	99.70(5)
S(3)-Sb(1)-S(1)	98.65(6)	S(3)-Ag(4)-S(7) ^[b]	104.72(5)
S(3)-Sb(1)-S(2)	91.11(5)	S(7) ^[b] -Ag(4)-S(4)	113.79(5)
S(5)-Sb(2)-S(2) ^[a]	90.32(5)	S(3)-Ag(4)-S(4)	114.92(5)
S(5)-Sb(2)-S(4)	101.16(6)	S(3)-Ag(4)-S(6)	126.58(6)
S(4)-Sb(2)-S(2)	103.10(5)	S(5) ^[a] -Ag(5)-S(6)	118.57(6)
S(7)-Sb(3)-S(8)	100.61(5)	S(5) ^[a] -Ag(5)-S(1) ^[a]	123.18(5)
S(8)-Sb(3)-S(6)	101.55(6)	S(1) ^[a] -Ag(5)-S(6)	108.21(5)
S(7)-Sb(3)-S(6)	100.51(5)	S(7) ^[b] -Ag(1)-S(1)	126.32(6)
S(3) ^[b] -Ag(1)-S(1)	96.23(5)	S(7) ^[b] -Ag(1)-S(3) ^[b]	119.46(5)
S(8) ^[c] -Ag(2)-S(4)	134.66(6)	S(8) ^[c] -Ag(2)-S(5) ^[d]	114.69(6)
S(4)-Ag(2)-S(5) ^[d]	101.83(5)	S(4)-Ag(3)-S(1) ^[a]	126.49(6)
S(4)-Ag(3)-S(6)	102.37(5)	S(4)-Ag(3)-S(2) ^[e]	106.01(5)
S(6)-Ag(3)-S(2) ^[e]	110.34(5)		

Symmetry codes: ^[a] -x+1.5, y+0.5, -z+1.5; ^[b] x+1, y, z; ^[c] -x+0.5, y-0.5, -z+1.5; ^[d] x-1, y, z;
^[e] -x+0.5, y+0.5, -z+1.5; ^[f] -x+1.5, y-0.5, -z+1.5.

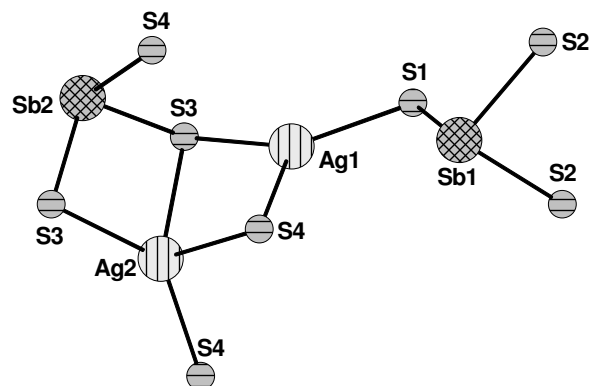


Fig. 1: The primary building units in compound **I** with labeling. Note that the disordered $\text{Ag2}'$ atom is not displayed.

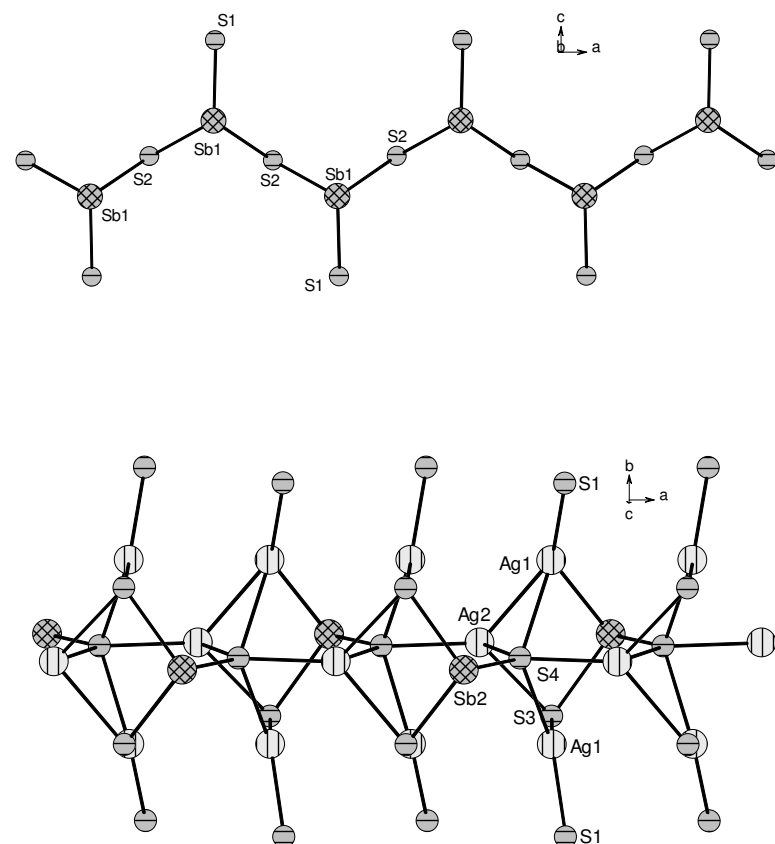


Fig. 2: The one-dimensional $[\text{Sb}_2\text{S}_5]$ chain in **I** formed by interconnection of the $\text{Sb}(1)\text{S}_3$ pyramids (top) and the $\text{Ag}_3\text{Sb}\text{S}_5$ units joined by the $\text{S}(4)$ atoms (bottom).

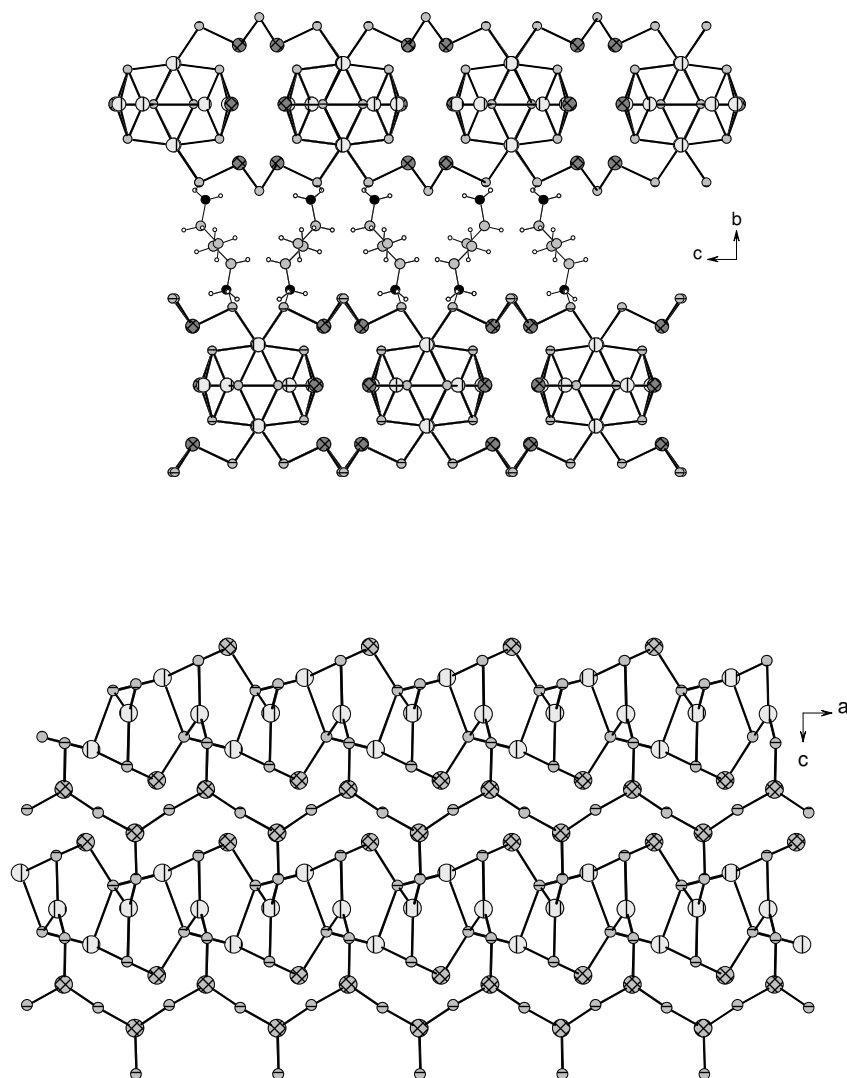


Fig. 3: Two different views of the layers in **I**. Top: View along $[100]$ showing the sandwich-like arrangement of the anionic layers and the organic cations. Bottom: View along $[010]$ showing the interconnection of the two different chains.

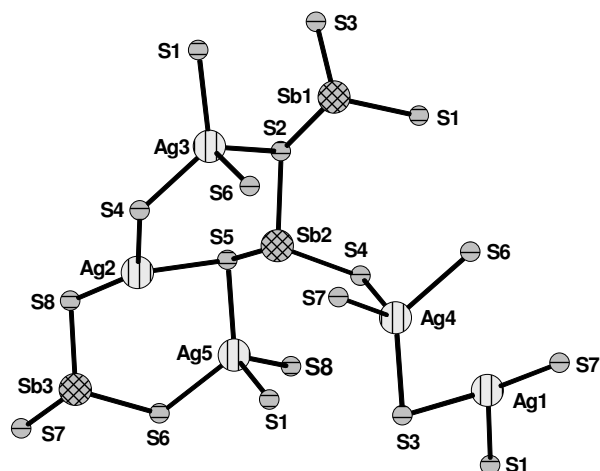


Fig. 4: The primary building units in compound **II** together with atom labeling.

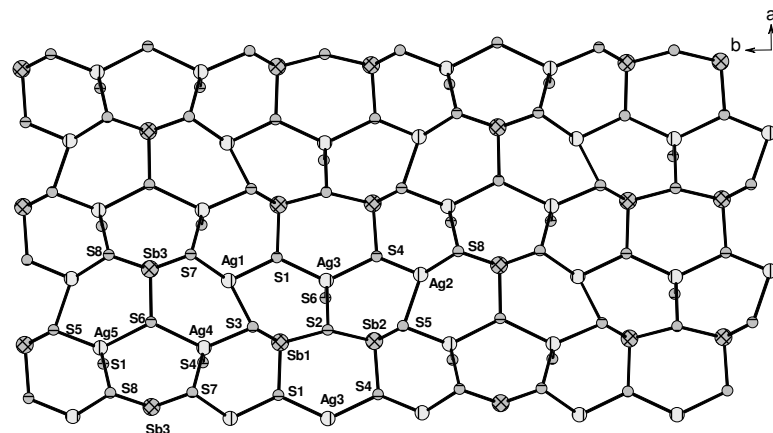


Fig. 5: The condensed six-membered rings in compound **II** forming a single layer.

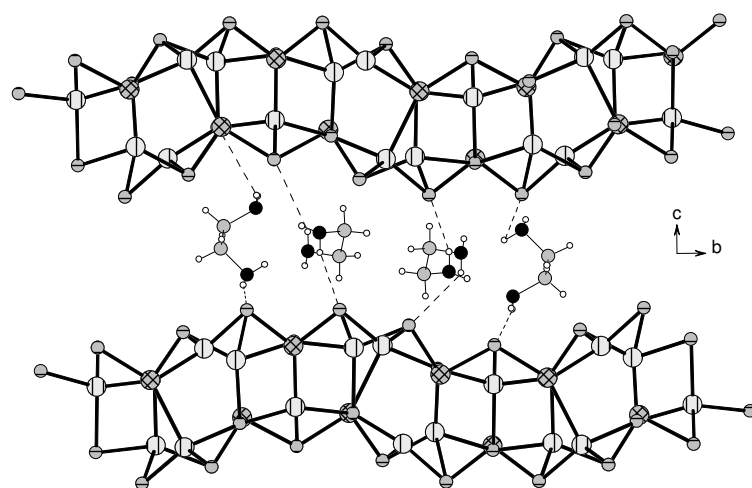


Fig. 6: The buckled double layers in compound **II** with view along [100] and the arrangement of the organic cations. Dotted lines indicate S...H hydrogen bonding.

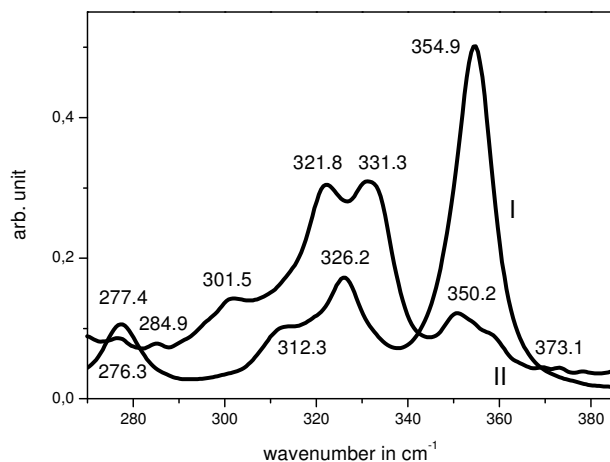


Fig. 7 Raman spectra of $[C_4N_2H_{14}]Ag_2Sb_2S_5$ (**I**) and $[C_2N_2H_9)_2][Ag_5Sb_3S_8]$ (**II**).

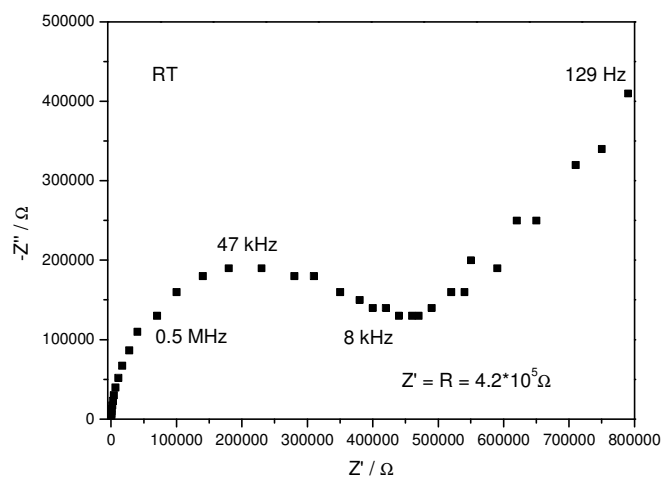


Fig. 8 Nyquistplot of the impedance measurement of a non-blocking interface at room temperature (RT) (**II**).

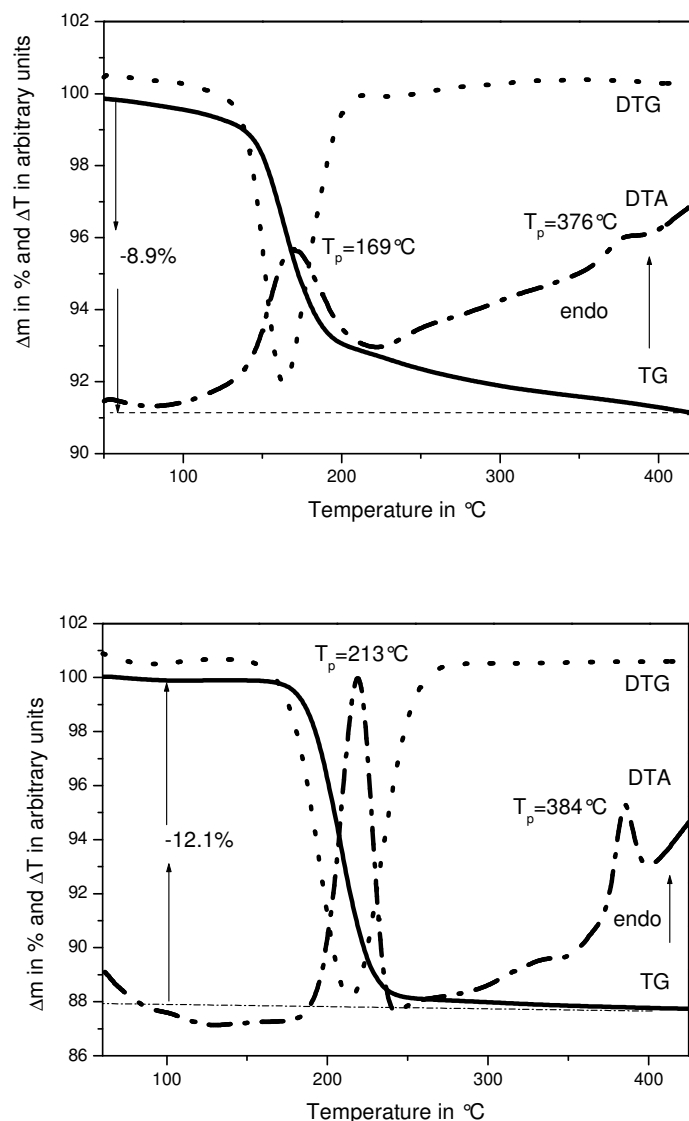


Fig. 9 TG-DTG-DTA curves of $[\text{C}_4\text{N}_2\text{H}_{14}][\text{Ag}_3\text{Sb}_3\text{S}_7]$ (I) (bottom) and $[\text{C}_2\text{N}_2\text{H}_9]_2[\text{Ag}_5\text{Sb}_3\text{S}_8]$ (II) (top).

4. Zusammenfassung und Ausblick

4.1 Thioantimonate (III) mit der allgemeinen Formel RSb_xS_y ($R = \text{Amin}$)

Die Verbindung $(C_6N_3H_{17})Sb_6S_{10}$ [56] gehört zur Gruppe der Thioantimonate(III) mit dem Sb:S-Verhältnis von 1:1.667. Auch die Anionen $[Sb_3S_5]^-$ [49-53], $[Sb_6S_{10}]^{2-}$ [54, 55, 56], $[Sb_9S_{15}]^{3-}$ [56] und $[Sb_{12}S_{20}]^{4-}$ [57] weisen das gleiche Sb-S-Verhältnis auf. In die Serie der Verbindungen mit dem Verhältnis 1:1.75 ($[Sb_4S_7]^{2-}$ [58-71], $[Sb_{12}S_{21}]^{6-}$ [69]) ist die neue Verbindung $(C_6N_2H_{18})Sb_4S_7$ einzuordnen. Unstrittig ist, dass organische Amine als strukturdirigierende Reagentien in der Synthese von nanoporösen Materialien eine bedeutende Rolle spielen. In wieweit aber gibt es gesicherte Erkenntnisse über die Mechanismen der Reaktionsprozesse? Aufgrund der vielen Variablen ist eine Vorhersage der Produkte kaum möglich und die Mechanismen bei der Entstehung der Festkörper aus den primären Baueinheiten ist kaum bekannt. Dennoch gibt es eine interessante Strategie für die Untersuchung von Templatmechanismen, die von Parise und Mitarbeitern entwickelt wurde [51]. Polymere Chalkogenidometallate der Gruppen 14 und 15 wurden mit kleineren Alkylammoniumionen als Gegenionen unter hydrothermalen Bedingungen synthetisiert. In manchen Fällen sind diese Gegenionen erst unter pyrolytischen Bedingungen aus grösseren Aminen entstanden. So wurde aus Triethylentetramin (TETN), $C_6N_4H_{18}$, das Piperazinium-Ion $[\text{pipzH}_2]^{2+}$ in der Verbindung $[\text{pipzH}_2]Sb_4S_7$ identifiziert [62]. Die Bildung eines anderen „Templats“ konnte auch bei der solvothermalen Synthese von $(C_8N_4H_{22})_{0.5}Cu_2SbS_3$ beobachtet werden [94]. Dabei cyclisierte während der Reaktion TETN zu 1,4-bis(2-aminoethyl)-Piperazin ($C_8N_4H_{20}$), wobei das im TETN zu 30% enthaltene TREN [tris(2-aminoethyl)amin = $C_6N_4H_{18}$] für diese Ringbildung ebenfalls verantwortlich sein könnte. In der Literatur ist bekannt, dass TETN unter bestimmten Versuchsbedingungen in Ethyldiamin und cyclisierte Amine einschließlich Piperazin übergeht [51].

Ein für Templatmechanismen typisches Indiz ist bei Netzwerken die Grösse der Hohlräume, die im allgemeinen die Geometrie der eingesetzten Amine widerspiegelt.

Dennoch kann ein einzelnes Amin zur Bildung von einer Vielzahl verschiedener anionischer Strukturen führen. Als Beispiel dafür kann 1,2-Diaminopropan ($C_3N_2H_{10}$) herangezogen werden, welches in den Verbindungen $(C_3N_2H_{12})Sb_{10}S_{16}$, $(C_3N_2H_{12})_2Sb_8S_{14}$ und $(C_3N_2H_{11})_2Sb_8S_{13}$ beobachtet wird [95]. Die Formel $(C_3H_{10}NO)_2Sb_4S_7$ steht für zwei Verbindungen mit verschiedenen anionischen Netzwerken [96]. Andererseits gibt es Gegenbeispiele, in denen ein spezielles Thioantimonatanion mit unterschiedlichen Aminen erhalten werden kann wie $(iPrH)_2Sb_8S_{13}$ und $(1,2-dapH)_2Sb_8S_{13}$ oder $(dienH_2)Sb_8S_{13}\cdot1.5H_2O$ und $(C_6H_9N_2)Sb_8S_{13}\cdot2.5H_2O$ zeigen [95]. Interessant ist ebenfalls, dass einige Thioantimonate(III) unter solvothermalem Bedingungen mit Übergangsmetallen gebildet wurden, ohne dass diese an der Struktur beteiligt sind. Beispiele dafür stellen die Synthesen von $(C_6N_4H_{20})Sb_4S_7$ mit Kupfer [93] und die Verbindungen $(trans-1,4-C_6N_2H_{15})Sb_3S_5$, $(trans-1,2-C_6N_2H_{15})Sb_3S_5$ [53], $(C_3NH_{10})_2Sb_4S_7$ und $(C_4NH_{12})_2Sb_4S_7$ mit Mangan dar [95]. Das Thioantimonat $(C_6N_2H_{18})Sb_4S_7$ wurde zuerst mit $AgNO_3$, Sb, S und 1,6-DAH hergestellt. Die anschließende Synthese mit Sb und S im Molverhältnis 1:3 bei $T = 170^\circ C$ führte zu einer wesentlich höheren Ausbeute der Verbindung. Bemerkenswert ist die Bildung von $[Sb_4S_7]^{2-}$ -Schichten mit parallel zu den Schichten angeordneten Aminmolekülen. Die Thioantimonate(III) weisen einige chemische und strukturelle Merkmale der Silikatchemie auf. Thioantimonate bilden analog zu Silikaten Ketten, Schichten und dreidimensionale Netzwerke, wobei letztere allerdings sehr selten auftreten. Ein Beispiel für ein Thioantimonat mit dreidimensionalem Netzwerk stellt $K_2Sb_4S_7$ dar [57]. Mit Zunahme der Kationengröße reduziert sich die Dimensionalität auf 2D-Schichten [60, 62, 63, 64, 66] und 1D-Ketten [59, 61, 68].

Die wesentlichen Unterschiede zwischen den Thioantimonaten(III) und Silikaten bestehen einerseits darin, dass Si immer tetraedrisch von O umgeben ist, während Sb drei bis sechs S-Atome binden kann. Andererseits ist die Si-O-Bindung mit Werten von ca. 1.6-1.7 Å relativ starr [97], während die Sb-S-Abstände von 2.3-3.8 Å einen grossen Wertebereich überstreichen. Die Silikate weisen mit Si-O-Si-Winkeln von ungefähr $90-180^\circ$ eine grössere Flexibilität als die Thioantimonate(III) auf, für die die Sb-S-Sb-Winkel im Bereich von 85 bis 110° liegen (S. 6, Abb. 1.2.2).

Die Struktur-Vielfalt der Thioantimonate(III) ist sehr gross und weitere neue Verbindungen können beim Einsatz anderer Amine erwartet werden, wobei auch der Einsatz von Aminoalkoholen als Strukturdirektoren von grosser Bedeutung sein könnte [96].

4.2 Kupfer(I)-Thioantimonate(III) mit der allgemeinen Formel RCu_2SbS_3 ($\text{R} = \text{Amin}$)

Einige interessante Aspekte ergeben sich bei der Betrachtung der Kupfer(I)-Thioantimonate(III) mit der allgemeinen Formel RCu_2SbS_3 ($\text{R} = \text{Amin}$).

Tab. 4.2.1 Gitterparameter der Kupfer(I)-Thioantimonate(III) mit der allgemeinen Formel RCu_2SbS_3 ($\text{R} = \text{Amin}$)

Amine Zuordnung ¹⁾	En (1)	1,3-DAP (2)	1,4-DAB (3)	1,6-DAH (I)	DIEN (II)	1,4-pip (III)
a [\AA]	6.173(2)	6.131(2)	6.159(2)	6.140(1)	6.170(4)	6.159(2)
b [\AA]	18.657(5)	21.504(4)	21.254(3)	24.77(5)	22.470(2)	27.480(6)
c [\AA]	6.502(2)	6.558(2)	6.544(2)	6.555(1)	6.546(4)	6.549(2)
β [°]	113.05(2)	113.01 °(1)	111.50 °(3)	112.53(1)	112.47(6)	112.25(3)
Zellvol. [\AA^3]	689.0(3)	795.9(2)	797.0(3)	919.0(2)	842.20(1)	1026.01(4)
Sb-S [\AA] ²⁾	2.440	2.442	2.443	2.440	2.448	2.443
Sb-S [\AA] ²⁾	3.839	3.840	3.849	3.871	3.840	3.849
Cu(1)-S [\AA] ²⁾	2.293	2.298	2.306	2.302	2.310	2.308
Cu(2)-S ²⁾ [\AA]	2.337	2.334	2.333	2.333	2.333	2.328
Cu(1)-Sb(1) [\AA] ³⁾	3.096	3.108	3.085	3.075	3.094	3.086
Cu(2)-Sb(1) [\AA] ³⁾	2.706	2.741	2.701	2.726	2.737	2.726
Cu-Cu [\AA] ³⁾	2.666	2.643	2.638	2.633	2.646	2.635

¹⁾ Die Zuordnung der Verbindungen entspricht der in der Veröffentlichung [93],

²⁾ Angabe von Mittelwerten, ³⁾ Angaben ohne Standardabweichungen.

En = Ethyldiamin, 1,3-DAP = 1,3-Diaminopropan, 1,4-DAB = 1,4-Diaminobutan, 1,6-DAH = 1,6-Diaminohexan, DIEN = Diethylentriamin, 1,4-pip = 1,4-bis(2-aminoethyl)-Piperazin.

Die mittleren Sb-S-Abstände liegen im Rahmen der Werte für Thioantimonate ohne Übergangsmetalle [44-85] und die so genannten sekundären Sb-S-Bindungen sind grösser als die Summe der van-der-Waals-Radien von 3.8 Å. Die mittleren Cu-S-Bindungen sind deutlich kürzer als die Summe der Ionenradien von Cu^+ und S^{2-} ($0.91 \text{ \AA} + 1.84 \text{ \AA} = 2.75 \text{ \AA}$). Interessant sind auch die kurzen **Cu(2)-Sb(1)**-Abstände (Tab. 4.2.1 und Abb. 4.2.1).

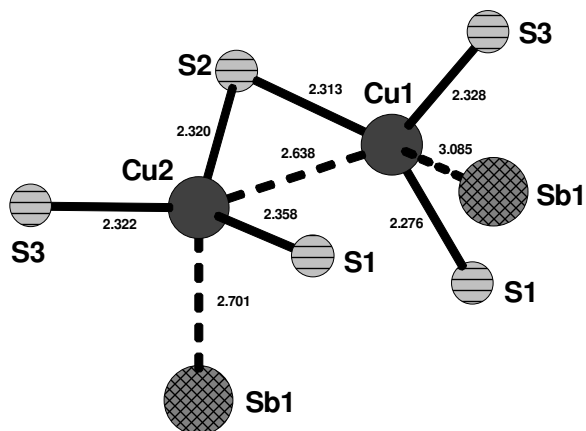


Abb. 4.2.1 Die Umgebung von Cu(1) und Cu(2) am Beispiel der Verbindung 3
(die Werte in Å sind ohne die Standardabweichungen angegeben)

Es ist deutlich zu erkennen, dass das Sb(III) $5s^2$ lone-pair in Richtung des Cu(I)-Zentrums weist, was zu den kurzen mittleren Cu(2)-Sb(1)-Abständen von 2.701–2.741 Å führt (Tab. 4.2.1). Die relativ kurzen **Cu-Cu**-Abstände (Tab. 4.2.1) sind etwas länger als im Cu-Metall mit 2.556 Å, aber dennoch könnte es sich hier um d^{10} - d^{10} -Wechselwirkungen handeln [22].

Bemerkenswert sind auch die unterschiedlichen **Cu(1)-S-** und **Cu(2)-S-**Abstände (Tab. 4.2.1 und Abb. 4.2.2).

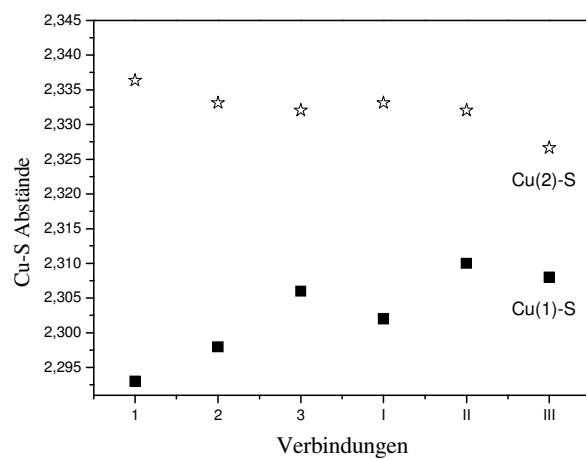


Abb. 4.2.2: Die gemittelten Cu(1)-S und Cu(2)-S Abstände in den Verbindungen **1-III** (in Å).

Die mittleren Cu(2)-S-Abstände sind zwischen 0.020 Å (**III**) und 0.044 Å (**1**) länger als die Cu(1)-S-Abstände. Dabei wird deutlich, dass die längeren Cu(2)-S-Abstände mit dem kürzeren Cu(2)-Sb-Abstand einhergehen (Tab. 4.2.1 und Abb. 4.2.1). Dieses ist möglicherweise auf eine Wechselwirkung zwischen Cu^I und dem 5s² lone-pair von Sb^{III} zurückzuführen. In der Verbindung Cu₂SbS₃·0.5en unterscheiden sich die Cu(1)-S- von den Cu(2)-S-Bindungen um ca. 0.057 Å und auch hier tritt die längere Cu-S-Bindung an dem Cu-Atom auf, das einen kürzeren Cu-Sb-Abstand aufweist [29].

Interessant sind auch die Analysen der **Interschichtabstände** (Tab. 4.2.2).

Tab. 4.2.2. Interschichtabstände von Kupfer(I)-Thioantimonaten(III) mit der allgemeinen Formel $\text{RCu}_2\text{SbS}_3 \cdot (\text{R} = \text{Amin})$

<u>Verbindung</u>	<u>Amin</u>	<u>Schicht-abstand</u> (Å) (gerundet)	<u>Parameter</u> b (Å)	<u>Winkel</u> β (°)	<u>C-Atome</u>
1 $(\text{en})_{0.5}\text{Cu}_2\text{SbS}_3$	Ethylendiamin	4.4	18.657 (5)	112.92(1)	2
3 $(1,4\text{-DAB})_{0.5}\text{Cu}_2\text{SbS}_3$	1,4-Diamino-butanol	5.93	21.254 (3)	111.50(3)	4
2 $(1,3\text{-DAP})_{0.5}\text{Cu}_2\text{SbS}_3$	1,3-Diamino-propan	5.98	21.504 (4)	113.01(1)	3
II $(\text{DIEN})_{0.5}\text{Cu}_2\text{SbS}_3$	Diethylentriamin	7.4	22.469 (2)	112.47(6)	4
I $(1,6\text{-DAH})_{0.5}\text{Cu}_2\text{SbS}_3$	1,6-Diamino – hexan	7.8	24.770 (5)	112.53(1)	6
III $(1,4\text{-pip})_{0.5}\text{Cu}_2\text{SbS}_3$	1,4-bis(2-amino ethyl)-Piperazin	8.8	27.480 (6)	112.25(3)	8

Die Werte in Tabelle 4.2.2 zeigen deutlich, dass mit Zunahme der Länge der b-Achse der Interschichtabstand von **1** bis **III** um über 4 Å zunimmt. Eine Abhängigkeit vom monoklinen Winkel β ist nicht eindeutig erkennbar. Eine Abhängigkeit des Interschichtabstandes von der Anzahl der C-Atome des Strukturdirektors ist nicht zwingend. Bei vielen Wirtsgittern wie z.B. TaS_2 sind die Interschichtabstände bei eingelagerten Alkylen mit weniger als 6 C-Atomen unabhängig von der Alkylkettenlänge [98]. Die Abbildung 4.2.3 zeigt exemplarisch für **1** und **III**, dass die protonierten Amine in Richtung der anionischen Schicht ausgerichtet sind, was darauf hindeutet, dass der N-H···S-Bindung eine wichtige Bedeutung zukommt.

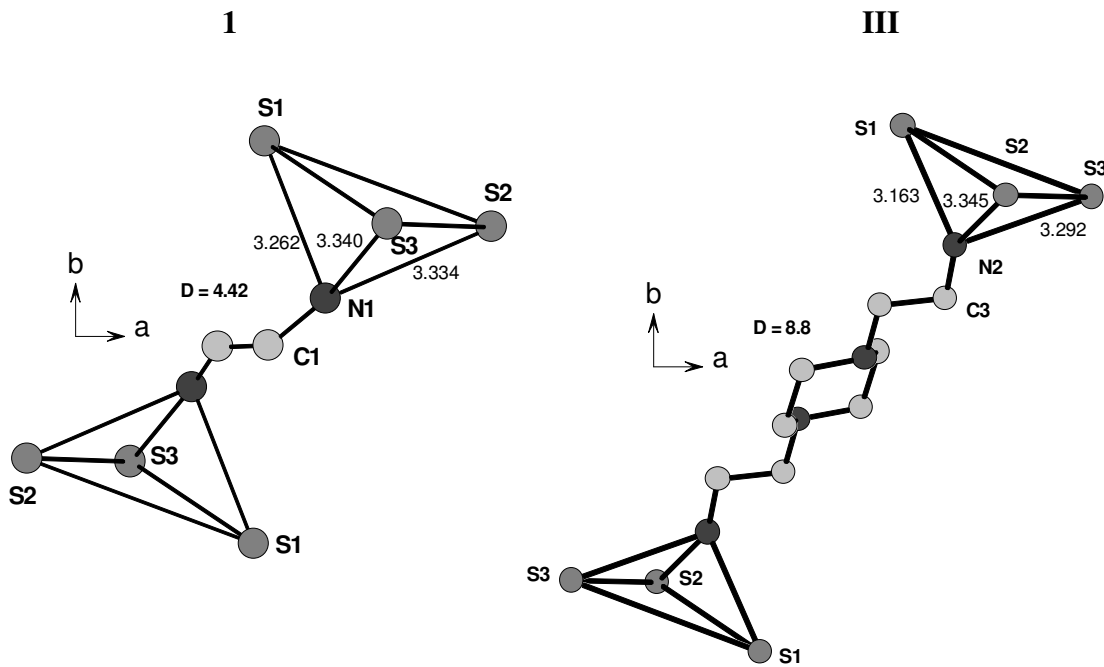


Abb. 4.2.3 Die Orientierung der Amine in $(en)_{0.5}Cu_2SbS_3$ (**1**) und in $(1,4\text{-pip})_{0.5}Cu_2SbS_3$ (**III**) mit N-H \cdots S -Bindungen (die Abstände sind in Å angegeben, D = Schichtabstände in Å)

Die Schichtdicke anorganischer Wirtsgitter bewegt sich oft zwischen 3-10 Å, während die Interschichtabstände durch den Einbau von „Templaten“ wie Aminen von 3-50 Å variieren können. Die Verbindung $(Octadecylamin)_xTaS_2$ weist mit 56.1 Å einen besonders grossen Interschichtabstand auf [98]. Solche Verbindungen zählt man zu den so genannten “Nanostruktur-Systemen”. Ein solch grosser Interschichtabstand wird bei den Kupferthioantimonaten nicht beobachtet. Trotzdem gehören diese Verbindungen zu den anorganisch-organischen Hybridverbindungen bzw. zu den nanostrukturierten Systemen.

Die Anionenschichten der Kupfer(I)-Thioantimonate(III) mit der allgemeinen Formel RCu_2SbS_3 werden aus kondensierten Cu-Sb-S-Ringen gebildet. Dabei wird nur ein Typ eines 6 MR (Cu_2SbS_3) und eines 10 MR ($Cu_3Sb_2S_5$) gefunden. Das ist bemerkenswert, da man sich viele Kombinationen für 6 MR und 10 MR vorstellen kann.

Tab. 4.2.3 Übersicht über die Synthesebedingungen der Kupfer(I)-Thioantimonate(III)

Verbindung	Eduktverhältnis (mmol)	V (mL)	Konz. (%)	Dauer (d)	Temp. (°C)
$(1,4\text{-DABH}_2)_{0.5}\text{Cu}_2\text{SbS}_3$ (1)	2:2:5 (Sb_2S_3 , CuCl_2 , S)	5	100	6	120
$(1,6\text{-DAHH}_2)_{0.5}\text{Cu}_2\text{SbS}_3$ (2)	2:2:5 (Sb, Cu, S)	5	100	7	140
$(\text{dienH}_2)_{0.5}\text{Cu}_2\text{SbS}_3$ (3)	2:2:5 (Sb, Cu, S)	5	100	7	140
$(1,4\text{-pipH}_2)_{0.5}\text{Cu}_2\text{SbS}_3$ (4)	2:2:5 (Sb, Cu, S)	5	70 (TETN)	7	140
$(\text{dienH})\text{Cu}_3\text{Sb}_2\text{S}_5$ (5)	2:2:5 (Sb, Cu, S)	5	100	7	140
$(\text{TETN}_2)_{0.5}\text{Cu}_3\text{Sb}_2\text{S}_5$ (6)	2:2:5 (Sb, Cu, S)	5	97	9	140

In der Tabelle 4.2.3 sind die Synthesebedingungen für die 6 neuen Kupfer(I)-Thioantimonate(III) zusammengefaßt. Auf den ersten Blick erscheinen die Versuchsbedingungen für alle Produkte sehr ähnlich zu sein. Ein Unterschied besteht im Einsatz der Edukte für Verbindung **1** im Vergleich zu den Verbindungen **2 - 6**. Scheinbar ist das Cu_2SbS_3 -Netzwerk unter den gewählten Bedingungen so stabil, dass die Eduktwahl nicht besonders wichtig zu sein scheint. Es stellte sich heraus, dass die Temperatur von 140 °C eine höhere Ausbeute bewirkt, wohingegen die Reaktionszeit und das Eduktverhältnis sowie das Volumen des Amins nicht besonders wichtig sind. Die Änderung der Konzentration der Amine führte im Unterschied zu Synthesen von Mangan- und Zink-Thioantimonaten(III/V) [99] zu keinen besonderen Ergebnissen. Interessant ist, dass sehr viele Mangan- und Zink-Thioantimonate(III/V) mit TREN (tris(2-aminoethyl)amin) erhalten wurden [99]. Versuche mit TREN oder 1,8-Diaminoctan führten nur zur Bildung von braunen amorphen Pulvern. Eventuell müssen mit diesen Aminen andere Versuchsbedingungen gefunden werden.

4.3 Kupfer(I)-Thioantimonate(III) mit der allgemeinen Formel $RCu_3Sb_2S_5$ (R = Amin)

Die Kupfer(I)-Thioantimonate(III) ($C_4N_3H_{14}Cu_3Sb_2S_5$) (**IV**) [$C_4N_3H_{13}$ = Diethylentriamin = DIEN] und ($C_6N_4H_{20}$)_{0.5} $Cu_3Sb_2S_5$ (**V**) [$C_6N_4H_{18}$ = Triethylentetramin = TETN] weisen bei gleicher Formel für das Anion $[Cu_3Sb_2S_5]^-$ völlig unterschiedliche Strukturen auf. In der Verbindung ($C_4N_3H_{14}Cu_3Sb_2S_5$) (**IV**) wird mit 2.622(1) Å der kürzeste **Cu-Cu**-Abstand für die Kupfer(I)-Thioantimonate(III) gefunden, welcher jedoch etwas länger als im metallischen Kupfer (2.556 Å) ist. Trotzdem könnten d^{10} - d^{10} -Wechselwirkungen vorliegen, welche die längeren Cu(2,3)-S- und Cu(2)-Sb-Abstände erklären könnten. Die Verbindung ($C_6N_4H_{20}$)_{0.5} $Cu_3Sb_2S_5$ (**V**) weist mit 2.683(3) Å den kürzesten **Cu(3)-Sb(2)**-Abstand auf. Die anionischen Schichten werden aus verschiedenen 6 MR aufgebaut und es entsteht ein verzerrtes 6^3 Netz. Die $Cu_2SbS_3^-$ und $CuSb_2S_3$ -Ringe treten im Verhältnis 4:1 auf, was zu der chemischen Formel $Cu_9Sb_6S_{15}$ führt und $Cu_3Sb_2S_5$ entspricht. Die Möglichkeiten der Kondensation unterschiedlicher Ringe wird bei der Verbindung ($C_4N_3H_{14}Cu_3Sb_2S_5$) (**IV**) deutlich. Das Verhältnis der 6 MR Cu_2SbS_3 : $CuSb_2S_3$ beträgt 3:2, und neben den fünf 6 MR sind in den Schichten noch zwei 4 MR ($Sb(2)Cu(3)S_2$, $Cu(2)Cu(3)S_2$) und ein 10 MR $CuSb_4S_5$ vorhanden (Abb. 4.2.3).

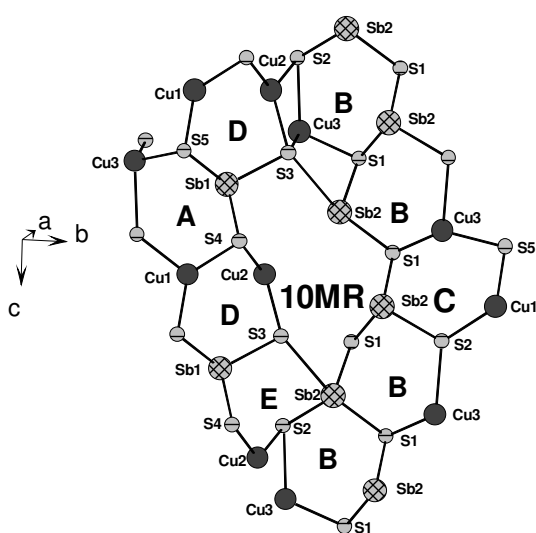


Abb. 4.2.3 Das Ringsystem in den Schichten der Verbindung $(C_4N_3H_{14})Cu_3Sb_2S_5$ (IV).

Um neue Kupfer(I)thioantimonate(III) mit unterschiedlichen Ringverhältnissen $\text{Cu}_2\text{SbS}_3:\text{CuSb}_2\text{S}_3$ und damit neue Netzwerktopologien zu erhalten, wurden die Molverhältnisse der Edukte verändert (Tab. 4.2.3). Allerdings wurden jeweils $(\text{C}_4\text{N}_3\text{H}_{14})\text{Cu}_3\text{Sb}_2\text{S}_5$, und CuSbS_2 [19] gebildet. Auf dem Blatt Papier lassen sich durch Kombination unterschiedlicher Heteroringe neue Netzwerktopologien designen.

Damit die Synthesen zielgerichteter durchgeführt werden können, ist ein grundsätzliches Verständnis der Bildungsmechanismen und der Wachstumskinetik erforderlich. Dieses Verständnis ist möglicherweise mit „in-situ“-Untersuchungen zu erreichen.

4.4 Die Silber(I)-Thioantimonate(III) $(C_4N_2H_{14})_2Ag_3Sb_3S_7$ und $(C_2N_2H_9)_2Ag_5Sb_3S_8$

Es gibt nur wenige unter solvothermalen Bedingungen synthetisierte Silber(I)-Thioantimonate(III) mit Aminen als Strukturdirektoren [42, 43]. In den beiden Silber(I)-Thioantimonaten(III) $(C_4N_2H_{14})_2Ag_3Sb_3S_7$ (**I**) und $(C_2N_2H_9)_2Ag_5Sb_3S_8$ (**II**) werden die Schichtanionen durch Verknüpfung der **primären Baueinheiten** - trigonale SbS_3 -Pyramiden, AgS_4 -Tetraeder und AgS_3 -Gruppen - gebildet. Die Netzwerktopologien dieser Verbindungen sind sehr unterschiedlich. Das zweidimensionale $[Ag_3Sb_3S_7]^{2-}$ -Anion wird durch Kondensation einer eindimensionalen $[Sb_2S_5]$ -Kette mit $[Ag_3SbS_5]$ -Einheiten, welche Ag_3SbS_3 -Halbwürfel als Zentralmotiv enthalten, gebildet. In der Verbindung **II** werden in den Schichten acht verschiedene 6 MR gefunden, von denen sieben aus zwei Ag-, einem Sb- und drei S-Atomen bestehen, während der achte Ring ein Ag-, zwei Sb- und drei S-Atome enthält. Zwischen den anionischen **Schichten** sind die protonierten Amine sandwichartig angeordnet. Diese anorganisch-organischen Hybridverbindungen weisen Interschichtabstände von 5.4 Å (**II**) und 7.4 Å (**I**) auf. Wie bei den Kupfer(I)-Thioantimonaten(III) sind auch hier die Ammoniumgruppen des organischen Moleküls unter Ausbildung von S···H-Brückenbindungen zur anionischen Schicht ausgerichtet. Interessant ist in der Verbindung **I** die ungewöhnliche Bindung von S(4) an vier Ag- und ein Sb-Atom. Das führt dazu, dass der Ag(1)-S(4)-Abstand länger ist als die Ag(1,3)-S-Abstände. Als Erklärung dafür könnte eine analoge Beobachtung bei den Verbindungen $Mn_2(L)Sb_2S_5$ (L = Amin) dienen. Ein sehr langer Mn-S-Abstand wird dadurch erklärt, dass dieses S-Atom an 3 Mn^{2+} - und 2 Sb(III)-ionen gebunden ist, während die S-Atome, die in die kürzeren Mn-S-Abstände involviert sind, nur Bindungen zu einem Mn^{2+} - und 2 Sb(III)-ionen oder 2 Mn^{2+} und 2 Sb(III)-ionen haben [100]. Ein weiterer interessanter Aspekt ist die Beobachtung, dass drei nicht isostrukturelle Verbindungen mit dem $[Ag_5Sb_3S_8]^{2-}$ -Anion bekannt sind, die unter verschiedenen solvothermalen Bedingungen hergestellt wurden [42, 43]. Die Synthese der beiden Verbindungen mit Ethylendiamin als Strukturdirektor [42] erfolgte mit unterschiedlichen Eduktverhältnissen und bei unterschiedlichen Temperaturen.

Die Silber(I)-Thioantimonat(III)-Chemie steht erst am Anfang. Da beide Verbindungen unter nahezu gleichen solvothermalen Bedingungen wie die Kupfer(I)-Thioantimonate(III) hergestellt wurden, könnten bei einem Einsatz der gleichen Amine (Tab. 4.2.3) neue Verbindungen im Ag-Sb-S-System gebildet werden.

4.5 Synthese von Kupfer(I)- Silber(I)- Thioantimonat(III): ein Anfang?

Silber- und Kupferthioantimonate sind nicht isostrukturell. Eine Überlegung war daher, Verbindungen mit unterschiedlichen Cu-Sb-S- und Ag-Sb-S-Blöcken darzustellen. Eine typische Synthese wurde mit Cu, Ag, Sb und S in den Molverhältnissen 1:1:2:5 bzw. 1:1:1:2.5 und 4 mL Ethylenediamin (en) bei 140°C 7 Tage durchgeführt. Dabei wurde eine neue Verbindung erhalten, welche aus braunen Plättchen besteht (Abb. 4.5.1) und in der triklinen Raumgruppe $P\bar{1}$ kristallisiert.

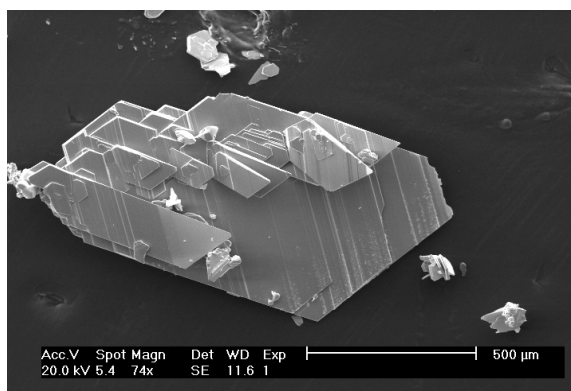


Abb. 4.5.1 SEM-Bild von Kristallen der Verbindung $(C_2N_2H_{10})_2Cu_3Ag_5Sb_4S_{12}$

Mit Hilfe der **Atomabsorptionsspektrometrie** (AAS) wurde die molare Zusammensetzung zu $[Cu_3Ag_5Sb_4S_{12}]^{4-}$ bestimmt. Der Ladungsausgleich erfolgt durch zweifach protonierte $(enH_2^{2+})_2$ -Kationen ($en =$ Ethylenediamin). Die CHN-Analyse ergab: C_{exp}: 2.4%, H_{exp}: 0.8%, N_{exp}: 2.6%, C_{theor.}: 2.7%. H_{theor.}: 1.2% N_{theor.}: 3.1%. Der thermische Abbau der Verbindung beginnt bei 179°C und wird von mehreren endothermen Ereignissen begleitet: T_p = 198°C, T_p = 361°C, T_p = 401°C, T_p = 417°C (Abb. 4.5.2). Als Abbauprodukte konnten Sb₂S₃, AgSbS₂, Ag₃SbS₃ und Cu₃SbS₃ im Pulverdiffraktogramm nachgewiesen werden.

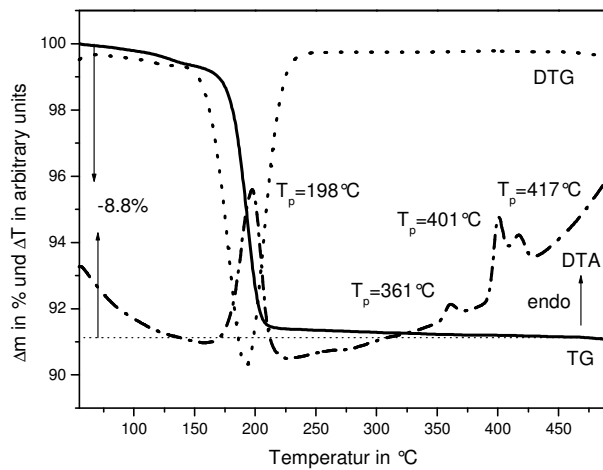


Abb. 4.5.2 TG-DTG-DTA-Kurven der Verbindung $(\text{C}_2\text{N}_2\text{H}_{10})_2\text{Cu}_3\text{Ag}_5\text{Sb}_4\text{S}_{12}$

Die **primären Baueinheiten** in der Struktur bilden fünf AgS_3^- , zwei CuS_3^- und vier SbS_3^- -Einheiten (Abb. 4.5.3).

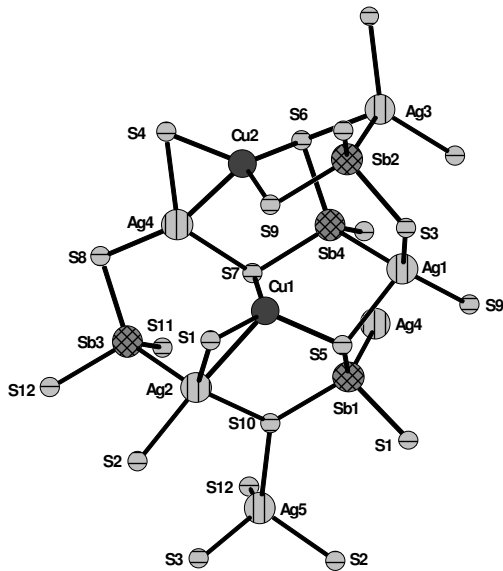


Abb. 4.5.3 Umgebung von $\text{Ag}1-5$, $\text{Cu}1-2$ und $\text{Sb}1-4$.

Die Sb-S-Abstände und S-Sb-S-Winkel entsprechen den aus der Literatur bekannten Werten [44-85] und die Cu-S- und Ag-S-Abstände sowie die entsprechenden Winkel stimmen mit den Daten für Kupfer(I)-Thioantimonate(III) [93, 94] und Silber(I)-Thioantimonate(III) überein. Die primären Baueinheiten sind zu verschiedenen

Ringen verbunden, welche zu **Einfachschichten** kondensieren. Die Einfachschichten sind über S-Brücken zu **Doppelschichten** verknüpft. Zwischen den Anionenschichten ist das zweifach protonierte Amin sandwichartig angeordnet. Dabei beträgt der Interschichtabstand 4.61 Å.

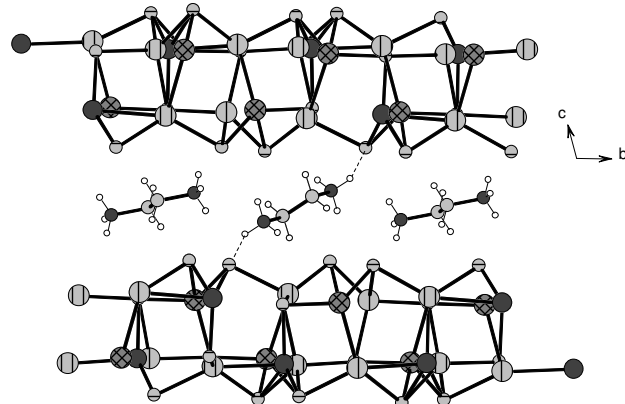


Abb. 4.5.6 Schichtstruktur der Verbindung $(\text{C}_2\text{N}_2\text{H}_{10})_2\text{Cu}_3\text{Ag}_5\text{Sb}_4\text{S}_{12}$

Bei der Strukturverfeinerung traten erhebliche Probleme bei der Zuordnung von Ag und Cu im anionischen Netzwerk auf, so dass kein befriedigendes Strukturmodell erhalten werden konnte.

5. Publikationsliste und Tagungsbeiträge

5.1 Publikationsliste

Novel Copper(I)- Thioantimonates(III): Solvothermal Synthesis, Crystal Structures, Thermal Stability and Magnetic Properties of $(C_2N_2H_{10})_{0.5}Cu_2SbS_3$, $(C_3N_2H_{12})_{0.5}Cu_2SbS_3$ and $(C_4N_2H_{14})_{0.5}Cu_2SbS_3$

V.Spetzler, H. Rijnberk, C. Näther, W. Bensch

Z. Anorg. Allgem. Chem., **630**, 142-148, 2004

Two novel Thioantimonates(III) with the Same Stoichiometric Sb: S Ratio but Different Crystal Structures: Solvothermal Synthesis, Crystal Structures, Thermal Stability and Spectroscopy of $(C_6N_3H_{17})Sb_6S_{10}$ and $(C_7N_2H_{13})Sb_9S_{15}$

V.Spetzler, R. Kiebach, C. Näther, W. Bensch

Z. Anorg. Allgem. Chem., **630**, 2398-2404, 2004

Template Assisted Solvothermal Synthesis of Five New Copper(I)-Thioantimonates(III) Composites: Crystal Structures, Optical and Thermal Properties of $(C_6N_2H_{18})_{0.5}Cu_2SbS_3$, $(C_4N_3H_{15})_{0.5}Cu_2SbS_3$, $(C_8N_4H_{22})_{0.5}Cu_2SbS_3$, $(C_4N_3H_{14})_{0.5}Cu_3Sb_2S_5$ and $(C_6N_4H_{20})_{0.5}Cu_3Sb_2S_5$

V.Spetzler, C. Näther, W. Bensch

Inorg. Chem., **44**, 5805-5812, 2005

$(C_6N_2H_{18})Sb_4S_7$ a thioantimonate(III) with a layered $[Sb_4S_7]^{2-}$ anion in the presence of a diprotonated amine as structure director.

V.Spetzler, C. Näther, W. Bensch

Z. Naturforsch. **61b**,(2006); received 2006

The new silver(I)thioantimonate(III) $(C_4N_2H_{14})Ag_3Sb_3S_7$ and a new structural variant of the silver(I)thioantimonate(III) $(C_2N_2H_9)_2Ag_5Sb_3S_8$ both synthesized under solvothermal conditions

V. Spetzler, C. Näther, W. Bensch

Manuskript wurde eingereicht

5.2 Tagungsbeitrag

Synthesen und Kristallstrukturen neuer Kupferthioantimonat-Komposite

V.Spetzler, C. Näther, W. Bensch

12. Jahrestagung der Deutschen Gesellschaft für Kristallographie, 2004, Jena

Z. Kristallogr. Suppl. **21**, 74, 2004

6. Strukturdaten

6.1 Single Crystal Structure Determination of (1,6-DAHH₂)Sb₄S₇

Table 1. Crystal data and structure refinement for (1,6-DAHH₂)Sb₄S₇

Identification code	vs745o	
Empirical formula	(C ₆ H ₁₈ N ₂)Sb ₄ S ₇	
Habitus	orange needles	
Formula weight	829.64 g/mol	
Temperature	293(2) K	
Wavelength	0.71073 Å	
Crystal system	triclinic	
Space group	P-1	
Unit cell dimensions	a = 6.9834(5) Å b = 11.8748(10) Å c = 13.6588(12) Å	α= 115.248(9)°. β= 100.165(9)°. γ= 92.568(9)°.
Volume	999.18(14) Å ³	
Z	2	
Density (calculated)	2.758 g/cm ³	
Absorption coefficient	6.070 mm ⁻¹	
F(000)	768	
Crystal size	1 · 0.2 · 0.1 mm ³	
Theta range for data collection	3.10 to 28.06°.	
Index ranges	-8 ≤ h ≤ 8, -15 ≤ k ≤ 15, -18 ≤ l ≤ 18	
Reflections collected	7421	
Independent reflections	3620 [R(int) = 0.0735]	
Completeness to theta = 28.06°	74.5 %	
Refinement method	Full-matrix least-squares on F ²	
Data / restraints / parameters	3620 / 0 / 173	
Goodness-of-fit on F ²	0.982	
Final R indices [I>2sigma(I)]	R1 = 0.0462, wR2 = 0.1154	
R indices (all data)	R1 = 0.0665, wR2 = 0.1230	
Extinction coefficient	0.0022(5)	
Largest diff. peak and hole	1.075 and -1.280 e.Å ⁻³	

Table 2. Atomic coordinates ($\cdot 10^4$) and equivalent isotropic displacement parameters ($\text{\AA}^2 \cdot 10^3$).**U(eq) is defined as one third of the trace of the orthogonalized U_{ij} tensor.**

	x	y	z	U(eq)
Sb(1)	8679(1)	5062(1)	3652(1)	21(1)
Sb(2)	10559(1)	8342(1)	4612(1)	22(1)
Sb(3)	16270(1)	9084(1)	5708(1)	19(1)
Sb(4)	16511(1)	6510(1)	6483(1)	20(1)
S(1)	10381(4)	3535(3)	2348(2)	30(1)
S(2)	5470(4)	3796(3)	2352(2)	30(1)
S(3)	8337(4)	6473(3)	2821(2)	30(1)
S(4)	12609(4)	6826(3)	4791(2)	31(1)
S(5)	13523(4)	10232(2)	6121(2)	23(1)
S(6)	16928(4)	8793(2)	7485(2)	29(1)
S(7)	18648(4)	11041(2)	6800(2)	23(1)
N(1)	7930(20)	811(14)	2135(12)	62(4)
C(1)	7930(30)	-60(20)	954(15)	71(6)
C(2)	7360(30)	-1380(20)	668(13)	79(7)
C(3)	5260(20)	-1710(20)	629(15)	62(4)
C(4)	4770(30)	-2980(20)	662(15)	77(6)
C(5)	2690(30)	-3316(19)	605(15)	63(4)
C(6)	2360(30)	-4188(17)	1114(15)	60(4)
N(2)	3360(20)	-3601(14)	2296(11)	57(4)

Table 3. Bond lengths [\AA] and angles [$^\circ$]

Sb(1)-S(3)	2.390(3)	Sb(3)-S(7)	2.491(3)
Sb(1)-S(1)	2.460(3)	Sb(3)-S(6)	2.562(3)
Sb(1)-S(2)	2.539(3)	Sb(4)-S(2)#2	2.409(3)
Sb(2)-S(4)	2.415(3)	Sb(4)-S(6)	2.435(3)
Sb(2)-S(7)#1	2.471(3)	Sb(4)-S(1)#3	2.475(3)
Sb(2)-S(3)	2.653(3)	Sb(2)-S(5)	2.775(3)

S(4)-Sb(2)-S(5)	88.38(8)	Sb(3)-S(5)-Sb(2)	97.97(9)
S(7)#1-Sb(2)-S(5)	86.70(8)	Sb(4)-S(6)-Sb(3)	93.40(10)
S(3)-Sb(2)-S(5)	165.37(9)	Sb(2)#1-S(7)-Sb(3)	104.09(10)
S(5)-Sb(3)-S(7)	91.58(9)		
S(5)-Sb(3)-S(6)	95.49(9)		
S(7)-Sb(3)-S(6)	85.15(9)		

Symmetry transformations used to generate equivalent atoms:

#1 -x+3,-y+2,-z+1 #2 -x+2,-y+1,-z+1 #3 -x+3,-y+1,-z+1

Table 4. Anisotropic displacement parameters ($\text{\AA}^2 \cdot 10^3$). The anisotropic displacement factor exponent takes the form: $-2\pi^2 [h^2 a^{*2} U_{11} + \dots + 2 h k a^{*} b^{*} U_{12}]$

	U ₁₁	U ₂₂	U ₃₃	U ₂₃	U ₁₃	U ₁₂
Sb(1)	19(1)	20(1)	29(1)	15(1)	6(1)	5(1)
Sb(2)	19(1)	18(1)	32(1)	12(1)	10(1)	3(1)
Sb(3)	17(1)	15(1)	30(1)	13(1)	4(1)	5(1)
Sb(4)	18(1)	19(1)	26(1)	12(1)	5(1)	4(1)
S(1)	22(2)	30(1)	33(2)	10(1)	3(1)	14(1)
S(2)	20(2)	40(2)	30(2)	16(1)	3(1)	-8(1)
S(3)	30(2)	21(1)	38(2)	19(1)	-8(1)	-3(1)
S(4)	32(2)	21(1)	40(2)	18(1)	-6(1)	2(1)
S(5)	18(1)	20(1)	29(1)	10(1)	3(1)	9(1)
S(6)	39(2)	18(1)	35(2)	18(1)	1(1)	4(1)
S(7)	23(1)	17(1)	31(1)	13(1)	3(1)	0(1)
N(1)	51(9)	55(9)	64(9)	14(7)	14(6)	-9(6)
C(1)	70(12)	73(13)	51(10)	24(9)	-8(7)	-7(9)
C(2)	68(13)	115(19)	20(8)	0(9)	-4(6)	31(10)
C(3)	54(11)	71(13)	58(11)	29(9)	6(7)	10(7)
C(4)	98(16)	94(18)	34(9)	26(10)	9(8)	20(11)
C(5)	81(13)	54(11)	43(10)	18(8)	1(7)	-10(7)
C(6)	77(13)	48(10)	64(11)	30(8)	24(8)	21(7)
N(2)	70(9)	69(10)	58(8)	42(7)	34(6)	52(7)

Table 5. Hydrogen coordinates ($\cdot 10^4$) and isotropic displacement parameters ($\text{\AA}^2 \cdot 10^3$)

	x	y	z	U(eq)
H(1A)	8285	1600	2265	92
H(1B)	8771	609	2585	92
H(1C)	6729	739	2257	92
H(1A)	7032	182	469	85
H(1B)	9235	44	823	85
H(2A)	8168	-1587	1207	95
H(2B)	7641	-1895	-51	95
H(3A)	4471	-1740	-44	74
H(3B)	4880	-1047	1252	74
H(4A)	5169	-3639	46	92
H(4B)	5541	-2942	1340	92
H(5A)	1997	-3711	-165	75
H(5B)	2130	-2554	982	75
H(6A)	963	-4382	1043	72
H(6B)	2864	-4969	723	72
H(2A)	3141	-4121	2591	85
H(2B)	2893	-2886	2653	85
H(2C)	4643	-3443	2358	85

6.2 Single Crystal Structure Determination of (1-pipH₂)Sb₆S₁₀

Table 1. Crystal data and structure refinement for (1-pipH₂)Sb₆S₁₀

Identification code	vs554	
Empirical formula	(C ₆ N ₃ H ₁₇)Sb ₆ S ₁₀	
Habitus	red needles	
Formula weight	1182.33 g/mol	
Temperature	293(2) K	
Wavelength	0.71073 Å	
Crystal system	monoclinic	
Space group	P2 ₁	
Unit cell dimensions	a = 6.1202(4) Å b = 17.7589(13) Å c = 11.4781(7) Å	α = 90°. β = 90.699(7)°. γ = 90°.
Volume	1247.44(14) Å ³	
Z	2	
Density (calculated)	3.148 g/cm ³	
Absorption coefficient	7.243 mm ⁻¹	
F(000)	1080	
Crystal size	2 · 1 · 1 mm ³	
Theta range for data collection	2.29 to 27.99°.	
Index ranges	-7 ≤ h ≤ 7, -23 ≤ k ≤ 23, -15 ≤ l ≤ 15	
Reflections collected	12065	
Independent reflections	5770 [R(int) = 0.0370]	
Completeness to theta = 27.99°	97.8 %	
Refinement method	Full-matrix least-squares on F ²	
Data / restraints / parameters	5770 / 1 / 228	
Goodness-of-fit on F ²	1.029	
Final R indices [I>2sigma(I)]	R1 = 0.0322, wR2 = 0.0789	
R indices (all data)	R1 = 0.0353, wR2 = 0.0810	
Absolute structure parameter	-0.03(3)	
Extinction coefficient	0.0055(3)	
Largest diff. peak and hole	1.250 and -1.312 e.Å ⁻³	

Table 2. Atomic coordinates ($\cdot 10^4$) and equivalent isotropic displacement parameters ($\text{\AA}^2 \cdot 10^3$). U(eq) is defined as one third of the trace of the orthogonalized U_{ij} tensor.

	x	y	z	U(eq)
Sb(1)	-5143(1)	7235(1)	966(1)	23(1)
Sb(2)	-533(1)	6915(1)	3072(1)	17(1)
Sb(3)	-365(1)	5062(1)	5089(1)	17(1)
Sb(4)	4389(1)	3929(1)	6149(1)	19(1)
Sb(5)	-390(1)	3917(1)	8042(1)	16(1)
Sb(6)	-1045(1)	5776(1)	10164(1)	17(1)
S(1)	-1480(4)	7485(1)	413(2)	26(1)
S(2)	-4569(4)	7014(1)	3055(2)	24(1)
S(3)	-360(4)	5607(1)	2253(2)	24(1)
S(4)	-557(4)	6480(1)	5105(2)	0(1)
S(5)	3620(4)	5178(1)	5252(2)	20(1)
S(6)	-1417(4)	5159(1)	7170(2)	19(1)
S(7)	865(4)	3466(1)	5579(2)	19(1)
S(8)	3494(4)	4251(1)	8181(2)	25(1)
S(9)	-1206(4)	4364(1)	10075(2)	17(1)
S(10)	-5059(4)	5905(1)	10225(2)	24(1)
N(1)	3825(12)	8058(4)	7487(6)	18(1)
C(1)	5138(17)	7593(5)	6716(8)	26(2)
C(2)	5293(17)	6793(5)	7192(9)	28(2)
N(2)	3019(14)	6472(4)	7291(7)	27(2)
C(3)	1565(15)	6974(5)	7964(7)	23(2)
C(4)	1594(15)	7772(5)	7491(7)	22(2)
C(5)	3859(15)	8866(5)	7171(7)	23(2)
C(6)	5967(18)	9236(6)	7583(8)	29(2)
N(3)	6259(14)	9088(4)	8849(6)	26(2)

Table 3. Bond lengths [Å] and angles [°].

Sb(1)-S(1)	2.379(3)	Sb(4)-S(8)	2.470(2)
Sb(1)-S(2)	2.450(2)	Sb(4)-S(5)	2.487(2)
Sb(1)-S(10)#1	2.512(2)	Sb(5)-S(8)	2.453(2)
Sb(2)-S(4)	2.457(2)	Sb(5)-S(6)	2.499(2)
Sb(2)-S(2)	2.476(2)	Sb(5)-S(9)	2.5209(19)
Sb(2)-S(3)	2.510(2)	Sb(6)-S(3)#2	2.448(2)
Sb(3)-S(5)	2.452(2)	Sb(6)-S(10)	2.469(2)
Sb(3)-S(6)	2.488(2)	Sb(6)-S(9)	2.512(2)
Sb(3)-S(4)	2.522(2)	Sb(4)-S(7)	2.393(2)
S(1)-Sb(1)-S(2)	99.62(8)	S(6)-Sb(5)-S(9)	92.34(6)
S(1)-Sb(1)-S(10)#1	93.54(8)	S(3)#2-Sb(6)-S(10)	98.18(8)
S(2)-Sb(1)-S(10)#1	100.22(8)	S(3)#2-Sb(6)-S(9)	85.60(7)
S(4)-Sb(2)-S(2)	90.72(8)	S(10)-Sb(6)-S(9)	93.17(7)
S(4)-Sb(2)-S(3)	93.76(7)	Sb(1)-S(2)-Sb(2)	98.65(8)
S(2)-Sb(2)-S(3)	96.26(8)	Sb(6)#1-S(3)-Sb(2)	104.24(8)
S(5)-Sb(3)-S(6)	100.93(7)	Sb(2)-S(4)-Sb(3)	107.83(7)
S(5)-Sb(3)-S(4)	87.81(7)	Sb(3)-S(5)-Sb(4)	98.02(7)
S(6)-Sb(3)-S(4)	84.92(6)	Sb(3)-S(6)-Sb(5)	104.86(7)
S(7)-Sb(4)-S(8)	97.36(7)	Sb(5)-S(8)-Sb(4)	96.22(7)
S(7)-Sb(4)-S(5)	91.63(7)	Sb(6)-S(9)-Sb(5)	110.11(7)
S(8)-Sb(4)-S(5)	98.13(8)	Sb(6)-S(10)-Sb(1)#2	96.98(8)
S(8)-Sb(5)-S(6)	92.94(8)	S(8)-Sb(5)-S(9)	93.80(7)

Symmetry transformations used to generate equivalent atoms: #1 x,y,z-1 #2 x,y,z+1.

Table 4. Anisotropic displacement parameters ($\text{\AA}^2 \times 10^3$). The anisotropic displacement factor exponent takes the form: $-2\pi^2[h^2 a^{*2}U_{11} + \dots + 2 h k a^{*} b^{*} U_{12}]$

	U ₁₁	U ₂₂	U ₃₃	U ₂₃	U ₁₃	U ₁₂
Sb(1)	23(1)	24(1)	20(1)	-2(1)	-4(1)	9(1)
Sb(2)	19(1)	16(1)	15(1)	1(1)	0(1)	-1(1)
Sb(3)	20(1)	18(1)	13(1)	0(1)	-2(1)	-2(1)
Sb(4)	17(1)	22(1)	17(1)	-1(1)	3(1)	3(1)
Sb(5)	17(1)	14(1)	16(1)	-1(1)	1(1)	-1(1)
Sb(6)	21(1)	17(1)	14(1)	1(1)	3(1)	0(1)
S(1)	31(1)	22(1)	25(1)	-2(1)	6(1)	-2(1)
S(2)	20(1)	34(1)	19(1)	-2(1)	4(1)	1(1)
S(3)	36(1)	18(1)	16(1)	-3(1)	-5(1)	7(1)
S(4)	30(1)	16(1)	14(1)	0(1)	-1(1)	3(1)
S(5)	18(1)	19(1)	24(1)	1(1)	3(1)	-2(1)
S(6)	23(1)	17(1)	17(1)	1(1)	2(1)	6(1)
S(7)	24(1)	15(1)	19(1)	-2(1)	-2(1)	-1(1)
S(8)	18(1)	42(1)	14(1)	-3(1)	-2(1)	-4(1)
S(9)	23(1)	16(1)	13(1)	0(1)	3(1)	2(1)
S(10)	20(1)	23(1)	28(1)	-2(1)	-2(1)	2(1)
N(1)	19(4)	13(3)	21(3)	3(2)	3(3)	0(3)
C(1)	27(5)	20(4)	30(4)	0(3)	10(4)	0(3)
C(2)	34(5)	17(4)	34(5)	2(3)	9(4)	5(4)
N(2)	27(4)	19(3)	34(4)	-2(3)	4(3)	-10(3)
C(3)	18(4)	32(4)	18(4)	-1(3)	1(3)	-2(3)
C(4)	17(4)	33(4)	16(4)	1(3)	0(3)	-6(3)
C(5)	28(5)	16(4)	24(4)	0(3)	3(3)	-1(3)
C(6)	42(6)	26(4)	18(4)	-2(3)	3(4)	-7(4)
N(3)	25(4)	31(4)	22(3)	-5(3)	-7(3)	-4(3)

Table 5. Hydrogen coordinates ($\cdot 10^4$) and isotropic displacement parameters ($\text{\AA}^2 \cdot 10^3$).

	x	y	z	U(eq)
H(1A)	6592	7806	6654	31
H(1B)	4477	7585	5944	31
H(2A)	6153	6484	6674	34
H(2B)	6006	6797	7951	34
H(2C)	2449	6404	6573	32
H(2D)	3093	6020	7643	32
H(3A)	2033	6978	8774	27
H(3B)	84	6780	7928	27
H(4A)	996	7778	6704	27
H(4B)	692	8093	7971	27
H(5A)	2625	9118	7523	27
H(5B)	3719	8917	6332	27
H(6A)	7193	9033	7158	34
H(6B)	5901	9774	7443	34
H(3C)	7492	9303	9101	39
H(3D)	6328	8594	8971	39
H(3E)	5134	9279	9234	39

6.3 Single Crystal Structure Determination of $(1.4\text{-DABH}_2)_{0.5}\text{Cu}_2\text{SbS}_3$

Table 1. Crystal data and structure refinement for $(1.4\text{-DABH}_2)_{0.5}\text{Cu}_2\text{SbS}_3$

Identification code	vs80
Empirical formula	$(\text{C}_4\text{N}_2\text{H}_{14})_{0.5}\text{Cu}_2\text{SbS}_3$
Habitus	orange needles
Formula weight	780.19 g/mol
Temperature	293(2) K
Wavelength	0.71073 Å
Crystal system	monoclinic
Space group	P2 ₁ /n
Unit cell dimensions	a = 6.1590(12) Å α = 90°. b = 21.254(3) Å β = 111.50(3)°. c = 6.5440(13) Å γ = 90°.
Volume	797.0(3) Å ³
Z	2
Density (calculated)	3.251 g/cm ³
Absorption coefficient	9.346 mm ⁻¹
F(000)	732
Crystal size	0.05 · 0.05 · 0.1 mm ³
Theta range for data collection	3.48 to 29.96°.
Index ranges	0 ≤ h ≤ 8, -29 ≤ k ≤ 29, -9 ≤ l ≤ 8
Reflections collected	4873
Independent reflections	2297 [R(int) = 0.0506]
Completeness to theta = 29.96°	99.0 %
Refinement method	Full-matrix least-squares on F ²
Data / restraints / parameters	2297 / 0 / 92
Goodness-of-fit on F ²	1.124
Final R indices [I>2sigma(I)]	R1 = 0.0304, wR2 = 0.0684
R indices (all data)	R1 = 0.0658, wR2 = 0.0772
Extinction coefficient	0.0061(4)
Largest diff. peak and hole	1.305 and -1.349 e.Å ⁻³

Table 2. Atomic coordinates ($\cdot 10^4$) and equivalent isotropic displacement parameters ($\text{\AA}^2 \cdot 10^3$). U(eq) is defined as one third of the trace of the orthogonalized U_{ij} tensor.

	x	y	z	U(eq)
Sb(1)	7018(1)	7040(1)	6261(1)	14(1)
Cu(2)	6072(1)	8216(1)	7265(1)	24(1)
Cu(1)	6565(1)	6907(1)	1428(1)	28(1)
S(1)	10655(2)	7064(1)	5589(2)	19(1)
S(3)	4746(2)	6327(1)	3363(2)	17(1)
S(2)	8140(2)	6302(1)	9377(2)	16(1)
N(1)	7380(8)	4206(3)	1904(9)	30(1)
C(1)	7028(15)	4821(4)	2740(15)	61(3)
C(2)	8863(14)	4924(4)	5106(16)	31(2)
C(2')	9720(40)	5103(13)	3810(30)	30(6)

Table 3. Bond lengths [Å] and angles [°].

Sb(1)-S(3)	2.4304(14)	Cu(2)-S(3)#3	2.3221(15)
Sb(1)-S(1)#1	2.4366(13)	Cu(2)-Cu(1)#4	2.6380(12)
Sb(1)-S(1)	2.4366(13)	Cu(1)-S(1)#2	2.2758(17)
Sb(1)-S(2)	2.4625(14)	Cu(1)-S(2)#5	2.3129(15)
Sb(1)-Cu(2)	2.7010(9)	Cu(1)-S(3)	2.3277(16)
Sb(1)-Cu(1)	3.0845(10)	Cu(2)-S(2)#2	2.3199(16)
S(3)-Sb(1)-S(1)	100.16(5)	Cu(1)#4-Cu(2)-Sb(1)	99.36(3)
S(3)-Sb(1)-S(2)	98.93(5)	S(1)#2-Cu(1)-S(2)#5	120.86(6)
S(1)-Sb(1)-S(2)	99.50(5)	S(1)#2-Cu(1)-S(3)	121.04(6)
S(3)-Sb(1)-Cu(2)	130.78(4)	S(2)#5-Cu(1)-S(3)	114.15(6)
S(1)-Sb(1)-Cu(2)	108.62(4)	S(1)#2-Cu(1)-Cu(2)#6	106.99(5)
S(2)-Sb(1)-Cu(2)	114.09(4)	S(2)#5-Cu(1)-Cu(2)#6	55.42(4)
S(3)-Sb(1)-Cu(1)	48.15(4)	S(3)-Cu(1)-Cu(2)#6	120.96(5)
S(1)-Sb(1)-Cu(1)	63.92(4)	S(1)#2-Cu(1)-Sb(1)	94.64(4)
S(2)-Sb(1)-Cu(1)	133.08(4)	S(2)#5-Cu(1)-Sb(1)	138.29(5)
Cu(2)-Sb(1)-Cu(1)	112.82(2)	S(3)-Cu(1)-Sb(1)	51.06(4)
S(2)#2-Cu(2)-S(3)#3	116.51(6)	Cu(2)#6-Cu(1)-Sb(1)	95.94(4)
S(2)#2-Cu(2)-S(1)#4	123.18(5)	Cu(1)#3-S(1)-Cu(2)#6	111.37(6)
S(3)#3-Cu(2)-S(1)#4	104.07(6)	Cu(1)#3-S(1)-Sb(1)	97.91(5)
S(2)#2-Cu(2)-Cu(1)#4	55.16(4)	Cu(2)#6-S(1)-Sb(1)	125.42(6)
S(3)#3-Cu(2)-Cu(1)#4	159.65(5)	Cu(2)#2-S(3)-Cu(1)	102.61(6)
S(1)#4-Cu(2)-Cu(1)#4	72.81(5)	Cu(2)#2-S(3)-Sb(1)	101.37(6)
S(2)#2-Cu(2)-Sb(1)	112.56(4)	Cu(1)-S(3)-Sb(1)	80.79(5)
S(3)#3-Cu(2)-Sb(1)	100.97(4)	Cu(1)#7-S(2)-Cu(2)#3	69.42(5)
S(1)#4-Cu(2)-Sb(1)	95.60(4)	Cu(1)#7-S(2)-Sb(1)	94.38(5)
Cu(2)#3-S(2)-Sb(1)	106.94(6)		

Symmetry transformations used to generate equivalent atoms:

#1 x,y,z #2 x-1/2,-y+3/2,z-1/2 #3 x+1/2,-y+3/2,z+1/2 #4 x-1/2,-y+3/2,z+1/2 #5 x,y,z-1 #6 x+1/2,-y+3/2,z-1/2 #7 x,y,z+1.

Table 4. Anisotropic displacement parameters ($\text{\AA}^2 \cdot 10^3$). The anisotropic displacement factor exponent takes the form: $-2\pi^2 [h^2 a^*{}^2 U_{11} + \dots + 2 h k a^* b^* U_{12}]$

	U ₁₁	U ₂₂	U ₃₃	U ₂₃	U ₁₃	U ₁₂
Sb(1)	13(1)	16(1)	13(1)	-2(1)	5(1)	1(1)
Cu(2)	17(1)	30(1)	21(1)	3(1)	3(1)	1(1)
Cu(1)	32(1)	28(1)	30(1)	2(1)	20(1)	4(1)
S(1)	17(1)	25(1)	18(1)	-1(1)	10(1)	-2(1)
S(3)	14(1)	20(1)	15(1)	-3(1)	5(1)	-1(1)
S(2)	16(1)	21(1)	12(1)	0(1)	5(1)	-1(1)
N(1)	21(2)	28(3)	31(3)	-5(2)	-2(2)	2(2)
C(1)	47(4)	40(5)	62(6)	-25(4)	-21(4)	11(4)
C(2)	27(4)	29(5)	40(5)	-13(4)	17(4)	-6(3)
C(2')	21(10)	45(15)	12(9)	17(9)	-8(8)	-18(9)

Table 5. Hydrogen coordinates ($\cdot 10^4$) and isotropic displacement parameters ($\text{\AA}^2 \cdot 10^3$)

	x	y	z	U(eq)
H(1N1)	6010	4014	1287	45
H(2N1)	8309	3973	3008	45
H(3N1)	8037	4257	909	45
H(1A)	5467	4844	2769	73
H(1B)	7183	5149	1774	73
H(2A)	8382	5268	5819	37
H(2B)	9010	4547	5980	37
H(2C)	10748	4910	3175	36
H(2D)	9755	5557	3675	36

6.4 Single Crystal Structure Determination of $(1.6\text{-DAHH}_2)_{0.5}\text{Cu}_2\text{SbS}_3$

Table 1. Crystal data and structure refinement for $(1.6\text{-DAHH}_2)_{0.5}\text{Cu}_2\text{SbS}_3$

Identification code	vs489
Empirical formula	$(\text{C}_6\text{N}_2\text{H}_{18})_{0.5}\text{Cu}_2\text{SbS}_3$
Habitus	orange needles
Formula weight	808.24 g/mol
Temperature	293(2) K
Wavelength	0.71073 Å
Crystal system	monoclinic
Space group	P2 ₁ /n
Unit cell dimensions	a = 6.1350(10) Å α = 90°. b = 24.751(3) Å β = 112.530(10)°. c = 6.5520(10) Å γ = 90°.
Volume	919.0(2) Å ³
Z	2
Density (calculated)	2.921 g/cm ³
Absorption coefficient	8.112 mm ⁻¹
F(000)	764
Crystal size	2 · 1 · 1 mm ³
Theta range for data collection	3.29 to 28.02 °
Index ranges	0 ≤ h ≤ 8, -32 ≤ k ≤ 32, -8 ≤ l ≤ 7
Reflections collected	4745
Independent reflections	2215 [R(int) = 0.0232]
Completeness to theta = 28.02 °	99.9 %
Refinement method	Full-matrix least-squares on F ²
Data / restraints / parameters	2215 / 0 / 97
Goodness-of-fit on F ²	1.129
Final R indices [$I > 2\sigma(I)$]	R1 = 0.0161, wR2 = 0.0395
R indices (all data)	R1 = 0.0190, wR2 = 0.0401
Extinction coefficient	0.0065(2)
Largest diff. peak and hole	0.532 and -0.529 e.Å ⁻³

Table 2. Atomic coordinates ($\cdot 10^4$) and equivalent isotropic displacement parameters ($\text{\AA}^2 \cdot 10^3$). U(eq) is defined as one third of the trace of the orthogonalized U_{ij} tensor.

	x	y	z	U(eq)
Sb(1)	7214(1)	2101(1)	3892(1)	16(1)
Cu(1)	6757(1)	1988(1)	-929(1)	29(1)
Cu(2)	6291(1)	3120(1)	4919(1)	26(1)
S(1)	10894(1)	2126(1)	3250(1)	20(1)
S(2)	8291(1)	1471(1)	7004(1)	18(1)
S(3)	4974(1)	1480(1)	989(1)	19(1)
N(1)	2747(4)	1036(1)	5847(4)	29(1)
C(1)	2912(6)	568(1)	4529(5)	35(1)
C(2)	716(6)	489(1)	2496(5)	39(1)
C(3)	1098(8)	53(2)	1028(5)	36(1)
C(3')	-320(80)	15(14)	1000(50)	64(10)

Table 3. Bond lengths [Å] and angles [°].

Sb(1)-S(1)	2.4503(7)	Cu(1)-S(2)#2	2.3099(7)
Sb(1)-S(2)	2.4487(6)	Cu(1)-S(3)	2.3265(7)
Sb(1)-S(3)	2.4222(6)	Cu(1)-Cu(2)#3	2.6330(7)
Sb(1)-Cu(2)	2.7263(5)	Cu(2)-S(1)#5	2.3672(7)
Sb(1)-Cu(1)	3.0747(6)	Cu(2)-S(2)#1	2.3163(7)
Cu(1)-S(1)#1	2.2705(7)	Cu(2)-S(3)#4	2.3156(7)
S(3)-Sb(1)-S(2)	98.08(2)	S(1)#5-Cu(2)-Cu(1)#5	72.21(2)
S(3)-Sb(1)-S(1)	99.47(2)	S(3)#4-Cu(2)-Sb(1)	101.51(2)
S(2)-Sb(1)-S(1)	100.77(2)	S(2)#1-Cu(2)-Sb(1)	112.06(2)
S(3)-Sb(1)-Cu(2)	132.243(18)	S(1)#5-Cu(2)-Sb(1)	95.360(19)
S(2)-Sb(1)-Cu(2)	113.528(17)	Cu(1)#5-Cu(2)-Sb(1)	98.978(14)
S(1)-Sb(1)-Cu(2)	108.103(17)	Cu(1)#4-S(1)-Cu(2)#3	111.73(3)
S(3)-Sb(1)-Cu(1)	48.303(16)	Cu(1)#4-S(1)-Sb(1)	97.52(2)
S(2)-Sb(1)-Cu(1)	133.397(17)	Cu(2)#3-S(1)-Sb(1)	125.36(3)
S(1)-Sb(1)-Cu(1)	63.476(18)	Cu(1)#6-S(2)-Cu(2)#4	69.38(2)
Cu(2)-Sb(1)-Cu(1)	113.067(11)	Cu(1)#6-S(2)-Sb(1)	95.43(2)
S(1)#1-Cu(1)-S(2)#2	120.45(2)	Cu(2)#4-S(2)-Sb(1)	106.49(3)
S(1)#1-Cu(1)-S(3)	122.32(2)	Cu(2)#1-S(3)-Cu(1)	102.22(3)
S(2)#2-Cu(1)-S(3)	113.46(3)	Cu(2)#1-S(3)-Sb(1)	99.24(2)
S(1)#1-Cu(1)-Cu(2)#3	106.27(2)	Cu(1)-S(3)-Sb(1)	80.68(2)
S(2)#2-Cu(1)-Cu(2)#3	55.422(18)	Cu(2)#3-Cu(1)-Sb(1)	96.860(17)
S(3)-Cu(1)-Cu(2)#3	120.55(2)	S(3)#4-Cu(2)-S(2)#1	115.95(3)
S(1)#1-Cu(1)-Sb(1)	94.412(18)	S(3)#4-Cu(2)-S(1)#5	105.33(2)
S(2)#2-Cu(1)-Sb(1)	139.05(2)	S(2)#1-Cu(2)-S(1)#5	122.88(3)
S(3)-Cu(1)-Sb(1)	51.022(16)	S(3)#4-Cu(2)-Cu(1)#5	159.51(2)

Symmetry transformations used to generate equivalent atoms:

#1 x-1/2,-y+1/2,z-1/2 #2 x,y,z-1 #3 x+1/2,-y+1/2,z-1/2 #4 x+1/2,-y+1/2,z+1/2 #5 x-1/2,-y+1/2,z+1/2 #6 x,y,z+1.

Table 4. Anisotropic displacement parameters ($\text{\AA}^2 \cdot 10^3$). The anisotropic displacement factor exponent takes the form: $-2\pi^2 [h^2 a^*{}^2 U_{11} + \dots + 2 h k a^* b^* U_{12}]$

	U ₁₁	U ₂₂	U ₃₃	U ₂₃	U ₁₃	U ₁₂
Sb(1)	15(1)	18(1)	14(1)	-1(1)	6(1)	1(1)
Cu(1)	34(1)	29(1)	31(1)	2(1)	21(1)	4(1)
Cu(2)	19(1)	33(1)	23(1)	3(1)	4(1)	1(1)
S(1)	19(1)	24(1)	19(1)	-1(1)	11(1)	-1(1)
S(2)	18(1)	22(1)	14(1)	-1(1)	6(1)	-1(1)
S(3)	16(1)	24(1)	15(1)	-3(1)	6(1)	-2(1)
N(1)	29(1)	27(1)	30(1)	-5(1)	8(1)	1(1)
C(1)	39(2)	27(1)	37(1)	-4(1)	14(1)	5(1)
C(2)	49(2)	30(2)	33(1)	-8(1)	9(1)	-2(1)
C(3)	40(3)	30(2)	29(2)	-11(1)	4(2)	-1(2)

Table 5. Hydrogen coordinates ($\cdot 10^4$) and isotropic displacement parameters ($\text{\AA}^2 \cdot 10^3$).

	x	y	z	U(eq)
H(1N1)	4083	1067	7030	44
H(2N1)	1548	988	6277	44
H(3N1)	2510	1334	5033	44
H(1A)	3203	246	5435	42
H(1B)	4243	618	4095	42
H(2A)	295	825	1681	47
H(2B)	-577	385	2921	47
H(3A)	2374	162	590	43
H(3B)	1567	-280	1868	43
H(3C)	-2027	31	509	76

6.5 Single Crystal Structure Determination of $(\text{dienH}_2)_{0.5}\text{Cu}_2\text{SbS}_3$

Table 1. Crystal data and structure refinement for $(\text{dienH}_2)_{0.5}\text{Cu}_2\text{SbS}_3$

Identification code	vs611o	
Empirical formula	$(\text{C}_4\text{N}_3\text{H}_{15})_{0.5}\text{Cu}_2\text{SbS}_3$	
Habitus	orange needles	
Formula weight	795.21 g/mol	
Temperature	293(2) K	
Wavelength	0.71073 Å	
Crystal system	monoclinic	
Space group	P2 ₁ /n	
Unit cell dimensions	a = 6.1962(4) Å b = 22.4696(18) Å c = 6.5461(4) Å	α = 90°. β = 112.470(6)°. γ = 90°.
Volume	842.20(10) Å ³	
Z	2	
Density (calculated)	3.136 g/cm ³	
Absorption coefficient	8.850 mm ⁻¹	
F(000)	748	
Crystal size	0.05 · 0.05 · 0.1 mm ³	
Theta range for data collection	3.49 to 27.99°	
Index ranges	-8 ≤ h ≤ 8, -29 ≤ k ≤ 29, -8 ≤ l ≤ 8	
Reflections collected	7639	
Independent reflections	1954 [R(int) = 0.0485]	
Completeness to theta = 27.99°	96.1 %	
Refinement method	Full-matrix least-squares on F ²	
Data / restraints / parameters	1954 / 0 / 108	
Goodness-of-fit on F ²	1.036	
Final R indices [I>2sigma(I)]	R1 = 0.0299, wR2 = 0.0736	
R indices (all data)	R1 = 0.0371, wR2 = 0.0766	
Largest diff. peak and hole	0.823 and -1.839 e.Å ⁻³	

Table 2. Atomic coordinates ($\cdot 10^4$) and equivalent isotropic displacement parameters ($\text{\AA}^2 \cdot 10^3$). U(eq) is defined as one third of the trace of the orthogonalized U_{ij} tensor.

	x	y	z	U(eq)
Sb(1)	7735(1)	2067(1)	5710(1)	10(1)
Cu(2)	6777(1)	3189(1)	6759(1)	20(1)
Cu(1)	7259(1)	1942(1)	849(1)	25(1)
S(1)	11393(2)	2077(1)	5093(2)	15(1)
S(2)	8823(2)	1365(1)	8825(2)	12(1)
S(3)	5464(2)	1386(1)	2781(2)	13(1)
N(1)	13402(9)	863(2)	7505(10)	37(1)
C(1)	13622(17)	357(6)	6350(30)	61(4)
C(2)	11540(40)	163(7)	4490(30)	117(10)
N(2)	10540(30)	-173(8)	6330(30)	31(5)
C(1')	13170(30)	267(6)	8020(30)	49(5)
C(2')	10990(50)	-3(8)	7110(60)	87(12)
N(2')	10780(40)	-135(10)	4410(40)	17(4)

Table 3. Bond lengths [Å] and angles [°].

Sb(1)-S(3)	2.4351(11)	Cu(2)-S(1)#3	2.3606(13)
Sb(1)-S(1)	2.4496(10)	Cu(2)-Cu(1)#3	2.6464(9)
Sb(1)-S(2)	2.4588(11)	Cu(1)-S(1)#1	2.2798(12)
Sb(1)-Cu(2)	2.7370(7)	Cu(1)-S(2)#4	2.3132(12)
Sb(1)-Cu(1)	3.0942(8)	Cu(1)-S(3)	2.3383(12)
Cu(2)-S(2)#1	2.3145(12)	Cu(1)-Cu(2)#5	2.6464(9)
Cu(2)-S(3)#2	2.3259(11)		
S(3)-Sb(1)-S(1)	99.70(4)	Cu(1)#3-Cu(2)-Sb(1)	98.84(2)
S(3)-Sb(1)-S(2)	98.24(4)	S(1)#1-Cu(1)-S(2)#4	122.19(5)
S(1)-Sb(1)-S(2)	99.49(4)	S(1)#1-Cu(1)-S(3)	120.83(4)
S(3)-Sb(1)-Cu(2)	131.33(3)	S(2)#4-Cu(1)-S(3)	113.65(4)
S(1)-Sb(1)-Cu(2)	109.63(3)	S(2)#4-Cu(1)-Cu(2)#5	55.14(3)
S(2)-Sb(1)-Cu(2)	113.53(3)	S(3)-Cu(1)-Cu(2)#5	120.01(4)
S(3)-Sb(1)-Cu(1)	48.24(3)	S(1)#1-Cu(1)-Sb(1)	93.28(4)
S(1)-Sb(1)-Cu(1)	64.01(3)	S(2)#4-Cu(1)-Sb(1)	138.05(4)
S(2)-Sb(1)-Cu(1)	133.07(3)	S(3)-Cu(1)-Sb(1)	50.97(3)
Cu(2)-Sb(1)-Cu(1)	113.40(2)	Cu(2)#5-Cu(1)-Sb(1)	95.84(3)
S(2)#1-Cu(2)-S(3)#2	116.07(4)	Cu(1)#2-S(1)-Cu(2)#5	110.27(5)
S(2)#1-Cu(2)-S(1)#3	123.31(4)	Cu(1)#2-S(1)-Sb(1)	97.41(4)
S(3)#2-Cu(2)-S(1)#3	105.83(5)	Cu(2)#5-S(1)-Sb(1)	125.23(5)
S(2)#1-Cu(2)-Cu(1)#3	55.10(3)	Cu(1)#6-S(2)-Cu(2)#2	69.76(4)
S(3)#2-Cu(2)-Cu(1)#3	161.52(4)	Cu(1)#6-S(2)-Sb(1)	94.26(4)
S(1)#3-Cu(2)-Cu(1)#3	73.04(3)	Cu(2)#2-S(2)-Sb(1)	106.85(4)
S(2)#1-Cu(2)-Sb(1)	111.66(4)	Cu(2)#1-S(3)-Cu(1)	104.08(5)
S(3)#2-Cu(2)-Sb(1)	99.61(3)	Cu(2)#1-S(3)-Sb(1)	100.21(4)
S(1)#3-Cu(2)-Sb(1)	96.17(3)	Cu(1)-S(3)-Sb(1)	80.79(4)

Symmetry transformations used to generate equivalent atoms:

#1 x-1/2,-y+1/2,z-1/2 #2 x+1/2,-y+1/2,z+1/2 #3 x-1/2,-y+1/2,z+1/2 #4 x,y,z-1 #5 x+1/2,-y+1/2,z-1/2 #6 x,y,z+1.

Table 4. Anisotropic displacement parameters ($\text{\AA}^2 \cdot 10^3$). The anisotropic displacement factor exponent takes the form: $-2\pi^2[h^2 a^* a^* U_{11} + \dots + 2 h k a^* b^* U_{12}]$

	U ₁₁	U ₂₂	U ₃₃	U ₂₃	U ₁₃	U ₁₂
Sb(1)	7(1)	13(1)	10(1)	-2(1)	4(1)	0(1)
Cu(2)	11(1)	28(1)	18(1)	3(1)	1(1)	1(1)
Cu(1)	28(1)	27(1)	29(1)	2(1)	21(1)	5(1)
S(1)	11(1)	21(1)	15(1)	-2(1)	8(1)	-2(1)
S(2)	10(1)	17(1)	10(1)	-1(1)	4(1)	-1(1)
S(3)	8(1)	19(1)	12(1)	-4(1)	3(1)	-1(1)
N(1)	26(2)	32(2)	48(4)	0(2)	9(2)	-6(2)
C(1)	15(5)	49(6)	108(13)	-39(7)	12(6)	-1(4)
C(2)	113(16)	49(9)	99(16)	-23(9)	-58(12)	8(9)
C(1')	57(11)	17(6)	45(12)	0(6)	-12(9)	-1(6)
C(2')	110(20)	22(9)	190(30)	-34(14)	130(30)	-16(11)

Table 5. Hydrogen coordinates ($\cdot 10^4$) and isotropic displacement parameters ($\text{\AA}^2 \cdot 10^3$).

	x	y	z	U(eq)
H(1N1)	14746	932	8632	56
H(2N1)	12278	805	8016	56
H(3N1)	13041	1176	6600	56
H(4N1)	14720	1009	8501	56
H(5N1)	12198	1078	7511	56
H(6N1)	13463	879	6170	56
H(1A)	14138	30	7393	73
H(1B)	14848	431	5804	73
H(2A)	11876	-116	3538	140
H(2B)	10575	483	3650	140
H(1N2)	11043	29	7619	37
H(1C)	14241	34	7584	59
H(1D)	13697	237	9615	59
H(2C)	9764	252	7157	105
H(2D)	10970	368	7867	105
H(2N2)	10979	-528	4288	21

6.6 Single Crystal Structure Determination of $(1,4\text{-pipH}_2)_{0.5}\text{Cu}_2\text{SbS}_3$

Table 1. Crystal data and structure refinement for $(1,4\text{-pipH}_2)_{0.5}\text{Cu}_2\text{SbS}_3$

Identification code	slvs369o		
Empirical formula	$(\text{C}_8\text{N}_4\text{H}_{22})_{0.5}\text{Cu}_2\text{SbS}_3$		
Habitus	orange crystal		
Formula weight	862.30 g/mol		
Temperature	293(2) K		
Wavelength	0.71073 Å		
Crystal system	monoclinic		
Space group	P2 ₁ /n		
Unit cell dimensions	$a = 6.1594(12)$ Å	$\alpha = 90^\circ$.	
	$b = 27.480(6)$ Å	$\beta = 112.24(3)^\circ$.	
	$c = 6.5491(13)$ Å	$\gamma = 90^\circ$.	
Volume	1026.0(4) Å ³		
Z	2		
Density (calculated)	2.791 g/cm ³		
Absorption coefficient	7.278 mm ⁻¹		
F(000)	820		
Crystal size	0.05 · 0.05 · 0.1 mm ³		
Theta range for data collection	2.97 to 25.88 °		
Index ranges	-7 ≤ h ≤ 7, -33 ≤ k ≤ 33, -8 ≤ l ≤ 8		
Reflections collected	7681		
Independent reflections	1975 [R(int) = 0.0516]		
Completeness to theta = 25.88 °	99.5 %		
Refinement method	Full-matrix least-squares on F ²		
Data / restraints / parameters	1975 / 0 / 109		
Goodness-of-fit on F ²	1.024		
Final R indices [$I > 2\sigma(I)$]	R1 = 0.0280, wR2 = 0.0685		
R indices (all data)	R1 = 0.0341, wR2 = 0.0709		
Largest diff. peak and hole	0.742 and -1.436 e.Å ⁻³		

Table 2. Atomic coordinates ($\cdot 10^4$) and equivalent isotropic displacement parameters ($\text{\AA}^2 \cdot 10^3$).

U(eq) is defined as one third of the trace of the orthogonalized U_{ij} tensor.

	x	y	z	U(eq)
Sb	834(1)	2143(1)	5788(1)	14(1)
Cu(2)	1765(1)	3059(1)	4739(1)	24(1)
Cu(1)	1285(1)	2042(1)	10624(1)	27(1)
S(1)	-2841(2)	2158(1)	6413(2)	18(1)
S(3)	3093(2)	1589(1)	8701(2)	17(1)
S(2)	-289(2)	1575(1)	2671(2)	16(1)
N(2)	-1329(10)	252(2)	7962(9)	49(1)
N(1)	-4909(7)	1174(2)	3874(7)	30(1)
C(2)	-1912(12)	685(3)	6574(14)	61(2)
C(3)	1175(14)	156(4)	8634(14)	70(2)
C(1)	-4491(11)	741(2)	5288(11)	44(2)
C(4)	1856(15)	-306(3)	10073(15)	66(2)

Table 3. Bond lengths [Å] and angles [°].

Sb-S(3)	2.4268(12)	Cu(2)-S(2)#2	2.3142(14)
Sb-S(1)	2.4486(12)	Cu(2)-S(1)#3	2.3578(13)
Sb-S(2)	2.4539(12)	Cu(2)-Cu(1)#3	2.6345(10)
Sb-Cu(2)	2.7258(8)	Cu(1)-S(1)#2	2.2766(14)
Sb-Cu(1)	3.0861(9)	Cu(1)-S(2)#4	2.3164(13)
Cu(2)-S(3)#1	2.3129(13)	Cu(1)-S(3)	2.3317(13)
S(3)-Sb-S(1)	99.79(4)	S(3)-Cu(1)-Cu(2)#5	120.40(4)
S(3)-Sb-S(2)	98.69(4)	S(1)#2-Cu(1)-Sb	93.83(4)
S(1)-Sb-S(2)	99.34(4)	S(2)#4-Cu(1)-Sb	138.54(4)
S(3)-Sb-Cu(2)	131.71(3)	S(3)-Cu(1)-Sb	50.93(3)
S(1)-Sb-Cu(2)	108.84(3)	Cu(2)#5-Cu(1)-Sb	96.12(4)
S(2)-Sb-Cu(2)	113.48(3)	Cu(1)#1-S(1)-Cu(2)#5	110.85(5)
S(3)-Sb-Cu(1)	48.24(3)	Cu(1)#1-S(1)-Sb	97.60(4)
S(1)-Sb-Cu(1)	63.86(4)	Cu(2)#5-S(1)-Sb	125.12(6)
S(2)-Sb-Cu(1)	133.12(3)	Cu(2)#2-S(3)-Cu(1)	103.42(5)
Cu(2)-Sb-Cu(1)	113.38(2)	Cu(2)#2-S(3)-Sb	100.02(5)
S(3)#1-Cu(2)-S(2)#2	115.73(5)	Cu(1)-S(3)-Sb	80.84(4)
S(3)#1-Cu(2)-S(1)#3	105.41(5)	Cu(2)#1-S(2)-Cu(1)#6	69.35(4)
S(2)#2-Cu(2)-S(1)#3	123.65(5)	Cu(2)#1-S(2)-Sb	107.38(5)
S(3)#1-Cu(2)-Cu(1)#3	160.54(4)	Cu(1)#6-S(2)-Sb	94.61(4)
S(2)#2-Cu(2)-Cu(1)#3	55.36(4)	Cu(1)#3-Cu(2)-Sb	98.81(3)
S(1)#3-Cu(2)-Cu(1)#3	72.97(5)	S(1)#2-Cu(1)-S(2)#4	121.25(5)
S(3)#1-Cu(2)-Sb	100.64(4)	S(1)#2-Cu(1)-S(3)	121.17(5)
S(2)#2-Cu(2)-Sb	111.47(4)	S(2)#4-Cu(1)-S(3)	114.02(5)
S(1)#3-Cu(2)-Sb	95.97(4)	S(1)#2-Cu(1)-Cu(2)#5	106.91(4)

Symmetry transformations used to generate equivalent atoms:

#1 x-1/2,-y+1/2,z-1/2 #2 x+1/2,-y+1/2,z+1/2 #3 x+1/2,-y+1/2,z-1/2 #4 x,y,z+1 #5 x-1/2,-y+1/2,z+1/2 #6 x,y,z-1.

Table 4. Anisotropic displacement parameters ($\text{\AA}^2 \cdot 10^3$). The anisotropic displacement factor exponent takes the form: $-2\pi^2 [h^2 a^*{}^2 U_{11} + \dots + 2 h k a^* b^* U_{12}]$

	U ₁₁	U ₂₂	U ₃₃	U ₂₃	U ₁₃	U ₁₂
Sb	11(1)	17(1)	13(1)	2(1)	5(1)	0(1)
Cu(2)	15(1)	32(1)	22(1)	-3(1)	3(1)	-1(1)
Cu(1)	29(1)	29(1)	30(1)	-1(1)	19(1)	-3(1)
S(1)	15(1)	24(1)	20(1)	2(1)	11(1)	2(1)
S(3)	11(1)	23(1)	15(1)	2(1)	3(1)	1(1)
S(2)	13(1)	21(1)	13(1)	1(1)	5(1)	1(1)
N(2)	46(3)	42(3)	47(3)	7(3)	4(3)	4(2)
N(1)	23(2)	28(2)	34(2)	4(2)	6(2)	3(2)
C(2)	44(4)	50(4)	70(5)	25(4)	-1(4)	-4(3)
C(3)	53(4)	89(6)	67(5)	34(5)	22(4)	23(4)
C(1)	40(3)	28(3)	48(4)	9(3)	0(3)	-4(2)
C(4)	63(5)	54(5)	80(6)	10(4)	27(4)	14(4)

Table 5. Hydrogen coordinates ($\cdot 10^4$) and isotropic displacement parameters ($\text{\AA}^2 \cdot 10^3$).

	x	y	z	U(eq)
H(2A)	-6441	1207	3110	44
H(2B)	-4172	1140	2947	44
H(2C)	-4367	1436	4709	44
H(1A)	-1111	670	5554	74
H(1B)	-1341	970	7498	74
H(2A)	2063	431	9461	84
H(2B)	1555	113	7337	84
H(3A)	-5094	455	4386	52
H(3B)	-5305	775	6292	52
H(4A)	1002	-583	9227	79
H(4B)	3519	-369	10494	79

6.7 Single Crystal Structure Determination of (dienH)Cu₃Sb₂S₅

Table 1. Crystal data and structure refinement for(dienH)Cu₃Sb₂S₅

Identification code	vs611a
Empirical formula	(C ₄ N ₃ H ₁₄)Cu ₃ Sb ₂ S ₅
Habitus	red needles
Formula weight	594.42 g/mol
Temperature	293(2) K
Wavelength	0.71073 Å
Crystal system	monoclinic
Space group	C2/c
Unit cell dimensions	a = 23.6408(16) Å α= 90 °. b = 20.4108(15) Å β= 100.153(7)°. c = 6.4599(4) Å γ = 90 °.
Volume	3068.3(4) Å ³
Z	8
Density (calculated)	2.574 g/cm ³
Absorption coefficient	8.197 mm ⁻¹
F(000)	2152
Crystal size	2 · 1 · 1 mm ³
Theta range for data collection	2.65 to 27.98 °.
Index ranges	-31 ≤ h ≤ 31, -26 ≤ k ≤ 26, -8 ≤ l ≤ 8
Reflections collected	14654
Independent reflections	3587 [R(int) = 0.0790]
Completeness to theta = 27.98 °	96.8 %
Refinement method	Full-matrix least-squares on F ²
Data / restraints / parameters	3587 / 0 / 92
Goodness-of-fit on F ²	0.925
Final R indices [I>2sigma(I)]	R1 = 0.0407, wR2 = 0.0944
R indices (all data)	R1 = 0.0609, wR2 = 0.1002
Extinction coefficient	0.00050(6)
Largest diff. peak and hole	1.063 and -1.272 e.Å ⁻³

Table 2. Atomic coordinates ($\cdot 10^4$) and equivalent isotropic displacement parameters ($\text{\AA}^2 \cdot 10^3$).

U(eq) is defined as one third of the trace of the orthogonalized \mathbf{U}_{ij} tensor.

	x	y	z	U(eq)
Sb(1)	2092(1)	2158(1)	6728(1)	22(1)
Sb(2)	2950(1)	410(1)	8625(1)	27(1)
Cu(1)	3303(1)	2327(1)	8611(2)	38(1)
Cu(2)	2408(1)	1533(1)	11747(2)	39(1)
Cu(3)	3317(1)	1310(1)	14630(2)	55(1)
S(1)	3640(1)	339(1)	6185(3)	25(1)
S(2)	3287(1)	1388(1)	10624(3)	26(1)
S(3)	2247(1)	1135(1)	4938(3)	27(1)
S(4)	1590(1)	1732(1)	9389(3)	29(1)
S(5)	1297(1)	2686(1)	4370(3)	26(1)

Table 3. Bond lengths [Å] and angles [°].

Sb(1)-S(4)	2.4163(17)	Cu(1)-Cu(2)#2	2.8571(15)
Sb(1)-S(3)	2.4467(17)	Cu(2)-S(4)	2.278(2)
Sb(1)-S(5)	2.4496(18)	Cu(2)-S(3)#5	2.309(2)
Sb(1)-Cu(1)	2.9265(13)	Cu(2)-S(2)	2.336(2)
Sb(1)-Cu(2)#2	3.0155(12)	Cu(2)-Cu(3)	2.6221(16)
Sb(2)-S(2)	2.4339(18)	Cu(2)-Cu(1)#2	2.8571(15)
Sb(2)-S(1)	2.4643(17)	Cu(2)-Sb(1)#2	3.0155(12)
Sb(2)-S(1)#3	2.6052(18)	Cu(3)-S(5)#2	2.290(2)
Cu(1)-S(5)#4	2.2895(19)	Cu(3)-S(1)#5	2.2907(19)
Cu(1)-S(4)#2	2.304(2)	Cu(3)-S(2)	2.581(2)
Cu(1)-S(2)	2.3197(19)	Cu(3)-S(3)#5	2.595(2)
S(4)-Sb(1)-S(3)	99.35(6)	S(2)-Cu(2)-Cu(3)	62.44(6)
S(4)-Sb(1)-S(5)	100.45(6)	S(4)-Cu(2)-Cu(1)#2	51.83(5)
S(3)-Sb(1)-S(5)	104.11(6)	S(2)-Cu(2)-Cu(1)#2	128.37(6)
S(4)-Sb(1)-Cu(1)	108.29(5)	Cu(3)-Cu(2)-Cu(1)#2	126.55(5)
S(3)-Sb(1)-Cu(1)	94.57(5)	S(4)-Cu(2)-Sb(1)#2	107.32(6)
S(5)-Sb(1)-Cu(1)	142.52(5)	S(2)-Cu(2)-Sb(1)#2	83.99(5)
S(4)-Sb(1)-Cu(2)#2	107.43(5)	Cu(3)-Cu(2)-Sb(1)#2	72.38(4)
S(3)-Sb(1)-Cu(2)#2	145.92(5)	Cu(1)#2-Cu(2)-Sb(1)	59.71(3)
S(5)-Sb(1)-Cu(2)#2	91.54(5)	S(5)#2-Cu(3)-S(1)#5	124.39(8)
Cu(1)-Sb(1)-Cu(2)#2	57.46(3)	S(5)#2-Cu(3)-S(2)	99.58(7)
S(2)-Sb(2)-S(1)	101.30(6)	S(1)#5-Cu(3)-S(2)	116.17(8)
S(2)-Sb(2)-S(1)#3	92.00(6)	S(5)#2-Cu(3)-S(2)#1	99.58(7)
S(1)-Sb(2)-S(1)#3	87.73(5)	S(1)#5-Cu(3)-S(3)#5	95.83(7)
S(5)#4-Cu(1)-S(2)	120.84(7)	S(2)-Cu(3)-S(3)#5	103.33(7)
S(4)#2-Cu(1)-S(2)	112.66(7)	S(5)#2-Cu(3)-Cu(2)	106.29(6)
S(2)-Cu(3)-Cu(2)	53.34(5)	 	
S(4)#2-Cu(1)-Cu(2)#	51.02(6)	S(3)#5-Cu(3)-Cu(2)	52.54(5)
S(2)-Cu(1)-Cu(2)#2	130.58(6)	Cu(3)#6-S(1)-Sb(2)	91.27(7)
S(5)#4-Cu(1)-Sb(1)	99.65(6)	Cu(3)#6-S(1)-Sb(2)#7	96.09(7)
S(4)#2-Cu(1)-Sb(1)	109.49(6)	Cu(1)-S(2)-Cu(2)	99.97(8)
S(2)-Cu(1)-Sb(1)	91.38(6)	Cu(1)-S(2)-Sb(2)	114.58(8)
Cu(2)#2-Cu(1)-Sb(1)	62.84(3)	Cu(2)-S(2)-Sb(2)	92.47(7)
S(4)-Cu(2)-S(3)#5	113.92(8)	Cu(1)-S(2)-Cu(3)	127.80(8)
S(4)-Cu(2)-S(2)	120.77(7)	Cu(2)-S(2)-Cu(3)	64.22(6)
S(3)#5-Cu(2)-S(2)	121.88(8)	Sb(2)-S(2)-Cu(3)	115.46(7)
S(4)-Cu(2)-Cu(3)	176.79(7)	Cu(2)#6-S(3)-Sb(1)	100.56(7)

S(3)#5-Cu(2)-Cu(3)	63.13(6)	Cu(2)-S(4)-Cu(1)#2	77.15(7)
Sb(1)-S(3)-Cu(3)#6	98.49(7)	Cu(2)-S(4)-Sb(1)	94.25(7)
Cu(1)#4-S(5)-Sb(1)	97.66(7)	Cu(3)#2-S(5)-Sb(1)	89.67(7)

Symmetry transformations used to generate equivalent atoms:

#1 x,y,z #2 -x+1/2,-y+1/2,-z+2 #3 x,-y,z+1/2 #4 -x+1/2,-y+1/2,-z+1 #5 x,y,z+1 #6 x,y,z-1 #7 x,-y,z-1/2

Table 4. Anisotropic displacement parameters ($\text{\AA}^2 \cdot 10^3$). The anisotropic displacement factor exponent takes the form: $-2\pi^2 [h^2 a^{*2} U_{11} + \dots + 2 h k a^{*} b^{*} U_{12}]$

	U ₁₁	U ₂₂	U ₃₃	U ₂₃	U ₁₃	U ₁₂
Sb(1)	30(1)	19(1)	19(1)	0(1)	7(1)	-1(1)
Sb(2)	38(1)	21(1)	23(1)	-1(1)	9(1)	-4(1)
Cu(1)	61(1)	29(1)	26(1)	-1(1)	15(1)	-1(1)
Cu(2)	49(1)	43(1)	25(1)	2(1)	10(1)	5(1)
Cu(3)	69(1)	21(1)	66(1)	7(1)	-14(1)	0(1)
S(1)	36(1)	19(1)	20(1)	-1(1)	6(1)	2(1)
S(2)	43(1)	18(1)	20(1)	-2(1)	10(1)	2(1)
S(3)	40(1)	19(1)	21(1)	1(1)	7(1)	4(1)
S(4)	40(1)	27(1)	22(1)	-1(1)	11(1)	-6(1)
S(5)	34(1)	23(1)	22(1)	1(1)	7(1)	2(1)

6.8 Single Crystal Structure Determination of $(\text{TETNH}_2)_{0.5}\text{Cu}_3\text{Sb}_2\text{S}_5$

Table 1. Crystal data and structure refinement for $(\text{TETNH}_2)_{0.5}\text{Cu}_3\text{Sb}_2\text{S}_5$

Identification code	vs655	
Empirical formula	$(\text{C}_6\text{N}_4\text{H}_{20})_{0.5}\text{Cu}_3\text{Sb}_2\text{S}_5$	
Habitus	red needles	
Formula weight	594.42 g/mol	
Temperature	293(2) K	
Wavelength	0.71073 Å	
Crystal system	triclinic	
Space group	P-1	
Unit cell dimensions	$a = 6.3188(8)$ Å	$\alpha = 103.376(14)^\circ$.
	$b = 9.9523(13)$ Å	$\beta = 91.420(14)^\circ$.
	$c = 11.3630(13)$ Å	$\gamma = 108.340(14)^\circ$.
Volume	656.19(14) Å ³	
Z	2	
Density (calculated)	3.008 g/cm ³	
Absorption coefficient	9.583 mm ⁻¹	
F(000)	538	
Crystal size	2 · 1 · 1 mm ³	
Theta range for data collection	3.24 to 25.02°	
Index ranges	-7 ≤ h ≤ 7, -11 ≤ k ≤ 10, -13 ≤ l ≤ 12	
Reflections collected	3712	
Independent reflections	2173 [R(int) = 0.0874]	
Completeness to theta = 25.02°	93.7 %	
Refinement method	Full-matrix least-squares on F ²	
Data / restraints / parameters	2173 / 0 / 91	
Goodness-of-fit on F ²	0.961	
Final R indices [$ I > 2\sigma(I)$]	R1 = 0.0639, wR2 = 0.1623	
R indices (all data)	R1 = 0.0863, wR2 = 0.1691	
Largest diff. peak and hole	2.448 and -2.630 e.Å ⁻³	

Table 2. Atomic coordinates ($\cdot 10^4$) and equivalent isotropic displacement parameters ($\text{\AA}^2 \cdot 10^3$).

U(eq) is defined as one third of the trace of the orthogonalized \mathbf{U}_{ij} tensor.

	x	y	z	U(eq)
Sb(1)	1814(2)	3799(1)	8870(1)	14(1)
Sb(2)	4065(2)	7927(1)	9241(1)	11(1)
Cu(1)	-316(4)	410(3)	8968(3)	35(1)
Cu(2)	2372(3)	4168(2)	11451(2)	22(1)
Cu(3)	4649(3)	8341(2)	11661(2)	23(1)
S(1)	4050(6)	5619(4)	7738(4)	15(1)
S(2)	1877(6)	1520(4)	7592(4)	17(1)
S(3)	6022(6)	9466(4)	8001(4)	17(1)
S(4)	296(6)	8095(4)	8953(4)	17(1)
S(5)	-1847(6)	3634(5)	8028(5)	24(1)

Table 3. Bond lengths [Å] and angles [°].

Sb(1)-S(2)	2.406(4)	Cu(1)-S(2)	2.351(5)
Sb(1)-S(5)	2.423(4)	Cu(1)-S(4)#2	2.449(5)
Sb(1)-S(1)	2.547(4)	Cu(1)-S(4)#3	2.482(5)
Sb(1)-Cu(2)	2.869(3)	Cu(1)-Cu(1)#4	2.715(5)
Sb(2)-S(3)	2.398(5)	Cu(2)-S(5)#3	2.262(4)
Sb(2)-S(4)	2.459(4)	Cu(2)-S(4)#3	2.284(5)
Sb(2)-S(1)	2.522(4)	Cu(2)-S(1)#5	2.348(4)
Sb(2)-Cu(3)	2.683(3)	Cu(3)-S(2)#5	2.284(4)
Cu(1)-S(3)#1	2.340(5)	Cu(3)-S(5)#3	2.299(5)
Cu(3)-S(3)#6	2.301(4)		
S(2)-Sb(1)-S(5)	96.11(14)	S(1)#5-Cu(2)-Sb(1)	115.49(14)
S(2)-Sb(1)-S(1)	101.45(14)	S(2)#5-Cu(3)-S(5)#3	112.76(17)
S(5)-Sb(1)-S(1)	95.89(15)	S(2)#5-Cu(3)-S(3)#6	115.26(17)
S(2)-Sb(1)-Cu(2)	117.22(12)	S(5)#3-Cu(3)-S(3)#6	117.39(17)
S(5)-Sb(1)-Cu(2)	115.78(13)	S(2)#5-Cu(3)-Sb(2)	114.83(14)
S(1)-Sb(1)-Cu(2)	124.93(11)	S(3)#6-Cu(3)-Sb(2)	91.88(14)
S(3)-Sb(2)-S(4)	100.22(14)	S(5)#3-Cu(3)-Sb(2)	102.16(16)
S(3)-Sb(2)-S(1)	93.00(15)	Cu(2)#5-S(1)-Sb(2)	92.14(15)
S(4)-Sb(2)-S(1)	106.21(13)	Cu(2)#5-S(1)-Sb(1)	96.97(16)
S(3)-Sb(2)-Cu(3)	128.86(13)	Sb(2)-S(1)-Sb(1)	97.70(15)
S(4)-Sb(2)-Cu(3)	101.64(12)	Cu(3)#5-S(2)-Cu(1)	100.02(18)
S(1)-Sb(2)-Cu(3)	123.54(11)	Cu(3)#5-S(2)-Sb(1)	97.06(16)
S(3)#1-Cu(1)-S(2)	105.02(18)	Cu(1)-S(2)-Sb(1)	85.99(16)
S(3)#1-Cu(1)-S(4)#2	98.57(17)	Cu(3)#6-S(3)-Cu(1)#7	96.62(18)
S(2)-Cu(1)-S(4)#2	109.54(17)	Cu(3)#6-S(3)-Sb(2)	113.28(18)
S(2)-Cu(1)-S(4)#3	119.04(18)	Cu(1)#7-S(3)-Sb(2)	102.72(18)
S(4)#2-Cu(1)-S(4)#3	113.18(15)	Cu(2)#3-S(4)-Cu(1)#8	126.75(16)
S(4)#2-Cu(1)-Cu(1)#4	57.17(14)	Cu(2)#3-S(4)-Sb(2)	110.80(16)
S(4)#3-Cu(1)-Cu(1)#4	56.02(14)	Cu(1)#8-S(4)-Sb(2)	122.31(17)
S(5)#3-Cu(2)-S(4)#3	127.62(16)	Cu(2)#3-S(4)-Cu(1)#3	112.50(19)
S(5)#3-Cu(2)-S(1)#5	109.77(17)	Cu(1)#8-S(4)-Cu(1)#3	66.82(15)
S(4)#3-Cu(2)-S(1)#5	116.93(16)	Sb(2)-S(4)-Cu(1)#3	96.78(15)
S(5)#3-Cu(2)-Sb(1)	96.22(16)	Cu(2)#3-S(5)-Cu(3)#3	117.14(19)
S(4)#3-Cu(2)-Sb(1)	84.51(14)	Cu(2)#3-S(5)-Sb(1)	110.84(18)
Cu(3)#3-S(5)-Sb(1)	112.33(19)		

Symmetry transformations used to generate equivalent atoms:

#1 x-1,y-1,z #2 x,y-1,z #3 -x,-y+1,-z+2 #4 -x,-y,-z+2 #5 -x+1,-y+1,-z+2 #6 -x+1,-y+2,-z+2 #7 x+1,y+1,z #8 x,y+1,z.

Table 4. Anisotropic displacement parameters ($\text{\AA}^2 \cdot 10^3$). The anisotropic displacement factor exponent takes the form: $-2\pi^2 [h^2 a^{*2} U_{11} + \dots + 2 h k a^{*} b^{*} U_{12}]$

	U_{11}	U_{22}	U_{33}	U_{23}	U_{13}	U_{12}
Sb(1)	11(1)	15(1)	19(1)	7(1)	5(1)	8(1)
Sb(2)	9(1)	15(1)	14(1)	6(1)	1(1)	9(1)
Cu(1)	22(1)	41(2)	47(2)	26(1)	3(1)	8(1)
Cu(2)	14(1)	16(1)	40(2)	8(1)	2(1)	9(1)
Cu(3)	18(1)	28(1)	32(1)	13(1)	1(1)	15(1)
S(1)	10(2)	18(2)	21(2)	5(2)	2(2)	11(2)
S(2)	13(2)	22(2)	21(2)	8(2)	4(2)	12(2)
S(3)	12(2)	19(2)	28(3)	12(2)	4(2)	11(2)
S(4)	6(2)	20(2)	32(3)	11(2)	2(2)	10(2)
S(5)	9(2)	20(2)	45(3)	7(2)	1(2)	11(2)

6.9 Single Crystal Structure Determination of (1,4-DAB)Ag₃Sb₃S₇

Table 1. Crystal data and structure refinement for (1,4-DAB)Ag₃Sb₃S₇

Identification code	vs750	
Empirical formula	(C ₄ N ₂ H ₁₄)Ag ₃ Sb ₃ S ₇	
Habitus	yellow needles	
Formula weight	1003.45 g/mol	
Temperature	293(2) K	
Wavelength	0.71073 Å	
Crystal system	orthorombic	
Space group	Pnma	
Unit cell dimensions	a = 6.6689(9) Å b = 30.440(3) Å c = 9.1538(8) Å	α= 90°. β= 90°. γ = 90°.
Volume	1858.2(3) Å ³	
Z	4	
Density (calculated)	3.587 g/cm ³	
Absorption coefficient	8.171 mm ⁻¹	
F(000)	1832	
Crystal size	1.2 · 0.2 · 0.1 mm ³	
Theta range for data collection	2.32 to 25.03°	
Index ranges	-7 ≤ h ≤ 7, -35 ≤ k ≤ 36, -10 ≤ l ≤ 10	
Reflections collected	12238	
Independent reflections	1648 [R(int) = 0.0620]	
Completeness to theta = 25.03°	98.9 %	
Refinement method	Full-matrix least-squares on F ²	
Data / restraints / parameters	1648 / 0 / 98	
Goodness-of-fit on F ²	1.082	
Final R indices [I>2sigma(I)]	R1 = 0.0346, wR2 = 0.0888	
R indices (all data)	R1 = 0.0371, wR2 = 0.0909	
Extinction coefficient	0.0027(2)	
Largest diff. peak and hole	2.245 and -2.272 e.Å ⁻³	

Table 2. Atomic coordinates ($\cdot 10^4$) and equivalent isotropic displacement parameters ($\text{\AA}^2 \cdot 10^3$). U(eq) is defined as one third of the trace of the orthogonalized U_{ij} tensor.

	x	y	z	U(eq)
Sb(1)	6627(1)	6453(1)	3618(1)	14(1)
Sb(2)	8171(1)	7500	10924(1)	20(1)
Ag(1)	6181(1)	6776(1)	7471(1)	38(1)
Ag(2)	3568(2)	7500	9335(2)	72(1)
Ag(2')	3609(11)	7500	10734(15)	53(3)
S(1)	6706(2)	6110(1)	5984(2)	19(1)
S(2)	4043(2)	5957(1)	2569(2)	17(1)
S(3)	6091(3)	6883(1)	10213(2)	24(1)
S(4)	10098(4)	7500	8682(3)	35(1)
N(1)	8366(7)	4201(2)	4386(6)	20(1)
C(1)	8880(9)	4978(2)	5144(9)	27(2)
C(2)	7842(11)	4662(2)	4106(8)	30(2)

Table 3. Bond lengths [Å] and angles [°].

Sb(1)-S(1)	2.4050(16)	Ag(2)#10-S(4)-Ag(2) # 5	124.75(10)
Sb(1)-S(2)#1	2.4616(15)	S(1)-Ag(1)-Ag(2)	155.89(5)
Sb(1)-S(2)	2.4859(15)	S(3)-Ag(1)-Ag(2)	52.16(5)
Sb(2)-S(4)	2.421(3)	S(4)#4-Ag(1)-Ag(2)	58.99(8)
Sb(2)-S(3)	2.4240(17)	Ag(2)#5-Ag(1)-Ag(2)	94.03(4)
Ag(1)-S(1)	2.4658(17)	S(1)-Ag(1)-Ag(1) #5	82.35(4)
Ag(1)-S(3)	2.5322(17)	S(3)-Ag(1)-Ag(1) #5	90.45(5)
Ag(1)-S(4) #4	2.5484(14)	S(4)#4-Ag(1)-Ag(1) #5	106.86(6)
Ag(1)-Ag(1) #5	3.3349(5)	Ag(2)#5-Ag(1)-Ag(1) #5	60.53(3)
Ag(2)-S(4) #6	2.390(3)	Ag(2)-Ag(1)-Ag(1) #5	121.44(3)
Ag(2)-S(3)	2.647(2)	S(3)-Ag(1)-Ag(1) #4	87.72(5)
Ag(2)-S(4) #4	2.944(4)	S(4)#4-Ag(1)-Ag(1) #4	73.94(6)
Ag(2)-Ag(1) #4	3.1821(13)	Ag(2)#5-Ag(1)-Ag(1) #4	120.57(3)
Ag(2)-Ag(1) #7	3.1821(13)	Ag(2)-Ag(1)-Ag(1) #4	57.43(2)
Ag(2)-Ag(1) #2	3.2874(14)	Ag(1) #5-Ag(1)-Ag(1) #4	178.16(4)
		S(4) #6-Ag(2)-S(3)	133.73(4)
S(1)-Sb(1)-S(2) #1	96.69(5)	S(3) #2-Ag(2)-S(3)	90.43(8)
S(1)-Sb(1)-S(2)	95.69(5)	S(4) #6-Ag(2)-S(4) #4	95.80(9)
S(2) #1-Sb(1)-S(2)	84.82(4)	S(3) #2-Ag(2)-S(4) #4	93.71(6)
S(4)-Sb(2)-S(3)	94.39(6)	S(4) #6-Ag(2)-Ag(1) #4	52.10(4)
S(3)-Sb(2)-S(3) #2	101.60(9)	S(3) #2-Ag(2)-Ag(1) #4	165.34(8)
S(1)-Ag(1)-S(3)	131.01(6)	S(4) #4-Ag(2)-Ag(1) #4	71.71(5)
S(1)-Ag(1)-S(4) #4	121.50(7)	S(4) #6-Ag(2)-Ag(1) #7	52.10(4)
S(3)-Ag(1)-S(4) #4	107.01(7)	S(3) #2-Ag(2)-Ag(1) #7	89.09(4)
S(1)-Ag(1)-Ag(2) #5	102.22(5)	S(3)-Ag(2)-Ag(1) #7	165.34(8)
S(3)-Ag(1)-Ag(2) #5	115.96(5)	S(4) #4-Ag(2)-Ag(1) #7	71.71(5)
Ag(1) #4-Ag(2)-Ag(1) #7	87.69(4)		
Sb(1) #9-S(2)-Sb(1)	104.53(6)	Ag(2) #10-S(4)-Ag(2) # 5	124.75(10)
Sb(2)-S(3)-Ag(1)	110.62(6)	Sb(2)-S(4)-Ag(2) #5	127.66(11)
Sb(2)-S(3)-Ag(2)	83.98(6)	Ag(1) #5-S(4)-Ag(2) #5	73.13(7)
Ag(1)-S(3)-Ag(2)	78.77(6)	Ag(1)-S(3)-Ag(2)	78.77(6)
Ag(2) #10-S(4)-Sb(2)	107.59(13)	Ag(2) #10-S(4)-Ag(1) #1	118.17(7)
Ag(2) #10-S(4)-Ag(1) #	1118.17(7)	Ag(2) #10-S(4)-Sb(2)	107.59(13)

Symmetry transformations used to generate equivalent atoms:

#1 x+1/2,y,-z+1/2 #2 x,-y+3/2,z #3 x+1/2,y,-z+5/2 #4 x-1/2,y,-z+3/2 #5 x+1/2,y,-z+3/2 #6 x-1,y,z #7 x-1/2,-y+3/2,-z+3/2 #8 x-1/2,y,-z+5/2 #9 x-1/2,y,-z+1/2 #10 x+1,y,z #11 x+1/2,-y+3/2,-z+3/2.

Table 4. Anisotropic displacement parameters ($\text{\AA}^2 \cdot 10^3$) . The anisotropic displacement factor exponent takes the form: $-2\pi^2 [h^2 a^*{}^2 U_{11} + \dots + 2 h k a^* b^* U_{12}]$

	U_{11}	U_{22}	U_{33}	U_{23}	U_{13}	U_{12}
Sb(1)	16(1)	15(1)	12(1)	1(1)	0(1)	1(1)
Sb(2)	28(1)	17(1)	15(1)	0	-4(1)	0
Ag(1)	64(1)	25(1)	25(1)	-4(1)	2(1)	4(1)
Ag(2)	27(1)	80(1)	108(1)	0	-7(1)	0
Ag(2')	13(4)	64(7)	83(9)	0	-5(4)	0
S(1)	27(1)	19(1)	12(1)	1(1)	1(1)	2(1)
S(2)	11(1)	21(1)	18(1)	1(1)	-2(1)	-1(1)
S(3)	38(1)	15(1)	19(1)	2(1)	5(1)	-7(1)
S(4)	36(1)	23(1)	47(2)	0	22(1)	0
N(1)	27(3)	14(3)	19(3)	-2(2)	-1(2)	-1(2)
C(1)	30(4)	14(3)	36(4)	-9(3)	1(3)	3(3)
C(2)	36(4)	20(3)	35(4)	6(3)	-9(3)	-5(3)

Table 5. Hydrogen coordinates ($\cdot 10^4$) and isotropic displacement parameters ($\text{\AA}^2 \cdot 10^3$).

	x	y	z	$U(\text{eq})$
H(1N1)	7724	4029	3754	30
H(2N1)	8010	4129	5292	30
H(3N1)	9683	4165	4282	30
H(1A)	8682	4877	6139	32
H(1B)	8260	5265	5057	32
H(2A)	6402	4697	4199	36
H(2B)	8207	4736	3110	36

6.10 Single Crystal Structure Determination of $(\text{en})_2\text{Ag}_5\text{Sb}_3\text{S}_8$

Table 1. Crystal data and structure refinement for $(\text{en})_2\text{Ag}_5\text{Sb}_3\text{S}_8$

Identification code	vs703	
Empirical formula	$(\text{C}_2\text{N}_2\text{H}_9)_2\text{Ag}_5\text{Sb}_3\text{S}_8$	
Habitus	orange needles	
Formula weight	1281.29 g/mol	
Temperature	293(2) K	
Wavelength	0.71073 Å	
Crystal system	monoclinic	
Space group	P2 ₁ /n	
Unit cell dimensions	$a = 6.2712(4)$ Å	$\alpha = 90^\circ$.
	$b = 15.9008(11)$ Å	$\beta = 93.376(7)^\circ$.
	$c = 23.0119(14)$ Å	$\gamma = 90^\circ$.
Volume	2290.7(3) Å ³	
Z	4	
Density (calculated)	3.715 g/cm ³	
Absorption coefficient	8.391 mm ⁻¹	
F(000)	2336	
Crystal size	0.1 · 0.1 · 0.05 mm ³	
Theta range for data collection	2.56 to 28.01 °	
Index ranges	-8 ≤ h ≤ 8, -21 ≤ k ≤ 21, -30 ≤ l ≤ 30	
Reflections collected	22261	
Independent reflections	5303 [R(int) = 0.0423]	
Completeness to theta = 28.01 °	95.5 %	
Refinement method	Full-matrix least-squares on F ²	
Data / restraints / parameters	5303 / 0 / 215	
Goodness-of-fit on F ²	1.025	
Final R indices [I>2sigma(I)]	R1 = 0.0332, wR2 = 0.0768	
R indices (all data)	R1 = 0.0471, wR2 = 0.0815	
Extinction coefficient	0.00049(6)	
Largest diff. peak and hole	3.553 and -2.785 e.Å ⁻³	

Table 2. Atomic coordinates ($\cdot 10^4$) and equivalent isotropic displacement parameters ($\text{\AA}^2 \cdot 10^3$). U(eq) is defined as one third of the trace of the orthogonalized U_{ij} tensor.

	x	y	z	U(eq)
Sb(1)	4887(1)	3605(1)	7136(1)	16(1)
Sb(2)	10146(1)	5913(1)	7797(1)	16(1)
Sb(3)	-547(1)	7307(1)	6621(1)	15(1)
Ag(1)	10356(1)	5061(1)	6624(1)	35(1)
Ag(2)	4914(1)	4557(1)	8340(1)	35(1)
Ag(3)	4563(1)	7264(1)	7687(1)	38(1)
Ag(4)	5204(1)	5790(1)	6663(1)	35(1)
Ag(5)	5140(1)	8754(1)	6862(1)	49(1)
S(1)	8709(3)	3671(1)	7034(1)	23(1)
S(2)	4014(3)	2238(1)	6630(1)	20(1)
S(3)	3728(3)	4386(1)	6278(1)	19(1)
S(4)	6281(3)	5819(1)	7802(1)	20(1)
S(5)	11208(3)	5079(1)	8627(1)	21(1)
S(6)	3309(3)	7295(1)	6545(1)	20(1)
S(7)	-1573(3)	6136(1)	5999(1)	18(1)
S(8)	-1597(3)	8474(1)	5994(1)	22(1)
N(1)	990(15)	8232(5)	4214(3)	50(2)
C(1)	1090(20)	9042(6)	4528(4)	59(3)
C(2)	3022(17)	9124(5)	4918(3)	42(2)
N(2)	3156(11)	8465(4)	5379(3)	32(1)
N(3)	4582(9)	6930(4)	4975(2)	39(2)
C(3)	3465(9)	6139(4)	5067(2)	45(2)
C(4)	1680(15)	6003(5)	4616(4)	41(2)
N(4)	-43(12)	6629(4)	4650(3)	39(2)

Table 3. Bond lengths [Å] and angles [°].

Sb(1)-S(3)	2.4085(15)	Ag(3)-Ag(5)	3.0708(9)
Sb(1)-S(1)	2.4241(18)	Ag(3)-Ag(4)	3.3659(9)
Sb(1)-S(2)	2.5100(15)	Ag(4)-S(3)	2.5546(16)
Sb(1)-Ag(2)	3.1559(7)	Ag(4)-S(7)#3	2.6621(17)
Sb(2)-S(5)	2.3887(15)	Ag(4)-S(4)#1	2.6678(17)
Sb(2)-S(4)#1	2.4290(17)	Ag(4)-S(4)	2.6678(17)
Sb(2)-S(4)	2.4290(17)	Ag(4)-S(6)	2.6785(16)
Sb(2)-S(2)#2	2.5243(15)	Ag(4)-Ag(1)#5	3.2499(10)
Sb(2)-Ag(1)	3.0293(7)	Ag(4)-Ag(1)#5	3.2499(10)
Sb(3)-S(7)	2.4127(15)	Ag(5)-S(5)#2	2.5122(17)
Sb(3)-S(8)	2.4184(15)	Ag(5)-S(1)#2	2.6032(19)
Sb(3)-S(6)	2.4348(17)	Ag(5)-S(6)	2.6719(16)
Ag(1)-S(7)#3	2.5007(16)	Ag(3)-S(4)#1	2.5440(16)
Ag(1)-S(3)#3	2.5407(17)	Ag(3)-S(4)#1	2.5440(16)
Ag(1)-S(1)	2.6376(16)	Ag(3)-S(4)	2.5440(16)
Ag(1)-Ag(4)#3	3.2499(9)	Ag(3)-S(1)#2	2.5512(16)
Ag(2)-S(8)#4	2.4968(17)	Ag(3)-S(6)	2.6993(17)
Ag(2)-S(4)#1	2.5349(16)	Ag(3)-S(2)#6	2.8132(18)
Ag(2)-S(4)	2.5349(16)		
S(3)-Sb(1)-S(1)	98.65(6)	S(1)#2-Ag(3)-S(6)	108.93(5)
S(3)-Sb(1)-S(2)	91.11(5)	S(4)-Ag(3)-S(2)#6	106.01(5)
S(1)-Sb(1)-S(2)	100.52(6)	S(6)-Ag(3)-S(2)#6	110.34(5)
S(3)-Sb(1)-Ag(2)	117.24(4)	S(4)-Ag(3)-Ag(5)	134.11(5)
S(1)-Sb(1)-Ag(2)	96.34(5)	S(6)-Ag(3)-Ag(5)	54.71(4)
S(2)-Sb(1)-Ag(2)	144.29(4)	S(4)-Ag(3)-S(6)	102.37(5)
S(5)-Sb(2)-S(4)	101.16(6)	S(4)-Ag(3)-Ag(4)	51.40(4)
S(5)-Sb(2)-S(2)#2	90.32(5)	S(1)#2-Ag(3)-Ag(4)	136.10(5)
S(4)-Sb(2)-S(2)#2	103.10(5)	S(6)-Ag(3)-Ag(4)	50.98(3)
S(5)-Sb(2)-Ag(1)	116.08(4)	S(2)#6-Ag(3)-Ag(4)	120.85(4)
S(4)#1-Sb(2)-Ag(1)	94.16(4)	Ag(5)-Ag(3)-Ag(4)	94.66(3)
S(2)#2-Sb(2)-Ag(1)	145.06(4)	S(3)-Ag(4)-S(7)#3	104.72(5)
S(7)-Sb(3)-S(8)	100.61(5)	S(3)-Ag(4)-S(4)	114.92(5)
S(8)-Sb(3)-S(6)	101.55(6)	S(3)-Ag(4)-S(6)	126.58(6)
S(7)#3-Ag(1)-S(3)#3	119.46(5)	S(7)#3-Ag(4)-S(6)	95.98(5)
S(7)#3-Ag(1)-S(1)	126.32(6)	S(4)-Ag(4)-S(6)	99.70(5)

S(3)#3-Ag(1)-S(1)	96.23(5)	S(3)-Ag(4)-Ag(1)#5	50.18(4)
S(7)#3-Ag(1)-Sb(2)	99.31(4)	S(7)#3-Ag(4)-Ag(1)#5	143.01(4)
S(3)#3-Ag(1)-Sb(2)	123.29(4)	S(4)#1-Ag(4)-Ag(1)#5	102.43(4)
S(1)-Ag(1)-Sb(2)	91.04(4)	S(6)-Ag(4)-Ag(1)#5	84.66(4)
S(7)#3-Ag(1)-Ag(4)#3	101.08(4)	S(3)-Ag(4)-Ag(3)	142.70(4)
S(3)#3-Ag(1)-Ag(4)#3	50.56(4)	S(7)#3-Ag(4)-Ag(3)	112.57(4)
S(1)-Ag(1)-Ag(4)#3	132.42(4)	S(4)#1-Ag(4)-Ag(3)	48.18(3)
Sb(2)-Ag(1)-Ag(4)#3	84.61(2)	S(6)-Ag(4)-Ag(3)	51.53(4)
S(8)#4-Ag(2)-S(4)	134.66(6)	Ag(1)#5-Ag(4)-Ag(3)	96.73(2)
S(8)#4-Ag(2)-S(5)#5	114.69(6)	S(5)#2-Ag(5)-S(1)#2	123.18(5)
S(4)#1-Ag(2)-S(5)#5	101.83(5)	S(5)#2-Ag(5)-S(6)	118.57(6)
S(4)-Ag(2)-S(5)#5	101.83(5)	S(1)#2-Ag(5)-S(6)	108.21(5)
S(8)#4-Ag(2)-Sb(1)	100.84(4)	S(5)#2-Ag(5)-Ag(3)	151.13(5)
S(4)#1-Ag(2)-Sb(1)	86.31(4)	S(1)#2-Ag(5)-Ag(3)	52.66(4)
S(4)-Ag(2)-Sb(1)	86.31(4)	S(6)-Ag(5)-Ag(3)	55.55(4)
S(5)#5-Ag(2)-Sb(1)	114.82(4)	Sb(1)-S(1)-Ag(3)#7	110.19(6)
S(4)-Ag(3)-S(1)#2	126.49(6)	Sb(1)-S(1)-Ag(5)#7	97.26(6)
S(2)#6-Ag(3)-Ag(5)	118.89(4)	Ag(3)-S(4)-Ag(4)	80.41(5)
Ag(3)#7-S(1)-Ag(5)#7	73.13(5)	Sb(2)-S(5)-Ag(5)#7	92.07(6)
Sb(1)-S(1)-Ag(1)	118.78(6)	Sb(2)-S(5)-Ag(2)#3	100.71(6)
Ag(3)#7-S(1)-Ag(1)	130.94(7)	Sb(3)-S(6)-Ag(5)	112.69(6)
Ag(5)#7-S(1)-Ag(1)	102.35(6)	Sb(3)-S(6)-Ag(4)	115.89(6)
Sb(1)-S(2)-Sb(2)#7	116.56(6)	Ag(5)-S(6)-Ag(4)	124.58(6)
Sb(1)-S(2)-Ag(3)#4	83.57(5)	Sb(3)-S(6)-Ag(3)	99.42(6)
Sb(2)#7-S(2)-Ag(3)#4	82.51(5)	Ag(5)-S(6)-Ag(3)	69.74(4)
Sb(1)-S(3)-Ag(1)#5	100.24(6)	Ag(4)-S(6)-Ag(3)	77.49(4)
Sb(1)-S(3)-Ag(4)	94.64(5)	Sb(3)-S(7)-Ag(1)#5	94.75(5)
Ag(1)#5-S(3)-Ag(4)	79.26(5)	Sb(3)-S(7)-Ag(4)#5	90.24(5)
Sb(2)-S(4)-Ag(2)	114.66(6)	Ag(1)#5-S(7)-Ag(4)#5	83.45(5)
Sb(2)-S(4)-Ag(3)	111.13(6)	Sb(3)-S(8)-Ag(2)#6	94.15(6)
Ag(2)-S(4)-Ag(3)	127.76(7)	Ag(2)-S(4)-Ag(4)	113.12(6)
Sb(2)-S(4)-Ag(4)	101.03(6)		

Symmetry transformations used to generate equivalent atoms:

#1 x,y,z #2 -x+3/2,y+1/2,-z+3/2 #3 x+1,y,z #4 -x+1/2,y-1/2,-z+3/2 #5 x-1,y,z #6 -x+1/2,y+1/2,-z+3/2 #7 -x+3/2,y-1/2,-z+3/2

Table 4. Anisotropic displacement parameters ($\text{\AA}^2 \cdot 10^3$). The anisotropic displacement factor exponent takes the form: $-2\pi^2[h^2 a^*{}^2 U_{11} + \dots + 2 h k a^* b^* U_{12}]$

	U ₁₁	U ₂₂	U ₃₃	U ₂₃	U ₁₃	U ₁₂
Sb(1)	16(1)	14(1)	17(1)	1(1)	2(1)	1(1)
Sb(2)	17(1)	14(1)	16(1)	1(1)	2(1)	1(1)
Sb(3)	17(1)	13(1)	15(1)	-1(1)	2(1)	-1(1)
Ag(1)	40(1)	29(1)	37(1)	3(1)	2(1)	15(1)
Ag(2)	44(1)	24(1)	38(1)	6(1)	6(1)	7(1)
Ag(3)	38(1)	24(1)	51(1)	2(1)	-5(1)	0(1)
Ag(4)	40(1)	27(1)	39(1)	-4(1)	4(1)	-10(1)
Ag(5)	71(1)	27(1)	46(1)	1(1)	-21(1)	8(1)
S(1)	15(1)	21(1)	32(1)	7(1)	0(1)	1(1)
S(2)	22(1)	14(1)	24(1)	0(1)	-3(1)	0(1)
S(3)	19(1)	15(1)	21(1)	2(1)	-2(1)	1(1)
S(4)	15(1)	18(1)	26(1)	2(1)	1(1)	1(1)
S(5)	23(1)	18(1)	21(1)	5(1)	-1(1)	2(1)
S(6)	16(1)	16(1)	27(1)	0(1)	1(1)	0(1)
S(7)	19(1)	14(1)	20(1)	-1(1)	-1(1)	-1(1)
S(8)	19(1)	16(1)	29(1)	3(1)	-4(1)	1(1)
N(1)	59(6)	60(5)	29(3)	7(3)	-16(3)	12(4)
C(1)	97(9)	42(5)	35(4)	22(4)	-20(5)	8(5)
C(2)	68(7)	35(4)	24(3)	6(3)	2(4)	-15(4)
N(2)	38(4)	36(3)	21(3)	0(2)	-1(3)	-3(3)
N(3)	29(4)	50(4)	38(4)	-2(3)	-5(3)	9(3)
C(3)	63(7)	41(4)	31(4)	0(3)	-1(4)	19(4)
C(4)	49(6)	36(4)	38(4)	-15(3)	5(4)	-5(4)
N(4)	34(4)	49(4)	35(3)	-4(3)	4(3)	-10(3)

Table 5. Hydrogen coordinates ($\cdot 10^4$) and isotropic displacement parameters ($\text{\AA}^2 \cdot 10^3$).

	x	y	z	U(eq)
H(1N1)	-162	8211	3993	75
H(2N1)	2083	8187	4008	75
H(1A)	1046	9497	4247	71
H(1B)	-163	9094	4755	71
H(2A)	3031	9674	5100	51
H(2B)	4270	9086	4689	51
H(1N2)	560	8021	5202	48
H(2N2)	2016	8563	5557	48
H(1N3)	5627	7009	5228	59
H(2N3)	5060	6929	4632	59
H(3A)	2895	6145	5450	54
H(3B)	4470	5677	5055	54
H(4A)	2244	6031	4233	49
H(4B)	1093	5445	4664	49
H(1N4)	545	7079	4529	59
H(2N4)	-449	6630	5001	59

6.11 Single Crystal Structure Determination of $(\text{enH}_2)_2\text{Cu}_3\text{Ag}_5\text{Sb}_4\text{S}_{12}$

Table 1. Crystal data for $(\text{enH}_2)_2\text{Cu}_3\text{Ag}_5\text{Sb}_4\text{S}_{12}$

Identification code	vs795	
Empirical formula	$(\text{C}_4\text{N}_4\text{H}_{20})_2\text{Cu}_3\text{Ag}_5\text{Sb}_4\text{S}_{12}$	
Habitus	brown plates	
Formula weight	738.26 g/mol	
Temperature	293(2) K	
Wavelength	0.71073	
Crystal system	triclinic	
Space group	P-1	
Unit cell dimensions	a = 6.7552(5) Å b = 11.3515(9) Å c = 20.4847(14) Å	$\alpha = 105.229(9)^\circ$ $\beta = 98.177(9)^\circ$ $\gamma = 94.933(10)^\circ$
Volume	1487.67(19) Å ³	
Density	1.648 g/cm ³	
Z	2	
Absorption coefficient	3.998 mm ⁻¹	
F(000)	678	
Crystal size	0.5 · 0.5 · 0.05 mm	
Theta range for data collection	2.39 to 28.00 °	
Index ranges	-8 ≤ h ≤ 8, -14 ≤ k ≤ 14, -26 ≤ l ≤ 26	
Reflections collected	16160	
Independent reflections	7013 [R(int) = 0.0722]	
Completeness to theta =	28.00 98.1 %	
Refinement method	Full-matrix least-squares on F ²	
Data / restraints / parameters	7013 / 0 / 250	
Goodness-of-fit on F ²	1.724	
Final R indices [$ I > 2\sigma(I)$]	R1 = 0.1864, wR2 = 0.4304	
R indices (all data)	R1 = 0.2276, wR2 = 0.4591	
Extinction coefficient	0.0032	
Largest diff. peak and hole	44.392 and -10.037 e Å ⁻³	

Table 2. Atomic coordinates ($\cdot 10^4$) and equivalent isotropic displacement parameters ($\text{\AA}^2 \cdot 10^3$). U(eq) is defined as one third of the trace of the orthogonalized U_{ij} tensor.

	x	y	z	U(eq)
Sb(1)	6124(3)	554(2)	3079(1)	7(1)
Sb(2)	10878(3)	-4447(2)	3082(1)	7(1)
Sb(3)	7932(4)	-2541(2)	1910(1)	9(1)
Sb(4)	12914(4)	-7511(2)	1931(1)	10(1)
Ag(1)	15474(5)	-6163(3)	3229(2)	21(1)
Ag(2)	10415(5)	-1277(3)	3230(2)	21(1)
Ag(3)	12228(5)	-4452(3)	1780(2)	22(1)
Ag(4)	7198(5)	550(3)	1761(2)	22(1)
Ag(5)	5817(6)	-3429(5)	3133(2)	38(1)
Cu(1)	11292(8)	1183(6)	3135(3)	20(1)
Cu(2)	18110(130)	-7120(80)	1900(40)	290(40)
Cu(2')	17470(140)	-6050(90)	1820(50)	350(40)
Cu(3)	17884(12)	-6734(11)	1847(3)	46(3)
S(1)	9204(15)	725(8)	3876(5)	13(2)
S(2)	9308(14)	-2929(8)	3838(5)	13(2)
S(3)	13952(16)	-4382(10)	3899(5)	18(2)
S(4)	15164(15)	-8208(10)	1122(5)	15(2)
S(5)	4473(14)	2072(8)	3805(5)	11(2)
S(6)	10535(14)	-6751(9)	1179(5)	12(2)
S(7)	11069(15)	-9470(9)	1958(6)	16(2)
S(8)	5602(15)	-1751(9)	1177(5)	14(2)
S(9)	9079(15)	-6436(9)	3037(6)	19(2)
S(10)	4197(16)	-1378(8)	3095(6)	16(2)
S(11)	10233(19)	-3216(11)	1103(6)	24(2)
S(12)	6074(15)	-4488(9)	1911(6)	21(2)
N(1)	8570(60)	-3710(40)	5330(20)	27(9)
C(1)	10500(120)	-4390(70)	5170(40)	56(18)
N(2)	13550(60)	-1550(40)	4770(20)	27(9)
C(2)	13890(60)	-150(40)	4920(20)	18(8)
C(3)	5960(80)	-4910(50)	-90(30)	37(12)
N(3)	6200(90)	-3690(50)	-250(30)	51(13)
N(4)	1640(80)	-1000(50)	270(30)	49(13)
C(4)	-900(200)	-630(120)	20(70)	120(40)

Table 3. Bond lengths [Å] and angles [°]

Sb(1)-S(1)	2.415(10)	Sb(3)-Ag(2)	2.905(4)
Sb(1)-S(5)	2.426(9)	Sb(4)-S(6)	2.436(10)
Sb(1)-S(10)	2.463(9)	Sb(4)-S(4)	2.433(10)
Sb(1)-Ag(4)	2.891(4)	Sb(4)-S(7)	2.471(9)
Sb(2)-S(2)	2.423(10)	Sb(4)-Ag(1)	2.915(4)
Sb(2)-S(9)	2.443(10)	Sb(4)-Cu(2)#1	3.31(9)
Sb(2)-S(3)	2.457(10)	Ag(1)-S(3)	2.516(10)
Sb(2)-Ag(3)	2.939(4)	Ag(1)-S(9)	2.553(11)
Sb(3)-S(8)	2.411(10)	Ag(1)-S(5)#3	2.665(10)
Sb(3)-S(11)	2.450(10)	Ag(1)-Ag(5)#2	3.152(6)
Sb(3)-S(12)	2.446(10)	Ag(2)-S(1)	2.576(10)
Ag(2)-S(10)#2	2.618(11)	Ag(2)-S(2)	2.622(10)
Ag(2)-Cu(1)	2.868(7)	Ag(3)-S(6)	2.652(10)
Ag(3)-S(11)	2.554(11)	Ag(3)-Ag(5)#2	3.290(6)
Ag(3)-S(12)#2	2.578(11)	Ag(4)-S(4)#4	2.526(10)
Ag(4)-S(7)#5	2.592(11)	Ag(4)-Cu(3)#4	3.032(13)
Ag(4)-S(8)	2.632(10)	Ag(5)-S(2)	2.518(10)
Ag(4)-Cu(2)#4	2.60(9)	Ag(5)-S(12)	2.514(13)
Ag(5)-S(3)#1	2.538(13)	S(9)-Cu(3)#1	2.379(14)
Ag(5)-S(10)	2.670(11)	S(9)-Cu(2)#1	2.24(8)
Ag(5)-Ag(1)#1	3.152(6)	S(9)-Cu(2')#1	2.74(9)
Ag(5)-Ag(3)#1	3.290(6)	S(9)-Ag(1)#1	2.553(11)
Cu(1)-S(7)#5	2.307(12)	S(10)-Ag(2)#1	2.618(11)
Cu(1)-S(1)	2.338(11)	S(12)-Cu(2')#1	2.05(10)
Cu(1)-S(5)#2	2.362(11)	S(12)-Ag(3)#1	2.578(11)
Cu(2)-Cu(2')	1.37(11)	Cu(3)-S(9)#2	2.379(14)
Cu(2)-S(6)#2	2.43(9)	Cu(3)-Ag(4)#3	3.032(13)
Cu(2)-S(4)	2.38(8)	Cu(2')-S(6)#2	2.68(9)
Cu(2)-S(9)#2	2.24(8)	Cu(2')-S(12)#2	2.05(10)
Cu(2)-Ag(4)#3	2.60(9)	Cu(2')-S(4)	2.71(9)
Cu(2)-Sb(4)#2	3.31(9)	Cu(3)-S(4)	2.402(12)
Cu(2')-S(9)#2	2.74(9)	Cu(3)-S(6)#2	2.402(11)
S(1)-Sb(1)-S(5)	98.3(3)	S(2)-Sb(2)-Ag(3)	130.6(3)
S(1)-Sb(1)-S(10)	103.9(4)	S(9)-Sb(2)-Ag(3)	112.1(3)
S(5)-Sb(1)-S(10)	101.3(3)	S(3)-Sb(2)-Ag(3)	105.7(3)
S(1)-Sb(1)-Ag(4)	107.9(3)	S(8)-Sb(3)-S(11)	98.1(4)
S(5)-Sb(1)-Ag(4)	127.8(2)	S(8)-Sb(3)-S(12)	103.2(3)
S(10)-Sb(1)-Ag(4)	114.5(3)	S(11)-Sb(3)-S(12)	102.6(4)
S(2)-Sb(2)-S(9)	105.3(3)	S(11)-Sb(3)-Ag(2)	107.0(3)

S(2)-Sb(2)-S(3)	97.5(3)	S(8)-Sb(3)-Ag(2)	129.5(3)
S(9)-Sb(2)-S(3)	100.8(4)	S(12)-Sb(3)-Ag(2)	112.7(3)
S(6)-Sb(4)-S(4)	97.6(3)	S(6)-Sb(4)-S(7)	103.3(3)
S(4)-Sb(4)-S(7)	102.3(4)	S(4)-Sb(4)-Cu(2)#1	138.4(15)
S(6)-Sb(4)-Ag(1)	129.0(3)	S(7)-Sb(4)-Cu(2)#1	72.6(16)
S(4)-Sb(4)-Ag(1)	106.5(3)	Ag(1)-Sb(4)-Cu(2)#1	113.2(15)
S(7)-Sb(4)-Ag(1)	114.0(3)	S(6)-Sb(4)-Cu(2)#1	47.1(15)
S(3)-Ag(1)-S(9)#2	132.4(4)	S(3)-Ag(1)-S(5)#3	102.0(3)
S(9)#2-Ag(1)-S(5)#3	104.0(3)	S(5)#3-Ag(1)-Sb(4)	91.3(2)
S(3)-Ag(1)-Sb(4)	113.2(3)	S(3)-Ag(1)-Ag(5)#2	51.7(3)
S(9)#2-Ag(1)-Sb(4)	105.3(3)	S(9)#2-Ag(1)-Ag(5)#2	94.1(3)
S(5)#3-Ag(1)-Ag(5)#2	153.4(2)	S(1)-Ag(2)-Sb(3)	114.7(3)
Sb(4)-Ag(1)-Ag(5)#2	102.62(14)	S(2)-Ag(2)-Cu(1)	154.4(3)
S(1)-Ag(2)-S(2)	105.4(3)	S(10)#2-Ag(2)-Cu(1)	82.9(2)
S(1)-Ag(2)-S(10)#2	121.6(3)	S(1)-Ag(2)-Cu(1)	50.5(2)
S(2)-Ag(2)-S(10)#2	108.8(3)	S(2)-Ag(2)-Sb(3)	94.8(2)
S(10)#2-Ag(2)-Sb(3)	108.0(3)	Cu(1)#1-S(5)-Ag(1)#4	101.4(4)
Cu(1)-Ag(2)-Sb(3)	103.22(16)	Cu(3)-Cu(2)-S(9)#2	100(10)
S(11)-Ag(3)-S(12)#2	125.2(4)	Cu(2')-Cu(2)-S(9)#2	96(6)
S(11)-Ag(3)-S(6)	103.1(4)	S(6)#2-Cu(2)-S(9)#2	118(4)
S(12)#2-Ag(3)-S(6)	106.6(3)	S(4)-Cu(2)-S(9)#2	137(4)
S(11)-Ag(3)-Sb(2)	113.6(3)	Cu(3)-Cu(2)-Ag(4)#3	147(10)
S(12)#2-Ag(3)-Sb(2)	109.9(3)	Cu(2')-Cu(2)-Ag(4)#3	148(7)
S(6)-Ag(3)-Sb(2)	92.6(2)	S(6)#2-Cu(2)-Ag(4)#3	112(3)
S(11)-Ag(3)-Ag(5)#2	128.5(3)	S(4)-Cu(2)-Ag(4)#3	61(2)
S(12)#2-Ag(3)-Ag(5)#2	48.9(3)	S(9)#2-Cu(2)-Ag(4)#3	100(3)
S(6)-Ag(3)-Ag(5)#2	128.3(3)	Cu(3)-Cu(2)-Sb(4)#2	118(10)
Sb(2)-Ag(3)-Ag(5)#2	66.20(11)	Cu(2')-Cu(2)-Sb(4)#2	120(7)
S(4)#4-Ag(4)-S(7)#5	128.3(4)	S(6)#2-Cu(2)-Sb(4)#2	47.3(16)
S(4)#4-Ag(4)-S(8)	104.8(3)	S(4)-Cu(2)-Sb(4)#2	131(3)
S(7)#5-Ag(4)-S(8)	106.0(3)	S(9)#2-Cu(2)-Sb(4)#2	83(3)
S(8)-Ag(4)-Cu(2)#4	158.4(19)	Ag(4)#3-Cu(2)-Sb(4)#2	90(3)
S(4)#4-Ag(4)-Sb(1)	114.7(3)	Cu(2)-Cu(2')-S(9)#2	55(5)
S(7)#5-Ag(4)-Sb(1)	103.6(3)	Cu(2)-Cu(2')-S(6)#2	65(6)
S(8)-Ag(4)-Sb(1)\tab	93.6(2)	S(9)#2-Cu(2')-S(6)#2	95(3)
Cu(2)#4-Ag(4)-Sb(1)	102.4(19)	Cu(2)-Cu(2')-S(12)#2	164(8)
S(4)#4-Ag(4)-Cu(3)#4	50.2(3)	S(9)#2-Cu(2')-S(12)#2	115(4)
S(7)#5-Ag(4)-Cu(3)#4	89.2(3)	S(6)#2-Cu(2')-S(12)#2	131(4)
S(8)-Ag(4)-Cu(3)#4	154.1(3)	Cu(2)-Cu(2')-S(4)	61(5)
Sb(1)-Ag(4)-Cu(3)#4	103.17(16)	S(9)#2-Cu(2')-S(4)	104(3)
S(2)-Ag(5)-S(12)	108.6(3)	S(6)#2-Cu(2')-S(4)	90(3)
S(2)-Ag(5)-S(3)#1	100.2(4)	S(12)#2-Cu(2')-S(4)	116(4)
S(12)-Ag(5)-S(3)#1	125.0(4)	Cu(2)-Cu(3)-S(4)	81(10)

S(2)-Ag(5)-S(10)	111.0(4)	Cu(2)-Cu(3)-S(6)#2	87(10)
S(12)-Ag(5)-S(10)	105.8(4)	S(4)-Cu(3)-S(6)#2	105.6(4)
S(3)#1-Ag(5)-S(10)	105.9(3)	Cu(2)-Cu(3)-S(9)#2	68(10)
S(2)-Ag(5)-Ag(1)#1	91.8(3)	S(4)-Cu(3)-S(9)#2	127.6(5)
S(12)-Ag(5)-Ag(1)#1	81.6(3)	S(6)#2-Cu(3)-S(9)#2	113.5(5)
Cu(2)-Cu(3)-Ag(4)#3	28(10)	S(6)#2-Cu(2)-S(4)	106(3)
S(3)#1-Ag(5)-Ag(1)#1	51.1(2)	S(4)-Cu(3)-Ag(4)#3	53.9(3)
S(10)-Ag(5)-Ag(1)#1	151.4(3)	S(6)#2-Cu(3)-Ag(4)#3	99.6(5)
S(2)-Ag(5)-Ag(3)#1	159.2(3)	S(9)#2-Cu(3)-Ag(4)#3	85.6(5)
S(12)-Ag(5)-Ag(3)#1	50.6(2)	Cu(1)-S(1)-Sb(1)	94.2(4)
S(3)#1-Ag(5)-Ag(3)#1	94.5(3)	Cu(1)-S(1)-Ag(2)	71.2(3)
S(10)-Ag(5)-Ag(3)#1	78.5(3)	Sb(1)-S(1)-Ag(2)	96.8(3)
Ag(1)#1-Ag(5)-Ag(3)#1	85.97(15)	Sb(2)-S(2)-Ag(5)	97.2(4)
S(7)#5-Cu(1)-S(1)	132.5(4)	Sb(2)-S(2)-Ag(2)	90.2(3)
S(7)#5-Cu(1)-S(5)#2	118.0(4)	Ag(5)-S(2)-Ag(2)	93.0(3)
S(1)-Cu(1)-S(5)#2	107.4(4)	Sb(2)-S(3)-Ag(1)	100.4(4)
S(7)#5-Cu(1)-Ag(2)	92.7(3)	Sb(2)-S(3)-Ag(5)#2	86.2(4)
S(1)-Cu(1)-Ag(2)	58.3(3)	Ag(1)-S(3)-Ag(5)#2	77.2(3)
S(5)#2-Cu(1)-Ag(2)	109.4(3)	Cu(3)-S(4)-Sb(4)	90.6(4)
Cu(3)-Cu(2)-S(6)#2	81(10)	Sb(4)-S(4)-Ag(4)#3	99.5(4)
Cu(2')-Cu(2)-S(6) # 2	85(6)	Cu(2)-S(4)-Cu(2')	30(3)
Cu(3)-Cu(2)-S(4)	87(10)	Sb(4)-S(4)-Cu(2')	83.6(19)
Cu(2')-Cu(2)-S(4)	89(6)	Ag(5)-S(12)-Ag(3)#1	80.5(4)
Ag(4)#3-S(4)-Cu(2')	94(2)	Cu(2')#1-S(12)-Ag(3)#1	125(3)
Cu(1)#1-S(5)-Sb(1)	90.9(3)	Sb(3)-S(12)-Ag(3)#1	113.2(4)
Sb(1)-S(5)-Ag(1)#4	94.0(3)	Sb(3)-S(12)-Ag(5)	85.9(4)
Cu(2)#1-S(6)-Sb(4)	86(2)	Cu(2')#1-S(12)-Ag(5)	113(3)
Cu(3)#1-S(6)-Sb(4)	95.3(4)	Sb(3)-S(12)-Cu(2')#1	121(3)
Cu(2)#1-S(6)-Cu(2')#1	31(3)	Sb(3)-S(11)-Ag(3)	97.7(4)
Cu(3)#1-S(6)-Cu(2')#1	19(2)	Ag(2)#1-S(10)-Ag(5)	119.2(4)
Sb(4)-S(6)-Cu(2')#1	109(2)	Sb(1)-S(10)-Ag(5)	124.3(4)
Cu(2)#1-S(6)-Ag(3)	104(2)	Sb(1)-S(10)-Ag(2)#1	116.1(4)
Cu(3)#1-S(6)-Ag(3)	96.9(4)	Cu(2')#1-S(9)-Ag(1)#1	79.4(19)
Sb(4)-S(6)-Ag(3)	90.9(3)	Sb(2)-S(9)-Ag(1)#1	109.3(4)
Cu(2')#1-S(6)-Ag(3)	84(2)	Cu(2)#1-S(9)-Ag(1)#1	92(2)
Cu(1)#6-S(7)-Sb(4)	92.3(4)	Cu(3)#1-S(9)-Ag(1)#1	87.3(4)
Cu(1)#6-S(7)-Ag(4)#6	92.0(4)	Sb(2)-S(9)-Cu(2')#1	77(2)
Sb(4)-S(7)-Ag(4)#6	112.0(4)	Cu(2)#1-S(9)-Cu(2')#1	30(3)
Sb(3)-S(8)-Ag(4)	93.3(3)	Cu(3)#1-S(9)-Cu(2')#1	18(2)

Symmetry transformations used to generate equivalent atoms:

#1 x-1,y,z #2 x+1,y,z #3 x+1,y-1,z #4 x-1,y+1,z #5 x,y+1,z #6 x,y-1,z #7 -x+2,-y-1,-z+1 #8 -x+3,-y,-z+1 #9 -x+1,-y-1,-z #10 -x,-y,-z.

Table 4. Anisotropic displacement parameters ($\text{\AA}^2 \cdot 10^3$). The anisotropic displacement factor exponent takes the form: $2\pi^2[h^2 a^* a^* U_{11} + \dots + 2 h k a^* b^* U_{12}]$

	U ₁₁	U ₂₂	U ₃₃	U ₂₃	U ₁₃	U ₁₂
Sb(1)	9(1)	8(1)	4(1)	-1(1)	6(1)	1(1)
Sb(2)	10(1)	8(1)	3(1)	1(1)	2(1)	0(1)
Sb(3)	12(1)	9(1)	2(1)	-1(1)	-2(1)	-1(1)
Sb(4)	16(1)	7(1)	6(1)	2(1)	-3(1)	-2(1)
Ag(1)	23(2)	15(2)	23(2)	-2(1)	6(1)	5(1)
Ag(2)	29(2)	15(2)	20(2)	6(1)	3(1)	7(1)
Ag(3)	25(2)	23(2)	20(2)	9(1)	2(1)	7(1)
Ag(4)	25(2)	23(2)	19(2)	7(1)	3(1)	10(1)
Ag(5)	22(2)	61(3)	36(2)	21(2)	9(2)	6(2)
Cu(1)	11(2)	37(3)	12(3)	8(2)	3(2)	-5(2)
Cu(3)	22(3)	89(7)	0(2)	-14(3)	-1(2)	52(4)
S(1)	18(4)	9(4)	10(4)	1(3)	2(3)	5(3)
S(2)	14(4)	9(4)	15(5)	1(3)	1(3)	4(3)
S(3)	19(5)	18(5)	12(5)	-3(4)	-5(4)	10(4)
S(4)	19(5)	23(5)	7(4)	6(4)	0(3)	11(4)
S(5)	15(4)	8(4)	9(4)	-1(3)	6(3)	4(3)
S(6)	18(4)	12(4)	8(4)	3(3)	6(3)	6(3)
S(7)	16(4)	10(4)	21(5)	5(4)	2(4)	-3(3)
S(8)	18(4)	12(4)	12(5)	6(4)	-1(3)	5(3)
S(9)	13(4)	15(5)	30(6)	3(4)	9(4)	-1(3)
S(10)	27(5)	5(4)	21(5)	3(4)	17(4)	3(3)
S(11)	37(6)	30(6)	18(6)	13(5)	19(5)	27(5)
S(12)	12(4)	13(5)	36(6)	13(4)	-9(4)	-3(4)

7. Literatur

- [1] M. G. Kanatzidis, A. C. Sutorik, *Prog. Inorg. Chem.* **1995**, *43*, 151.
- [2] D. W. Beck, *Zeolithe Molecular Sieves*, Krieger, Malbar, FL, **1984**.
- [3] G. A. Ozin, *Supramolecular Chemistry*, **1995**, Vol. 6, 125.
- [4] C. L. Bowes and G. A. Ozin, *Adv. Mater.* **1996**, *8*, No. 1.
- [5] (a) H. Eckert, *Angew. Chem. Int. Ed. Engl.* **1989**, *28*, 1723, (b) G. Sakane, S. Shi et al, *Inorg. Chem.* **1995**, *34*, 4785.
- [6] M. Ciampolini, N. Nardi, *Inorg. Chem.* **1966**, *1*, 41.
- [7] M. Ciampolini, N. Nardi, *Inorg. Chem.* **1966**, *1*, 45.
- [8] M. T. Czyzyk and R. A. de Groot, *Physical Review B*, **1989**, *39*, 763.
- [9] W. S. Sheldrick, M. Wachhold, *Angew. Chem.* **1997**, *109*, 214.
- [10] M. Schur, C. Näther, W. Bensch, *Z. Naturforsch.* **2001**, *56b*, 79.
- [11] M. Schur, W. Bensch, *Z. Naturforsch.* **2002**, *57b*, 1.
- [12] R. Stähler, W. Bensch, *J. Chem. Soc., Dalton Trans.* **2001**, 2518.
- [13] R. Stähler, W. Bensch, *Eur. J. Inorg. Chem.* **2001**, 3073.
- [14] R. Kiebach, C. Näther, W. Bensch, *Z. Anorg. Allg. Chem.* **2002**, *628*, 2176.
- [15] R. Kiebach, C. Näther, W. Bensch, R. – D. Hoffmann, R. Pöttgen, *Z. Anorg. Allg. Chem.* **2003**, *629*, 532.
- [16] J. Rijnberk, C. Näther, M. Schur, I. Jeß, W. Bensch, *Acta Crystallogr.* **1998**, *C54*, 920.
- [17] G. L. Schimek, J. W. Kolis, *Inorg. Chem.* **1997**, *36*, 1689.
- [18] K. Volk, H. Schäfer, *Z. Naturforsch.* **1979**, *34b*, 172.
- [19] A. F. Wels, *Structural Inorganic Chemistry*, 4. Auflage, Oxford Univ. Press, London, **1975**, 437.
- [20] B. J. Wuensch, *Z. Kristallogr.* **1964**, *119*, 437.
- [21] A. Pfitzner, *Z. Anorg. Allg. Chem.* **1994**, *620*, 1992.
- [22] M. Jansen, *Angew. Chem.* **1987**, *99*, 1136; *Angew. Chem. Int. Ed. Engl.* **1987**, *26*, 1098.
- [23] J. Garin, E. Parthe', *Acta Crystallogr.* **1972**, *B28*, 3672.
- [24] R. M. Imamov, Z. G. Pinsker, A. I. Ivchenko, *Kristallografiya*, **1964**, *9*, 853.
- [25] A. Pfitzner, *Z. Allg. Chem.* **1995**, *621*, 685.

- [26] E. Jerome, G. L. Schimek, G. W. Drake, J. W. Kolis, *Eur. J. Solid State Inorg. Chem.* **1996**, *33*, 765.
- [27] Zh. Chen, R. E. Dillks, R.-J. Wang, J. Y. Lu, J. Li, *Chem. Mater.* **1998**, *10*, 3184.
- [28] A. V. Powell, S. Boissiere, A. M. Chippindale, *Chem. Mater.* **2002**, *14*, 1220.
- [29] A. V. Powell, S. Boissiere, A. M. Chippindale, *J. Chem. Soc., Dalton Trans.* **2000**, 4192.
- [30] F. Sauerwald, Dissertation der Philipps Universität Marburg, **2005**.
- [31] J. Schwenzel, Dissertation, Universität Kiel, **2003**.
- [32] R. D. Armstrong, T. Dickensen, P. M. Willis, *Electroanal. Chem. Interfacial Electrochem.* **1974**, *53*, 389.
- [33] R. D. Armstrong, T. Dickensen, R. Whitfield, *J. Electroanal. Chem.* **1972**, *39*, 257.
- [34] R. D. Armstrong, T. Dickensen, J. Turner, *J. Electroanal. Chem.* **1973**, *44*, 157.
- [35] R. D. Armstrong, T. Dickensen, P. M. Willis, *J. Electroanal. Chem.* **1973**, *48*, 47.
- [36] C. J. Wen, C. Ho, B. A. Boukamp, I. D. Raistrick, W. Weppner, R. A. Huggins, *International Metals Reviews*, **1981**, No. 5.
- [37] C. R. Knowles, *Acta Crystallogr.* **1964**, *17*, 847.
- [38] D. Harker, *J. Chem. Phys.* **1936**, *4*, 381.
- [39] B. Ribar, W. Nowacki, *Acta Crystallogr.* **1970**, *B26*, 201.
- [40] G. L. Schimek, W. T. Pennington, P. T. Wood, J. W. Kolis, *J. Solid State Chem.* **1996**, *123*, 277.
- [41] P. T. Wood, G. L. Schimek, J. W. Kolis, *Chem. Mater.* **1996**, *8*, 721.
- [42] P. Vaqueiro, A. M. Chippindale, A. R. Cowley, A. V. Powell, *Inorg. Chem.* **2003**, *42*, No. 24, 7846.
- [43] A. V. Powell, J. Thun, A. M. Chippindale, *J. Solid State Chem.* **2005**, *178*, 3414.
- [44] K. Volk, H. Schäfer, *Z. Naturforsch.* **1979**, *34b*, 1637.
- [45] X. Wang, F. Liebau, *J. Solid State Chem.* **1994**, *111*, 385.
- [46] X. Wang, L. Liu, A. J. Jacobson, *J. Solid State Chem.* **2000**, *155*, 409.

- [47] K. Tan, Y. Ko, J. B. Parise, *Acta Crystallogr.* **1994**, C50, 1439.
- [48] Y. Ko, K. Tan, J. B. Parise, A. Darowsky, *Chem. Mater.* **1996**, 8, 493.
- [49] J. B. Parise, *Science*. **1991**, 251, 293.
- [50] K. Volk, H. Schäfer, *Z. Naturforsch.* **1979**, 34b, 172.
- [51] J. B. Parise, Y. Ko, *Chem. Mater.* **1992**, 4, 1446.
- [52] M. Gostojic, W. Nowacki, P. Engel, *Z. Kristallogr.* **1982**, 159, 217.
- [53] L. Engelke, C. Näther, W. Bensch, *Eur. J. Inorg. Chem.* **2002**, 2936.
- [54] J. Rijnberk, C. Näther, W. Bensch, *Monatsh. Chem.* **2000**, 131, 721.
- [55] R. Stähler, C. Näther, W. Bensch, *Eur. J. Chem.* **2001**, 1835.
- [56] V. Spetzler, R. Kiebach, C. Näther, W. Bensch, *Z. Anorg. Allg. Chem.* **2004**, 630, 2398.
- [57] X. Wang, A. J. Jacobson, F. Liebau, *J. Solid State Chem.* **1998**, 140 , 387.
- [58] H. A. Graf, H. Schäfer, *Z. Naturforsch.* **1972**, 27b, 735.
- [59] G. Dittmar, H. Schäfer, *Z. Anorg. Allg. Chem.* **1977**, 437, 183.
- [60] G. Dittmar, H. Schäfer, *Z. Anorg. Allg. Chem.* **1978**, 441, 93.
- [61] G. Dittmar, H. Schäfer, *Z. Anorg. Allg. Chem.* **1978**, 441, 98.
- [62] B. Eisenmann, H. Schäfer, *Z. Naturforsch.* **1979**, 34b, 383.
- [63] G. Cordier, H. Schäfer, C. Schwidetzky, *Z. Naturforsch.* **1984**, 39b, 131.
- [64] W. S. Sheldrick, H.-J. Häusler, *Z. Anorg. Allg. Chem.* **1988**, 557, 105.
- [65] H.-O. Stephan, M. G. Kanatzidis, *Inorg. Chem.* **1997**, 36, 6050.
- [66] W. Bensch, M. Schur, *Z. Naturforsch.* **1997**, 52b, 405.
- [67] P. Vaqueiro, D. P. Darlow, A. M. Chippindale, A. V. Powell, *Solid States Ionics*. **2004**, 601, 172.
- [68] M. Schur, W. Bensch, *Eur. J. Solid State Inorg. Chem.* **1997**, 34, 457.
- [69] R. Stähler, C. Näther, W. Bensch, *J. Solid State Chem.* **2003**, 174, 264.
- [70] M. Schaefer, D. Kurowski, A. Pfitzner, C. Näther, W. Bensch, *Acta Cryst.* **2004**, E60, m183.
- [71] A. Puls, M. Schaefer, C. Näther, W. Bensch, A. V. Powell, S. Boissière, A. M. Chippindale, *J. Solid State Chem.* **2005**, 178, 1171.
- [72] W. S. Sheldrick, H.-J. Häusler, *Z. Anorg. Allgem. Chem.* **1988**, 561, 149.
- [73] J. B. Parise, *J. Chem. Soc. Chem. Commun.* **1990**, 1553.

- [74] K. Volk, P. Bickert, R. Kolmer, H. Schäfer, *Z. Naturforsch.* **1979**, *34b* 380.
- [75] H. A. Graf, H. Schäfer, *Z. Anorg. Allg. Chem.* **1975**, *414*, 211.
- [76] G. Cordier, C. Schwidetzky, H. Schäfer, *J. Solid State Chem.* **1984**, *54*, 84.
- [77] R. Kiebach, F. Studt, C. Näther, W. Bensch, *Eur. J. Inorg. Chem.* **2004**, 2553- 2556.
- [78] T. J. McCarthy, M. G. Kanatzidis, *Inorg. Chem.* **1994**, *33*, 1205.
- [79] W. Bensch, C. Näther, R. Stähler, *Chem. Commun.* **2001**, 477.
- [80] J. Oliver-Fourcade, J. Izghouti, E. Philippot, *Rev. Chim. Min.* **1981**, *18*, 207.
- [81] G. Cordier, H. Schäfer, *Rev. Chim. Min.* **1981**, *18*, 218.
- [82] R. Stähler, W. Bensch, *Z. Anorg. Allg. Chem.* **2002**, *628*, 1657.
- [83] W. Bensch, M. Schur, *Eur. J. Solid State Inorg. Chem.* **1996**, *33*, 1149.
- [84] W. S. Sheldrick, M. Wachhold, *Coordination Chem. Rev.* **1998**, *176* 211.
- [85] H.-O. Stephan, M. G. Kanatzidis, *J. Am. Chem. Soc.* **1996**, *118*, 12226.
- [86] X. Wang, F. Liebau, *Acta Crystallogr.* **1996**, *B52*, 7.
- [87] W. Dörrscheidt, H. Schäfer, *Z. Naturforsch.* **1981**, *86b*, 410.
- [88] A. Bondi, *J. Phys. Chem.* **1964**, *68*, 44.
- [89] L. Pauling, *Die Natur der chemischen Bindung*, VCh, Weinheim, **1962**.
- [90] A. Pfitzner, *Chem. Eur. J.* **1997**, *3*, 2032.
- [91] A. Pfitzner, D. Kurowski, *Z. Kristallogr.* **2000**, *215*, 373.
- [92] <http://www-ph.postech.ac.kr/~yktwon/phy-esp2/web/egap/egap.html>; Pohang University of Science and Technology, **1986**.
- [93] V. Spetzler, C. Näther, W. Bensch, *Inorg. Chem.* **2005**, *44*, 5805.
- [94] V. Spetzler, H. Rijnberk, C. Näther, W. Bensch, *Z. Anorg. Allg. Chem.* **2004**, *630*, 142.
- [95] A. Puls, Dissertation, Christian-Albrechts-Universität zu Kiel, **2006**.
- [96] R. Kiebach, A. Griebe, C. Näther W. Bensch, Solid State Sci. accepted 22.12.2005.
- [97] Holleman – Wiberg, Lehrbuch der Anorganischen Chemie, Berlin, New York **1995**.

- [98] A. Lerk in “*Handbook of Nanostructured Materials and Nanotechnology*”, ed. H. S. Nalwa, Academic Press **2000**, Vol. 5.; *Intercalated Layered Materials*, ed. F. A. Lévy, D. Reidel Publishing, Dordrecht, Boston, London, **1979**.
- [99] M. Schaefer, Dissertation, Christian-Albrechts-Universität zu Kiel, **2003**.
- [100] L. Engelke, R. Stähler, M. Schur, C. Näther, W. Bensch, R. Pöttgen, M. H. Möller, *Z. Naturforsch.* **2004**, 59b, 869.

Danksagung

An erster Stelle danke ich meiner Frau, die meine Begeisterung für die Chemie mitgetragen hat und dadurch auf viele gemeinsame Tätigkeiten verzichten musste.

Mein Dank gilt Herrn Prof. Dr. W. Bensch, der mir als „Altlast“ mit unendlicher Mühe und Geduld stets Hilfestellungen und Anregungen gegeben hat.

Der gesamten Arbeitsgruppe danke ich für die ständige Hilfsbereitschaft und freundschaftliche Arbeitsatmosphäre während dieser Zeit. Besonders hervorheben möchte ich Frau Dipl.-Chem. A. Puls, Frau Dipl.-Chem. N. Pienack, Herrn Dipl.-Chem. D. Pitzschke, Herrn Dipl.-Chem. H. Lühmann und Herrn Dipl.-Chem. R. Kiebach für ihre Unterstützung bei praktischen und theoretischen Fragen.

Mein Dank gilt auch Herrn Dr. C. Näther für seine ständige Hilfe bei der Lösung kristallographischer Probleme.

Für die Hilfe bei der Charakterisierung der Proben möchte ich mich herzlich bei Frau I. Jeß (Einkristallstrukturanalyse), Herrn Dr. C. Teske (thermische Analysen) und Frau U. Cornelsen (Spektroskopie) bedanken.

Herrn Prof. Dr. W. Weppner vom Institut für Materialwissenschaft der Technischen Fakultät der Universität Kiel danke ich für die Bereitstellung eines Laborplatzes und die Geräte zur Durchführung der Impedanzanalysen. Herrn Dipl. Chem. C. Knittlmayer danke ich für die Hilfestellung bei den Messungen.

Gedankt sei auch meinem ehemaligen Kollegen Herrn StD. D. Neumann für die Unterstützung bei der Lösung physikalischer Probleme.

Erklärung

Die experimentellen Untersuchungen zu dieser Arbeit wurden in der Zeit von Oktober 2003 bis Dezember 2005 am Institut für Anorganische Chemie der Christian-Albrechts-Universität zu Kiel unter Leitung von Herrn Prof. Dr. W. Bensch durchgeführt.

Hiermit versichere ich an Eides statt, dass ich die vorliegende Arbeit selbständig – abgesehen von der Beratung durch meinen wissenschaftlichen Lehrer – und nur unter Verwendung der angegebenen Hilfsmittel angefertigt habe. Die Dissertation wird ausschließlich an dieser Stelle zur Promotion vorgelegt.

Zusätzlich erkläre ich, dass ich noch keinen Promotionsversuch, an dieser oder einer anderen Hochschule, gemacht habe.

Kiel, den 15.5.2006

Volker Spetzler

Lebenslauf

Name: Volker Spetzler
Adresse: Am Traveeck 19
23558 Lübeck
Geburtsdatum: 29.04.1941
Staatsangehörigkeit: deutsch
Familienstand: verheiratet, 2 Kinder

Schulausbildung

1948 – 1952 Volksschule Niendorf/Ostsee
1952 – 1962 Ostsee-Gymnasium Timmendorfer Strand

Hochschulausbildung

1962 – 1967 Studium für das Lehramt an Gymnasien
in den Fächern Chemie und Erdkunde

Beruf

1967 – 2005 Lehrer am Gymnasium Johanneum zu Lübeck
(Altersteilzeit der Arbeitsphase 2001 – 2003)
Altersteilzeit der Freistellungsphase bis 2005)

Hochschulausbildung

2000 – 2003 Probezeit für die Zulassung zur Promotion
2003 – 2006 Doktorarbeit bei Herrn Prof. Dr. W. Bensch am
Institut für Anorganische Chemie der Christian-
Albrechts-Universität zu Kiel
Abschluss: Promotion im Fachbereich Chemie